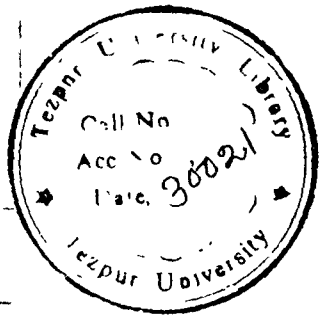

# *Swift heavy ion irradiation effects on electrodeposited conducting polymer based electrodes for redox supercapacitors*

**Abu Mohd. Pharhad Hussain** (M.Sc. M.Phil.)

Registration Number 010 of 2003

A thesis
submitted in partial fulfillment of the requirements
for the degree of
Doctor of Philosophy (Ph.D.)



February, 2006

School of Science & Technology
Department of Physics
Tezpur University
Napaam, Tezpur - 784 028
(India)

*I dedicate this work*

*to my beloved MAA,*

*who first taught me to hold the pencil,*

*&*

*to my dearest ABBA,*

*who first showed me way to find the answers of*

*'what', 'why', 'how'.*

# ABSTRACT

Organic conducting polymers have recently attracted much attention worldwide in view[a] of both scientific interest and a variety of possible applications. The electrical conductivities of the intrinsically conducting polymers (ICPs) typically range from that of insulators (<$10^{-10}$ S/cm) to that of semiconductors such as silicon (~$10^{-5}$ S/cm), even to that of metals such as copper ~5 x $10^5$ S/cm depending upon their doping level. The ICPs are transformed from insulating to conducting form through the process of doping. Both *p*-type (electron accepting e.g. $I_2$, $PF_6$, $BF_6$, Cl, $AsF_6$) and *n*-type (electron donating e.g. Na, K, Li, Ca, $[CH_3(CH_2)_3]_4$) dopants have been utilized to induce an insulator-to-conductor transition in electronic polymers. The conducting polymers have begun to find applications, which include molecular electronics, battery materials, electrochemical capacitors, non-linear optics, conductive layers for light-emitting polymer devices, sensor technology, actuators, electromagnetic-interference (EMI) shielding, electromagnetic-radiation absorbers, welding of plastics, and anticorrosion coatings for iron and steel.

Swift heavy ions (SHI) irradiation of polymers is an emerging area of research and recently SHI irradiation has been successfully employed for modification and improvement of properties such as conductivity, crystallinity, density, environmental stability, solubility etc. of polymeric materials. Irradiating ions have velocities around or above the velocity of K-shell electrons, which correspond to energies ranging from a few MeV/amu to about 100 MeV/amu. They interact with matter mainly by inelastic collision process leading to excitations and ionization of the target atoms. Almost all of the SHI energy is lost in the electronic stopping creating large number of active chemical species, cations, anions, radicals and electrons along the ion track. Violent Coulombic interactions among these charged species may give rise to bond breaking as well as cross-linking between the polymer chains.

A supercapacitor is an electrochemical capacitor that has an unusually large energy storage capacity (~20-2000 times) as compared to that of a conventional capacitor for the same size. These are of particular interest in automotive applications as supplemental storage device to batteries for electric vehicles. The first supercapacitor based on a double layer mechanism was developed in 1957 by General Electronics using a porous carbon electrode.

The present work aims to develop a deeper understanding of the monomer level processes of electrochemical polymerization of conducting polymers polyaniline, polypyrrole and poly(3-methylthiophene) for improvement and control of conductivity, morphology and porosity and to standardize parameters like monomer and dopant concentrations and type of solvent to synthesize homogeneous, dense, uniform and smooth conducting polymer films with higher conductivity and higher charge storage capacity. All-polymer redox supercapacitors have been fabricated using unirradiated and irradiated conducting polymer electrodes and their performance characteristics studied by cyclic voltammetry and charge-discharge studies. SHI irradiation of the conducting polymer films has been carried out to study the effects of ion irradiation on conducting polymers from the point of view of their application as electrodes in all-polymer redox supercapacitors.

In the present thesis, chapter I deals with the review of literature on conducting polymers, SHI irradiation of polymers and electrochemical supercapacitors. Basic characteristics and different types and methods of doping of conducting polymers are presented. At the end of the chapter, scope of the thesis along with the statement of the problem and objectives of understanding the present work has been spelt out.

In chapter II different theories of charge transport in conducting polymers have been discussed. The theoretical aspects involved in the electropolymerization of polymers, SHI irradiation and supercapacitors are also included in this chapter.

Chapter III describes the materials viz. monomers, dopants and solvents used in the present work and the method of synthesis of conducting polymer

films by oxidative electropolymerization. Different parameters such as fluence, ion track, nuclear and electronic energy loss etc. of SHI irradiation have been discussed. Various techniques employed in the present work such as cyclic voltammetry, four probe measurement, XRD, SEM, UV-Vis and FTIR for characterization of the conducting polymer films have been briefly reviewed. Charge-discharge technique for characterization of the all-polymer redox supercapacitors has also been described in detail in this chapter.

Electropolymerization, characterization and SHI irradiation of polyaniline conducting polymer films and the results thereof have been discussed in chapter IV. The conducting polymer films exhibited good electroactive behaviour in the cyclic voltammetry studies with electrochromism. The oxidation/reduction peak heights show an increase in magnitude upon SHI irradiation, which could be attributed to the increase in conductivity of the polymer films as other conditions of cyclic voltammetry have been kept unchanged. Electropolymerized polyaniline films doped with different dopants show highest conductivity for $HClO_4$ doping (~78 S/cm), which upon SHI irradiation increases to 124 S/cm. The enhancement of dc conductivity upon SHI irradiation could be attributed to electronic stopping of the irradiated beam in the polymer, which creates large number of active chemical species, cations, anions, radicals and electrons along the ion track. The Coulombic interactions among these charged species may lead to cross-linking between the polymer chains. The cross-linking of polymer chains upon SHI irradiation decreases the resistance of the polymer films as the charge carriers can move from one chain to the other through the cross-links, which otherwise takes place by inter-chain hopping resulting in high resistance. The conductivity of polymer films increases with the increase in fluence of irradiation. The morphological studies by SEM show that potentiodynamic method of electropolymerization produces polymer films with denser and smoother surface morphology as compared to those prepared by the potentiostatic method. The SEM studies also show that upon SHI irradiation the

surface becomes dense and smooth with increase in grain size, which could be attributed to the huge amount of energy transferred from the incident ion upon SHI irradiation. The UV-Vis spectroscopy shows that upon SHI irradiation the position of the carrier absorption peak shifts to higher wavelength resulting in decrease in the band gap, which could be attributed to the broadening of polaron/bipolaron band. The formation of polyaniline and the presence of dopants have been confirmed from the study of the FTIR spectra. The XRD studies reveal that the polyaniline conducting polymer films are semi-crystalline in nature, which upon SHI irradiation show significant increase in the degree of crystallinity. Upon SHI irradiation, collective excitations (plasmons) produce a large excited volume in which, the backbone bonds may rotate and adopt a variety of conformations. Upon cooling, the lower-energy configurations of bonds are preferred. Stereoregular chains then favour regular helical zigzag shapes. At the same time, the regular sections of chain may align together to form regions of crystallinity. The degree of crystallinity of conducting polymer films show increase with the increase in fluence of SHI irradiation. At the end of the chapter a brief summary of results and discussion of various characterizations carried out on polyaniline conducting polymer films has been presented.

In chapter V, the electropolymerization, characterization and SHI irradiation of polypyrrole conducting polymer films have been discussed. The cyclic voltammograms of the polypyrrole conducting polymer films show good redox behaviour with well-constructed oxidation and reduction peaks. The magnitude of oxidation/reduction current peak height increases upon SHI irradiation, which is attributed to the increase of conductivity after irradiation. The polypyrrole films doped with different dopants showed conductivity in the range on 100 - 115 S/cm, which increases by about 60% upon SHI irradiation. This could be ascribed to the creation of large number of radicals, cations, anions and charged chemical species and also to the cross-linking of the polymer chains. The conductivity is fluence dependent and increases with the increase in fluence of SHI irradiation. The SEM studies show that upon SHI

irradiation the granular size increases with densification of the polypyrrole conducting polymer film, which could be attributed to the huge energy transfer by the electronic stopping process. The carrier absorption peak position upon SHI irradiation shows increase in intensity and also shifts towards higher wavelength in the UV-Vis study indicating lowering of band gap, which is attributed to the broadening of the polaron/bipolaron bands that occurs due to the increase in carrier concentration in the polymer films as large number of cations, anions, radicals and electrons are created upon SHI irradiation due to electron stopping mechanism. The FTIR spectra confirm that the polypyrrole films synthesized by electrochemical polymerization are in doped state. The semi-crystalline nature of the conducting polymer films is revealed by XRD study shows increase in the degree of crystallinity upon SHI irradiation, which may be ascribed to cross-linking occurring due to collective excitations (plasmons), which produces a large excited volume resulting in coercive interaction among the ions and radical pairs produced in the adjacent chains within the volume as a result of electron stopping mechanism. The degree of crystallinity increases with the increase of fluence of SHI irradiation. At the end of the chapter, the results and discussion of various characterizations carried out on polypyrrole have been summarized.

Electropolymerization, SHI irradiation and characterization of poly(3-methylthiophene) have been presented in chapter VI. The cyclic voltammograms of poly(3-methylthiophene) conducting polymer films doped with different dopants show good electroactivity with electrochromism. The conductivity measurements show that the $LiClO_4$ p-doped poly(3-methylthiophene) possesses highest conductivity of the order of 120 S/cm, which upon SHI irradiation increases upto ~198 S/cm, which could be attributed to the increase in charge carrier concentration, lowering of band gap and cross-linking of polymer chains upon SHI irradiation. The increase in charge carrier concentration and the lowering of band gap have been confirmed from the studies of UV-Vis spectra, which could be attributed to the creation of

large number of cations, anions, radicals and charged active chemical species upon SHI irradiation of the conducting polymer films. The cross-linking of the polymer chains upon SHI irradiation could be predicted from the FTIR study. The XRD studies of the poly(3-methylthiophene) conducting polymer films show that the poly(3-methylthiophene) films are semi-crystalline in nature and the degree of crystallinity has been observed to increase upon SHI irradiation. This could be attributed to the cross-linking occurring due to collective excitation (plasmons), which produce a large excited volume resulting in coercive interaction among the ions and radical pairs produced in the adjacent chains within the volume as a result of electron stopping mechanism. The conductivity and the degree of crystallinity of the poly(3-methylthiophene) conducting polymer films increase with the increase in fluence of SHI irradiation. The summary of the results and discussion on various characterizations carried out on poly(3-methylthiophene) has been presented at the end of this chapter.

The characterization of the all-polymer solid state supercapacitors of type I, II and III configurations with conducting polymer electrodes and gel polymer electrolytes and the various characteristic properties of the supercapacitors have been presented in chapter VII. The supercapacitors with conducting polymer electrodes show capacitance in the range of 150 -250 F/gm, the highest capacitance (~250 F/gm) has been obtained for type I supercapacitor with $[CH_3(CH_2)_3]_4NBF_4$ doped poly(3-methylthiophene) conducting polymer electrode. The highest energy density has been obtained for type III supercapacitors with p and n-doped poly(3-methylthiophene) electrodes (~76 WH/kg). All-polymer supercapacitors with conducting polymer electrodes show coulombic efficiency in the range of 85-95%. The supercapacitors with conducting polymer electrodes show an initial sharp decrease in capacitance, which could be attributed to the charge consumption or loss due to irreversible Faradic reactions at the electrodes due to the presence of volatile reactive surface groups such as $OH^-, CN^-, CH_3^+$ etc. The supercapacitors with SHI irradiated conducting polymer electrodes show

remarkably increase in electrochemical stability and the initial decrease of capacitance is decreased, which may be attributed to the stabilization or removal of the volatile reactive surface groups from the electrodes upon SHI irradiation. The decrease of total charge-discharge time observed for supercapacitors with SHI irradiated electrodes, which could be attributed to the increase in conductivity of the polymer electrodes upon SHI irradiation, which gives rise to faster charging and discharging of the supercapacitors.

The conclusions drawn from the present work with a brief mention of the future scope in the related research field have been presented in the last chapter VIII. The electropolymerization of polyaniline, polypyrrole and poly(3-methylthiophene) conducting polymer films doped with different dopants has been carried out on ITO coated glass substrates. The conducting polymer films have been irradiated with 160 MeV $Ni^{12+}$ and 120 MeV $Si^{9+}$ ion beams of three different fluences of $5x10^{10}$, $5x10^{11}$ and $3x10^{12}$ ions/$cm^2$. The cyclic voltammetry, dc conductivity measurement, UV-Vis and FTIR spectroscopy, SEM and XRD studies have been carried out on both the unirradiated and irradiated conducting polymer films. All-polymer solid state redox supercapacitors with conducting polymer electrodes and PVDF-HFP(20w/o)-PMMA(10w/o)-$LiCF_3SO_3$(10w/o)-PC+DEC (57w/o)-$SiO_2$(3w/o) gel polymer electrolyte have been fabricated and characterized by cyclic voltammetry and tested for 10,000 charge-discharge cycles for electrochemical stability.

# Declaration

*I hereby declare that the thesis entitled "**Swift heavy ion irradiation effects on electrodeposited conducting polymer based electrodes for redox supercapacitors**", being submitted to the Dept. of Physics, Tezpur University, is a record of original research work carried out by me. Any text, figures, theories, results, or designs that are not of own devising are appropriately referenced in order to give credit to the original author(s). All sources of assistance have been assigned due acknowledgment. I also declare that neither this work as a whole nor a part of it has been submitted to any other University or Institute for any other degree, diploma or award.*

*Date:* 14.02.2006

*Place: Napaam, Tezpur*

*(Abu Mohd. Pharhad Hussain)*

# Department of Physics :: Tezpur University

Dr. Ashok Kumar
*Reader*

P.O.: Napaam, Tezpur
Sonitpur, -784 028
Assam, (India)

## CERTIFICATE

This is to certify that the thesis entitled "**Swift heavy ion irradiation effects on electrodeposited conducting polymer based electrodes for redox supercapacitors**" submitted to the Tezpur University in the Department of Physics, under the School of Science and Technology, in partial fulfillment for the award of the degree of Doctor of Philosophy (Ph.D.) in Physics is a record of research work carried out by **Mr. Abu Mohd. Pharhad Hussain** under my personal supervision and guidance.

All helps received by him from various sources have been duly acknowledged.

No part of this thesis has been reproduced elsewhere for award of any other degree.

(A. Kumar)
Reader
School of Science and Technology
Department of Physics

Date: 14.02.2006
Place: Napaam, Tezpur

# CONTENTS

# LIST OF TABLE

# LIST OF FIGURE

# ACKNOWLEDGMENT

*It is a matter of immense pleasure and fortune for me to express deep sense of gratitude to Dr. Ashok Kumar for his dynamic & meticulous supervision that I have received all through my research work at Tezpur University. His valuable suggestions and discussions were inspiring enough to put me best efforts into my work. Needless to say, I shall be highly obliged to him.*

*I extend my sincere gratitude to Dr. D. K. Avasthi, IUAC (NSC), New Delhi, for his keen interest and inspiring suggestions for swift heavy ion irradiation of conducting polymers. His constructive comments, immense help and assistance at various stage of my work shall remain noteworthy. Help & suggestions extended by Mr. Fouran Singh, IUAC, New Delhi is also highly acknowledged.*

*I extend my sincere thanks to Prof. A. Choudhury, Dr. J. K. Sarma, Dr. N. Das, Dr. G. A. Ahmed, Dr. Biren Das, Dr. D Mohanta, Dr. K. Baruah and Dr. N. S. Bhattacharyya of Tezpur University and Dr. S. Gogoi and Dr. S. Rai of Dibrugarh University for their encouragement, criticism and inspiration to carry out this work.*

*I would like to thank RSIC-NEHU, Shillong, specially Dr. S. Dey, Consortium for Scientific Research-DAE facility Indore, Dept. of Molecular Biology and Biotechnology and Dept. of Chemical Sciences, Tezpur University, for co-operation and concerns to characterize the samples on various aspects.*

*I sincerely acknowledge Shyamalima for her support, inspiration & affection at different stage of my work, especially during my depressed & frustrated moments and I also heartily acknowledge Boby baideu for her care, support & encouragement during this work. My special thanks are due to Anjan da, Mamoon & Deep daju for their help, love and goodwill.*

*I would like to thank Diganta, Robin (Doley), Kishore (KD), Juti, Nazir, Tulika, Rummy, Sanjeev, Taslima, Babita, Pranjal da, Anu, Kaushik da, Nandini, Nava, Upamanyu, Parthada, Pathakda, Narayanda for their help, company and*

*goodwill. Help extended by technical staff of Tezpur University Computer Center specially Dhiraj da, library staff of Tezpur University central library, IUAC library staff, Pelletron group of IUAC, New Delhi and canteen staff of A.T. Hostel are also acknowledged.*

*I am indebted to my parents, Baitimoni & Rupamoni for their constant encouragement, inspiration and moral support all throughout my work. I sincerely acknowledge Rahim bhai, Monoj sir for their encouragement & support and Saanu, Rhiya & Babu for their love.*

*Finally I thank University Grant Commission (UGC) New Delhi for financial support [vide project no. F.10-53/2001 (SR-I)] and Council for Scientific and Industrial Research (CSIR), New Delhi, for financial support as Senior Research Fellow (SRF) [9/796/(8)/2004/E.M.R.I.] of the council which helped to carryon this work and come to this stage.*

*Date : 14.02.2006*

*(Abu Mohd. Pharhad Hussain)*
*Dept. of Physics, T.U.*
*Napaam, Tezpur*

# CHAPTER I

# INTRODUCTION

## 1.1 Historical developments:

When we think of polymers what comes to mind first are the plastics such as polyethylene, which owing to their specific properties such as light weight, mechanical strength and easy processability occupy ubiquitous place in our everyday life. Almost all the polymers that we come across in daily life are insulators, which give them significant advantage for a wide range of applications in electronics and electrical industry. It is a general view that plastics and electrical conductivity are mutually exclusive and their inability to carry electricity distinguishes them from metals and semiconductors. The past two decades, however, have seen the development of a new class of organic polymers with the remarkable ability to conduct electrical current. Conducting polymers are a completely different class of polymers in the sense that they are intrinsically conducting and do not have any conducting fillers. Intrinsically conducting polymers (ICPs) are exciting electronic materials that have the potential of combining the high conductivities of metals with the low density, processability and corrosion resistance associated with polymers. These polymers also referred to as conjugated polymers or organic polymeric conductors, have conjugated bond structure in their main chain i.e. alternate single double or single triple bonds (Fig. 1.1). ICPs are beginning to find applications in molecular electronics [1, 2], battery electrode materials [3], electrochemical capacitors [4] non-linear optics [5, 6], electrochromic displays [7, 8], sensor technology [9, 10], polymer actuators [11] and electromagnetic shielding [12].

The polymeric backbone of the conducting polymer needs to be oxidized or reduced to introduce charge centers before conductivity is observed. The oxidation or reduction is performed by doping with anions or cations called dopants, a somewhat misnomer term, since the doping in conducting polymers

is completely different from the doping of semiconductors where the substitutional dopant is added in ppm. The interest in conjugated polymers was initially focused mainly on electrical conduction properties. Electrons or holes can be injected into the chains by introducing a low molecular weight dopant. The polymer chains become oxidized or reduced and show electrical conduction due to the creation of polaron or charged soliton states in the band gap. Recent interest in the conjugated polymers is not only limited to conduction properties of doped materials but also optical properties of neutral conjugated polymers are extensively being studied. Conjugated polymers represent materials with both electronic and optical properties comparable to the properties of inorganic semiconductors and metals, but have in addition the benefit of attractive mechanical and processing properties of polymers. Many of the original conjugated polymers have been derivatized in order to control the processability of the polymers.

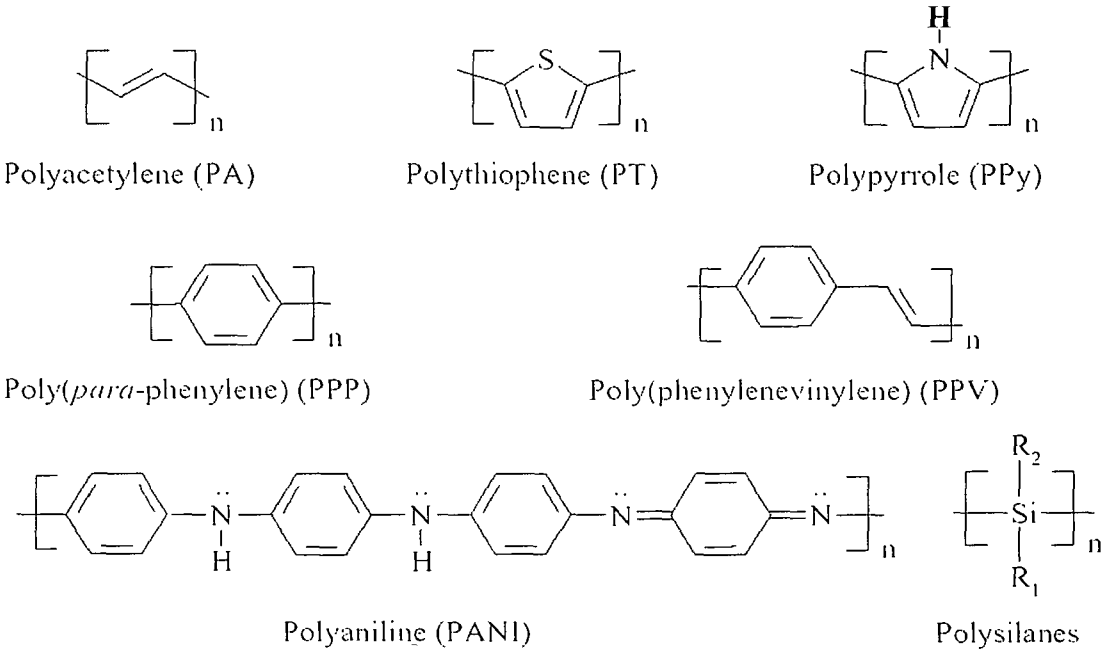


Figure 1.1: Molecular structure of some conjugated polymers.

Though conducting polymers have come into focus recently, many of the conducting polymers in their non-conducting forms were known earlier. Some were known even in their conducting form, but were not well characterized. Letheby [13] described chemical oxidative polymerization of aniline into

polyaniline in 1862 and Mohilner characterized it in 1962 [14], one complete century after its discovery. Polypyrrole was earlier known as pyrrole black and was found on the sides of container of pyrrole, which was formed by oxidation of pyrrole in air [15]. Well-defined syntheses of polyacetylene have been reported since 1971 [15]. Thus in many sense conducting polymers are rediscovered materials. The developments of importance that focused attention on conducting polymers as potential novel materials with highly promising conductivity and other properties started with the accidental discovery of conductivity of polyacetylene exposed to iodine vapors in a collaborative effort between Shirakawa, Heeger and McDiarmid [12]. A chemical route to a new conductive organic material was thus obtained. Diaz [15] gave the further impulse to the field by repetition and refinement of the electropolymerization of polyaniline films. Dall'Ollio and co-workers [16] started the electro-oxidative polymerization technique, which gave much better polypyrrole films. [16]. Polyacetylene was initially the most studied conducting polymer from both scientific and practical applications points of view, but due to its high chemical instability in air and related factors, interest in it has most recently been confined to scientific aspects only. Polyaniline, polypyrrole and polythiophene are the most extensively studied conducting polymers till date for both scientific and commercial or practical points of view. Brief historical developments of these three conducting polymers, which are the core materials investigated in the present thesis, are described below.

### *1.1.1 Polyaniline:*

Polyaniline was first polymerized electrochemically by oxidative polymerization of the monomer by Letheby in 1862 [13] when he observed the growth of a blue-green powdery pigment on a platinum anode during electrolysis of a solution of aniline in sulfuric acid. A similar product was synthesized when aniline was oxidized in hydrochloric acid [17]. But the detailed study of polyaniline took almost one century from its discovery when Mohilner and his group carried out its first systematic study in 1962 [14]. They

found that the oxidation of aniline takes place through a free-radical mechanism leading to the octamer emeraldine as the major product [14]. Their conclusion was based on the reaction kinetics and comparison of the properties of chemically synthesized emeraldine to the electrochemical product. Emeraldine is a blue-violet base that forms dark green salts [18]. Emeraldine loses two protons in oxidation with ammonia solution forming a dark blue base, nigraniline, which forms blue salts. Ohsaka et al. [19] clarified $p^H$ dependence of aniline by studying oxidation of aniline in acidic, neutral and basic media. Diaz and Logan [15] demonstrated that continuously varying potential between -0.2 and +0.8 V versus saturated calomel electrode (SCE) in a solution of 0.1M sulfuric acid and monomer aniline produces homogeneous coatings of high quality polyaniline films strongly adhered to platinum electrode. Four idealized forms of polyaniline have been proposed as shown in Fig. 1.2.

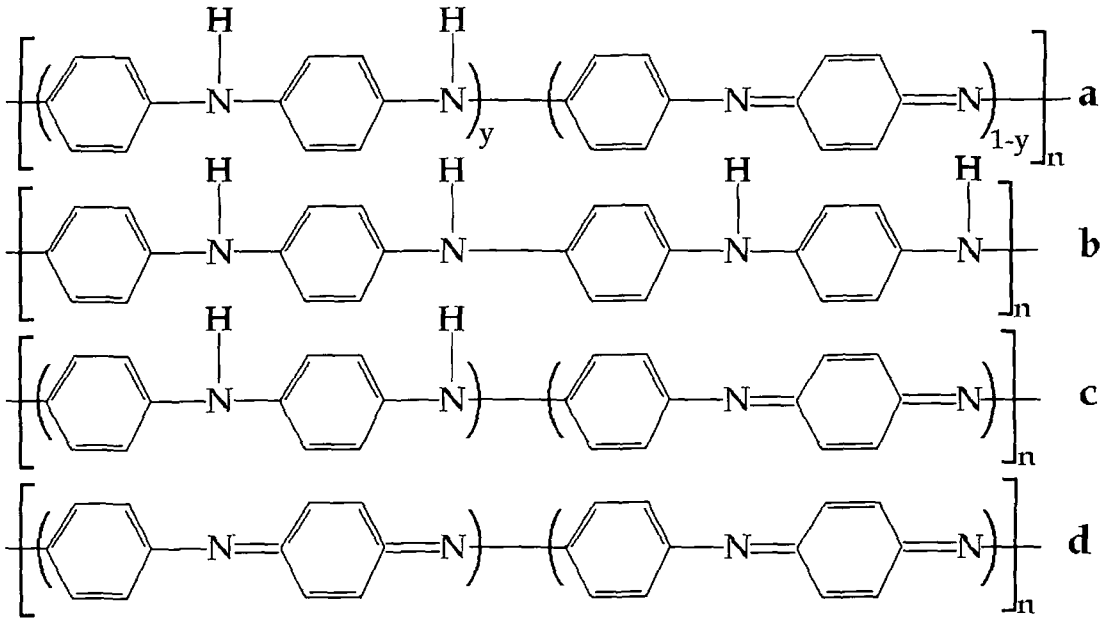


Figure 1.2: Structures of various forms of polyaniline (a) general form, (b) completely reduced form leucoemeraldine, (c) half oxidized form emeraldine base and (d) completely oxidized state pernigraniline.

In this general formula (Fig. 1.2a), there is alternating reduced units comprising the units contained in the left parenthesis and oxidized units comprising the units contained in the right parenthesis. The degree of polymerization is

denoted by n and (1-y) is the oxidation state that can have a value from 0.0 to 1.0. For (1-y) = 0, we get completely reduced polymer denoted as leucoemeraldine as shown in Fig. 1.2b. When (1-y) = 0.5, we have half-oxidized state of the polyaniline called emeraldine (Fig. 1.2c). The completely oxidized polyaniline conducting polymer called pernigraniline is obtained at (1-y) = 1.0, which is non-conducting form of polyaniline. In theory 'y' may have any value from 0.0 to 1.0, but practically it is usually found to be close to 0.5, which describes the emeraldine base form (Fig. 1.2c). These forms can be interconverted by chemical and electrochemical redox processes e.g. upon protonation of emeraldine base form (Fig. 1.2c) with HCl will produce emeraldine hydrochloride salt.

Polyaniline has been studied in various forms for different applications. Polyaniline films grown on semiconductor substrates such as cadmium selenide, silicon, gallium phosphide, gallium arsenide etc. may provide protection from corrosion in aqueous media [20]. Polyaniline films have been studied for electrochromic device applications [21], however only yellow to green transition was found to be reversible and repetition for $10^6$ cycles was obtained. De Surville and coworkers [22] were the first to investigate polyaniline as electrode material, following which both aqueous [23, 24] and non-aqueous (solid state) [25, 26] cells have been extensively investigated.

### *1.1.2 Polypyrrole:*

Polypyrrole, known as "pyrrole black" in conductive form was first found on the sides of pyrrole container, which was polymerized by spontaneous polymerization in air and chemical oxidative polymerization [3]. Dall'Ollio in 1968 [16] polymerized polypyrrole by electrochemical oxidative polymerization of pyrrole monomer and this was the first experiment to produce a conducting polymeric material and showed conductivity of 8 S/cm. In 1979, Diaz and coworkers [27] produced coherent films of polypyrrole, which could be peeled off from the platinum substrate, leading to the

electrochemical polymerization processes as major synthetic route to produce conducting polymer films.

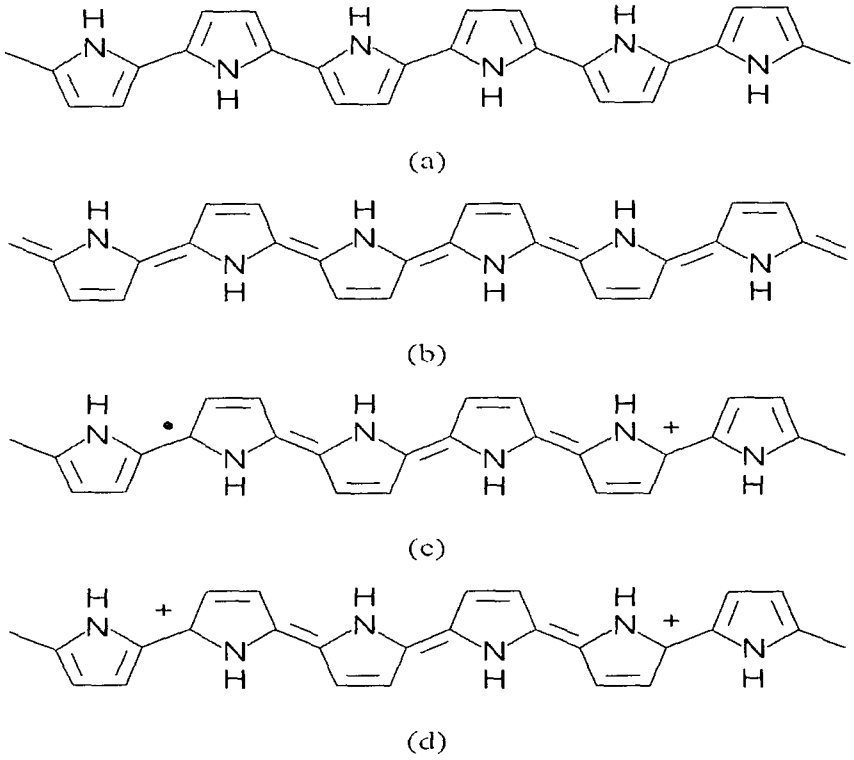

Figure 1.3: Possible structures of polypyrrole showing the (a) non-degenerate aromatic and (b) quinoid configurations (c) a polaron defect and (d) a bipolaron defect.

The structure of polypyrrole is pyrrole units coupled through their 2- and 5-positions (Fig. 1.3). Pyrrole monomers with substitutes at 2- or 5-positions forms only dimers, and monomers having substitutes at 2- or 5-positions or on both 2- and 5-position do not polymerize [28].Polypyrrole can be drawn with either heteroaromatic (Fig. 1.3(a)) or quinoid (Fig. 1.3(b)) structures, of which the latter possesses a higher energy configuration. Two neutral radicals on a single chain will recombine to eliminate the structural defect [29], although if one is charged, a polaron is formed, which is delocalised over about four rings (Fig. 1.3(c)). In contrast to polyacetylene, when both defects are charged they are predicted to pair up to form a 'bipolaron' [29] consisting of a doubly charged defect with no spin (Fig. 1.3(d)) and extending over a similar number of rings as for the polaron. At higher doping levels, bipolarons may also combine to form 'bipolaron bands' within the band gap [30].

The average chain lengths of polypyrrole are about 750 monomer units for electrodeposited polypyrrole films [31]. The electrical properties of polypyrrole films vary with nature of the solvent in which they are synthesized. The highest conductivity of ~100 S/cm in polypyrrole is found in electrochemically deposited films in organic solvent [32]. Polypyrrole films synthesized above 0.9 V show very poor conductivity and charge capacity due to overoxidation [33]. Electrochemically synthesized polypyrrole thin films are stable in air and retain their conductivity upto 250 $^{0}$C [34]. Substitution on the nitrogen of pyrrole decreases the conductivity to $10^{-3}$ S/cm and also becomes less air sensitive [35].

### *1.1.3 Polythiophene:*

Polythiophene, a five-membered heterocyclic ring conducting polymer contains one sulphur on the thiophene monomer in 1-position. The chemical polymerization of polythiophene using sulfuric acid catalyst has been known for more than 100 years [36]. Other catalysts such as hydrogen fluoride [37], iron chloride [38], aluminium chloride and trifluoroacetic acid [39] etc. could be used for polythiophene synthesis. Chemically synthesized polythiophene conducting polymer films often contain tetrahydrothiophene units in the polymer chain [40, 41]. Grignard reaction [42] was the first synthesis technique for preparing high purity polythiophene films. The oxidative electrochemical polymerization produces polythiophene conducting polymer films with greater purity and high quality as compared to the chemical synthesis [43]. Electrochemical oxidative polymerization of thiophene into polythiophene can be carried out by inserting a working electrode in a non-aqueous solution of thiophene and suitable salt and applying a potential of about 1.6V versus saturated calomel electrode (SCE) [43]. An alternative way of electrochemical polymerization of thiophene was reported by Zotti and Schiavon [44], which involve the reduction of nickel-thiophene complex to produce thin films on the cathode. When the potential of a solution with the nickel-thiophene complex in

acetonitrile was scanned between -0.5 V and -2.5 V versus SCE at a very slow scan rate, a thin film of polythiophene got deposited on the cathode [44].

The polymerization of thiophene follows the same path as that for pyrrole polymerization. Like pyrrole, thiophene monomer units also get coupled through their 2- and 5-positions [45] and hence thiophene monomers having substitutions either on 2- or 5-positions or on both 2- and 5-positions do not get polymerized. Polythiophene and almost all its derivatives polymerized electrochemically are insoluble in almost all solvents. However, poly-3-alkylthiophene chemically synthesized by Grignard reaction can be solubilized under certain conditions [46]. Average chain lengths of polythiophene are about 3000-8000 monomer units. Thiophene based conducting polymers, both in doped and undoped forms, are usually stable in air upto $350^0$C and even higher temperatures in inert atmosphere or in vacuum [47]. Electron spin resonance (ESR) study of polythiophene showed metallic nature of its conductivity [48].

**1.2 Characteristics of conducting polymers:**

Solid state materials can be classified into three broad categories according to their conductivity: insulators, semiconductors and conductors. The electronic states of atoms/molecules/monomers forming the solid materials overlap producing electronic bands. The energy states of valence electrons overlap to produce valence band and the electronic levels immediately above the valence band form the conduction band. An energy gap called band gap ($E_g$) exists between these two bands. If the band gap is large (> 5 eV), electrons are difficult to get excited from valence band to conduction band at room temperature and the material is an insulator. If the band gap is small (~1.0 eV), then electrons may be excited from the valence band to the conduction band by means of thermal, vibrational or photon excitations, the material is then a semiconductor. The conductivity of conducting polymers is achieved through simple chemical or electrochemical oxidation or in some cases reduction by a number of simple anionic or cationic species called dopants. Conjugated polymers have a framework of alternating single and double carbon-carbon

(sometimes carbon-nitrogen) bonds. Single bonds are referred to as σ-bonds and double bonds contain a σ-bond and a π-bond. All conjugated polymers have a σ-bond backbone of overlapping $sp^2$ hybrid orbitals. The remaining out-of-plane $p_z$ orbitals on the carbon (or nitrogen) atoms overlap with neighboring $p_z$ orbitals to give π-bonds. The characteristics of the π-bonds are the source of the (semi)conducting properties of these polymers. The π-bonds are delocalized over the entire molecule. Doped conducting polymers when in appropriate oxidized or reduced states are semiconductors as a result of their unique extended π-conjugation. The quantum mechanical overlap of $p_z$ orbitals actually produces two orbitals, a bonding (π) orbital and an antibonding (π*) orbital. The lower energy bonding π-orbital produces the valence band, and the higher energy antibonding π*-orbital forms the conduction band. These one-dimensional materials are generally conceived as having a two-band structure using the one-electron model approximation. The highest occupied molecular orbitals (HOMO) of the repeat units form the occupied π-band (valence band) of the polymer and the lowest unoccupied molecular orbitals (LUMO) of the repeat units form the π*-band (conduction band) of the polymer. As a consequence of the bond alternation the band gap of the neutral polymers lies in the range of 1.5 (near IR) to 4 eV (UV) resulting in semiconductor properties. At the high doping levels, overlap of the valence band and conduction band occurs and the metallic conductivities are achievable.

### *1.2.1 Structural distortion and charge carriers in conducting polymers:*

Condensed matter physics models for the semiconductors are the closest for arriving at a generalized understanding of conducting polymers. The conventional semiconductors can be described well by the band theory giving the semiconductors energy band structure of broad valence and conduction bands. Conducting polymers also develop broad valence and conduction bands stemming from extended overlap of the π-orbitals intrinsic to these systems. The π and π* orbital bands can be treated as valence and conduction bands respectively. As an important difference, the polymeric nature and two-fold co-

ordination of these organic systems allow much greater flexibility and susceptibility to structural distortion. The introduction of charges leads to a relaxation or structural distortion of the polymer structure about the charges, which functions to stabilize the charges. Conjugated polymers possess non-degenerate ground states, which affect the nature of charges that they can support [49]. In such polymers, where two nondegenerate regions are separated by a topological defect, the formation of single solitons is energetically unfavourable and paired sites are formed [29].

Local geometric distortion of the ground state in a conducting polymer possessing a standard semiconductor band structure requires distortion energy $E_{dis}$, giving rise to localized electronic states in the band-gap between the valence and conduction bands (Fig. 1.4a). The geometric distortion causes local upward shift of HOMO (highest occupied molecular orbit) i.e., the valence band and lowering of the LUMO (lowest unoccupied molecular orbit) i.e., the conduction band. If the conducting polymer is oxidized i.e. p-doped, the band structure looks like Fig. 1.4b.

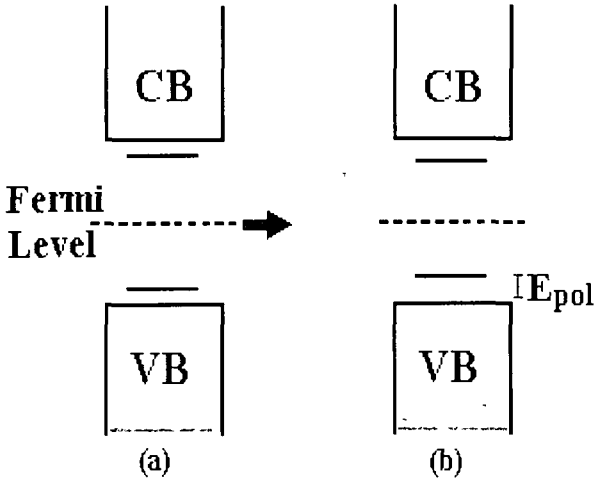


Figure 1.4: Formation of a polaron.

The energy required to remove an electron from the distorted structure of the conducting polymer is less than that required to remove an electron from the valence band, by an amount $E_{pol}$. If $E_{pol}$ is greater than $E_{dis}$, the formation of a charged entity is favored. The entity called a polaron is a radical cation (one

unpaired electron), which is locally associated with a structural distortion in the conducting polymer. Alternatively a polaron is a charge in an extended lattice, which is stabilized by a local distortion of the lattice. In actual case a polaron is formed by the removal of an electron from the conducting polymer structure causing a local distortion in the structure, which serves to stabilize the charge associated with the electron removal. This distortion of local structure by a charge in an extended lattice such as a conducting polymer chain arises from strong electron-phonon coupling. The polaron possesses a binding energy of $E_{pol} - E_{dis}$. It is important to note that in polaron formation the conduction band

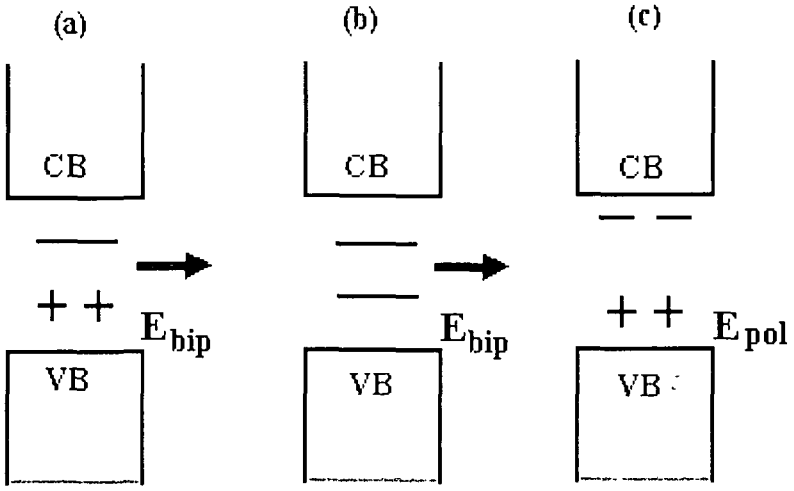


Figure 1.5: Formation of a bipolaron.

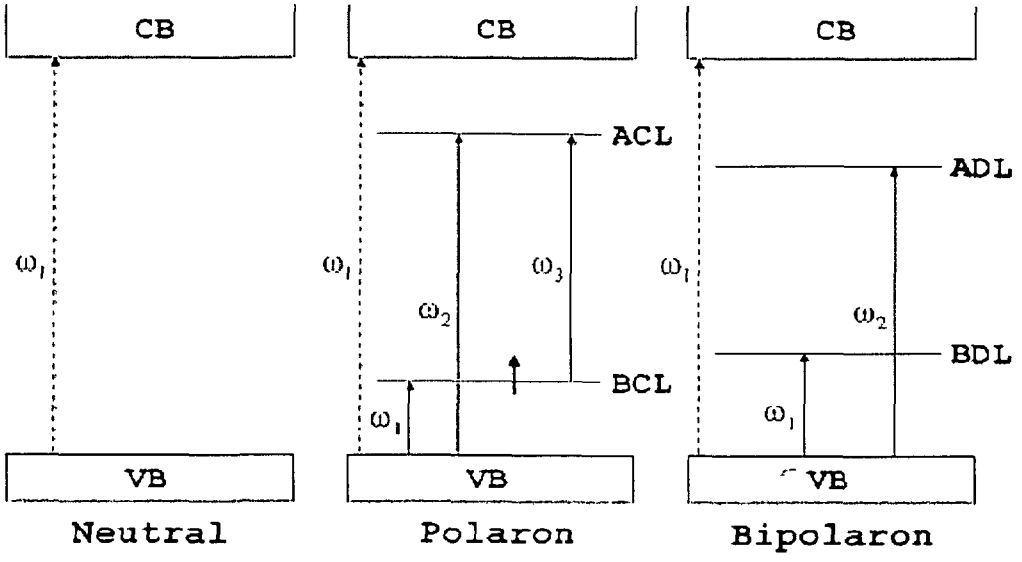


Figure 1.6: Electronic band model of a conducting polymer.

remains empty and the valence band remain full, and there is no resulting conductivity as in the case of electron removal from valence band in a conventional semiconductor. The newly generated half-occupied electron level remains localized in the band gap.

If the conducting polymer is again oxidized, it might be considered that it would happen through formation of another polaron in the conducting polymer chain at a different location. The second electron might also be taken away from the polaron itself, generating a bipolaron. It has been found that the distortion energy, $E_{dis}$, required to generate polaronic and bipolaronic distortions is almost the same [29]. Thus the bipolaron in such extended structure is more stable than two separate polarons. This stability, despite obvious Coulomb repulsion between two positive charges, can be considered to arise form the coupling of two charges to the lattice via lattice vibrations i.e., phonons like Cooper pair in condensed matter. At high doping levels, Coulomb repulsion between like charges of a bipolaron is also to a large extent screened by the dopants, further contributing to their stability. Another important feature regarding the bipolaron levels in particular is that they are either empty (p-type) or fully occupied (n-type) and hence spinless.

There exists another type of charge carrier in conducting polymers called soliton. The ground state structure of conjugated polymers are two fold degenerate, the charged cation/anion are not bound to each other by a higher energy bonding configuration and can freely separate along the chain. The effect of this is that the charged defects can form domain walls that separate two phases of opposite orientation and identical energy. These are called solitons and can be positive, negative or neutral. Solitons formation results in the creation of new localized electronic states that appear in the middle of the energy gap. The polarons, bipolarons and solitons are the charge carriers in the conducting polymers.

Although these charge carriers are responsible for electrical conductivity in conjugated polymers, many structural imperfections are also present in all polymers. Conductivity is not only a result of charge transfer along the chain,

but is also due to electron hopping between chains and between different conjugated segments of the same chain. In addition to these effects, which act at the molecular level, bulk conductivity values are also dominated by electron transfer between grain boundaries and variations in morphology [50, 51]. Thus, the bulk conductivity of a conjugated polymer may be described by

$$\sigma = \sum \frac{n_i Z_i e v_i}{E} \qquad (1.1)$$

where, σ= conductivity (S/cm),

$n_i$ = number of charge carriers of type i,

$Z_i$ = atomic number of i type charge carrier,

e = electronic charge ($1.6 \times 10^{-19}$ C),

$v_i$ = drift velocity of i type charge carrier (cm/s), and,

E = electric field (V/cm)



### *1.2.2 Comparison between conventional and polymer film electrodes:*

In case of conventional electrodes, the electrode reaction involves the mass transfer of the electroactive species from the bulk solution to the electrode surface and the electron transfer step occurs at the electrode surface. Other processes such as homogeneous chemical reactions and surface processes may accompany these processes. When an electric current flows in an electrochemical cell, the movement of ions carries the current in solution. These ions are not necessarily those that react at the metal surface. The mass transfer in solution occurs because of an electrochemical potential gradient ($\bar{\mu}$) i.e., by diffusion and/or migration, and by convection. It can be described with the help of the well known Nernst-Planck equation [52]

$$J_i = -D_i \nabla c_i - \frac{z_i F}{RT} D_i c_i \nabla \Phi + c_i v \qquad (1.2)$$

where $J_i$ is the flux, $D_i$ is the diffusion coefficient, $c_i$ is the concentration and $z_i$ is the atomic number of the 'i' th charge species, v is the velocity with which a volume element in solution moves in the solution and Φ is the electrostatic

potential. The three terms on the right hand side represents the contributions of diffusion, migration and convection to the flux respectively.

In the case of the polymer modified electrodes, because of the absence of the mediated reaction, the convection term in eqn (1.2) can be omitted since any stirring of the solution has no effect inside the electrode film as observed experimentally. However diffusion and migration of the electrochemically active species, especially in the case of redox polymers where redox sites are covalently bonded to the polymer chain, have to be reformulated as no free diffusion of the sites occurs. Moreover the polymer chains are trapped in a tangled network and the layer is more or less stably attached to the metal, mainly by adsorption (adhesion). The free energy of sticking is small for a monomer, hence stable films cannot be made from small molecules, but the energy per chain is large [53]. The fundamental observation that should also be brought into harmony with the theory is that even rather thick films, in which most of the sites are as far from the surface as 100-10,000 nm, which correspond to the surface concentration of $10^{-8}$-$10^{-6}$ mol/cm$^2$, may be oxidized or reduced in slow sweep rate cyclic voltammetric experiments. However, in many cases, all the redox sites do not undergo electrochemical transformations.

The transport of electrons in polymer film electrode can be assumed to occur via an electron exchange reaction or electron hopping between neighbouring redox sites if the segmental motions make it possible. Electron exchange reactions coupled to diffusion have been detected in the solutions of redox species [54 - 58]. The delocalized electrons can move through the conjugated systems (intrachain conduction), but an electron-hopping mechanism is likely to be operative between the chains (interchain conduction) and defects. This amounts to the fact that in contrast to the usual electrode reaction, we should assume long-range electron transport, which presumes an electronic conduction and/or a chemical reaction. In almost every case, the motion of electro-inactive ions carry the charge during electrolysis as it is necessarily coupled with the transfer of electrons in order to preserve

electroneutrality within the film. The motion of the counterion may also be the rate-determining step.

**1.3 Doping of conducting polymers:**

Undoped organic conducting polymers possess conductivity on the order of $10^{-10}$ to $10^{-2}$ S/cm i.e. they are either insulators or semiconductors. The semiconductor band structure of conducting polymers permits electronic excitation or electron removal/addition from the valence band to the conduction band, giving rise to the properties of interest in the conducting polymers. Excitation of electrons from the valence band to the conduction band yields typical excited state properties such as photoluminescence and nonlinear properties. On the other hand a chemical or electrochemical oxidation of the conducting polymer removes an electron from the valence band and creates a charge on the polymer chain. These charges are generally delocalized over several monomer units in the polymer. The charges also cause a relaxation of the geometry of the polymer to a more energetically favoured conformation. A charge also may be donated to the conduction band of the conducting polymer causing reduction of the conducting polymer. Oxidation i.e. removal of electron from the polymer backbone chain caused by a chemical species generates a positively charged conducting polymer and an associated anion. Similarly reduction i.e. addition of electron to the polymer chain generates a negatively charged conducting polymer and an associated cation.

$$P(Py) + MClO_4 \rightarrow P(Py)^+ClO_4^- + M^+ \text{ (oxidation)}$$

$$P(Ac) + NaA \rightarrow Na^+P(Ac)^- + A^- \text{ (reduction)}$$

The processes of oxidation and reduction impart conductive properties to the conducting polymers. The terminology of doping is used because of the analogy with the doping in inorganic semiconductors. However, the doping in conducting polymers is completely different from that in inorganic semiconductors. In inorganic semiconductors e.g. silicon, a few of the silicon atoms are substituted by electron rich (e.g. phosphorous) or electron deficient

(e.g. boron) atoms to create n and p-type semiconductors, respectively. On the other hand conducting polymer doping is essentially salt formation. The most important difference between inorganic and organic (semi)conductor is that the latter is highly anisotropic and possesses a quasi one-dimensional structure. The doping of organic conducting polymer increases its conductivity by several orders of magnitude e.g. conductivity of undoped polyaniline rises from $10^{-10}$ S/cm to $10^{2}$ S/cm after doping [59]. Thus conductivity of a conducting polymer can be controlled by controlling the degree of doping i.e. concentration of dopants in a conducting polymer. Depending on the mechanism, the doping of conducting polymers can be broadly divided into two types: (i) redox doping and (ii) non-redox doping [55 - 57].

### *1.3.1 Redox doping:*

Redox doping is a process of doping wherein the number of electrons in the conducting polymer backbone is changed by either oxidation or reduction and the charge neutrality of the conducting polymer backbone is maintained by the incorporation of cations or anions, respectively. The redox doping can be further subdivided into two classes, p-doping and n-doping depending on whether oxidation or reduction is taking place. Both oxidation and reduction of a conducting polymer can be attained by either chemical or electrochemical processes. The chemical doping involves exposing the polymer to an oxidant e.g. iodine vapors or a reductant e.g. alkali metal vapors. In the electrochemical doping a polymer coated working electrode is suspended in an electrolyte solution, in which the polymer is insoluble, along with separate counter and reference electrodes. A potential difference is applied between the electrodes that causes charge to cross into the polymer in the form of electron addition (n-doping) or removal (p-doping) and the appropriate counter ion from the electrolyte enters into the polymer film in order to maintain its electroneutrality.

*1.3.1.1 Redox p-doping:*

The p-doping of a conducting polymer involves oxidation of the polymer chain. The p-doping i.e. the oxidation can be accomplished either chemically or electrochemically. Chemical p-doping of a conducting polymer can be achieved by putting the polymer in a medium containing the oxidant such as iodine vapors that are incorporated into the polymer system. Oxidation of organic conducting polymer i.e. p-doping was first discovered while treating trans-polyacetylene (trans-$(CH)_x$) with oxidizing agent iodine [60, 61]. Iodine atoms being highly electronegative i.e., oxidizing in nature attracts $\pi$ electron of the polymer chain, thereby making the polymer chain electron deficient i.e., p-doped. The chemical p-doping process of trans-polyacetylene can be represented as:

$$trans\text{-}[CH]_x + 1.5xyI_2 \rightarrow [CH^{y+}(I_3)_y^-]_x, \qquad y \leq 0.07$$

The iodine doping of trans-polyacetylene by chemical doping increased the conductivity from ~$10^{-5}$ S/cm to ~$10^3$ S/cm [60,61].

The electrochemical p-doping of conducting polymers is carried out by anodic oxidation by immersing the polymer (generally in thin film form) coated working electrode into an electrolyte (e.g. $LiClO_4$ dissolved in acetonitrile) with desired dopant ions (anions e.g. $ClO_4^-$ for oxidation) in an electrochemical cell containing counter and reference electrodes. A potential difference is applied between the electrodes. An electron from the polymer is drawn out and the polymer gets oxidized. In order to maintain the charge neutrality of the polymer system, an anion enters into the polymer from the electrolyte. The electrochemical p-doping of *trans*-polyacetylene can be represented as [62]:

$$trans\text{-}[CH]_x + (xy)(ClO_4)^- \rightarrow [CH^{y+}(ClO_4)_y^-]_x + (xy)e^-, \qquad y \leq 0.1$$

The electrochemical p-doping of the polymer can also be accomplished during electro-polymerization of the conducting polymer by introducing the dopant anion into the electrolyte solution along with monomer. In this case doping occurs simultaneously with the process of electropolymerization.

### *1.3.1.2 Redox n-doping:*

Reduction of a polymer chain by adding an electron is termed as n-doping of the polymer. The n-doping could also be accomplished by both chemical and electrochemical methods. For chemical n-doping, the conducting polymer is immersed in a medium containing the desired reducing agent e.g. alkali ($Na^+$, $Li^+$) vapors. Since alkali atoms are highly electropositive i.e., reducing in nature, their outermost electrons are attracted by the electronic system of the polymer chain, thus destabilizing the polymer chain $\pi$ electron system and making the polymer chain negatively charged.

Table 1.1 : Common dopants and their degree of doping used for doping of conducting polymers.

| Dopant name | Symbol | Degree of doping |
|---|---|---|
| Chloride | $Cl^-$ | 3% - 42% |
| Sulphate | $SO_4^{2-}$ | 5% - 22% |
| Perchlorate | $ClO_4^-$ | 4% - 30% |
| Tetrafluoro borate | $BF_4^-$ | 5% - 33% |
| Hexafluoro arsenate | $AsF_6^-$ | 5% - 33% |
| Hexafluoro phosphate | $PF_6^-$ | 5% - 33% |
| Hydrogen sulphate | $HSO_4^-$ | 2% - 30% |
| Fluorosulfonate | $SO_3F^-$ | 5% - 15% |
| Trifluoro methane sulfonate | $CF_3SO_3^-$ | 4% - 31% |
| Benzene sulfonate | $C_6H_5SO_3^-$ | 2% - 33% |
| Bromobenzene sulfonate | Br $C_6H_4SO_3^-$ | 2 % - 33% |
| Trifluoro acetate | $CF_3COO^-$ | 4% - 25% |
| Chloroferrate | $FeCl_4^-$ | 3% - 42% |
| Poly(styrene sulfonate) | $PSS^{n-}$ | 3% - 15% |
| Iodine | $I_3^-$ | 2% - 25% |
| Sodium | $Na^+$ | 2% - 28% |
| Lithium | $Li^+$ | 6% - 44% |

The chemical reduction (n-doping) process of *trans*-polyacetylene can be represented as [60, 61]:

$$trans\text{-}[CH]_x + (xy)Na^+(Npth)^- \rightarrow [Na_y^+(CH)^{-y}]_x + Npth, \qquad y \leq 0.1$$

This process partially populates the antibonding π*-system of trans-polyacetylene giving rise of conductivity of the order of ~$10^3$ S/cm.

Electrochemical n-doping of conducting polymer can be accomplished by cathodic reduction [63] of polymer films in an electrochemical cell by immersing the polymer film into an electrolyte containing the desired dopant cations. By applying a potential difference between the electrodes, electrons are supplied to the polymer system from the source causing cations to move into the polymer system to maintain the charge neutrality. The electrochemical n-doping of *trans*-polyacetylene with $Li^+$ can be represented as:

$$trans\text{-}[CH]_x + (xy)Li^+ (xy)e^- \rightarrow [Li_y^+(CH)^{-y}]_x, \qquad y \leq 0.1$$

The most common dopants used for doping in both electrochemical and chemical methods are listed in Table1.1. The dopant ion could be from different compositions depending on the method of doping e.g. perchlorate ion ($ClO_4^-$) or tetrafluoroborate ($BF_4^-$) ion can be introduced as lithium perchlorate ($LiClO_4$) or tetraethyl ammonium tetrafluoro borate ($Et_4NBF_4$) salts respectively for electrochemical polymerization and doping, whereas for chemical polymerization and doping $CuBF_4$ may be used; $AsF_6^-$ could be taken as $AsF_5$ for vapor doping of polyacetylene while for electrochemical doping $LiAsF_6$ could be used as electrolyte salt. The degree of doping is defined as the number of monomer units per dopant ion e.g. if there is one $Cl^-$ ion for four aniline monomer then the degree of doping will be ¼ = 0.25, i.e., 25%. The range of degree of doping normally achieved in conducting polymers is also given in Table 1.1.

### *1.3.1.3 Redox doping involving no dopant ions:*

Redox doping of conducting polymers can also be achieved without introducing an anion or cation. The types of redox doping involving no dopant ions such as 'photo doping' and 'charge injection doping' are discussed below.

### *1.3.1.3.1 Photo-doping:*

When a conjugated polymer e.g. *trans*-polyacetylene, is irradiated with photons of energy higher than the band gap of the conducting polymer, electrons are promoted to the higher energy state across the band gap. The polymer is doped and the doping process is called photo doping. Spectroscopic signatures of solitons can be observed under appropriate experimental conditions of photo-doping [64].

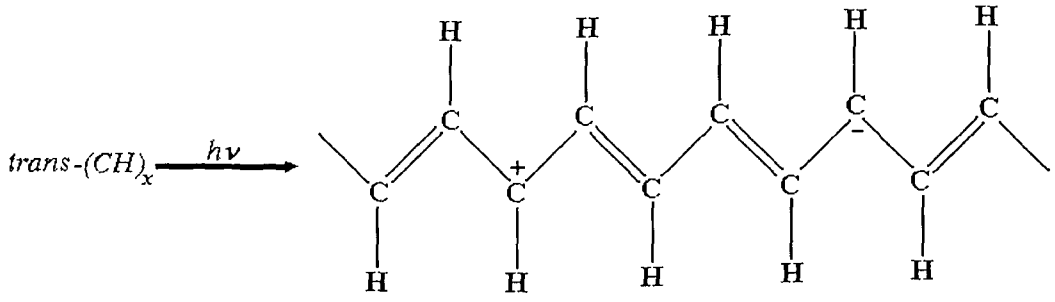


Figure 1.7: The positive and negative solitons in polyacetylene.

The positive and negative solitons, as shown in Fig. 1.7, are delocalized over about 15 CH units. Photo doping does not sustain after the irradiation is removed due to rapid recombination of electrons and holes when the irradiation is stopped. If a potential difference is applied during irradiation a photo-current can be obtained from the photo doped conducting polymer polyacetylene.

### *1.3.1.3.2 Charge-injection doping:*

Another type of redox doping called charge injection doping can also be used to dope an undoped conducting polymer. Here the conducting polymer is taken in thin film form over a metallic sheet separated by a high dielectric strength insulator. Charge injection is carried out using this metal/insulator/semiconductor structure. Application of an appropriate potential difference across the structure will give rise to surface charge layer. The charges are injected into the conducting polymer without involving any dopant ion. The accumulation of charge layer for conducting polymer has been extensively studied and the spectroscopic signature of solitons and mid gap

absorption have been observed in injected charge layer in polyacetylene in the absence of dopant ion [65 - 67].

*1.3.2 Non-redox doping:*

Unlike in redox doping, in non-redox doping the number of electrons associated with the polymer chain does not change in the doping process. In the non-redox doping process, the energy levels get rearranged. The emeraldine base form of polyaniline when treated with protic acid gets converted to protonated emeraldine base (polysemiquinone radical cation). This non-redox doping increases the conductivity of polyaniline by ~10 order of magnitude (upto ~3 S/cm) [68 -70].

*1.3.3 Doping by ion implantation:*

Ion implantation is a useful technique to dope a conducting polymer film by bombarding it with low energy (< 100 KeV) ions. A study of 100 keV $Ar^+$ ion and 24 keV $I^+$ ion bombardment on polyaniline at fluence $10^{16}$ ions/$cm^2$ has been reported [71]. The $Ar^+$ ion implantation showed little effect on conductivity whereas $I^+$ ion implantation produced environmentally stable films with conductivity increase from the undoped insulator state to doped conducting form with an increase in conductivity by 12 orders of magnitude.

*1.3.4 Doping by heat treatment:*

Heat treatment is an interesting method of doping that has been applied mainly to ladder type conducting polymers [72]. When a ladder type conducting polymer is subjected to heat treatment [72] of 50$^0$C increments for 2 minutes in a calorimeter chamber, a conductivity of $10^{-8}$ S/cm was obtained at 100$^0$C, the same polymer when treated at 350$^0$C, conductivity increased to$10^{-4}$ S/cm and when treated at 600$^0$C, the conductivity again decreased to $10^{-8}$ S/cm. The increase in conductivity on heat treatment has been ascribed to improved structural order and thermally excited charge carriers, but may also be due to

impurity doping, i.e. creation of oxidation centers which at high temperature behave as dopants.

### 1.4 Swift Heavy Ion irradiation of conducting polymers:

Swift heavy ion (SHI) irradiation of polymers has been found to produce useful modifications in their physical and chemical properties. Increase in hardness, strength and wear resistance [73 - 75], electrical conductivity [76 - 78], density [77], chain length [74-76], crystallinity[75-77], solubility [73-77]] and improvements in the optical transmission [75-78] properties of the polymers have been reported. These changes depend upon the sample parameters like composition, molecular weight, temperature and ion beam parameters such as energy, mass and fluence. The primary phenomena associated with ion beam and polymer interactions are cross-linking, chain scissions and emission of atoms, molecules and molecular fragments.

Most investigations of ion beam induced modifications of polymers have focused on low energy (< 100 KeV) ion irradiation resulting in ion implantation into the polymer. The degree of dopant ion concentration in the polymer films can be increased and different types of dopants can be implanted by low energy ion irradiation. The early works of Charlesby [79] and Chapiro [80] on ionizing radiation induced effects in polymers opened a new dimension of research, but interest in the modification of organic materials by ion beams increased rapidly through the impetus given by Venkatesan [81] of Bell Labs. Since then ion beam irradiation of polymers has been used to enhance the electric conductivity of polymers and to generate active sites for surface physical and chemical modifications. The enhancement of conductivity in organic polymers resulting from ion beam irradiation has been widely reported [82 - 87]. The change in electrical and optical properties induced by ion beams is generally attributed to the formation of peculiar carbonaceous clusters, along the latent track of energetic ions [88].

In early stages less attention was paid to the doping effects associated with ion implantation than to modifications of the bombarded materials.

However, Weber and coworkers [89] demonstrated the formation of conducting polyacetylene by ion implantation with doping ions, which also exhibited unusual air resistance to oxidation. Davenas and his group [90] showed an increase in conductivity by more than four orders of magnitude by ion implantation of polyacetylene with $I^+$ ions with a fluence of $5X10^{16}$ ions/$cm^2$. They also studied the effects of implantation of inert $Ar^+$ ions and electroactive $Cl^+$ ions on the electrical properties of polyacetylene and found that the electroactive $Cl^+$ ion implantation increases the conductivity almost by two orders of magnitude whereas the inert $Ar^+$ ions implantation induces a slight decrease in conductivity [91]. Lin and his group [92] studied the ion implantation effects on chemically doped polyacetylene by exposing the polymer to low energy ion beam irradiation ( 30 KeV, 2μA/$cm^2$, $K^+$ ion) and found that the chemically doped species became concentrated in the implanted region during implantation. They also obtained p-type and n-type doped conducting polyacetylene by ion implantation and observed diode like I -V behaviour, but the diode nature degraded with time [92-94].

Research efforts have been also made to study ion implantation induced p-n junction formation in polyacetylene film surface [95 - 97]. Another study on poly (2,6- dimethyl phenyl oxide) with $N^+$ ion implantation at 100KeV showed that the $N^+$ ion beam induces stable electrical conductivity and reduces the optical band gap with increasing fluence [98].

The irradiation of polyaniline shows that conductivity after irradiation is dependent on the incident ion dose, ion species and dose rate (ion-beam current) [77]. The conductivity increases with increasing deposited electronic energy density, which is proportional to the ion dose for a particular ion species. The conductivity at first increased progressively with increasing dose rate in the beam current range of 1-3 μA/$cm^2$, showed a maximum conductivity of $10^3$ S/cm corresponding to 4 μA/$cm^2$ followed by decrease in conductivity with further increase in dose rate. $N^+$ ion irradiation with 2MeV energy at 500nA/$cm^2$ in the $10^{13}$ to $10^{16}$ ions/$cm^2$ fluence range [99] showed an increase in conductivity. Inert $Ar^+$ ion implantation at 120KeV ($10^{16}$ ions/$cm^2$) also showed

increase in conductivity. Polystyrene-acrylonitrile (PSA) implanted with 20-175 KeV $N^+$ ions to a dose of $5x10^{13}$ - $5x10^{16}$ ions/$cm^2$ shows conductivity increase by more than 17 orders of magnitude with increasing ion dose and beam energy [78]. Hall coefficient study showed little Hall voltage indicating presence of large number of carriers ($10^{22}cm^{-2}$) in the implanted PSA film. The observed difference in the electrical conductivity of polymers before and after ion irradiation reveals a complex disordering of the polymer chain structure by the incident ions [100].

### 1.5 Electrochemical supercapacitors:

The concept of storing large quantities of electrical energy, comparable in magnitude with storage energy-densities attainable in batteries, in reasonably small capacitors was proposed about five decades ago [101, 102]. However, only over the past 15 years have the charge storage device [103] variously called 'supercapacitor' or 'ultra capacitor' became subject of practical and commercial development for possibility of utilizing them in a hybrid mode along with batteries for electric vehicle power system and for starting, lighting and

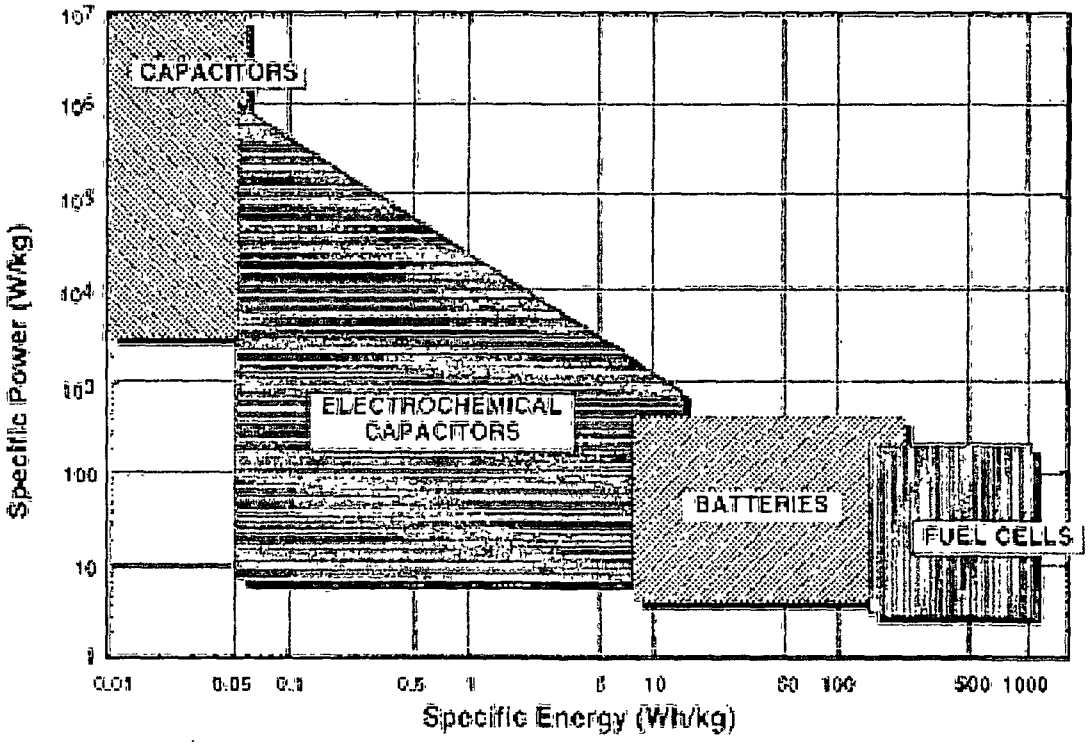


Figure 1.8: Ragone plot of various energy storage devices.

ignition, in regular internal combustion engine powered vehicles as well as for smaller scale consumer electronics applications [103]. Electrochemical supercapacitors bridge the gap between conventional capacitors and batteries. The two main characteristics, the large value of capacitance and high power storage and delivery, are unique in electrochemical supercapacitors. The current position of the electrochemical double layer capacitors (EDLC) can be visualized by means of a Ragone plot (Fig. 1.8) [104], which graphically represents a device's energy and power capabilities.

There is no difference in the design of supercapacitors and batteries, in either case an electrolyte is sandwiched between two active electrodes. However, but in supercapacitors both electrodes may be of same materials unlike in batteries, where the electrode materials are always different. An important and fundamental difference between charge storage in a capacitor and that in a battery is that in a capacitor actual positive (electron deficiency on one plate) and negative (electron excess on the complementary plate) electrostatic charges physically reside at a two-dimensional plate with certain surface charge density, and charges can be withdrawn from the surface, but in a battery charges are stored as chemical energy and when connected to an external circuit charges can be withdrawn from the electrodes, which accompanies electrochemical Faradic processes by charge transfer across an interface, involving changes of oxidation state of the chemical materials of the cell. The energy stored in a battery can be expressed as $E = Q.\ \Delta V$, where Q is the Faradic charge that could be obtained at Nernstian cell potential $\Delta V$. The energy stored in a supercapacitor can be expressed as $E = \frac{1}{2}\ Q.\ \Delta V$ where Q is the charge stored at the electrode at potential $\Delta V$, which also can be expressed as $E = \frac{1}{2}\ C\ (\Delta V)^2$ where C is the capacitance of the supercapacitor. The two types of processes are distinguished by the terms 'non- Faradic' or 'Faradic' respectively. Two principal types of supercapacitors have been developed, tested and investigated: (i) the electrical double-layer capacitors, and (ii) the redox or ad-species pseudo-capacitors [101].

### *1.5.1 Electrical double layer capacitors:*

At the electrode/electrolyte interfaces, a separation of ionic and electronic charges occurs giving rise to an electrical double layer [105, 106]. Accumulation of charges ($\Delta q$) of opposite signs takes place across the interfaces, which is dependent of potential ($\Delta V$) of the electrode, a capacitance $C = \Delta q / \Delta V$ or $d(\Delta q)/d(\Delta V)$ arises and is referred as the double layer capacitance [105, 106]. The capacitance arises at the electrode interfaces and it has a typical value between about 15 to 50 $\mu Fcm^{-2}$ in aqueous electrolyte [105, 106] and less in non-aqueous systems. The charge storage in double layer capacitor is essentially electrostatic in nature i.e., separation of ion and electron charges, and hence charging/discharging is highly reversible and hundreds of thousands of cycle are typically attainable. The double layer capacitance values per $cm^2$ are large compared with those attainable in conventional capacitors as the charge separation is over only about 3Å in the compact double layer capacitors [105, 106] or up to 1000 Å over the diffuse part of the double layer [106].

The high value of capacitance of double layer at the electrode/electrolyte interfaces using high surface area carbon electrodes has been utilized for electrical energy storage [101, 102, 107]. The technology has led to the development of large double layer capacitors capable of starting internal combustion engine and in hybrid mode in parallel with lead/acid or Zn-$Br_2$ batteries for electrical vehicle propulsion, where the supercapacitor function as load leveling device [108]. In recent years, it has been recognized that with carbon double layer capacitors a small but significant pseudocapacitance can also arise due to electrochemical reactions on the carbon e.g. reversible surface quinonoide-type redox reactions or chemisorptions processes involving partial faradic charge transfer [109 - 113].

### *1.5.2 Redox or ad-species pseudo-capacitors:*

A different kind of capacitance arises at certain electrodes e.g. ruthenium dioxide ($Ru_2O$), where the extent of faradically admitted charge depends linearly on the applied voltage. For such a situation, the electrode behavior is

equivalent to and measurable as a capacitance. This capacitance can be large but it is faradic in origin and arises from reversible faradic reactions occurring at the electrode. Therefore it is called "pseudocapacitance" in order to differentiate it from electrostatic capacitance. This kind of pseudocapacitance can originate when an electrochemical charge-transfer process takes place to an extent limited by a finite quantity of reagent or of available surface. Several examples of pseudocapacitance can arise, but the capacitance function is usually not constant and, in fact, is usually appreciably dependent on potential or state of charge. There are two types of reactions that can involve a voltage dependent charge transfer. The deposition of ions to form a monolayer on the electrode surface is a reversible process that results in a faradic charge transfer, and hence gives rise to a pseudocapacitance in a manner similar to that demonstrated in redox reactions. However, when the process is surface limited, and proceeds in several one-electron stages, a broad range of significant capacitance values arises. A very different basis for development of supercapacitors arises from utilization of pseudocapacitance. Such systems bridge the gap between the electrical double layer capacitors (EDLC) electrostatic charge and energy storage, and electrochemical battery charge and energy storage. Two types of pseudocapacitances can arise in electrochemical processes: (a) adsorption pseudocapacitance, and (b) redox pseudocapacitance.

Supercapacitors are well suited to replace batteries in many applications. Even though supercapacitors have a lower energy density as compared to that in batteries, they avoid many of the battery's disadvantages. Batteries have a limited number of charge/discharge cycles with a degrading performance and take time to charge and discharge because the process involves chemical reactions with non-instantaneous rates. These chemical reactions have parasitic thermal release, which causes the battery to heat up. Moreover acidic batteries are hazardous to the environment. On the other hand supercapacitors can be charged and discharged almost an unlimited number of times. The typical cycle life of a supercapacitor is more than $10^6$ charge-discharge cycles. They can charge/discharge on the time scale of milliseconds and are capable of

producing enormous currents, hence are very useful in load leveling applications in fields where a sudden boost of power is needed in fraction of a second. Supercapacitors do not release any thermal heat during discharge. The long life time of supercapacitors reduces maintenance costs. They do not release any substances hazardous to the environment and their performance does not degrade with time. Supercapacitors are extremely safe for charge storage as they have low internal resistances, even if many of them are coupled together. Even though they have a lower energy density and are bulkier and heavier than an equivalent battery, they have high power density and have replaced batteries in many applications due to their readiness in releasing power. They find most applications in the field of hybrid vehicles and handheld electronic devices. In rural areas, where there are voltage sags in the power grid, supercapacitors can be used to reduce the effect of fluctuations.

As conducting polymers can be obtained in both p and n-doped states, redox supercapacitors are classified into three types [114, 115], viz., type I, type II and type III. In type I configuration both the electrodes are p-doped same materials, in type II configuration both electrodes are p-doped but different materials and in type III configuration both electrodes are same materials but one electrode is p-doped and the other n-doped [115]. In type I configuration of a supercapacitor, in fully charged state one electrode is in fully oxidized state and the other in fully reduced state and a potential difference of 0.8 - 1.0 Volt [115] is attainable in this configuration. In type II configuration, since the two p-doped electrodes have different oxidation and reduction potential ranges, a wider potential range of application is obtainable in this configuration as compared to that in type I configuration. In type III supercapacitor in fully charged condition p-doped electrode is in fully oxidized state and the n-doped electrode in fully reduced state, as a result the potential range is wider compared to the type I and type II supercapacitors. A maximum potential of 3.1 Volt is reported in type III configuration [114, 115].

**1.6 Scope of the thesis and statement of the thesis problem:**

The present work aims to gain a deeper insight into the monomer level processes and mechanism of electropolymerization of polyaniline, polypyrrole and polythiophene/its derivative so as to effectively control the morphology, porosity and standardize various parameters such as potential window, monomer and dopant concentrations and type of solvent for obtaining dense, smooth, uniform and homogeneous conducting polymer films. The other prime objective is to study the effects of swift heavy ion irradiation on conducting polymer electrodes and to understand the interaction of the fast ions with the polymer films. Most research work on ion irradiation on conducting polymers has concentrated in the low energy region (< 100 KeV) resulting in ion implantation of the irradiating species in the target material. However, the effects of swift heavy ion (SHI) irradiation on conducting polymers with higher energies (>100 MeV) have not been investigated in detail. The emphasis in the present work is on the investigation of SHI irradiation effects on conducting polymers polyaniline, polypyrrole and poly(3-methylthiophene) from the viewpoint of their applications as electrode materials in all-polymer redox supercapacitors.

In order to achieve the abovementioned objectives, the following systems have been chosen for investigation in the present work:

- Polyaniline p-doped with hydrochloric acid (HCl), sulfuric acid ($H_2SO_4$), phosphoric acid ($H_3PO_4$), perchloric acid ($HClO_4$) and lithium perchlorate $LiClO_4$.
- Polypyrrole p-doped with lithium perchlorate ($LiClO_4$), sodium perchlorate ($NaClO_4$), lithium trifluoromethane sulfonate ($LiCF_3SO_3$), tetrabutyl-ammonium tetrafluoroborate ($[CH_3(CH_2)_3]_4NBF_4$) and tetrabutylammonium hexafluorophosphate ($[CH_3(CH_2)_3]_4NPF_6$) dopants.
- Poly(3-methylthiophene) p-doped with lithium perchlorate ($LiClO_4$), lithium trifluoromethanesulfonate ($LiCF_3SO_3$), tetrabutylammonium tetrafluoroborate ($[CH_3(CH_2)_3]_4NBF_4$) and tetrabutylammonium hexafluorophosphate ($[CH_3(CH_2)_3]_4NPF_6$).

- Poly(3-methylthiophene) n-doped with lithium perchlorate ($LiClO_4$).

The conducting polymer films of the above systems have been synthesized by electropolymerization technique in a three-electrode electrochemical cell potentiodynamically/potentiostatically. Cyclic voltammetry, XRD, FTIR, SEM, UV-Vis and conductivity measurements by four probe technique have been carried out on the conducting polymer films.

Swift heavy ion (SHI) irradiation is a relatively recent technique for modification of properties of materials by deposition of huge amount of energy by electronic and nuclear stopping processes. Conducting polymers have been used as electrode materials in supercapacitors. However, they show poor performance characteristics and low cycle life. Swift heavy ion irradiation has been employed to improve the performance characteristics of polyaniline, polypyrrole and polythiophene conducting polymer films. All characterizations carried out on unirradiated conducting polymer films have been conducted on the SHI irradiated films in order to study the SHI irradiation effects on them.

Redox supercapacitors with all its components i.e., both the electrodes and electrolyte made up of polymeric materials have been fabricated. P(VDF-HFP) (20 w/o) - PMMA (10 w/o) - $LiCF_3SO_3$ (10 w/o) -PC + DEC (57 w/o) + $SiO_2$ (3 w/o) polymer gel electrolyte and conducting polymer films as electrodes have been used to fabricate the supercapacitors. Redox supercapacitors with type I (p-doped same conducting polymeric material electrodes on either side), type II (p-doped different conducting polymeric material electrodes on either side) and type III (same p and n-doped conducting polymeric material of either side as electrode) configurations have been fabricated and their performance characterized by cycle life stability tests and charge-discharge characteristics. Both unirradiated and SHI irradiated conducting polymer films have been used to fabricate the all-polymer redox supercapacitors to study the SHI irradiation effects on the performance parameters of the supercapacitors.

# CHAPTER II

# THEORETICAL ASPECTS

In conducting polymers, conduction within a chain appears to occur through the delocalization of π-electrons across the chain, but an electron hopping mechanism is most likely to be operative between the chains. This conduction is different from that in metallic conductor and semiconductors and to explain the mechanism of charge transport in conducting polymer different models and theories have been put forward. A brief discussion of these models and theories are discussed in this chapter. The electropolymerization mechanism and factors influencing the electropolymerization are also presented.

## 2.1 Models of charge transport in electronically conducting polymer films:

The electronically conducting polymers consist of polyconjugated, polyaromatic or polyheterocyclic macromolecules and have the unusual property of possessing high electrical conductivity in the doped state. Two separate theoretical interpretations have been developed to describe the mechanism of charge transport in these systems because of the different approach of physicists and chemists. While physicists are interested in the properties of doped/undoped conducting polymers (mainly the conductivity) in dry state, electrochemists want to understand their behaviour in contact with electrolyte solutions. Polymer film electrodes based on conducting polymers are especially interesting, as electron transport through the surface layer by a delocalized band structure may be expected, which is distinct from the electron-hopping mechanism in redox polymer films. However, interactions between the polymer chains and the solution species (counter ions, solvent molecules) may influence the electron transport properties of the polymer. In addition, it is electron hopping that ensures the interchain electron transport. Electron hopping may also contribute to the intrachain conduction between different

conjugated segments on the same chain, because it is unlikely that a chain is fully conjugated and contains no imperfections. In the overall charge transport process during charging/discharging of the film, counterions also participate, thus the sorption/desorption of those counterions may also be rate-determining, as in the case of redox polymers. The doping process in conjugated polymers is essentially a charge transfer reaction, resulting in the partial oxidation or less frequently reduction of the polymer. Conducting polymer films have several peculiarities when compared to the redox polymers. In a half oxidized state, the film conductivity is much higher than that in a reduced state or that observed in redox polymer films [116, 117]. After the completion of the redox process, there is an unusually high capacitive current [118-127] and there is no saturation of the counterions in the film [128-133]. Protonation of the conducting polymer film in some cases causes an increase in the film conductivity. Both the charge transport and charge transfer processes are very fast [134-138] and the activation energies are small as compared to the redox polymer films [139].

Various models have been proposed to explain the mechanism of charge transport in conducting polymer film electrodes. Two extreme approaches exist. Some researchers [140-148] argue that a delocalized band model is operative i.e. the charges are delocalized over a large number of monomer units. Others prefer a chemical model, in which the charge is localized in the polymer chain, or at most only some monomer units are involved [149]. The precise nature of charge carriers in conjugated systems varies from material to material, and the mechanism of charge transport is not yet fully understood. Even for one material several structures may be considered and the nature of the charge carriers and mechanism may differ. In general charge carriers in conducting polymers may be solitons (neutral defect state), polarons (a neutral and a charged soliton in the same chain, which are essentially radical cations for chemists), and bipolarons (two charged defects form a pair, a doubly oxidized dication form).

For instance, in trans-polyacetylene solitons and polarons are mobile along the polymer chain giving rise to inherent conductivity of the material. The theoretical calculations show that two polarons repel each other, which lead to two isolated charged defects. In contrast to the polyacetylene, two charged defects tend to form a bipolaron in poly p-phenylene, which may contain a nondegenerate benzenoid and a higher energy quinoid configuration. Both polaron and bipolaron defects are delocalized over five rings. At high doping level bipolarons form bipolaron bands within the gap of the valence and conduction bands [150-152].

The situation is further complicated in the case of polyaniline. While the terms polaron and bipolaron are used to describe states resulting from $1e^-$ and $2e^-$ oxidation processes respectively, this nomenclature is questionable because none of these species need to be charged due to protonation of the polymer [143, 153-155]. For instance, on the basis of simultaneous cyclic voltammetric/esr results, Geniés and Lapkowski [153, 154] have assumed that the electron transfer processes result in the formation of both polarons and bipolarons, but their characteristics differ because of the structural change of the polymer in the course of oxidation. They also have emphasized that in high molecular mass polyaniline, the cation radicals are not stabilized via resonance, but stabilization occurs via deprotonation. Glarum and Marshall [140, 143] used a one-dimensional band model to explain the results of the electrochemical ESR experiments, but they also recognized the effect of the structure inhomogeneity of the polymer, as well as the role of protonation equilibria. There is disagreement regarding the explanation of esr data for oxidized polyaniline in terms of localized Curie spin, as against Pauli susceptibility of metallic islands [146-148, 151-157].

Some ESR results supported the suggestion that the fundamental charged species responsible for the charge transport in polypyrrole is the bipolaron [30]. Other results showed a good correlation between the conductivity and spin polaron concentration, and the decrease of conductivity at higher doping level was attributed to the formation of bipolaron [141, 158,

159], which seems to be more reasonable. The electrochemical ESR data for both polyaniline and polypyrrole are also interpreted in terms of a localized redox site model assuming a phase transition as the number of oxidized sites increases [149, 160-162].

The measured diffusion coefficients are attributed to spin diffusion [28], to interchain electron hopping [161], to intrachain and interchain electron transport coupled to counterion motion [149,163] or to ion diffusion [120]. In the later case, not only rate-determining counterion diffusion was assumed, but also co-ion motion [142], which explains the very rapid switching rate observed for polyaniline, proton migration [164]. In general, the experimental findings attest that the rate of charge transport very much depends on the morphology of the polymer, including its change with the potential. As for the redox systems, the morphology of conducting polymer films is influenced by the nature of the supporting electrolyte and the conditions of film preparation. Some reports suggest that the effect of the uncompensated ohmic potential drop is more substantial in the electrochemical switching of conducting polymers, as compared to the redox systems, due to the large-scale change in the film conductivity during charging [164]. When the ohmic drop was successfully eliminated or at least substantially reduced, a very high switching rate was detected [164].

The RC behaviour is certainly relevant in large amplitude potential step experiments. The values of diffusion co-efficient derived from the impedance data are model dependent. Also because of the absence of the diffusion controlled region in the impedance spectra of the conducting polymers, in many cases diffusion constant (D) values were derived from the low frequency data, which may prove to be seriously in error. This serves as an explanation for why D values, ranging from $10^{-3}$ to $10^{-11}cm^2/s$, were extracted from the experimental results. The role of iR drop was also emphasized in some works. Gottesfeld *et al.* [165] were able to explain the origin of the quasi-reversible behaviour and the appearance of prepeaks or shoulders in the cyclic voltammograms with a simple model. According to this model the film

resistivity is inversely related to the amount of oxidizing. The occurrence of sharp current peaks, however, can also be explained within the framework of the percolation theory. Aoki [166] investigated the connection between the electrode potential and the distribution of conductive species in the film by using percolation theory. When the ratio of the number of conductive elements to that of all the lattice elements in the cubic lattice model reaches the threshold value of the percolation (p=0.31), the percolation theory predicts that the maximum radius of a cluster is associated with a second order phase transition. Conductive sites for $p<0.31$ are localized to the electrode, whereas those for $p>0.33$ are uniform over the film. This model explains the appearance of a sharp current peak near the formal potential of the system in the voltammogram.

The combined application of electrochemical and non electrochemical techniques may offer an opportunity to gain a better insight into the mechanism. At present, it seems to be a reasonable assumption that the double-layer capacitance is associated with the metallic behaviour i.e., arising from an excess of surface density of mobile electronic charge carriers and as ionic double layer, which was proved by radiotracer measurements [167, 129]. Feldberg [122] suggested a model according to which the double-layer capacitance linearly increases with the fraction of the polymer converted to its oxidized (conducting) form.

## 2.2 Theories of electron transport in polymer film electrode:

### *2.2.1 Early models of charge propagation:*

The first models and their mathematical formulations appeared in a closely spaced series of publications by Andrieux and Savéant [168], Laviron [169] and Peerce and Bard [170]. They used the idea of Kaufman and Engler [171] that the electron transfer between neighbouring redox sites may take place via an electron-hopping mechanism. They relied on the early results obtained by potential sweep and potential step methods, which showed that the charge transport processes can be described within the framework of diffusion kinetics.

The three models share several common features and serve as the starting point for the subsequent models. First, the polymer films were treated as a macroscopic assembly of planar layers containing equal concentrations of evenly distributed redox centers, although in the model of Peerce and Bard [170] the consequences of uneven distribution of nonequivalent, interacting sites were also emphasized. Second, it was presumed that direct electron transfer between the metal and the film involves the redox sites situated in the layer immediately adjacent to the metal surface only. The third common feature of the early models is that the polymer films are electronically nonconductive.

Andrieux and Savéant [168] assumed that the propagation of electrons through the film occurs as a consequence of successive steps between redox centers located in sublayers, and rationalized the sweep rate dependence of the cyclic voltammograms in terms of a linear process occurring within a finite space. It was pointed out that as far as the charge transport under a concentration gradient is concerned, Fick's law can describe the electron hopping between adjacent redox sites of different oxidation states, i.e. , as a diffusion process of two immobile redox sites with the same diffusion coefficient,

$$D_e = k_e \delta^2 c$$

where $k_e$ is the bimolecular electron transfer rate constant, c is the total redox site concentration and $\delta$ is the mean distance between two adjacent redox sites, which is equal to the thickness of layer ($\Delta x$) in the film. Relying on this theory, Andrieux and Savéant calculated the values of $D_e$ and $k_e$ for poly(p-nitrostyrene) films. It was found that $D_e = 2X10^{-12}$ $cm^2/s$ and $k_e = 10^4$ $dm^3/mol/s$ taking $\Delta x = 0.8$ nm and using the heterogenous rate constant, $k_s = 5x10^{-5}$ cm/s. When these values were compared with the respective values obtained in solution, it was revealed that both the charge transport and charge transfer process are much slower in polymer films, which was assigned to different collision and environmental situations, as well as to the ohmic drop effects.

The model developed by Laviron [169] is basically similar to the model given by Andrieux and Savéant. Laviron emphasized that the model is valid when the transport of counter ions and solvent molecules do not appear as a limiting factor. In this model, the thickness of the first layer, $\Delta x_1$, may differ from $\Delta x$.

In the model proposed by Peerce and Bard [170], it was assumed that the electron transport within the layer is driven by the difference between the ratio of oxidized and reduced sites in the film. The rate at which equilibrium is attained depends on the rate of transport of counterions into or out of the film and the rate of electron transfer between the electroactive groups. They also considered that the appropriate orientation of the redox groups is related to the self-diffusion of the polymer chains. The combined effects of electron hopping and ion movement were treated in the model as diffusion processes. On the basis of this model a digital simulation was used to estimate the effect of D and $k_s$ on the shapes of the cyclic voltammograms in different cases. They analyzed the effect of site-site interactions, the distribution of nonequivalent redox sites, and their interconversion as a function of potential. The treatment was applied to simulate the results obtained for two ferrocene containing polymers in which the spacing between the electroactive groups was different. For poly(vinylferrocene) (PVF) films in 0.1 mol/dm$^3$ tetratbutylammonium perchlorate (TBAP)/acetonitrile D = 2x $10^{-10}$ cm$^2$/s and $k_s$ = 100-250 s$^{-1}$ were obtained, and it was found that the values of the diffusion coefficient depend on the film thickness, the nature of counterions and the spacing between the redox groups. The application of this model fits the experimental results quite well, which attests that, to the first approximation, the cyclic voltammetric behaviour of these films can be described in terms of a model including a heterogeneous electron transfer step and a diffusion process, even when interactions between the sites and interconversion of the different sites can be assumed.

Because of the phenomenological nature of these theories and the applied simplifications, several questions have remained unanswered

concerning the actual mechanism of charge transport in conducting polymers. The fundamental questions: (i) what does the measured diffusion co-efficient represent? and (ii) what is the rate determining step? remain unanswered. Among the possible explanations are the diffusion coefficients of the redox sites, the local segment or long-range chain motion, and diffusion or migration of counterions. The problem of coupling between the electron transport and counterion displacement also need to be resolved.

### *2.2.2 Theory of the electron exchange reaction:*

For the fast electron exchange process coupled to isothermal diffusion in solution, the theoretical description and its experimental verification were given by Dahms [54] and by Ruff and co-workers [55-58]. Ruff and co-workers studied the displacement of the centers of mass of particles, which is brought about by both common migrational and chemical exchange reaction of the type:

$$A + AX = AX + A \qquad (2.1)$$

It was concluded that the exchange reaction can be described in terms of second-order kinetics, and a relationship was given between the measured diffusion co-efficient (D) and the diffusion co-efficient ($D_0$) in the absence of any electron exchange reaction.:

$$D = D_0 + \frac{k_e \delta^2 \Pi}{4} c = D_0 + D_e \qquad (2.2)$$

where $k_e$ is the second-order rate constant of the exchange reaction, and c and $\delta$ are the concentration and the distance between the centers of the chemically equivalent species involved in the electron exchange, respectively. In fact, $\delta$ is the distance with which the hydrodynamic displacement is shortened for the species and can be estimated on the basis of independent data. Later Ruff and Botár [172] corrected the original thermodynamic derivation, which was affected by some errors. According to the corrected thermodynamical treatment, the constant factor in above equation is 1/6, 1/4 or 1/2 (instead of $\Pi/2$) for three, two and one dimensional diffusions, respectively i.e.,

$$D = D + k_e \delta^2 c/6 \tag{2.3}$$

On the basis of the random walk treatment, Ruff and Botár [173] derived two equations for the diffusion coefficients for A and AX:

$$D_A = \frac{1}{6}\left[\lambda_{AX}\delta^2 - \lambda_X \delta^2\right]\Phi_{AX}(i) \tag{2.4}$$

$$D_{AX} = \frac{1}{6}\left\{\lambda_{AX}\delta^2\left[1 - \Phi_A(j)\right] + \lambda_X \delta^2 \Phi_A(i)\right\} \tag{2.5}$$

where $\lambda_X$ and $\lambda_{AX}$ are the respective jump frequencies, $\delta$ is the distance between the lattice points, $\Pi_A(i)$ and $\Pi_{AX}(i)$ are the respective one-position distribution functions, which suggest the probability that position I is occupied by a particle A or AX, respectively. The $\Pi(i)$ functions can be regarded as concentrations. Buck [174] criticized the original treatment applied by Ruff et al. [55-58]. He made two anomalous steps in the derivation. The first was in the application of the time-dependent Fick's second law, the second in the differential formulation of the chemical rate expression. Buck observed that the spherical diffusion co-efficient (P/4) in Ruff equation was not necessary [175]. Despite the fact that considerable efforts have been made to find the linear concentration dependence of D predicted by Dahms-Ruff theory, it is yet to be formulated. This leads to the conclusion that either this simple model is not suitable for the adequate explanation of the observations or the experimental techniques employed and data evaluation do not supply correct information. There may be several reasons as to why this model has not yielded the expected results:

1. The uncertainty in the determination of D by potential-step, impedance, or other techniques is too substantial to obtain reliable data, due to problems such as the extraction of D from a $D^{1/2}c$ product, the difficulty arising from the insitu thickness estimation, nonuniform thickness, incomplete electroactivity, film homogeneity and ohmic drop effects.
2. The model is accurate, but the values of the electron jump distance $\delta$ used for the calculation are not correct, or even may change with c.

## 2.3 New theories predicting nonlinear D(c) function:

### *2.3.1 He-Chen Model:*

He and Chen [176] proposed a modified version of the original Dahms-Ruff theory. They assumed that systems where the electron exchange rate is high, the rate of the electron transport are determined by the physical diffusion of the redox species incorporated in an ion-exchange membrane, when the concentration of the redox couple is low. As the concentration of redox species increases in the film, and consequently some of the redox centers become immediately adjacent, several electron hops may be possible i.e., the charge donated to a given redox ion through diffusion encounter may propagate over more than one site in the direction of concentration gradient resulting in the enhancement of the total electron flux. This is equivalent to an increase of the electron-hopping distance by a certain factor f, thus the diffusion co-efficient D can be expressed as follows:

$$D = D_0 + \frac{\Pi k_e c \delta f}{4} = D_0 + D_c \qquad (2.6)$$

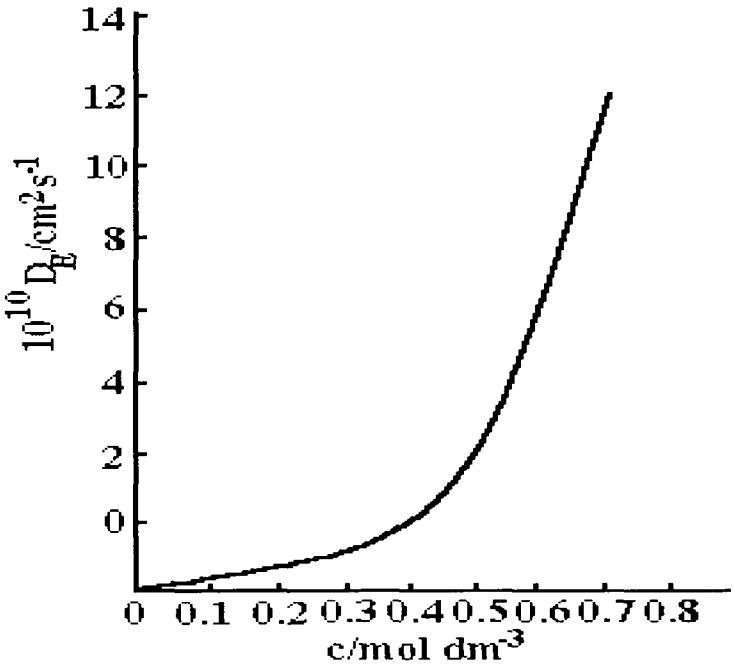


Figure 2.1: Concentration dependence of the electron diffusion calculated according to He-Chen equation assuming $k_e=10^4 dm^3/mols$ and $\delta=1.36x10^{-7}$ cm.

Assuming a Poisson distribution of the electroactive species, the enhancement factor can be expressed as power series of a probability function, collision distance is nearly zero and the factor f = 1. $D_e$ increases markedly at higher concentrations. He and Chen have found such concentration dependence of the electron diffusion co-efficient in Nafion films in contact with 0.05 mol/dm$^3$ $H_2SO_4$ solution. An attempt was made to explain the sharp increase of the D vs. c curve at high concentrations in terms of parallel conduction pathways. This model provided a satisfactory explanation for the data obtained at low values of concentration c, but gave overestimated values of D at high concentrations.

### *2.3.2 Fritsch-Faules-Faulkner model:*

Fritsch-Faules and Faulkner [177] developed a microscopic model to describe electron (or hole) diffusion in a rigid three-dimensional network. Their model takes excluded volume into consideration and is based on principles of probability distribution arguments and on random walk theory. The following conditions are assumed: (a) there is a homogeneous random distribution of hard-sphere redox centers of diameter $r_0$, the hard-sphere approximation simplifies the geometry and eliminates the orientation effects, (b) all redox centers are identical, noninteractive and immobilized i.e., there is no molecular motion, (c) each step corresponds to an electron transfer across the average nearest neighbour distance between redox species $r_{NN}$, (d) the electron transfer rate constant $k_e$, decreases exponentially with the edge-to-edge separation between reacting pairs, $r_{NN} - r_0$, and (e) the charge compensation occurs sufficiently rapidly on a local basis so that it does not limit the random hopping, except for its effect on the reorganization energies governing extended electron transfer.

The conception of Fritsch-Faules and Faulkner is closely related to that of Feldberg [178], who investigated the problem of coupling of semi-infinite linear diffusion and heterogeneous electron transfer with an exponentially decaying distance dependence, and it has some features in common with the distance dependence of electron transfer rates for homogeneous bimolecular reactions

[179-181]. The diffusion coefficient for the succession of electron transfer events in the network was derived from the relationship originated from the three-dimensional random walk model:

$$D_e = \frac{f\langle l^2 \rangle}{6} \tag{2.7}$$

where f is the number of displacement per unit time ($f=1/\tau$)and $\langle l^2 \rangle$ is the mean square displacement distance. This model is valid only for systems where redox species are truly immobilized in a rigid network. Polymer film electrodes, in contact with supporting electrolytes, do not usually fall into this category. In real systems, the physical diffusion of the redox centers, the segmental and chain motions of the polymer take place. Therefore the models that predict sharp rise of D with c at low concentration, but do not preclude bimolecular collisions, seem to be more realistic.

### *2.3.3 Percolation Theory:*

The electron transport that occurs via electron hopping between localized sites in films and the mediation reaction are also described in terms of percolation theory [182] using a model that is applied in solid state physics for electron hopping through insulating film. According to this theory, the probability $P_{ij}$ of electronic transition between two localized states depends on their spatial separation $r_{ij}$, and the difference $E_i$-$E_j$ in energy:

$$P_{ij} = A \exp [-\chi r_{ij} - | E_i - E_j | / kT ] \tag{2.8}$$

where $\chi$ characterizes the localization of the electronic wavefunction at a particular state. The preexponential factor A depends on the properties of the electronic state and the surrounding medium. The simulated current-potential relationship for a mediated reaction occurring at the film/solution interface is similar to the experimentally observed current-potential relationships. It is interesting to note that the current density is not proportional to the concentration of localized states, but follows a power law of the type $j \sim c^m$, with m~2-3.

### 2.3.4. *Theories of coupled electron hopping-ion displacement:*

When the oxidation state of the film is changed, in the simplest case counterions enter into the film in order to maintain the bulk electroneutrality in the surface layer of finite thickness. The phenomenon is independent of as to how the electrons traverse the film. Andrieux and Savéant [183] considered the consequence of the electroneutrality coupling of electron hopping between localized sites with electroinactive counterion displacement for the steady state [184] and transient current response [183]. They recognized that the electron-hopping process cannot be described by the usual combination of the classical Fick's and Nernst-Planck laws, when the effect of electric field is considered, but rather a second-order law should be derived from the bimolecular character of electron-hopping, as opposed to the unimolecular character of ion displacement. They investigated systems containing fixed redox ions, mobile electroinactive counterions, and fixed electroinactive counterions, under semi-infinite diffusion-migration conditions. This theory, however, has some limitations like it considered only those cases where the explicit consideration of the transport of counterions was unnecessary i.e., when mobile counterions are present in excess or when there are no mobile counterions.

### 2.3.5 *Ion association and electric field effects:*

The ion association within the polymer film plays an important role in the dynamics of electron hopping within the films [185]. Due to the high ionic content and the low dielectric constant that prevails in the interior of many redox polymers, an extensive ion association might be expected. The strikingly nonlinear increase in the apparent diffusion co-efficient of the incorporated redox ions as their concentration increase is related to the common effects of electric fields present within the redox polymer and the ion association. According to the model [185], the sharp rise in the apparent diffusion coefficient D as the concentration of the redox couple in the film approaches saturation and is an expected consequence of the shifting of the ionic association equilibrium to produce large concentrations of the oxidized half of

the redox couple, which is well matched for rapid electron acceptance from the reduced half of the couple. Electric field present in the films also contributes to the sharp increase of D with c, but the calculated effects of the electric fields by themselves are too small to account for the observed behaviour. It should be mentioned that in this study particular attention was devoted to measuring the molar fraction of the electroactive material in the coatings and to controlling the film preparation in order to avoid the problems of previous measurements, when large fraction of the incorporated complexes were found to be electroactive and data evaluation became uncertain.

### 2.3.6 *Diffusion-migration model for long distance electron hopping:*

Srinivasa Mohan and Sangaranarayanan [186] introduced a generalized diffusion-migration equation for long-distance electron hopping between redox centers taking the potential and concentration fluctuations into consideration. They demonstrated the advantages of employing a nondiscrete approach for the derivation of transport equations incorporating distance-dependent electron hopping. The explicit form of a typical rate constant depicting its dependence on the potential difference and distance was given by the following expression:

$$K_1(x,y) = k_0 \exp(-\beta y) \exp[(\alpha F/RT)(\Phi(x) - \Phi(x+y))] \quad (2.9)$$

where the variables x and y denote, respectively, the coordinate of species A and the hopping distance. The term $\exp(-\beta y)$ depicts the distance-dependent electron hopping. In their derivations they used the approximations that the potential difference term occurring in the exponent can be linearized and $\Phi(x+y) - \Phi(x)$ can be taken as $(d\Phi/dx)_y$. Assuming a second-order process for the electron transport and uniform discrete jumps to a distance $\Delta x$, the concentration dependence of $D_e$ was given as follows:

$$D_e = k_e\, c(\Delta x)^2 \exp(-\beta \Delta x)$$

The expression indicates the point of extremum in $D_e$ with respect to $\Delta x$. they identified the mean square displacement $\langle x^2 \rangle$ as:

$$\langle x^2 \rangle = \int_0^\infty y^2 \exp(-\beta)\, \omega(y)\, dy \quad (2.10)$$

where $\omega(y)$ is the probability distribution of hopping distances. With the help of this function the diverse concentration dependence of $D_e$ and the interactions between sites can be analyzed.

### 2.3.7 *Blauch-Savéant theory: Transition between percolation and diffusion behaviours:*

A systematic investigation of the interdependence between physical displacement and electron hopping in propagating charge through supramolecular redox systems showed that when physical motion is either nonexistent or much slower than electron hopping, charge propagation is fundamentally a percolation process, because the microscopic distribution of redox centers plays a critical role in dictating the rate of charge transport [187]. Any self-similarity of the molecular clusters between successive electron hopping imparts a memory effect, making the exact adjacent-site connectivity between the molecules important. In the opposite extreme, rapid molecular motion thoroughly rearranges the molecular distribution between successive electron hopping leading to the mean-field behaviour.

The mean-field approximation presupposes that the diffusion-controlled rate constant $k_d$ is higher than the activation-controlled rate constant for the electron exchange $k_{act}$. For this reason, the Dahms-Ruff approach does not accurately describe charge propagation occurring by means of electron hopping in systems, where the redox centers are irreversibly attached to the supramolecular structure, and they are thereby unable to contribute directly to the charge transport through their physical motion. The mean-field approximation leads to Dahms-Ruff-type behaviour for freely diffusing redox centers with the following corrected equation for diffusion co-efficient:

$$D = D_0 (1 - x) f_c + D_e x \qquad (2.11)$$

where x is the fractional loading, which is the ratio of the total number of molecules to the total number of lattice sites. The factor $(1 - x)$ in the first term accounts for the blocking of physical diffusion and $f_c$, introduced by Blauch-Savéant, is a correlation factor, which depends on x. In the framework of this

model, however, the fulfillment of mean-field conditions implies a descending variation of the apparent diffusion coefficient with x and not the commonly expected ascending variation. When $D_0$ becomes less than $D_e$, percolation effects appear. If $D_e >> D_0$, a characteristic static percolation behaviour should be observed. Blauch-Savéant emphasized that when redox centers are irreversibly attached to the supramolecular structures, but the rate of bounded diffusion- a concept introduced by them - is large enough to allow interactions between neighbouring redox centers, the rate constant in $D_e = k_e \delta^2 c$ is activation-controlled.

**2.4 Polymerization mechanism:**

According to elementary polymer chemistry or organic chemistry, all polymerization processes fall into either of the following two categories:

(i) Condensation polymerization (step-growth polymerization)

(ii) Addition polymerization (chain-growth polymerization)

Conducting polymers can be synthesized by either of the two methods:

(i) Chemical method and

(ii) Electrochemical method

Almost all electrochemical syntheses are addition polymerization and most chemical syntheses are condensation polymerization processes. A clear difference in mechanisms between chemical and electrochemical syntheses occurs for almost all conducting polymers.

*2.4.1 Electrochemical polymerization mechanism:*

Electrochemical polymerizations of almost all conducting polymers appear to follow a generic reaction pathway with the following common features:

1. The initiation step, (monomer) radical generation via electrochemical oxidation.
2. Propagation via (a) radical-radical recombination, not radical-monomer combination; (b) loss of two protons from the radical-radical

intermediate species, generating the dimer; (c) electrochemical oxidation of the dimer, generating another "oligomeric" radical; (d) combination of this or similar oligomeric radicals with monomer radicals and repeat of step 2b and 2c, building up the polymer.

3. Termination via exhaustion of reactive radical species in the vicinity of the electrode and accompanying oxidative or other chain termination processes.

Among other common features of the mechanism is the preferred polymer linkage at the α-position for most monomers. One of the first feature to note for an electrochemical polymerization is that once the initiating electrochemical potential is applied, the population of radical cations is likely to far exceed than that of the neutral monomers in the vicinity of the electrode surface and a generated radical cation is far more likely to be surrounded by other radical cations than by neutral monomers, oligomers or other species. Most important determining factor for this is rapid electron transfer kinetics for electro-oxidation of the monomers in comparison to the slower diffusion of monomers from the bulk of the reaction medium to electrode, thus causing a rapid depletion of monomer concentration at the electrode. This is in contrast to the situation in a typical chemical polymerization, where the concentration of monomers far exceeds that of radical and thus radical-monomer combination is more likely to be the next step after radical generation.

Apart from the usual spectroscopic structural evidence, for α-polymer linkages for most conducting polymers, it has been shown that 2,5-disubstituted pyrrole monomers do not polymerize, and the polymerization of 2-monosubstituted monomer stops at the dimer stage; 1- and 1,3-substituted azulenes do not to polymerize. The possible mechanism of oxidative polymerization of polyaniline, polypyrrole and polythiophene are shown in Figs. 2.2-2.4.

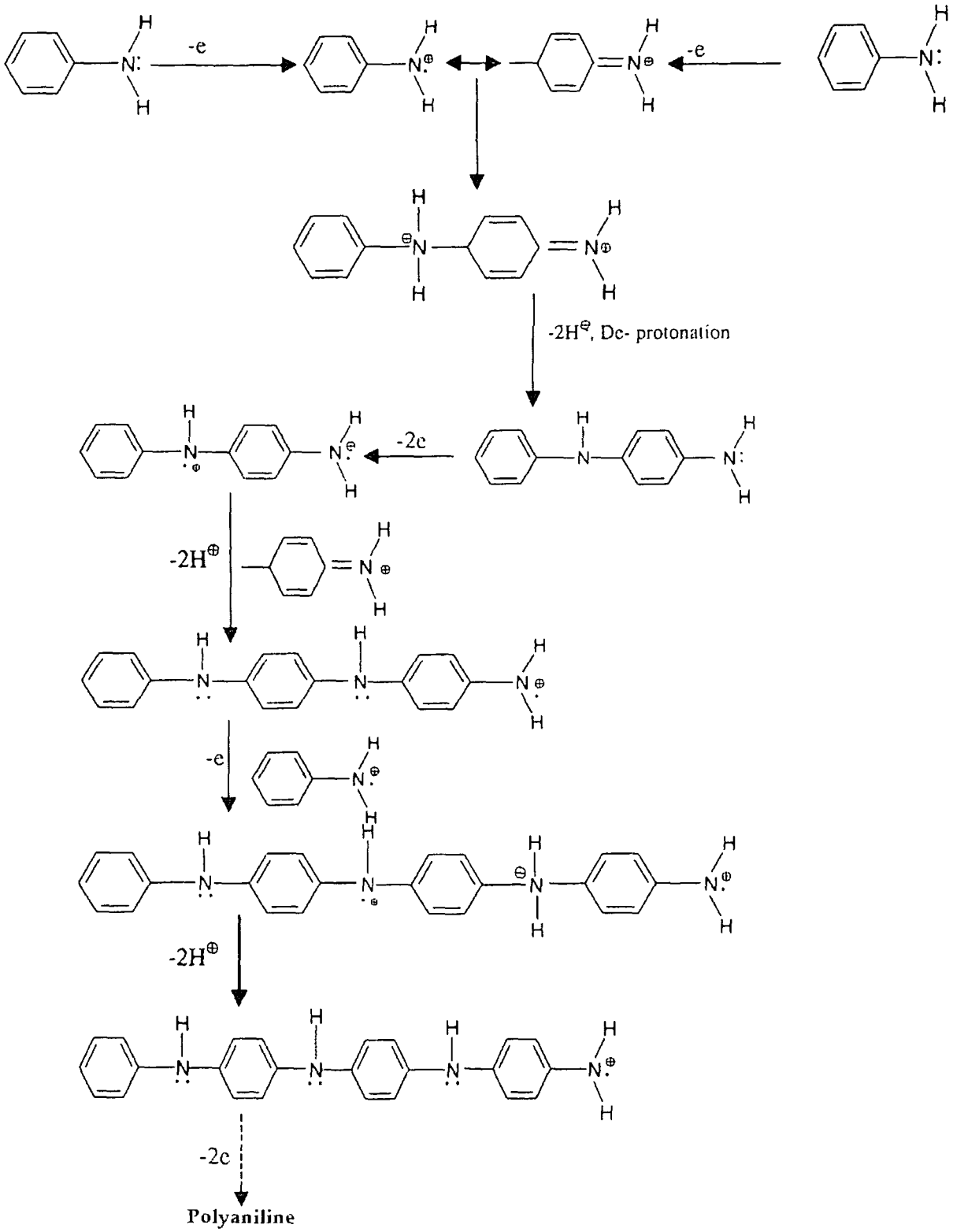


Figure 2.2: Oxidative polymerization of polyaniline conducting polymer.

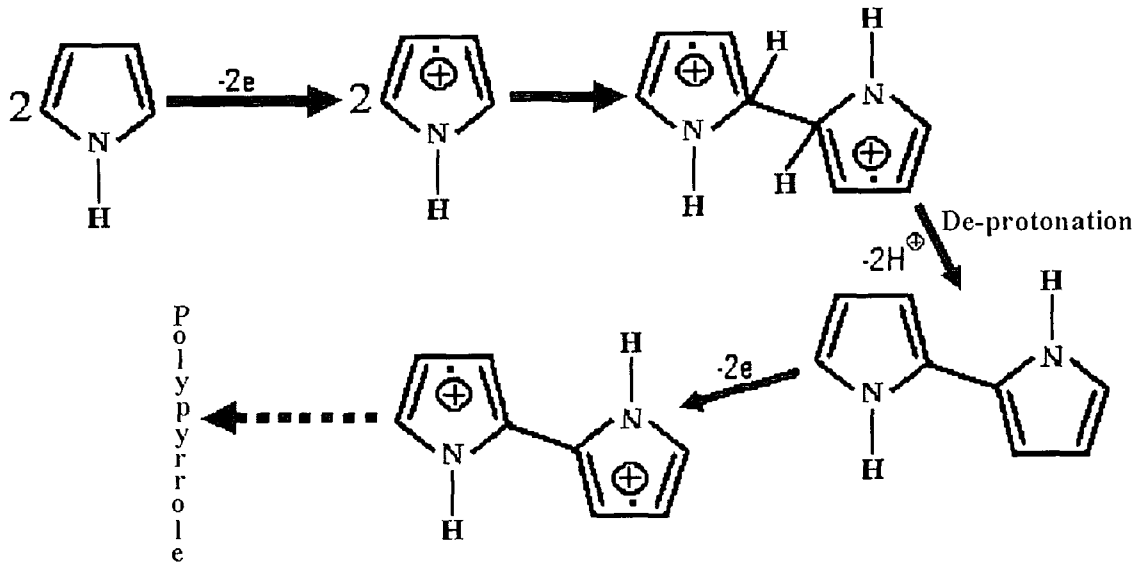


Figure 2.3: Oxidative polymerization of polypyrrole conducting polymer.

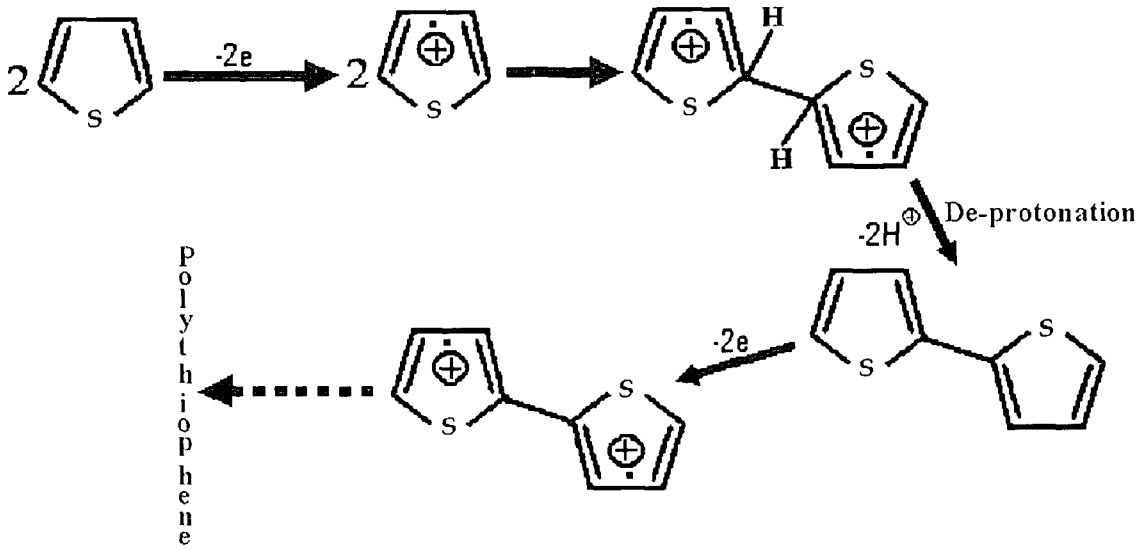


Figure 2.4: Oxidative polymerization of polythiophene conducting polymer.

### *2.4.2 Factors favouring polymerization:*

While it is true that electropolymerization is a generic technique usable for fast polymerization of conducting polymers, not all organic monomers undergo electropolymerization. The key to understand as to why only certain monomers electropolymerize to yield conducting polymers lie in a combination of factors of stability of the radical ions generated in the first step, and the oxidation potentials for generation of these. In nearly all cases where successful electropolymerization is observed, the radical ions are found to be highly

stabilized via mechanism such as charge delocalization, and electrochemical oxidation is reasonably facile. Carbazole, furan and indole monomers whose radical cations are less stable than that of, for example, pyrrole produce poorly formed polymers with low conductivity on electropolymerization. Steric crowding can also hinder electropolymerization or yield low conductivity polymers. Proton removal renders the dihydro-dimer or dihydro-oligomer formation, which is irreversible. Thus it is expected that proton acceptors including water, bases such as pyridine or lutidine and other nucleophiles enhance electrochemical polymerization. This is indeed found to be the case for a wide variety of conducting polymers [30]. It is also felt by many workers [31, 34, 142, 145] that this is one of the reasons that electropolymerizations are generally more successful in acetonitrile. A decrease in $p^H$ is sometimes observed during polymer formation. Indeed in many cases a little water about 1% v/v, is found necessary for electropolymerization [15] and when highly dried materials are used, yields are invariably poor [15]. Water or other nucleophiles may also serve the function of an effective counter electrode reaction during solution electropolymerization. It is observed that in the absence of an effective counter electrode reaction in most electropolymerizations, reduction of impurities such as trace metals or water serves as a poor substitute counter electrode reaction [30-34]. Excess water may in some case, however, lead to premature oxidative termination of the propagating polymer chain.

The dimers and subsequent oligomers produced invariably have oxidative potentials lower than that of the monomer. This is a thumb rule for conducting polymers as the chain length increases, the oxidation potential decreases. The variation of formal redox potentials for conducting polymer chains of different lengths is one of the factors contributing to peak broadening in the cyclic voltammograms of the conducting polymers. Thus in a typical potentiostatic or galvanostatic polymerization, the oligomer, once produced, is rapidly oxidized at the electrode to its radical cation. It then is more likely to react with monomeric radical cations. It is however intriguing to note that

attempts to electropolymerize dimers or trimers directly are unsuccessful. An excess of monomer radical cation appears to be necessary for successful electropolymerization.

**2.5 Swift heavy ion irradiation:**

Ion beams have become an integral part of numerous surface processing schemes and in the modification of surface layers of solids [188]. Recently there has been a growth of interest in high energy ion irradiation of polymers and other insulating materials [189-194]. Ions couple energy to the target atoms in a solid predominantly through electronic excitations and ionizations and through direct collisional displacement of the target atoms. In case of high energy ion irradiation of polymers, the electronic energy loss of the incident swift heavy ion is released into (i) radiative decay (ii) production of new reactive species (radicals, gases) and defects (instaurations, scissions, crosslinks) and heat. The decrease in crystallinity has also been reported after ion irradiation [195].

An important parameter characterizing ion-to-target energy transfer is the energy loss dE/dx (eV/Å), defined as the energy deposition per unit length along ion track. The value of (dE/dx) changes with ion energy. When an energetic particle penetrates into a polymer medium, depending upon its incident energy it loses energy by two main processes, viz. by interacting with target nuclei (screened) and by interacting with target electrons. The former process is called *nuclear energy loss or nuclear stopping* and the latter *electronic energy loss or electronic stopping* [196].

*2.5.1 Nuclear Energy Loss:*

Nuclear energy loss $S_n$ arises from the collisions between the energetic ion and the target nuclei, which cause atomic displacements and phonons [196]. Displacement occurs when the colliding particle imparts energy greater than certain displacement threshold energy, $E_d$, to a target atom. $E_d$ is the energy that a recoil atoms requires to overcome the binding forces and to move more than one atomic spacing away from its original site. Since the nuclear collision occurs

between two atoms with electrons around their nuclei, the interaction of an ion with a target nucleus is treated as the scattering of two screened particles. At low energies (~1 keV/nucleon) the incident ion primarily undergoes nuclear energy loss ($S_n$) [197]. Nuclear energy loss is derived with consideration of the momentum transfer from the incident ion to the target atom and inters atomic potential between them. Thus $S_n$ varies with ion velocity as well as the charges of two colliding ions/atoms. The nuclear energy loss becomes important when an ion slows down to approximately the Bohr velocity (orbital electron velocity, $2.2 \times 10^6$ m/s). Therefore, the maximum nuclear energy loss occurs near the end of the ion track for high energy ions.

### 2.5.2 *Electronic Energy Loss:*

Electronic energy loss $S_e$ arises from the electromagnetic interaction between the positively charged ion and the target electrons. One mechanism is called glancing collision (inelastic scattering, distant resonant collisions with small momentum transfer) and the other is called knock-on collision (elastic scattering, close collisions with large momentum transfer). Both glancing and knock-on collisions transfer energy in two ways: electronic excitation and ionization. All excited electrons eventually lose energy as they thermalize. Glancing collisions are quite frequent, but each collision involves a small energy loss (<100 eV). On the other hand, knock-on collisions are very infrequent, but each collision imparts a large energy (>100eV) to the target electrons. Theoretical and experimental evidence suggested that approximately one half of the electronic energy loss is due to glancing collisions and the other half to knock-on collisions [196]. At high energies (≥100 keV/nucleon) the incident ion primarily undergoes electronic energy loss [197] $(dE/dx)_e$, and if the films are sufficiently thin compared to the stopping range of the ion, the electronic energy loss is reasonably uniform throughout the film thickness.

On their way through matter, energetic ions lose energy and induce a continuous trail of excited and ionized target atoms. Due to their highly charged state, associated with a high energy transfer, heavy ions are especially

suited to create cylindrical zones of irreversible chemical and structural changes. These zones have a diameter of only a few nanometers and are known as latent tracks. Formation of tracks in polymers can be explained on the assumption that particles lose energy during its passage through matter in two ways: (i) along the trajectory, the energy yield being large, all chemical bonds are broken, and (ii) in the neighbourhood of the trajectory, only the bonds between monomer units are broken. Thus the breaking of chemical bonds plays a more critical role in the formation of tracks than the displacement of ions by mutual repulsion.

### 2.5.3 *Ion tracks:*

When an energetic ion enters into a target, the ion interacts with the atoms or molecules, loses its energy on its way through the target material. The path of the ion is called ion track. The electrons of the atoms of the target materials are pulled of by an electromagnetic force when a positively charged ion (in almost all ion irradiations) travels in the ion track producing a strong restoring force in the atoms of the target material. As a result, electrostatic oscillation of the electron density, velocity and electric field of the target atoms occurs, at the plasma frequency $\omega_p$ [196],

$$\omega_p = \frac{1}{4\pi\varepsilon_0}\frac{4\pi ne^2}{m_e} \qquad (2.12)$$

where e (Coulomb) and $m_e$ (kg) are the charge and mass of the electron, n ($m^{-3}$) is the electron number density of the medium. The oscillation occurs in a column of radius $r_c$ given as [198]

$$r_c = \frac{\beta c}{\omega_p} \qquad (2.13)$$

where $\beta = V_{ion}/c$, $r_c$ is termed as the physical core in which fluctuation of electron density or energy for a period of plasma frequency pulse occurs. In other words, it is the range of uncertainty in energy deposition. $r_c$ varies with ion velocity and defines the range of energy deposition, which occurs for a period of $10^{-16}$ sec for a relativistic high energy fast ion. Within this short time

only electronic processes are possible in the ion track as this time is too short for molecular motion. If the time is of the order of $10^{-14}$ sec, molecular vibration in the medium could occur. A local temperature rise could occur at $10^{-13}$ sec and diffusion processes could take place at $10^{-12}$ sec [199]. The time period of plasma frequency pulse can be calculated from the uncertainty relation $\Delta t \Delta E \approx \hbar$, where $\Delta E$ is an energy width over which absorption can take place, which is also termed as 'spur'.

Some energy loss outside the core defined by $r_c$ also occurs due to δ-rays. The maximum range of δ-rays can be calculated by using the relation [200,201]:

$$\delta_{max}\left[\frac{g}{cm^2}\right] = kW_{max}^{\alpha} \qquad (2.14)$$

where $k = 6\text{x}10^{-6}$ g cm$^{-2}$ (keV)$^{\alpha}$, $\alpha = 1.097$ for $W_{max} < 1$ keV and $\alpha = 1.677$ for $W_{max} > 1$ keV. $W_{max}$ is the maximum energy of δ-rays, which is derived from the kinematics consideration for head-on collision between ion and electrons in the medium as $W_{max} = 2m_e v_{ion}^2/(1 - \beta^2)$ with relativistic correction of mass for fast ions. The radial range of δ-rays, called the penumbra radius, is denoted by $r_p$. The energy density within the core ($r_c$) mostly occurs due to glancing collisions and a small fraction of low energy knock-on electrons, which are trapped inside the core. The energy density between $r_c$ and $r_p$ arises mainly due to the δ-rays.

The ion path i.e., the ion track is thus described by a cylindrical trajectory defined by the physical core with radius $r_c$, the approximate limiting distance from the fast ion trajectory at which an electronic excitation initially occurs. The penumbra with radius $r_p$ is the outermost cylindrical boundary of the δ-rays or secondary electrons. A chemical radius defines the radial distance from the ion trajectory to the point where diffusion and chemical reaction of active species such as radicals, cations, anions, electrons and other activated chemical species occurs. Some chemical species recombine and neutralize in a dense chemical sea, some diffuse out to the penumbra and mingle together with chemical species induced by δ-rays, establishing a fairly large effective radius. Since the chemical radius is difficult to measure or calculate in reality, a term effective radius, which defines the extent to which the energy density or radial

concentration is significant for a given process. Cross-linking, scission and other chemical reaction occur within this effective radius. Most cross-linking and other chemical reactions occur near $r_c$ where concentration of radicals and other ion pairs are high, because of slow migration of radicals in a viscous medium. In low energy loss per unit length situation, δ-rays develop independently and have very little effect on cross-linking.

*2.5.4 Spurs:*

The concept of linear energy transfer of the incident fast ion in the target medium or the stopping power is based on the assumption of continuous slowing down of the fast ion. The energy transfer of the fast ion to the target medium takes place discretely and not continuously as electronic excitation is restricted by quantized energy levels and ionization is restricted by certain potential energy barrier, which has to be overcome to take out an electron from the target atoms i.e. to eject electrons from the orbitals. Some threshold energy barrier has to be broken to displace an atom and also needs some minimum energy to start the atom moving in the field of the surrounding atoms. Creation of one ion pair requires removal of electrons where also again some minimum energy is needed. These discrete energy losses of the fast ion in the target medium are quantized in the quantum unit called spur. Most of the spurs are within 100 eV and in polymer a spur has an average value of 30-40 eV [199,202], which is almost equal to the average energy required for producing one ion or radical pair. Some of the energy is used for excitation, so the spur energy is larger than the of ionization energy needed for creation of one ion or radical pairs.

*2.5.5 Linear energy transfer (LET):*

The energy deposited per unit path length of an ion in the target medium, linear energy transfer (LET), is an important parameter for cross-linking of SHI irradiated polymer. Energy loss or transfer of the incident fast ion occurs in the target medium discretely as spurs instead of continuous

transfer of energy. Hence like spur, LET is also an important parameter in SHI irradiation. Change of LET also changes the spur separation in the ion track. The distance between spurs can be calculated by dividing the spur energy by LET. For low energy the spur distance is high, spurs are widely separated and occur independently. High LET produces more radical pairs within the track radius, spurs are connected or overlapped, high radical concentration gradient is established and hence effective radius increases. Effective radius for cross-linking in polymer can be estimated in terms of spur density. For this let us assume that first one radical pair or spur is required per unit volume since the distance between polymer chains is in the nm range for most of the polymers and two radicals must be in neighboring chains for cross-linking to occur. This assumption grossly overestimates the effective radius because a significant fraction of radicals recombines and do not contribute to cross-linking. In SHI irradiation several physical and chemical processes occur in the polymer. Atomic displacement is caused by nuclear collision causing chain scission and releasing of pendent atoms. Bond breaking of polymer chain occurs due to superposition of phonon waves, which has low probability as the energy density required for phonon wave to begin is very high. Polymer usually contains large free volume, sometimes more than 20% and the atomic density is relatively small as compared to those of the compact lattice structure. Thus in polymer, nuclear displacements take place independently increasing the polymer density. The probability of displacement of two radical ions from the two neighbouring chain simultaneously for cross-linking is low. Low energy ions with keV energy have high nuclear LET and generally are not suitable for cross-linking phenomena to occur [203]. When the electronic LET is high, a large volume around the ion track is affected due to the coulombic field induced by glancing collisions and ionizations (δ-rays) by knock-on collisions. This results in production of active chemical species, cations, anions, radicals and electrons along the polymer chains. The coulombic attraction and repulsion among these active species cause violent bond stretching and segmental motion in the polymer chains that could lead to cross-linking as well as bond breaking.

Thus electronic and nuclear LET, both can produce cross-linking and chain-scission in polymers, but high nuclear energy loss causes more scission due to the independent displacement damage and less number of radical creation, simultaneously in neighboring chain. High electronic energy loss i.e., high electronic LET produces more cross-linking due to collective excitations also termed as plasmons producing a large excited volume resulting in coercive interaction among the ions and radical pairs produced within the effective volume. This is established in G-value and hardness measurements as well as other experiments [204,205]. Electronic LET increases and the nuclear LET decreases with the increase in ion energy. The magnitude of ionization varies with the ion velocity and charge state. The charged atomic species with large atomic number and high energy are desirable for large $r_c$ and $r_p$ as fast ions have short interaction time and produce large $r_c$ and $r_p$. LET is also directly dependent of charge state of the ion and higher charge state produces high LET. However, increasing the energy of the fast ion beyond a certain limit does not increase the LET, only the penetration depth of the ion is increased. To obtain high LET, the charge state of the ion also should be high. The nuclear energy loss decreases and electronic energy loss increases with increase in ion energy, hence in case of SHI irradiation of polymers the scission yield decreases and cross-linking increases with the increase in ion energy as well as with increase in charge state. However, in the polymers, the cross-linking can occur only when two dangling radical pairs are in neighbouring chains, which is attainable in polymers with high energy incident ions with higher charge state and high atomic number.

**2.6 Supercapacitor:**

Supercapacitors are being developed as energy storage devices based on better understanding of the physical processes that take place therein. This section deals with the scientific principles involved in the electrochemical double layer capacitor (EDLC).

### 2.6.1 *Basic scientific principles:*

Electrochemical capacitors operate on principles similar to those of conventional electrostatic capacitors. Conventional capacitor stores energy in the form of electrical charge and a typical device consists of two conducting materials separated by a dielectric. The charge storage mechanism in electrochemical double layer capacitors (EDLC) is shown in Fig. 2.5 [206].

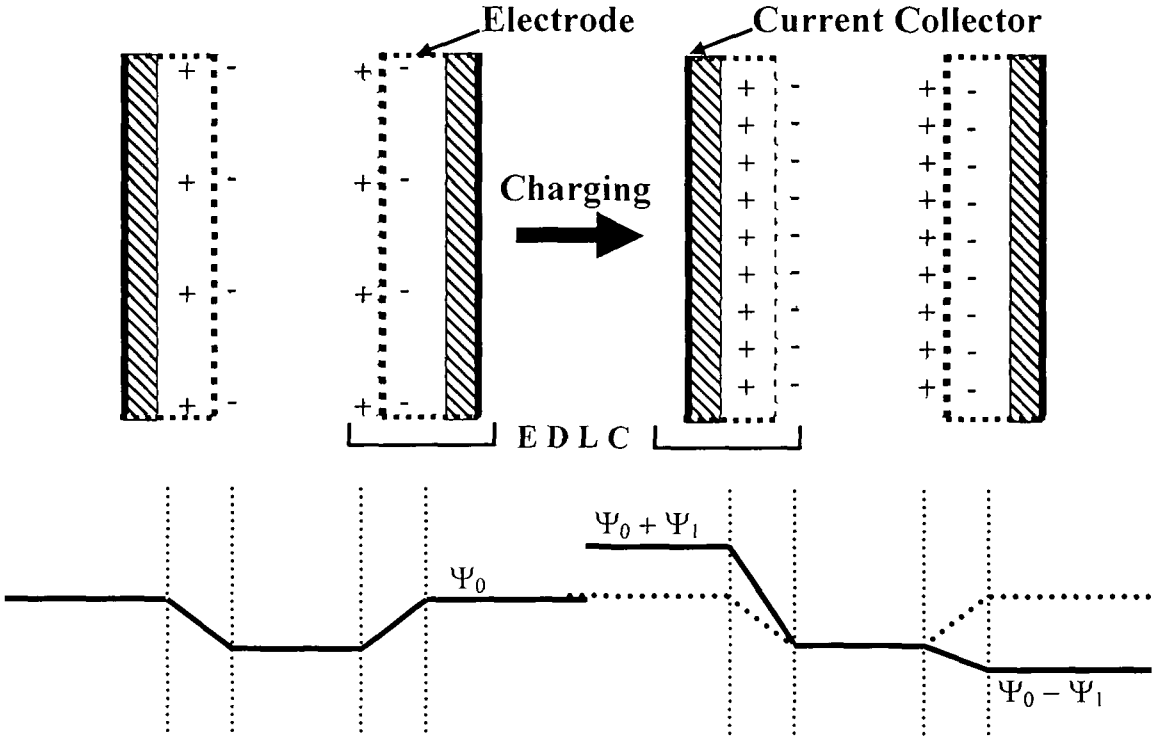


Figure 2.5: The charge storage mechanism in EDLC.

The amount of charge that can be stored in relation to the strength of the applied potential is known as the capacitance, and is a measure of a capacitor's energy storage capability. The capacitance and the stored energy in an electrostatic capacitor are given by following expressions:

$$C = \frac{Q}{V} = \varepsilon \frac{A}{d} \tag{2.15}$$

$$U = \frac{1}{2} CV^2 = \frac{1}{2} QV \tag{2.16}$$

where C is capacitance in Farads, Q is charge in Coulombs, V is electric potential in Volts, ε is the dielectric constant of the dielectric, *A* is conductor surface area, *d* is dielectric thickness, and U is the stored electrical energy.

EDLCs store electrical charge in a similar manner, but charge does not accumulate on two conductors separated by a dielectric. Instead the charge accumulates at the interface between the surface of a conductor and an electrolytic solution (Fig. 2.5). The accumulated charge hence forms an electric double-layer, the separation of each layer being of the order of a few Å. The specific capacitance of such a double-layer is given by Equation 2.17.

$$\frac{C}{A} = \frac{\varepsilon}{4\pi\delta} \tag{2.17}$$

$C$ is the capacitance, $A$ is the surface area, $\varepsilon$ is the relative dielectric constant of the medium between the two layers i.e., the electrolyte, and $\delta$ is the distance between the two layers i.e., the distance from the electrode surface to the centre of the ion layer [207]. This approximation is valid for concentrated electrolytic solutions. A supercapacitor consists of two electrodes to allow a potential to be applied across the cell, and there are two double-layers present, one at each electrode/electrolyte interface. The electrodes are made of high effective surface-area materials such as porous carbon or carbon aerogels in order to maximize the surface-area of the double-layer. High energy densities are achieved in EDLCs due to their high specific capacitance, attainable because of a high electrode/electrolyte interface surface-area and a small charge layer separation of atomic dimensions. In addition to the capacitance that arises from the separation of charge in the double-layer, a contribution to capacitance is also made from reactions that can occur on the surfaces of the electrodes. The charge required to facilitate these reactions is dependent on the potential, resulting in a Faradaic 'pseudocapacitance'. Pseudocapacitance arises from reversible Faradaic reactions occurring at the electrodes. The charge transfer that takes places in these reactions is voltage dependent, so a capacitive phenomenon occurs. There are two types of reactions that can involve a charge transfer that is voltage dependent. In a redox reaction involving an oxidant and reductant, the potential $E$ is given by the Nernst equation.

$$E = E^0 + \frac{RT}{zF} \ln \frac{r}{1-r} \tag{2.18}$$

where $E^0$ is the standard potential, $R$ is the gas constant, $T$ is the absolute temperature, $F$ is the Faraday constant, and r is defined as [ox] / ([ox]+[red]), (square brackets denote species concentrations). The amount of charge $q$ given by the product $zF$, is therefore a function of the potential $E$. Differentiation of Equation 2.18 produces a pseudocapacitive relation [101]. Utilization of the capacitance of the double-layer at electrode interface for electrical energy storage is the basis of so-called double-layer capacitors or supercapacitors, in principle, developed first by Becker [102] and later high-area carbon powder materials and tetraalkylammonium salt electrolytes were used by Sohio group [208]. The charge/discharge curve is a result of overlapping redox reactions as well as a significant double-layer capacitance due to the porous structure of the electrode [101]. The deposition of ions to form a monolayer on the electrode substrate is a reversible process that results in a Faradaic charge transfer, and hence gives rise to pseudocapacitance in a manner similar to that demonstrated in redox reactions. The adsorption/desorption process can be written as Equation 2.19,

$$A_c^{\pm} + \underset{1-\theta_A}{S} \pm e^- \leftrightarrow \underset{\theta_A}{\underset{V}{S}} A_{ads} \qquad (2.19)$$

where $A$ is the ionic species, $S$ is the substrate, $c$ is the concentration of depositable ions, $1-\theta_A$ is the fractional free surface area available for adsorption at a coverage $\theta_A$, and $V$ is the electrode potential [209]. If it assumed that the sites are occupied randomly in a fixed lattice, an equation for coverage can be determined from the Langmuir adsorption equation. This yields the relation shown in Equation 2. 20.

$$\frac{\theta_A}{1-\theta_A} = Kc\, exp\left(\frac{-VF}{RT}\right) \qquad (2.20)$$

$K$ being the electrochemical equilibrium constant. A change in coverage $d\theta$ is directly proportional to the charge $dq$, expressed by Equation 2.21.

$$dq = q_1 d\theta \qquad (2.21)$$

where $q_1$ is the amount of charge required to form or disperse a complete monolayer. Since θ is a function of $V$, differentiation of Equation 2. 21 results in a pseudocapacitive relation [101] described by Equation 2.22:

$$C_{\phi} = \frac{q_1 F}{RT} \frac{Kc \pm \exp\left(\frac{-VF}{RT}\right)}{\left(1 + Kc \pm \exp\left(\frac{-VF}{RT}\right)\right)^2} \qquad (2.22)$$

The high values of specific capacitance attainable for supercapacitor through EDLC technology are a result of double-layer capacitance, and often pseudocapacitance. Double-layer capacitors offer good high storage capabilities attributed to the high surface-area materials used as electrodes, and the fact that charge separation in them occurs at atomic dimensions. Pseudocapacitance that arises from redox or ion-sorption reactions further improves the achievable capacitance from the electrochemical double layer capacitors.

# CHAPTER III

# EXPERIMENTAL DETAILS

Conducting polymer films have been synthesized on stainless steel and indium doped tin oxide (ITO) coated glass substrates by different electrochemical methods. The conducting polymer films are characterized by cyclic voltammetry for the study of their redox response. The dc conductivity of the polymer films is measured by standard four probe technique. The UV-Vis and FTIR spectra are studied for electronic band structure and bonds present in the polymer chains respectively. SEM images are taken for surface morphological study. XRD studies of the polymer films have been carried out for determining the degree of crystallinity of the conducting polymer films.

## 3.1 Materials:

The electrochemical polymerization of the conducting polymer electrodes has been carried out using different monomers, solvents and dopants. For polymerization of the monomers, the substrate i.e. working electrode, counter electrode or secondary electrode and reference electrodes are used in a single compartment three electrode electrochemical cell. For electrochemical polymerization choosing the right combination of monomer, solvent and dopant and also the substrate (working electrode) are very important to produce good quality conducting polymer films.

### *3.1.1 Monomers:*

In the present work, for synthesizing the polyaniline, polypyrrole, and poly-3-methylthiophene conducting polymer films monomers aniline, pyrrole and 3-methylthiophene (Sigma-Aldrich, USA) are distilled under reduced pressure and stored in dark prior to use. Some of the physical properties and molecular structure of the monomers aniline, pyrrole and 3-methyl thiophene are presented in Table 3.1.

Table 3.1: Some physical properties of monomers used in the present work.

| Monomer | Molecular structure | Formula weight | Melting point (°C) | Boiling point (°C) | Density at 25°C gm/ml | Oxidation potentials (Volt) |
|---|---|---|---|---|---|---|
| Aniline | 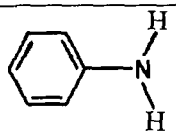 | 93.13 | -6 | 184 | 1.022 | 0.9 |
| Pyrrole | 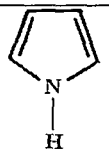 | 67.09 | -23 | 131 | 0.967 | 0.8 |
| 3-methyl thiophene | 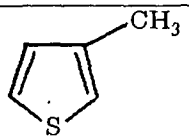 | 98.17 | -69 | 113 | 1.014 | 1.6 |

### *3.1.2 Solvents:*

The solvent is an important factor for electropolymerization governing not only the quality of the conducting polymer films but also its conductivity, morphology and subsequent electrochemical, physical and chemical properties. Acetonitrile is one of the most versatile solvents for several reasons, viz., good nucleophilicity facilitating proton removal during polymerization, insolubility or poor solubility of conducting polymers as well as of oligomers and relative dryness with sufficient water content for effective polymerization without early termination. Solvent such as propylene carbonate (PC), for instance, exhibits high solubility of oligomers giving reduced polymer yield. Retention of solvent affinity sites within the polymer matrix is also an important factor. Solvents may be too nucleophilic, besides its high solvation capability for doped conducting polymers. Dimethyl formamide (DMF) is a poor electropolymerization solvent due to its high nucleophilicity. Electropolymerization is observed if nucleophilicity is reduced with the addition of protic solvents. In cases where monomer has poor solubility in an otherwise ideal polymerization solvent such as acetonitrile, mixed solvents are used to facilitate solubility. In the present work, for electropolymerization double distilled water has been used in all aqueous solutions and as-received

acetonitrile (LOBA, India) is used as organic solvent. Table 3.2 presents some physical properties and molecular formula of acetonitrile.

Table 3. 2: Some physical properties of organic solvent used to synthesize conducting polymers in the present work.

| Solvents | Molecular structure | Mol. weight | Melting point (°C) | Boiling point (°C) | Density ρ at 25 $^0$C (g cm$^{-3}$) |
|---|---|---|---|---|---|
| Acetonitrile | $CH_3—C\equiv N$ | 41.05 | -48 | 81 | 0.786 |

*3.1.3 Dopants:*

It is usually noted that the net charge transfer is a little in excess of that indicated stoichiometrically due to the additional oxidation and doping that occurs during electrochemical preparation of conducting polymers. When a conducting polymer is electrochemically prepared in different solvents with a given dopant, it may not readily exchange in different solvents. Similarly when different dopants are used in a given solvent, the dopant ion may not readily exchange, even if dopant ion size is smaller. The conductivity and electrochemical characteristics of the film depend on the solvent and the dopant ion size.

Dopant salts like perchloric acid ($HClO_4$), phosphoric acid ($H_3PO_4$), lithium perchlorate ($LiClO_4$), sodium perchlorate ($NaClO_4$), lithium trifluoro methane sulfonate ($LiCF_3SO_3$), tetrabutyl ammonium tetrafluoro borate ($[CH_3(CH_2)_3]_4NBF_4$) and tetrabutyl ammonium hexafluoro phosphate ($[CH_3(CH_2)_3]_4NPF_6$) (Sigma-Aldrich, USA) are used as received. Hydrochloric acid and sulfuric acid (E-Merck, India) are used as received. Some of the physical properties of the dopants used in the present work are presented in Table 3.3.

Table 3.3: Some physical properties of dopants used in the present work.

| Dopants | Formula weight | Melting point (°C) | Boiling point (°C) | Density at 25 °C |
|---|---|---|---|---|
| Hydrochloric acid (HCl) | 36.46 | -- | >100 | 1.20 gm/ml |
| Sulfuric acid ($H_2SO_4$) | 98.08 | -- | ~290 | 1.840 gm/ml |
| Perchloric acid ($HClO_4$) | 100.46 | -- | 113 | 1.664 gm/ml |
| Phosphoric acid ($H_3PO_4$) | 98.00 | ~40 | 158 | 1.685 gm/ml |
| Lithium perchlorate ($LiClO_4$) | 106.39 | 236 | -- | 2.42 gm/cm$^3$ |
| Sodium perchlorate ($NaClO_4$) | 122.44 | 486 | -- | 2.0 gm/cm$^3$ |
| Lithium-trifluoro methane sulfonate ($LiCF_3SO_3$) | 156.01 | ~300 | -- | 0.64 gm/cm$^3$ |
| Tetrabutyl ammonium tetra fluoro borate ($[CH_3(CH_2)_3]_4NBF_4$) | 329.27 | ~158 | -- | 0.68 gm/cm$^3$ |
| Tetrabutyl ammonium hexa fluoro phosphate ($[CH_3(CH_2)_3]_4NPF_6$) | 387.43 | ~245 | -- | 0.71 gm/cm$^3$ |

### *3.1.4 Electrodes:*

Though any electrode that does not undergo oxidation at a potential equal to or less than the oxidation potential of the monomer can be used as electrode for electrodeposition of a conducting polymer, yet several electrodes are preferred for specific applications. For electrochromic and initial characterization studies, a transparent electrode such as indium doped tin oxide (ITO) or gold (Au)/platinum (Pt) on glass is preferred. For purely electrochemical characterizations the platinum (Pt) wires, on which adhesion of nearly all conducting polymers is excellent, are preferred. For preparation of free standing films, graphite or glassy carbon electrodes are preferred. Stainless steel electrode is of choice for corrosion studies and for semiconductor applications n-Si electrodes are used with success. Adhesion to such electrodes can be improved by using standard semiconductor rinses e.g., soap water, deionized water, acetone, methanol and acetonitrile. As counter electrodes also, any of the above electrode materials can be used. Pt coil or flag electrodes are

frequently used for electrochemical characterization. High quality stainless steel is also widely used as counter electrode.

In the present work ITO coated glass slides received from Bharat Heavy Electricals Limited (BHEL, India) are used as working electrodes for elctrodeposition of conducting polymer films. Saturated calomel electrode (SCE) is used as the reference electrode and stainless steel is used as the counter electrode in all the experiments.

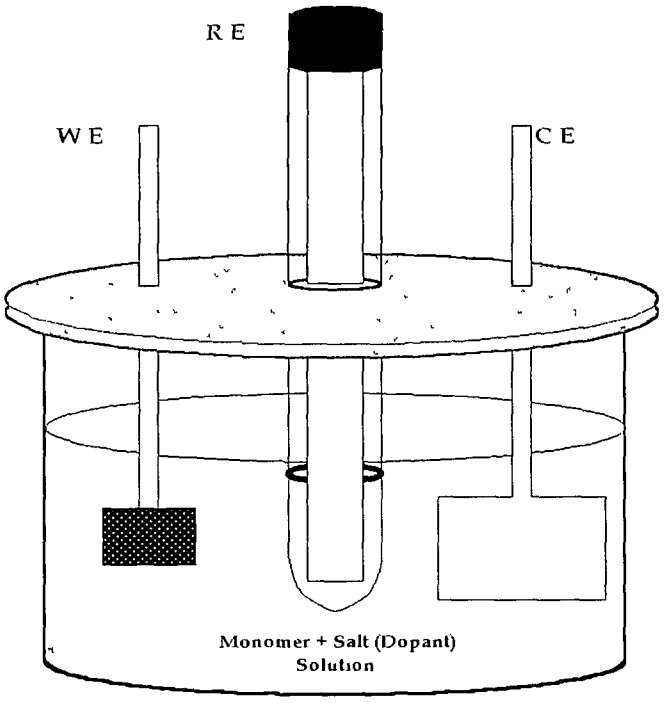


Figure 3.1: Single-compartment three-electrode electrochemical cell.

### 3.2 Synthesis of conducting polymer films by electrochemical process:

Electrochemical synthesis of conducting polymer films have been carried out in a three electrode single compartment electrochemical cell containing one primary or working electrode, one secondary or counter electrode and one reference electrode as shown in Fig. 3.1. Stainless steel and ITO coated glass substrates are used as working electrode. Stainless steel counter electrode with larger surface as area compared to the working electrode and saturated calomel electrode (SCE) as reference electrode are used in all experiments.

A potentiostatic i.e., constant potential deposition mode generally yields polymer with uniform morphology. Potentiodynamic cycling mode typically to

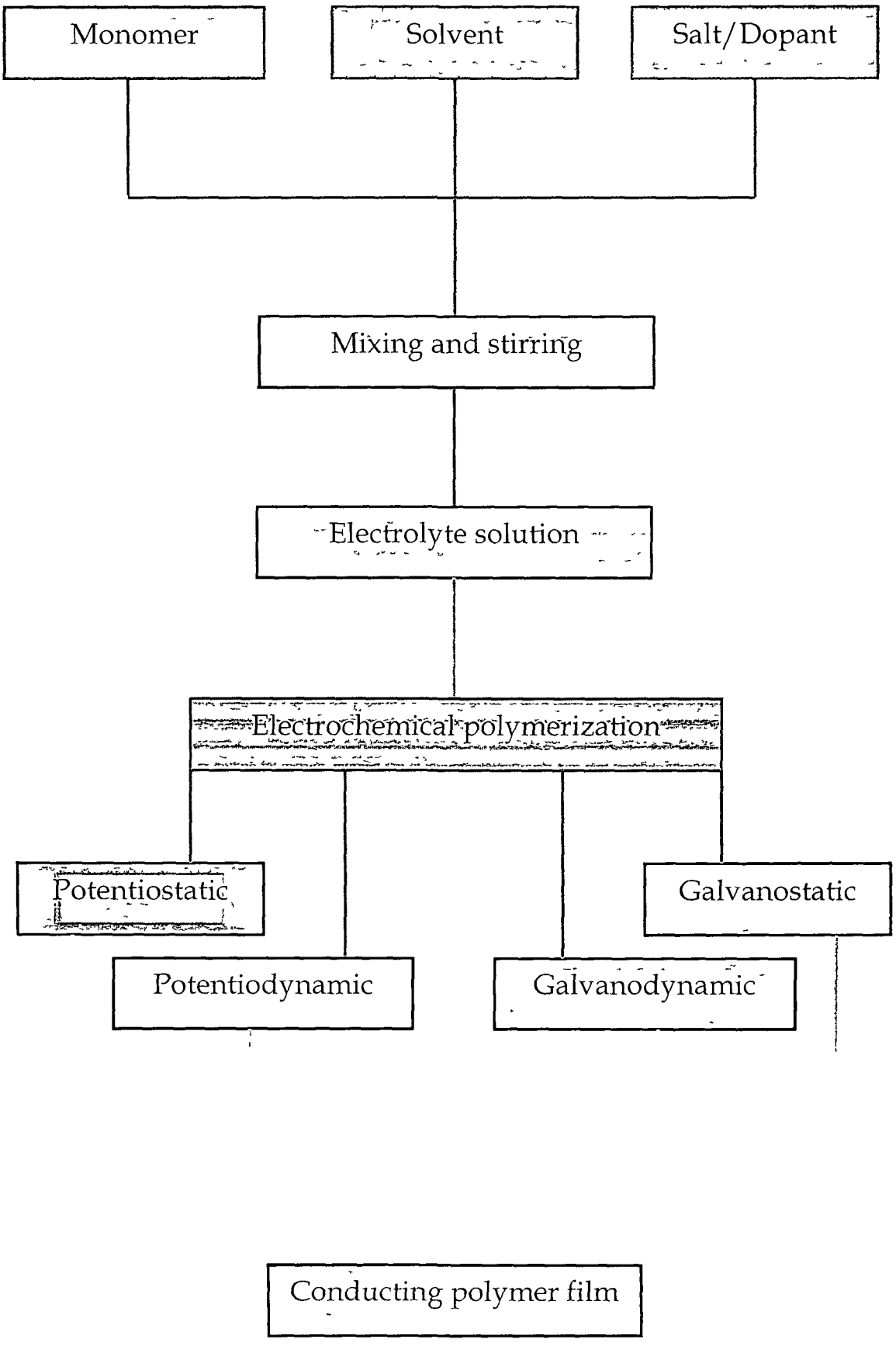


Figure 3.2: Block diagram of electropolymerization of conducting polymer film.

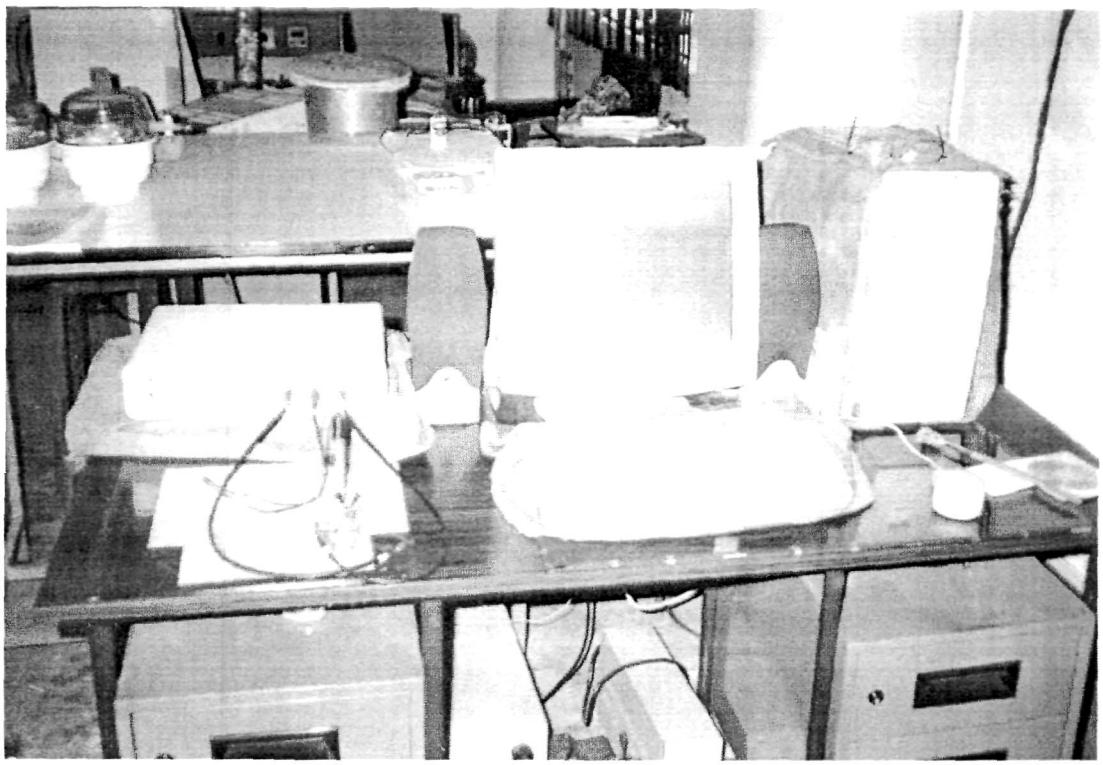

Figure 3.3: Potentiostate/galvanostate set up for electropolymerization of conducting polymer films.

a few hundred mV beyond the monomer oxidation potential is commonly used to produce conducting polymer films of almost comparable quality to that of potentiostatic polymerization. Galvanostatic i.e., constant current and galvanodynamic cyclic mode polymerizations can also be used when control of charge is desired. However it is well known that galvanostatic/galvanodynamic modes yield polymer films of poorer morphology, conductivity and general quality, hence these modes are not further tried in the present work.

Fig. 3.2 shows the block diagram of electropolymerization of conducting polymer films. The experimental set-up for electropolymerization is shown in Fig. 3.3. The electrolyte solution has been prepared by adding particular monomer (aniline, pyrrole or 3-methylthiophene) in desired molar concentration to the solvent (double distilled water or acetonitrile). The dopant salt or the protic acid is then added to the solution and stirred thoroughly to make a clear solution. Required amount of the electrolyte is then taken in the electrochemical cell. The stainless steel counter electrode, SCE reference

electrode and the working electrode, all three fitted in a holder are placed into the electrochemical cell and then connected to the potentiostate/galvanostate from where the desired potential is applied (Fig. 3.3).

The electropolymerization of polyaniline, polypyrrole and poly-3-methylthiophene conducting polymer films have been carried out potentiostatically as well as potentiodynamically from a solution containing the monomer and the dopant. Potentiostatic deposition of polyaniline has been carried out at constant potential of 950 mV against SCE reference electrode in three electrode system, whereas for two electrode set-up the applied potential is 1100 mV. The potentiodynamic polymerization of polyaniline has been carried out by sweeping the potential from -200 mV to 1200 mV in two electrode set-up of the electrochemical cell. When the SCE reference electrode is used, the potential range for potentiodynamic deposition is -100 mV to 950 mV because of the 241 mV potential of the SCE applied against the working electrode. Polypyrrole films are potentiostatically deposited at 800 mV with SCE reference electrode and for potentiodynamically deposition the voltage is swept between -200 mV and 850 mV with SCE as the third electrode. The potentiostatic deposition of poly-3-methylthiophene has been carried out by applying a constant potential of 1700 mV against SCE reference electrode. The duration of the deposition is dependent on the rate of polymerization and the thickness requirement. In most cases potentiostatic deposition has been carried out for about 5 to 10 minutes to obtain the desired thickness of about 25-30 μm. For poly-3-methylthiophene, the deposition time is about 20 minutes as the polymerization rate is slow in acetonitrile. The potentiodynamic deposition has been carried out for about 75 cycles to obtain the required thickness of about 25-30 μm.

**3.3 Preparation of gel polymer electrolyte:**

PVDF-HFP(20w/o)-PMMA(10w/o)-$LiCF_3SO_3$(10w/o)-PC+DEC(57w/o)-$SiO_2$(3w/o) gel polymer electrolyte has been prepared by solution casting technique [210] following the procedure as given below:

(i) P(VDF-HFP) (20 wt%) and PMMA (10 wt%) polymers are dissolved in tetrahydrofuran.

(ii) Salt $LiCF_3SO_3$ (10 wt%) is dissolved in propylene carbonate (PC) and diethyl carbonate (DEC) (57 wt%) with equal proportions of PC and DEC.

(iii) Both polymer and salt solution are mixed together and stirred at 50°C.

(iv) Ceramic filler $SiO_2$ (3 wt%) is added to the above polymer-salt solution and continuously stirred at 50°C for 12 - 14 hours to make the solution homogeneous and viscous.

(v) Above viscous solution is then cast on the glass plates and allowed to evaporate the solvent at room temperature.

The gel polymer electrolyte thus prepared is used as the electrolyte in fabrication of all-polymer redox supercapacitors.

### 3.4 Fabrication of all polymer redox supercapacitors:

All polymer redox supercapacitors have been fabricated with conducting polymer electrodes and gel polymer electrolyte having the following configuration:

**ITO | conducting polymer | gel polymer electrolyte | conducting polymer | ITO**

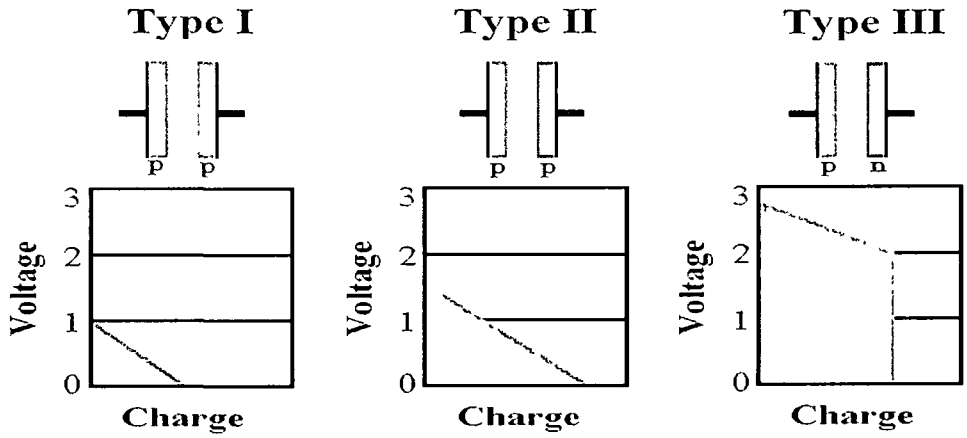


Figure 3.4: Configurations of type I, II and III supercapacitors.

ITO acts as current collector on both sides of the capacitor. With this configuration three types of supercapacitor can be fabricated which are termed as type I, II and III as shown in Fig. 3.4. Type I has symmetrical (same material) electrodes coated with polymers that are only p-dopable e.g.,

ITO | p-doped polyaniline | gel polymer electrolyte | p-doped polyaniline | ITO

Type II configuration utilizes asymmetrical (different materials) electrodes of p-dopable polymers e.g.,

ITO | p-doped polyaniline | gel polymer electrolyte | p-doped polypyrrole | ITO

The type III configuration employs symmetrical (same material) electrodes of a conducting polymer that can be both n- and p-doped:

ITO | p-doped polythiophene | gel polymer electrolyte | n-doped polythiophene | ITO

All three types of supercapacitors are fabricated and characterized by cyclic voltammetry, capacitance measurements, charge-discharge and electrochemical stability test for 10,000 cycles of charging-discharging.

### 3.5 Swift Heavy Ion (SHI) Irradiation:

Swift heavy ion irradiation experiments have been carried out in Material Science (MS) and General Purpose Scattering Chamber (GPSC) beam lines under high vacuum at Inter University Accelerator Centre (IUAC), New Delhi. For ion irradiation, conducting polymer samples are of 1cm × 1cm area on ITO glass substrate and fixed on sample holder (ladder) made up of copper (in MS) and Stainless Steel (in GPSC). Material Science (MS) ladder is rectangular and 24 samples can be loaded at a time with six samples on each side.

GPSC ladder

Figure 3.5: Material Science Beam Line and Chamber at IUAC, New Delhi.

is hexagonal and 36 samples can be loaded in a single run. The samples are put in the respective MS and GPSC vacuum chambers. Figs. 3.5 and 3.6 show the MS and GPSC beam lines and chambers respectively. The samples during SHI irradiation and ladder movement (up, down and rotation) are monitored and controlled from control room in IUAC, New Delhi.

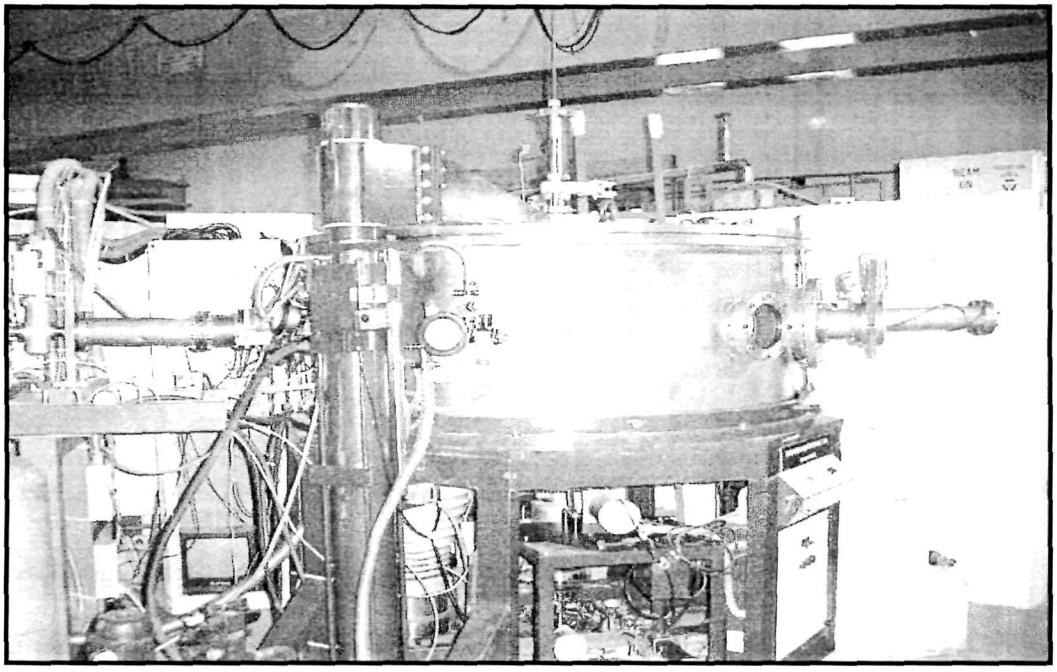

Figure 3.6: GPSC Beam Line and Chamber at IUAC, New Delhi.

### *3.5.1 Parameters Related to Ion Irradiation:*

#### *3.5.1.1 Fluence ($\phi$):*

Fluence is defined as the total number of irradiating ions incident per square centimeter (ions/$cm^2$) of sample. It varies from sample to sample depending upon its size and material.

Fluence is calculated using the following formula

$$\text{Fluence}\ (\phi) = \frac{\text{Time}\ (t) \times \text{Beam Current} \times \text{pnA}}{\text{Charge State}} \qquad (3.1)$$

Beam currents for ion irradiation experiments are usually taken in the range of 1-5 nA.

$$1\ \text{pnA}(\text{particle nano-ampere}) = \frac{10^{-9}\ \text{Coul/sec}}{1.6\text{x}10^{-19}\ \text{Coul}} = 6.25\text{x}10^{9}\ \text{particles/sec} \qquad (3.2)$$

### 3.5.1.2 Count:

During ion irradiation process, fluences have been recorded by using a counter. Following relation relates the counts and the fluences

$$\text{Counts} = \frac{\phi\, q\, e}{S} \qquad (3.3)$$

Where $\phi$ is the fluence,

q is the charge state of ion beam,

e is the electronic charge ($1.6\times10^{-19}$ coulomb ),

S is the scale of counter

### 3.5.1.3 Beam Energy:

The energy of the accelerated ion beam depends on charge state (q) of the ion and the terminal potential $V_T$

$$E\,(MeV) = (q + 1)\, V_T + V_{inj} \qquad (3.4)$$

For the 15 UD Pelletron at Inter University Accelerator Centre, New Delhi, India, the terminal potential $V_T$ is in the range of 10 MV to 15 MV and Injector potential ($V_{inj}$) is in the range of 250 to 350 keV. The projected range of $Ni^{12+}$and $Si^{10+}$ ion beams used in the present work is calculated by SRIM-2003 code (SRIM-Stopping and Ranges of Ions in Matter). Table 3.4 gives the incident energy, corresponding electronic energy loss ($S_e$), nuclear energy loss ($S_n$) and projected range obtained from the SRIM-2003 code for $Ni^{12+}$and $Si^{9+}$ ion beams in polyaniline, polypyrrole and poly(3-methylthiophene) conducting polymer films.

Table 3.4: SRIM data for $Ni^{12+}$ and $Si^{9+}$ ions in different conducting polymers.

| Polymer | Ion | Energy (MeV) | $S_e$ (MeV/mm) | $S_n$ (MeV/mm) | Projected Range (μm) |
|---|---|---|---|---|---|
| Polyaniline | Ni | 160 | $4.655\times10^{3}$ | $5.310\times10^{00}$ | 40.04 |
| | Si | 120 | $1.415\times10^{3}$ | $9.859\times10^{-1}$ | 64.46 |
| Polypyrrole | Ni | 160 | $4.489\times10^{3}$ | $5.135\times10^{00}$ | 41.63 |
| | Si, | 120 | $1.365\times10^{3}$ | $9.521\times10^{-1}$ | 66.90 |
| Poly-3-methylthiophene | Ni | 160 | $4.205\times10^{3}$ | $5.046\times10^{00}$ | 44.04 |
| | Si | 120 | $1.280\times10^{3}$ | $9.311\times10^{-1}$ | 71.38 |

The thicknesses of the conducting polymer films (25 - 30 μm) are kept less than the calculated range by SRIM programme such that all the incident ions crossed through the samples.

### 3.6 Characterization of conducting polymer films:

#### *3.6.1. Cyclic voltammetry:*

Cyclic Voltammetry (CV) is a versatile electroanalytical technique for the study of electroactivity of electrode and electrolyte combinations. CV consists of linearly cycling the potential of an electrode immersed in an unstirred solution while measuring the resulting current. Thus, a cyclic voltammogram is a display of current *versus* potential. The most useful aspect of this technique is its application to the qualitative diagnosis of electrode reactions. The cyclic voltammetry of conducting polymer film, one of the most basic electrochemical characterization, is a measurement of current resulting from application of a variable voltage to the conducting polymer film i.e., it is an I-V curve with a variable voltage fixed scan rate in mV/s. In linear sweep cyclic voltammetry, the potential applied to the working electrode of the cell is a triangular wave function of time. The potential of the working electrode is continuously swept back and forth between two set voltages at a constant scan/sweep rate. The initial potential is chosen to be a potential value where no electrode reactions take place. The current that flows through the working electrode is measured as a function of scanned potential. The reversal of the potential scan direction gives rise to a current flow due to the reversible electrode reaction in the forward sweep. The cyclic voltammogram can be directly correlated with electrochromism of the conducting polymer, if it is electrochemically active, in the sense that the redox peaks observed in the cyclic voltammogram usually coincide with the change of colour of the conducting polymer. While scanning towards positive potential, the current is denoted 'anodic' with corresponding peaks as anodic peaks and while scanning towards negative potential the current is called cathodic and, hence corresponding peaks are called cathodic peaks. The cyclic voltammogram of a conducting polymer provides information

regarding the electrochemical window within which the doping/dedoping i.e. the redox process is reproducible, though not necessarily electrochemically reversible and beyond which oxidative or reductive decomposition of the conducting polymer occurs. Thus the first measurement performed on a conducting polymer film is to determine this electrochemical window, oxidative peaks and reduction peaks. Cyclic voltammograms have well established characteristics for such properties as anodic/cathodic peak separation, peak full width at half maxima (FWHM) and scan rate dependence. Some other properties can also be obtained from cyclic voltammogram, such as oxidation potential $E_o$, reduction potential $E_r$, background (residual) current represented by plateau following the peaks and integrated current (area) under the peaks which represents the total charge Q.

Another aspect of cyclic voltammetry is the scan rate dependence. According to well established electrochemical treatments, for a behaviour dominated by diffusion effects, $i_p$ is proportional to $V^{1/2}$, whereas for a material localized on an electrode surface such as conducting polymer film, $i_p$ is proportional to V. For most conducting polymer films, the latter case obtains thus indicating surface-localized electroactive species. The structure of the cyclic voltammograms of conducting polymer films also depends on the dopant ion size. The slope of the cyclic voltammograms differs for different dopants. A lower slope usually implies slower dopant diffusion in and out of the conducting polymer giving broader peaks attributed to larger size dopant ions. In general, sharper large peaks are given by smaller size dopants, which find facile diffusion in and out of conducting polymer films.

The cyclic voltammetry of the electropolymerized conducting polymer films have been carried out in the three electrode single compartment electrochemical cell (Fig. 3.1) containing electrolyte solution of the salt. The electrochemical polymerization and the cyclic voltammetry studies have been carried out using a potentiostate/galvanostate (Analytical Electrochemical Workstation, AEW2, Sycopel Scientific, UK). All the cyclic voltammetry

experiments have been carried out within the electrochemical window while similar conditions are maintained for cyclic voltammetry as that for synthesis.

*3.6.2 Conductivity measurements:*

Four-point probe is the most reliable method for determining the conductivity of a conducting polymer film [211]. As shown in Fig. 3.7, the apparatus consists of four probes about 1 mm apart in a straight line that project down from a stage that can be raised and lowered. A current from a high impedance current source is supplied through the outer two and the resulting voltage is measured across the inner two probes that are at distance $X_1$ and $X_2$ from the positive tip of the current source. For a film of thickness t<<s, where s the distance between the inner and outer probes, the resistivity ρ of the film is given by the following relation [212]:

$$\rho = \frac{\pi t}{\ln 2}\left(\frac{V}{I}\right) \qquad (3.5)$$

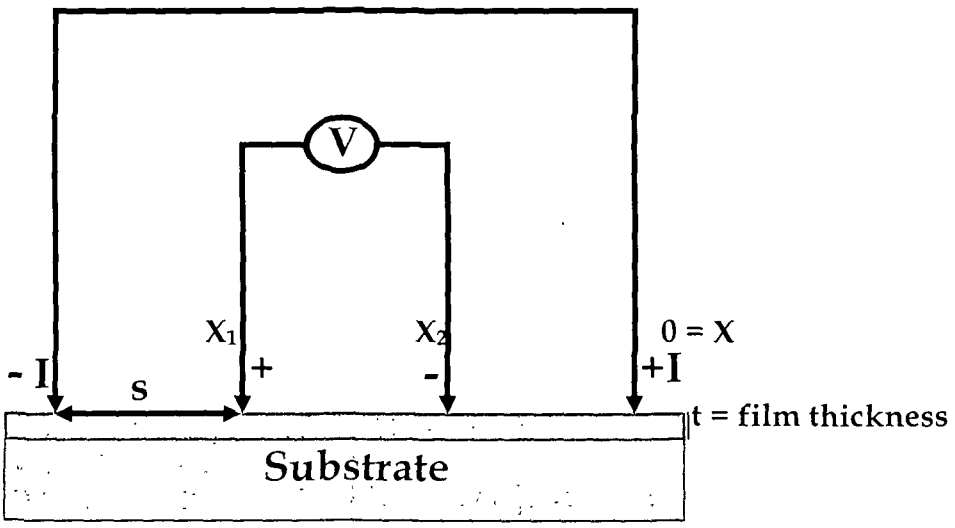


Figure 3.7: A schematic diagram of four-point probe for measuring conductivity of conducting polymer films.

For a known value of current I, by measuring the potential V, the resistivity ρ of the film of a given thickness can be calculated. The reciprocal of the resistivity ρ is the conductivity σ of the film. The only drawback of this type of measurement is that it is important to avoid deformation of the film while lowering the tips onto the film surface. This arrangement of probes eliminates

any contribution to the measurement of the resistance from the probes themselves. The dc conductivity studies of the conducting polymer films have been carried out using laboratory standard (Scientific Equipments, India, Model DFP-20) four-point probe set-up at room temperature.

### *3.6.3 UV-Vis absorption spectroscopy:*

UV-Vis spectroscopy provides key information about the electronic transitions and hence the electronic structure of the material. Ultraviolet-visible absorption spectroscopy involves the absorption of ultraviolet/visible light (wavelengths (λ) between 190 and 800 nm) by a molecule raising electrons from a ground/lower electronic state to an excited/higher electronic state.

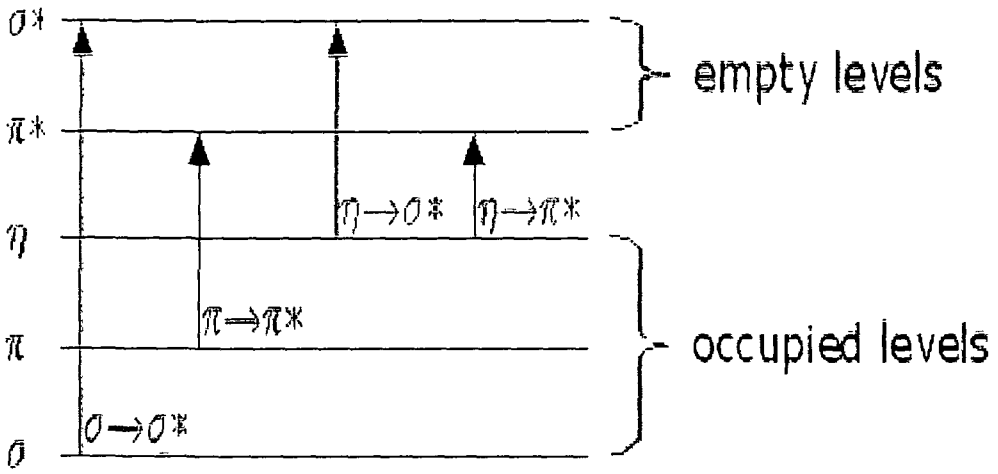


Figure 3.8: Types of electronic transitions.

There are several types of electronic transitions possible (Fig. 3.8) in a molecule including:

σ to $\sigma^*$ (alkanes)

σ to $\pi^*$ (carbonyl compounds)

π to $\pi^*$ (alkenes, carbonyl compounds, alkynes, azo compounds) (Fig. 3.9)

η to $\sigma^*$ (oxygen, nitrogen, sulfur, and halogen compounds)

η to $\pi^*$ (carbonyl compounds)

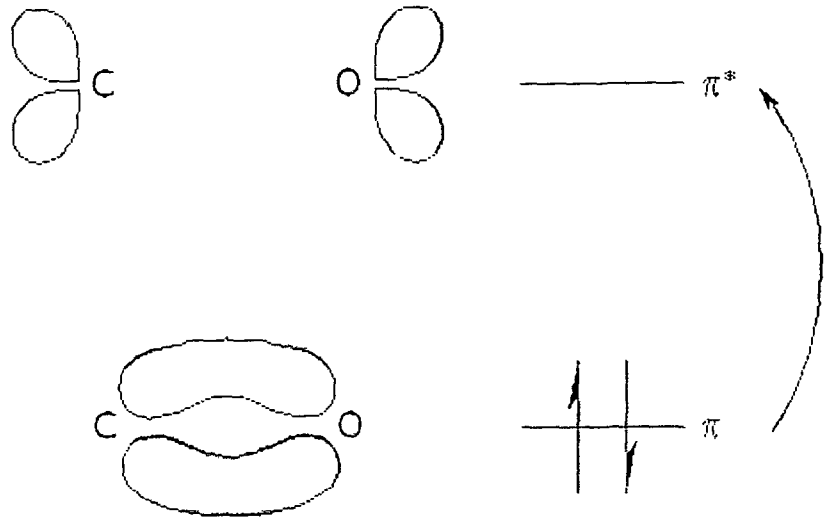


Figure 3.9 : π to π* transition of electrons.

Transitions from the highest occupied molecular orbital (HOMO) to the lowest occupied molecular orbital (LUMO) require the least amount of energy and are, therefore, usually the most important. Not all the transitions, those are possible, are observed. Some electronic transitions are "forbidden" by certain selection rules. UV absorptions are generally broad because vibrational and rotational levels are "superimposed" on the electronic levels.

UV-Vis spectroscopy studies of the conducting polymer films have been carried out for the study of optical absorption characteristics and hence the energy band structure of conducting polymer. The UV-Vis spectra are recorded using a Beckman DU® 530 Life Science UV-Vis spectrophotometer.

### *3.6.4 Fourier Transform Infrared (FTIR) spectroscopy:*

Fourier transform infrared (FTIR) spectroscopy is a powerful analytical tool for characterizing and identifying organic molecules, chemical bonds (functional groups) and the molecular structure of organic compounds. The wavelength of infrared radiation absorbed is characteristic of stretching/bending vibrational modes of a chemical bond. The most useful range for the identification of the compounds is the near and mid-infrared region as most of the molecular vibrations lie in these frequency regions. FTIR

spectra of pure compounds are generally so unique that they are like molecular fingerprints. Infrared radiation is absorbed by a molecule and converted into the energy of molecular vibration. A single vibrational energy change is accompanied by a number of rotational energy changes, consequently vibrational spectra appear as bands rather than as discrete lines. Band positions are presented as wave numbers (in $cm^{-1}$). Band intensities are expressed either as transmittance 'T', the ratio of the radiant power transmitted by the sample to the radiation incident on the sample or the absorbance 'A', logarithm to the base 10 of the reciprocal of the transmittance, $A = \log_{10}(1/T)$. Intensity in terms of percentage of transmission and frequencies in wavenumbers are depicted in a two dimensional plot called FTIR spectrum. Determination of frequencies, at which the sample absorbs IR radiation, allows the identification of the sample's chemical make-up, since functional groups are known to absorb radiation at specific frequencies. Identification of the sample composition is called qualitative analysis. FTIR spectroscopy is known to possess two main advantage over conventional techniques, viz., (i) it makes use of all the frequencies from the source simultaneously, and (ii) the sensitivity of the Fourier Transform method is greater. These advantages are called "Fellget" and "Jacquinot" effects respectively.

The key components of a Fourier Transform system are the source, the Michelson interferometer and the detector. To use the FTIR instrument, the light from a continuous source is directed onto the sample of interest and the intensity is measured using an infrared detector. The Michelson interferometer provides a means for the spectrometer to measure all optical frequencies simultaneously. The interferometer modulates the intensity of the individual frequencies of radiation before the detector picks up the signal.

The FTIR spectroscopy study of the conducting polymer films has been conducted for understanding the bond structure and compositional and doping studies of the conducting polymers. The FTIR spectra are recorded by using Nicolet Impact 410 FTIR spectrophotometer.

### *3.6.5 Scanning Electron Microscopy (SEM):*

The scanning electron microscope (SEM) is one of the most versatile instruments available for examination and analysis of microstructural and morphological features of solid objects. The primary reason for the usefulness of SEM lies in its high depth of focus and high resolution that can be obtained when bulk objects are examined. The SEM study has been carried out using JEOL JSM-35CF, JEOL JSM-5600 and JEOL JSM-6360, scanning electron microscopes with resolutions in the range of 5 - 15 nm to examine the surface morphology and porosity. The equipments provide a range of magnifications from 10X to 180,000X. The micrographs are taken at 20 kV accelerating voltage and magnification is fixed according to need from 2000X to 10000X.

### *3.6.6 X-ray diffraction (XRD):*

X-ray diffraction is one of the most important structural characterization tools used in materials science. X-ray diffraction patterns give information about different crystal structural parameters like crystallite size, d-spacing, diffraction planes, structure, phase and lattice constants. In addition to the crystal structure, XRD is applied for various other purposes such as chemical analysis, stress measurement, phase equilibria, measurement of particle size, determination or orientation of single crystals or the ensemble of orientations in a polycrystalline or polymeric aggregate, order-disorder transformation etc. The intensities and the angles of diffracted X-ray beams are related to atomic arrangement of the crystal. In the case of polymeric material, XRD is used to determine the proportions of crystalline and amorphous phases in terms of the degree of crystallinity. This technique is based on the scattering of X-rays by crystals defined by the Bragg's law. The X-ray diffraction patterns for various conducting polymer films have been recorded using the Rigaku make D-Max series diffractometer mounted on a Rigaku X-ray generator employing Cu $K_\alpha$ radiation. The generator is operated at 30 kV and 20 mA and scanning speed is fixed at 1 °/min in $2\theta$ varying from 5° to 80°.

### *3.6.6.1 Degree of crystallinity:*

Generally a polymer is neither fully crystalline nor fully amorphous. The degree of crystallinity of a polymer can be measured by X-ray diffraction. A typical X-ray diffractogram consists of a plot of X-ray counts received by a detector versus the scattering angle of the detector as shown in Fig. 3.10. Depending upon its degree of crystallinity, typical X-ray diffractogram of a polymer sample has sharp peaks superimposed on a broad amorphous hump as shown in Fig. 3.11. Total area under the diffractogram is the sum of the crystalline peaks and broad amorphous hump.

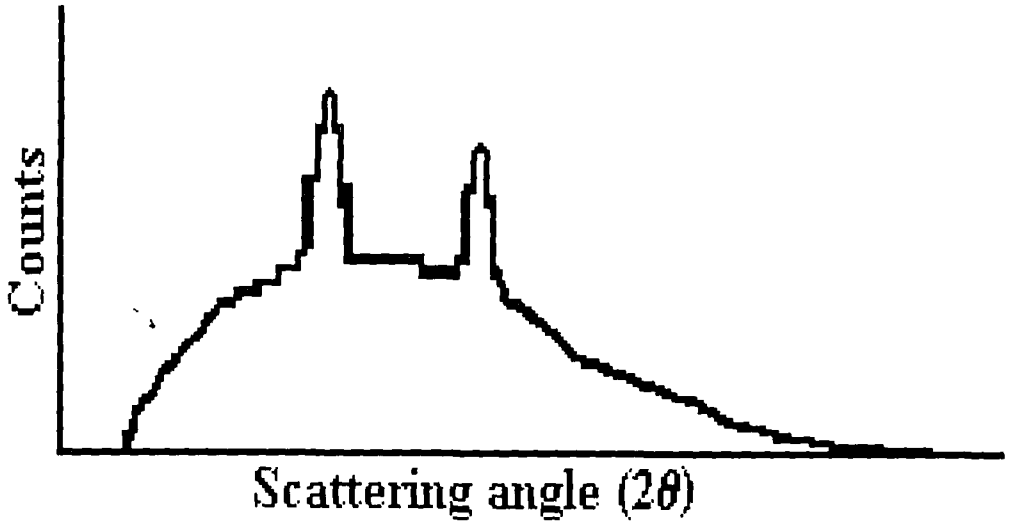


Figure 3.10: Typical X-ray diffractogram of a polymer sample.

For example, if a typical X-ray diffractogram has two crystalline peaks with areas A1 and A2 superimposed on a broad amorphous hump with an area of A3, then the degree (percentage) of crystallinity, K, of the polymer will be

$$K = \frac{k_c(A_1 + A_2)}{k_c(A_1 + A_2) + k_a A_3} \tag{3.5}$$

where $k_a$ and $k_c$ are proportionality constants for the amorphous and crystalline phases respectively. For reasonable accuracy for polymers assuming $k_a = k_c$, the expression (3.5) for the degree of crystallinity K becomes:

$$K = \frac{A_1 + A_2}{A_1 + A_2 + A_3} = \frac{S}{S_0} \qquad (3.6)$$

To define the degree of crystallinity in percentage, the equation (3.6) can be written as:

$$K = \frac{A_1 + A_2}{A_1 + A_2 + A_3} x100\% = \frac{S}{S_0} x100\% \qquad (3.7)$$

where S is the sum of areas of all the crystalline peaks and $S_0$ is the sum of areas of crystalline peaks and amorphous hump i.e. total area under the diffractogram. Area has been calculated by dividing the X-ray diffractogram into minute square (0.5 × 0.5 $mm^2$) grids and counting the number of grids.

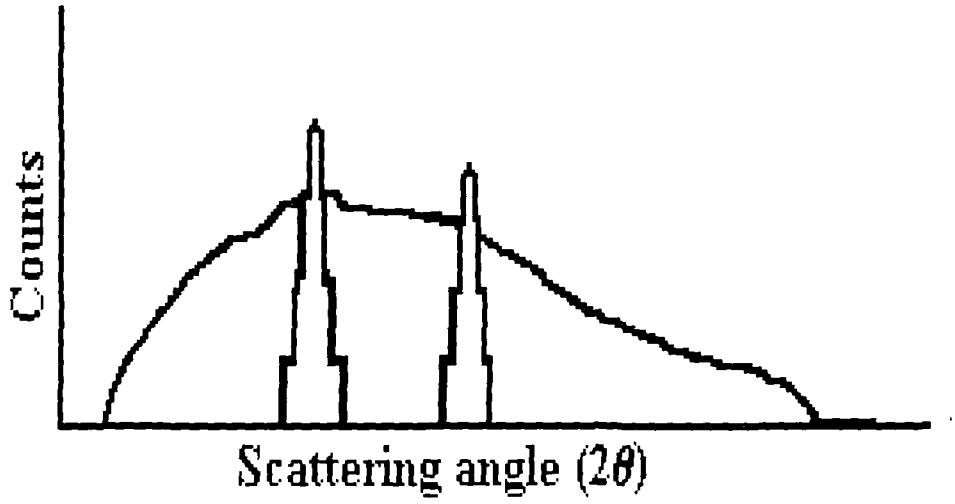


Figure 3.11: XRD pattern with crystalline peaks and a broad amorphous hump.

The degree of crystallinity in a polymer depends on the following parameters:

- the secondary valence bonds that can be formed
- the structure of the polymer chain (degree of order)
- the physical treatment of the polymer
- the thermal history of the polymer
- the molecular weight of the polymer

**3.7 Characterization of supercapacitors:**

The characterization of the all polymer redox supercapacitors have been carried out by recording the cyclic voltammograms at different scan rates,

galvanostatic charge discharge cycles at 100 μA and the stability of the supercapacitors are tested for 10,000 charge-discharge cycles.

### *3.7.1 Cyclic voltammetry and stability test of supercapacitor:*

Cyclic voltammetry provides a measure of a supercapacitor's charge-discharge response with regard to a changing voltage, and is therefore a means of evaluating capacitance. To perform cyclic voltammetry tests, a series of changing voltages at a constant sweep rate (dV/dt) is applied and the response current is recorded. The capacitance is then calculated by using the following equation 3.8, where *I* is the current and *s* is the sweep rate in V/s [213].

$$C = \frac{I}{s} \tag{3.8}$$

Where I is the current and S is the scan rate in V/S.

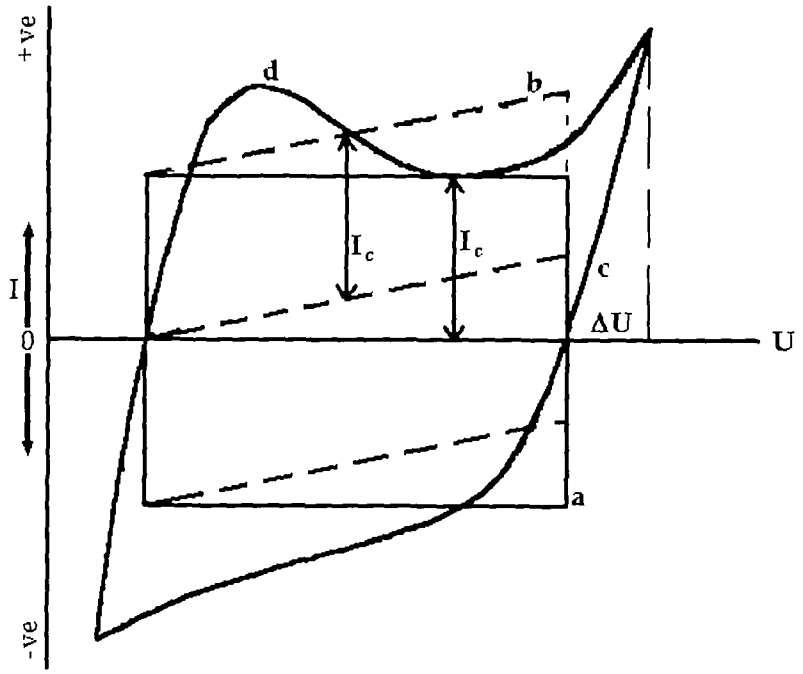


Figure 3.12: Comparison of ideal and real cyclic voltammograms (a) Ideal capacitor, (b) real capacitor with resistance, (c) capacitor with carbon material, (d) influence of redox reactions, ΔU- voltage delay and $I_c$- capacitive current.

An ideal capacitor with no internal resistance would display a rectangular shape, but most real electrochemical double layer capacitor (EDLC) voltammograms take the shape of a parallelogram with irregular peaks (Fig.

3.12). Prominent peaks that occur within narrow voltage windows are usually evidence of pseudocapacitive behaviour. Faster sweep rates correspond to charging and discharging at higher power levels. Multiple plots obtained at increasing sweep rates are therefore often displayed on the same graph to demonstrate the impact of power levels on the charging characteristics. From such plots it is evident that capacitance decreases at higher frequencies. Voltammetry can also provide an indication of the degree of reversibility of an electrode reaction. A voltammogram that depicts a mirror-image represents a reversible reaction, but an irreversible process will have two separate charge and discharge profiles, the ends of which do not meet. Reversibility is an important factor in the search for new materials.

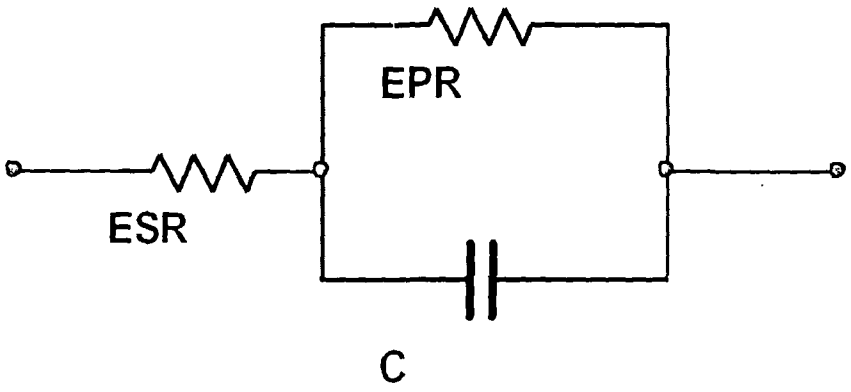


Figure 3.13: The classical equivalent circuit of an EDLC.

Fig. 3.13 shows an equivalent circuit representing a real Electrochemical Double Layer Capacitor (EDLC). The current flowing through the supercapacitor rises and falls with potential in the cyclic voltammetry could be described by this equivalent circuit. The cyclic voltammogram of the supercapacitor are recorded at different scan rate with the same potentiostate/galvanostate as described in the section 3.6.1. The capacitance of the supercapacitor is calculated using the eqn. 3.8. Cyclic voltammogram of the supercapacitor are taken for 10,000 cycles and the capacitance is measured after every 1000 cycles to check the stability i.e., the cycle life of the supercapacitors.

### *3.7.2 Charge discharge studies:*

The charge-discharge of the polymer redox supercapacitors have been carried out galvanostatically at 100 μA using a computer controlled battery testing unit (Maccor 2300). A simplified circuit for charging and discharging a capacitor is shown in Fig. 3.14, where C is the capacitor, V is a voltage/power source, $R_1$ and $R_2$ are two variable resistors. A and B are two switch positions for charging and discharging of the capacitor, respectively. The current in the circuit is adjusted by varying the value of the resistance $R_1$ for charging and $R_2$ for discharging, which is controlled automatically according to the inputs from the computer. There are different modes of charging and discharging e.g., constant current i.e., galvanostatic mode, constant potential i.e., potentiostatic mode and mixed mode i.e., combination of potentiostatic charging followed by galvanostatic discharging or vice versa. The potential is measured across the capacitor at fixed time intervals (say, 1 second) and thus a data sheet of voltage vs. time is obtained.

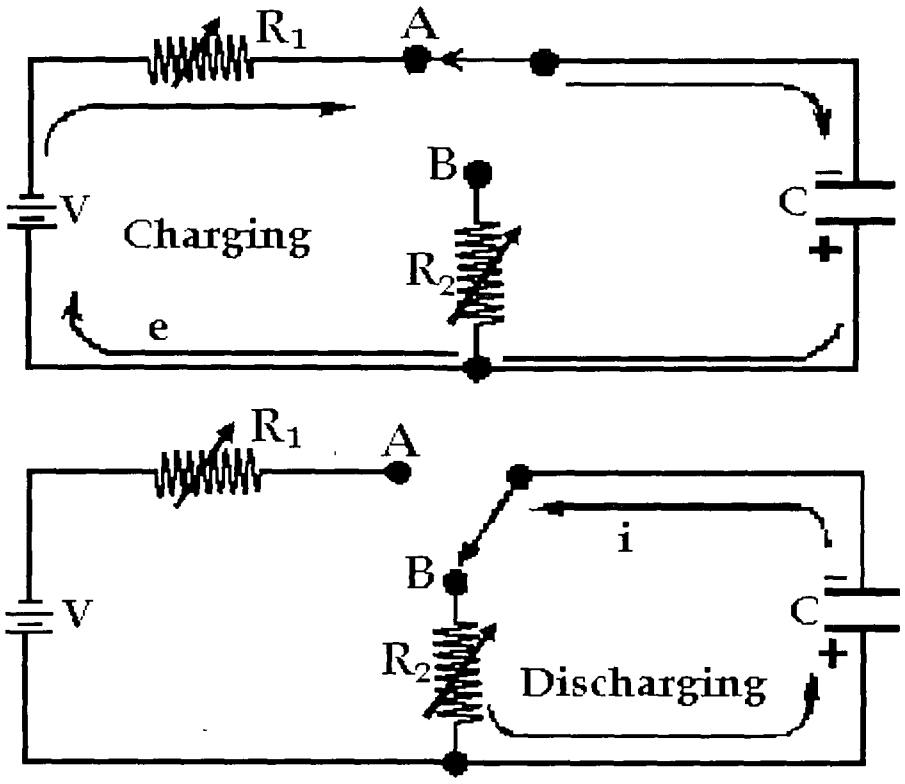


Figure 3.14: Circuit diagram for charging and discharging a capacitor.

A battery testing unit connected to a PC (Maccor 2300) (Fig. 3.15) is used for charge-discharge testing of the supercapacitors. In galvanostatic mode, the capacitor has been charged at a constant current of 100 μA and the potential rise is recorded against time. The capacitor has been charged up to 0.95 V and then the discharging started. In discharging the capacitor galvanostatically at 100 μA a load $R_2$ is connected and the fall in potential with time is recorded. The complete operation of charging-discharging i.e. adjusting the resistances $R_1$ and $R_2$, changing the switch position for first charging followed by discharging are controlled automatically according to the input values given to the computer.

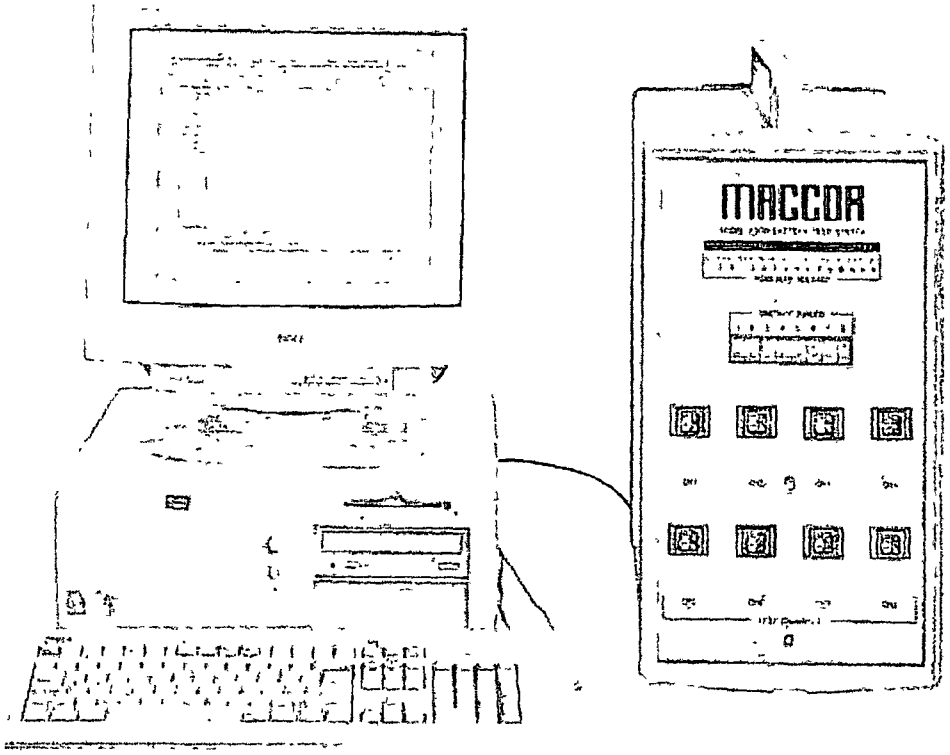


Figure 3.15: Battery testing unit connected to a PC (Maccor 2300).

When a capacitor cell is charged galvanostatically i.e. at constant current 'i', the voltage 'V' developed across the cell can be expressed as:

$$V = iR_s + \frac{\int i.dt}{C} \qquad (3.9)$$

Since current 'i' is constant, the expression can be written as:

$$V = i\left(R_i + \frac{t}{C}\right) \qquad (3.10)$$

Thus for a current step, the voltage across an ideal capacitor cell, whose capacitance is C, increases linearly with time (Fig. 3.16). After full charging up to the full capacity or to the desired value of potential, it can be discharged at constant current. The decrease in potential across the cell is also linear with time for an ideal capacitor (Fig. 3.16).

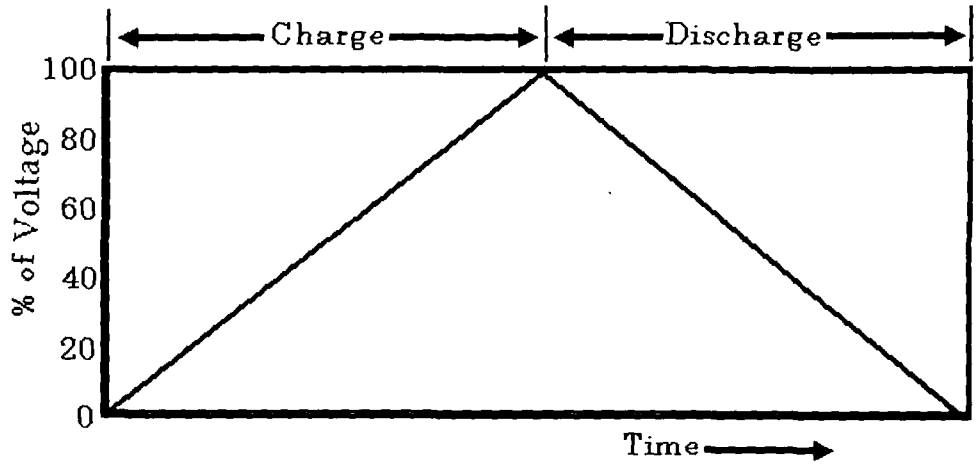


Figure 3.16: Charge discharge cycle of an ideal capacitor.

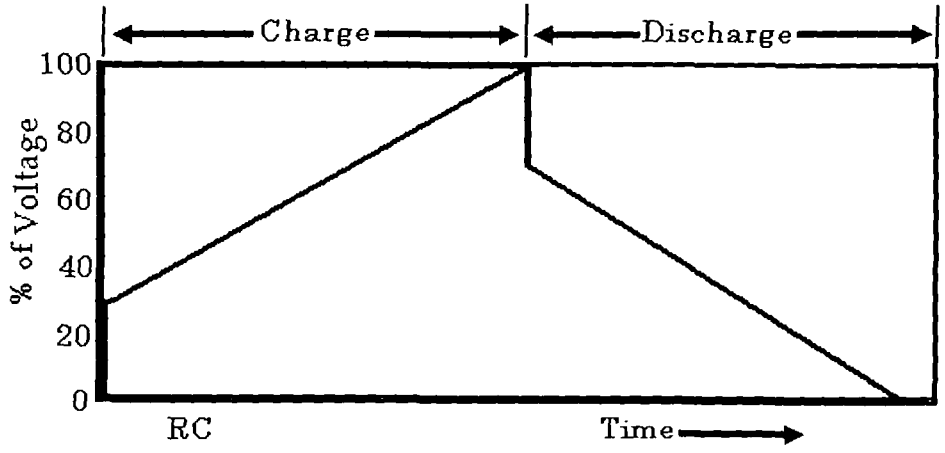


Figure 3.17: Charge discharge cycle of a real capacitor.

In real capacitors, the initial sharp rise and fall in potential is observed while charging and discharging respectively. This is attributed to an ohmic loss due to internal resistance of the capacitor cell (Fig. 3.17). The discharge capacitance of the capacitor cell can be evaluated from the linear region of the curve following the relation:

$$C = i\frac{\Delta t}{\Delta V} \qquad (3.11)$$

where $\Delta V$ is the change in potential in time $\Delta t$.

The coulombic efficiency $\eta$of the capacitor cell can also be calculated from the galvanostatic charge-discharge experiment using the following relation:

$$\eta = \frac{\Delta t_D}{\Delta t_C} \times 100\% \qquad (3.12)$$

where $\Delta t_D$ and $\Delta t_C$ are the times of charging and discharging respectively.

The internal resistance of the supercapacitors is calculated from the steep rise in potential of the charge-discharge plot using the relation:

$$R = V/i \qquad (3.13)$$

where 'i' is the charging current and V is the magnitude of vertical rise in or fall of potential during charging or discharging respectively.

The energy density of the supercapacitors with conducting polymer electrodes is calculated using the relation:

$$E_d = \tfrac{1}{2} CV^2 \qquad (3.14)$$

where C is the discharge capacitance of the electrode material (in F/gm) and V is the working potential i.e., the highest potential up to which the supercapacitor exhibit capacitive behaviour.

# CHAPTER IV

# POLYANILINE: ELECTROPOLYMERIZATION, CHARACTERIZATION AND SHI IRRADIATION

Polyaniline is an exceptionally versatile material among the class of conducting polymers with applications ranging from battery electrodes to chemical sensing [214-227]. Polyaniline can be easily synthesized electrochemically [15, 69, 228-237] as well as chemically [227]. Electrochemical polymerization of aniline monomer gives homogeneous polyaniline conducting polymer films on conducting or semiconducting substrates. Polyaniline can be synthesized in aqueous media and after drying the polymer films can be employed in any application, even in non-aqueous systems [237]. Polyaniline films can be grown from non-aqueous media like acetonitrile for non-aqueous applications. The electropolymerization of aniline in aqueous medium leads to partial oxidative degradation of the deposited polyaniline to p-aminophenol and p-bezoquinone, which decreases the charge capacity of the resulting polymer film [238]. The non-aqueous medium can provide access to higher cell voltage due to an increased potential window of electrochemical stability of the solvent [237]. A few studies on synthesis of polyaniline in organic medium have been reported as compared to those in aqueous medium. Polyaniline has been electropolymerized from three types of solutions [239-242]. The first one involved the electropolymerization of polyaniline from an organic solvent such as acetonitrile [239]. Larger donor level is required in organic solvent to keep both the aniline and aniline radical protonated to obtain a good conductivity. The second approach is based on the use of a similar solvent to which organic acid has been added that kept the aniline in the protonated state [240]. It is widely believed that the polymerization of polyaniline occurs in acidic medium involving the coupling of aniline radical cation [240]. Therefore, the addition of acid enhances the polymerization efficiency and also electroactivity of the resulting polymer. In the third approach, an anilinium tetrafluoroborate salt

dissolved in acetonitrile has been used as precursor for electropolymerization of polyaniline films [241, 242].

Tremendous efforts have been made on the studies of polyaniline conducting polymer films [15, 69, 220, 227, 230-237, 243-247]. Most of the reported works in literature deals with various studies like UV-Vis, FTIR, conductivity, cyclic voltammetry and corrosion etc. but few reports have appeared on the characterizations like XRD, SEM and electrode application [237, 245-247]. Swift heavy ion (SHI) irradiation on polymeric materials is a relatively recent area of research and a few studies of SHI irradiation on polyaniline conducting polymers have been reported [75]. SHI irradiation of polyaniline above 100 MeV energy for electrode application has been investigated for the first time in the present studies.

Polyaniline has several disadvantages like poor processability, environmental stability etc. In this study a sincere effort has been made for systematic study of polyaniline conducting polymer films synthesized in different electrolytes with different dopants and swift heavy ion (SHI) irradiation with 160 MeV $Ni^{12+}$ and 120 MeV $Si^{9+}$ ion beams have been carried out on the polyaniline films for enhancement of the properties such as the dc conductivity, charge storage capacity and electrochemical stability of the polymer as electrodes in solid state redox supercapacitors. In this chapter the electrochemical synthesis of polyaniline conducting polymer films on ITO coated glass substrates with different dopants are described in detail. Characterizations by cyclic voltammetry, four probe measurements for dc conductivity, surface morphological study by scanning electron microscopy, UV-Vis and FTIR spectroscopies and X-Ray diffraction have been carried out on polyaniline conducting polymer films before and after SHI irradiation and the results thereof are presented and analyzed in this chapter.

**4.1 Electrochemical polymerization:**

Conducting polymer films of polyaniline have been synthesized by oxidative electropolymerization of aniline monomer by potentiodynamic and

potentiostatic methods [227, 231-237] as described in chapter III, section 3.2. Monomer aniline (Aldrich, USA) has been distilled under reduced pressure and stored in darkness at room temperature prior to use. The monomer and the dopant are dissolved together in a common suitable solvent (double distilled de-ionized water for HCl, $H_2SO_4$, $H_3PO_4$ and $HClO_4$ doping and acetonitrile for $LiClO_4$). The electropolymerization of polyaniline has been carried out in a three electrode single compartment electrochemical cell. The polyaniline films have been deposited from an aqueous solution of monomer aniline and the protic acid (HCl, $H_2SO_4$, $H_3PO_4$ and $HClO_4$) in appropriate amounts. The $ClO_4^-$ ion doped polyaniline films have been synthesized from a solution of $LiClO_4$ salt and monomer aniline in organic solvent acetonitrile. The potentiodynamic polymerization of polyaniline has been carried out by sweeping the potential from -200 mV to 1200 mV in two electrode setup in the electrochemical cell. The potential range for potentiodynamic deposition is -100 mV to 950 mV with SCE reference electrode. Potentiostatic deposition of polyaniline has been carried out at constant potential of 950 mV against SCE reference electrode in three electrode electrochemical cell and for two electrode setup the applied potential is 1100 mV as in three electrode system the potential is applied against the reference electrode, the potential due to the reference electrode is also added to the total potential to the working electrode. The number of cycle for deposition has been taken according to the film thickness requirements. All potentials are applied against a saturated calomel reference electrode (SCE) in three electrode setup. Cleaning of the ITO coated glass substrate is also important for depositing a uniform polymer film [248]. The electrosynthesis of polyaniline produces deep green polymer films. Fig. 4.1 shows the plot of deposition current (a measure of polymerization rate) vs. monomer concentration of polyaniline deposition with protic acid dopant HCl in aqueous medium. The plot of deposition current as a function of monomer concentration (Fig. 4.1) shows that polymerization rate increases monotonically with monomer concentration and that at 0.15 M aniline concentration, the polymerization rate is quite high, but the films obtained have a rough and flaky surface and show

poor adhesion. This may be attributed to the faster rate of polymerization due to higher monomer concentration, which does not provide sufficient time for polymer chains to grow smoothly on the substrate. The polymer films obtained by varying the acid concentration however, does not show any notable change in surface morphology indicating that monomer concentration is more critical in conducting polymer film deposition.

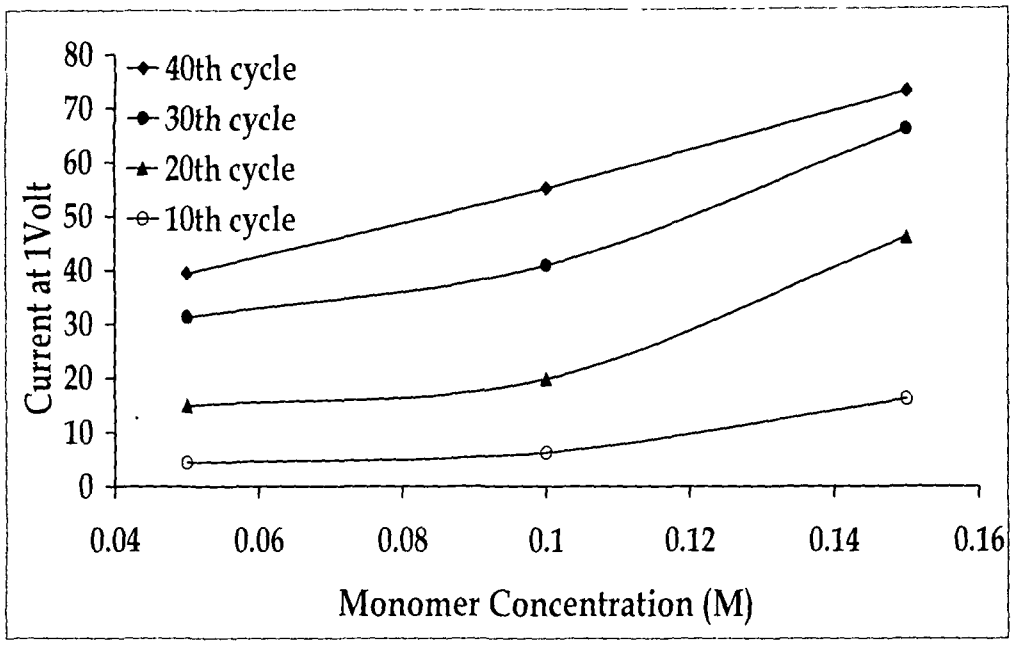


Figure 4.1: Deposition current vs. monomer concentration for deposition of polyaniline films at a fixed HCl concentration of 1.0 M.

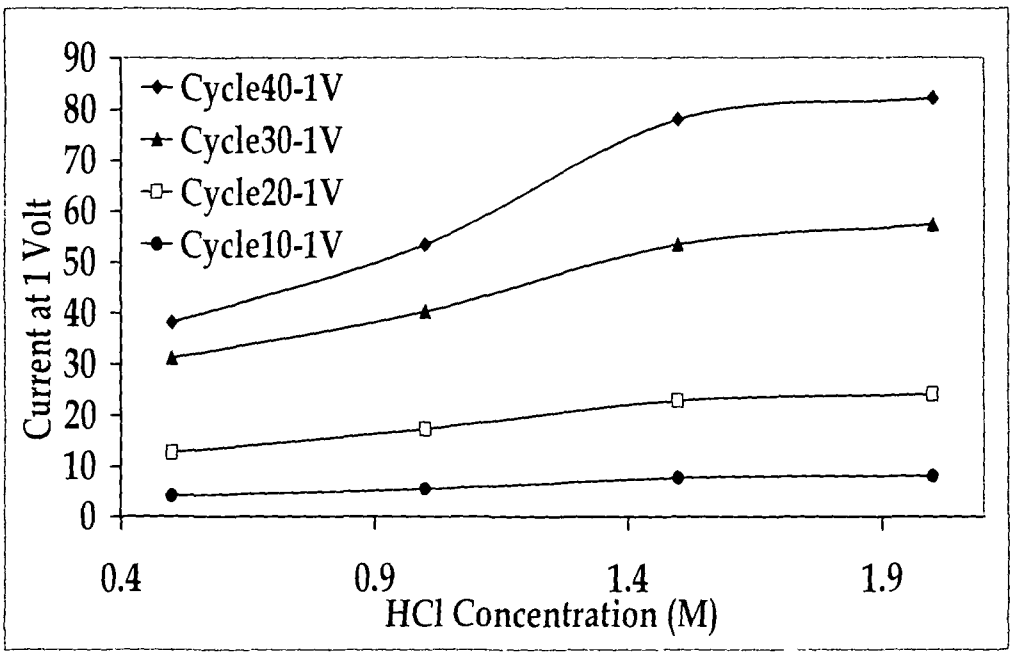


Figure 4.2: Deposition current vs. HCl concentration for deposition of polyaniline films as a fixed monomer concentration of 0.1 M.

The slow deposition rate at low hydrochloric acid concentration could be ascribed to lower proton concentration and hence lower protonation rate of the film. The rate of polymerization however, does not increase monotonically with HCl concentration. The deposition current vs. HCl concentration plot is shown in Fig. 4.2. The deposition current gets saturated as hydrochloric acid concentration exceeds 1.5 M (Fig. 4.2), which implies that higher proton concentration cannot increase polymerization rate beyond a certain limit. The chloride ions ($Cl^-$) from the electrolyte enter into the polymer film as dopant in the oxidative polymerization process so as to maintain the electroneutrality of the film. Undoped polyaniline is an insulator and shows conductivity of the order of $10^{-4}$ to $10^{-10}$ S/cm [245, 249, 250]. All the protic acid doped polyaniline conducting polymers are synthesized in aqueous medium and the lithium perchlorate doped polyaniline conducting polymer films are synthesized in organic solvent acetonitrile. Both potentiodynamic and potentiostatic synthesis methods produced smooth polyaniline films except for lithium perchlorate doped polyaniline films. The films doped with lithium perchlorate in acetonitrile produce very rough and uneven surface and the films get cracked when dried.

Different concentrations of monomer and dopant have been used for synthesis of polyaniline conducting polymer films. The optimum concentrations of monomer and dopant for the highest conductivity and film yield deposition are taken for detailed studies of the polyaniline films. For HCl, $H_2SO_4$, $H_3PO_4$ and $HClO_4$ doping, the highest conductivity of polyaniline films is obtained for 1.0 M of the protic acid with 0.1 M aniline monomer concentration. For $LiClO_4$ doping, the optimum conductivity and smooth surface film of polyaniline is obtained with 2.0 M $LiClO_4$ and 0.15 M aniline. Higher monomer concentration of 0.15 M is required because of slow polymerization rate of aniline in acetonitrile. Increasing the dopant concentration beyond these values does not increase the conductivity and made the surface rough and flaky. The increase of monomer concentration beyond this optimum value increases the rate of polymerization but the dc conductivity

has been observed to decrease and also the film becomes less adhesive to the substrate. Increase of concentration of both monomer and dopant in the same ratio does not make any difference except increase in the rate of polymerization.

## 4.2 Characterization of the polyaniline conducting polymer films:

### *4.2.1 Cyclic voltammetry:*

The cyclic voltammetry studies of all the conducting polymer films have been carried out for understanding their redox response. Fig. 4.3 shows the cyclic voltammograms (CVs) of the polyaniline films obtained in 1.0 M hydrochloric acid (HCl) at different scan rates of 10, 20, 40 and 50 mV/s. All the potentials are measured against SCE reference electrode.

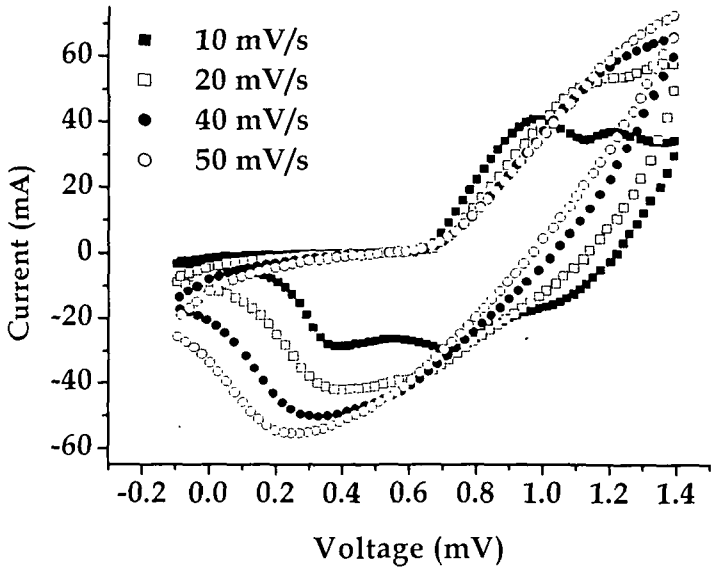


Figure 4.3: Cyclic voltammograms of polyaniline doped with HCl (1.5 M) at different scan rates.

Voltammograms of the HCl doped polyaniline (Fig. 4.3) at various scan rates can be differentiated into three main potential regions (i) from -0.2 V to +0.6 V polyaniline is in completely reduced state i.e., leucoemeraldine form, (ii) from about +0.6 V to +0.83 V, the polyaniline is in de-protonated state i.e., emeraldine form of polyaniline and (iii) from about +0.83 V to +1.4 V, polyaniline is in completely oxidized state i.e., pernigraniline. Separate de-protonation and oxidation peaks have been observed in the forward sweep at

low scan rate (10 mV/s), which get merged with the oxidation peak at higher scan rates. The reduction peak for low scan rate of 10 mV/s occurs at comparatively higher potential. Separate reduction and protonation peaks have been observed at low scan rate (10 mV/s), but the peaks get diffused into a single peak at higher scan rates. The colour of the polyaniline films changes from light green (bottle green) to deep green in the forward sweep and back to light green in the reverse sweep, which is an indication of the oxidation-reduction taking place in the polymer films during the potential sweep.

In the de-protonation process of the polyaniline film, the protons i.e., hydrogen positive ion bonded with the nitrogen of the aromatic amine are expelled from its chain and the fully reduced leucoemeraldine form of polyaniline is converted to partially oxidized emeraldine form. During oxidation in the forward sweep of potential, the $Cl^-$ ion entered into the polymer film from the electrolyte [244] and oxidation of the polymer chain occurs by giving out one electron from the chain. The electron deficiency imbalance thus created in the polymer chain has been neutralized by the dopant ion. The charge neutrality of the polymer chain is thus maintained as electrons are drawn from the polymer chain during oxidation. In the reverse sweep, the polymer film expels the dopant ions during reduction [244]. The evidence of ion entering into the polymer film during oxidation has been observed in experiments with electrochemical quartz crystal microbalance [251]. At slow scan rate (10 mV/s), separate reduction and deprotonation peaks have been observed in the reverse sweep. First the reduction of the polyaniline film occurs at 0.73 V (Fig. 4.3) and the pernigraniline form of polyaniline has been transformed into emeraldine form, which after protonation at 0.42 V (Fig. 4.3) turns back to completely reduced leucoemeraldine form of polyaniline. In the protonation process, the polyaniline film incorporates hydrogen ions (protons) form the electrolyte of protic acid. In the de-protonation process in forward sweep after bond re-arrangement the benzenoid form has been converted to quinoid form and reverse occurs in the reverse sweep. Although theoretically expulsion of all dopant ions from the polymer film is expected,

practically a certain dopant ions are trapped within the polymer chain, even some dopant ions are trapped during the synthesis of the polymer film. The colour of the polyaniline films changes from light green (bottle green) to deep green, which is also an indication of the oxidation-reduction taking place in the polymer electrode.

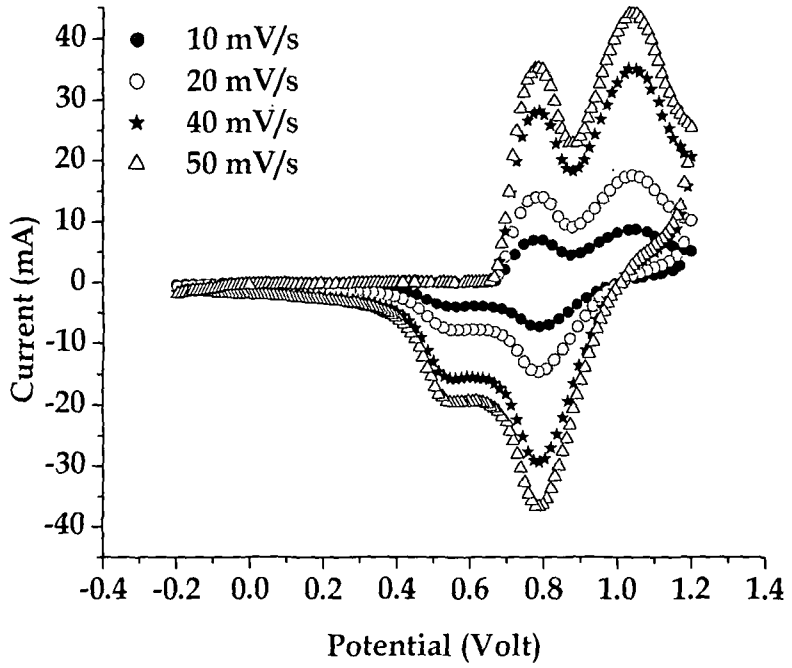


Figure 4.4: Cyclic voltammograms of polyaniline doped with $H_2SO_4$ (1.0 M) at different scan rates.

The cyclic voltammograms of polyaniline doped with 1.0 M sulfuric acid on ITO coated glass substrate with stainless steel counter electrodes are shown in Fig. 4.4. The cyclic voltammograms of polyaniline films doped with sulfuric acid also can be divided into three regions. In the -0.2 V to 0.6 V region the polyaniline is in completely reduced leucoemeraldine form. In the forward sweep of potential, the de-protonation of the polyaniline film starts from 0.6 V and the peak is reached at 0.78 V and the polyaniline conducting polymer film has been transformed into emeraldine form, which is partially oxidized. Above 0.82 V, the incorporation of dopant ions into the polymer films starts and oxidation of the polyaniline film occurs. The oxidation peak is observed at 1.02 V and the polyaniline has been transformed into completely oxidized

pernigraniline form. In the reverse sweep, the reduction of polyaniline take place at 0.8 V, the pernigraniline form of polyaniline has been reduced to emeraldine form. Then the protonation of the polyaniline film occurs at 0.52 V and the emeraldine form of polyaniline has been converted to completely reduced leucoemeraldine form.

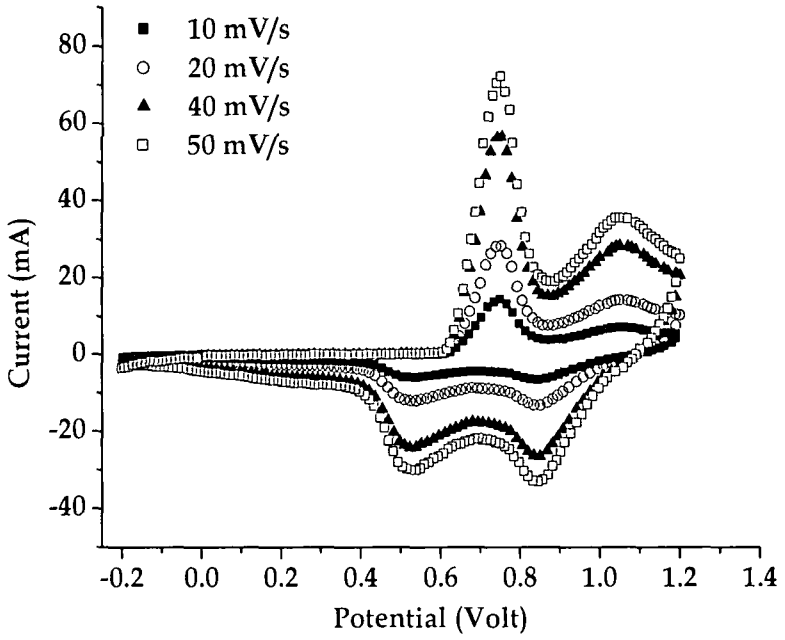


Figure 4.5: Cyclic voltammograms of polyaniline doped with $HClO_4$ (1.0 M) at different scan rates.

The cyclic voltammograms of perchloric acid doped polyaniline films are shown in Fig. 4.5. For perchloric acid doped polyaniline, the de-protonation of the polyaniline film occurs at 0.78 V and the oxidation peak is found at a potential of 1.05 V in the forward sweep. In the reverse sweep, reduction occurs at 0.81 V and the protonation peak appears at 0.51 V. The polyaniline film in the forward sweep transform to emeraldine from leucoemeraldine during de-protonation and on oxidation, emeraldine is converted to pernigraniline. The reverse transformation to emeraldine and then to leucoemeraldine take place in the reverse sweep.

The cyclic voltammograms of polyaniline films synthesized in phosphoric acid are shown in Fig. 4.6. Phosphoric acid doped polyaniline

conducting polymer films does not show any sharp reduction peaks although there is a sharp oxidation peak in the forward sweep (Fig. 4.6). No separate de-protonation peak has been observed in the forward sweep, but the anodic current starts rising from 0.7 V and continues to increase up to 1.38 V. A close look into the structure of cyclic voltammograms reveals the partial overlapping of the de-protonation peak into the oxidation peak at lower scan rates (<40 mV/s) which is believed to be completely overlapped at higher scan rates (≥ 50 mV/s) as the shift of de-protonation peak towards higher potential occurs at higher scan rates.

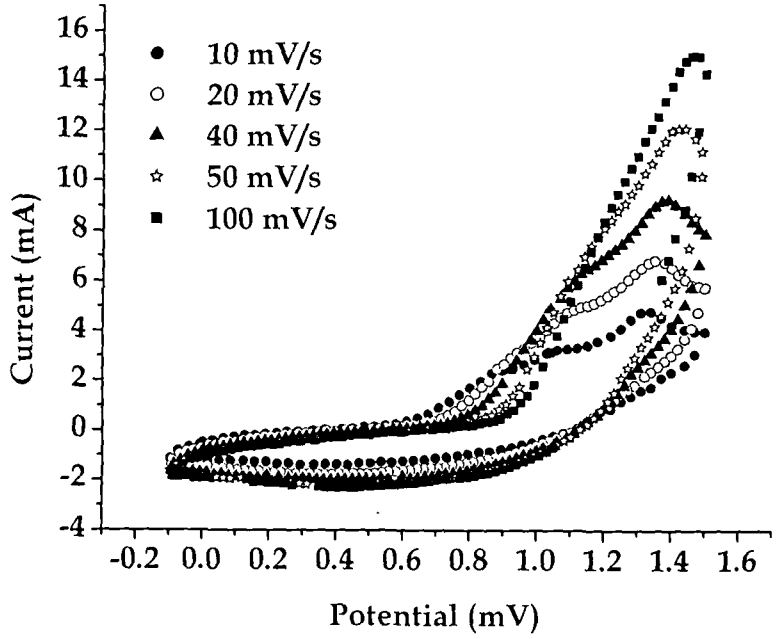


Figure 4.6: Cyclic voltammograms of polyaniline doped with $H_3PO_4$ (1.0 M) at different scan rates.

The oxidation of the phosphoric acid doped polyaniline occurs at higher potential possibly due to the larger size of the dopant ion $PO_4^-$, which has very low mobility. The nonoccurrence of reduction peak could also be attributed to the larger size of the dopant ion, most of them get trapped inside the polymer chains and the outward motion of $PO_4^-$ ions do not take place. However, a broad reduction peak is attributed to the protonation.

The cyclic voltammograms of $LiClO_4$ doped polyaniline are shown in Fig. 4.7. The structure of the cyclic voltammograms completely different from those of the perchloric acid doped polyaniline films with oxidation peaks occurring in the range 0.8-1.0 V, although the same dopant ion is involved in the doping process. At low scan rates (<20 mV/s) de-protonation and protonation peaks are dominating in the forward and reverse sweeps of potential respectively, but at higher scan rates (≥ 40 mV/s) the de-protonation and oxidation peaks merge into a broad peak. The oxidation peak occurs at a higher potential of 1.2 Volt at a high scan rate of 100 mV/s which is due to faster rate of change of potential. The reduction peaks occur in the range of 0.8-0.45V and here also the reduction peak shift towards lower potential with the increase in scan rate due to inertia of large perchlorate ($ClO_4^-$) ions unable to keep pace with the faster rate of change of potential.

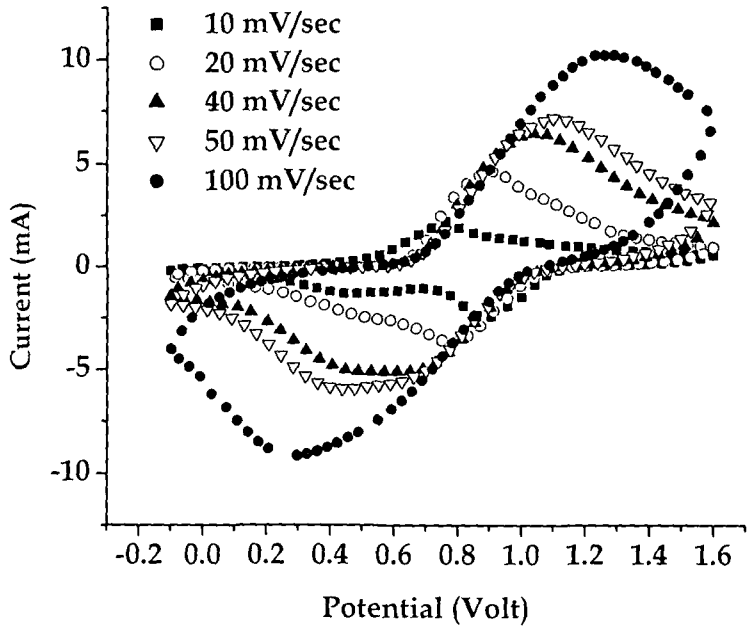


Figure 4.7: Cyclic voltammograms of polyaniline doped with $LiClO_4$ (1.5 M) at different scan rates.

The doping/dedoping of all the polyaniline films are electrochemically reversible and reproducible within the potential limit of cyclic voltammograms taken. All the cyclic voltammograms exhibit the expected scan rate dependence,

i.e. the current increases with the increase in the scan rate. Electrochromism i.e. the change of colour with oxidation-reduction of polyaniline films is also observed. The colour changes from bottle green to deep green in the forward sweep of potential and vice versa. The redox current peak height in the cyclic voltammogram of the conducting polymers is dependent on the active sites on the polymer chain [252] and more active site would give rise to higher current. Effective surface area is also an important factor and higher surface area of the conducting polymer film shows higher redox peak current in cyclic voltammograms [252].

### *4.2.2 Conductivity Studies:*

The conductivity of the doped polyaniline films has been measured by four probe technique at room temperature. The highest conductivity of 78 S/cm has been measured in perchloric acids ($HClO_4$) doped polyaniline films. The polyaniline films synthesized in acetonitrile with lithium perchlorate ($LiClO_4$) as dopant show conductivity of ~70 S/cm. The conductivity of perchlorate ion doped polyaniline is five orders of magnitude higher than the earlier reported value of conductivity of polyaniline synthesized in ethylene carbonate (EC) and dimethyl carbonate (DMC) [253]. The $Cl^-$ ion doped polyaniline films synthesized in HCl aqueous solution show conductivity of about 35 S/cm.

Table 4.1: The dc conductivity values of polyaniline conducting polymer films measured by four probe method.

| Dopant | Conductivity (S/cm) | |
|---|---|---|
| | Potentiostatic | Potentiodynamic |
| Hydrochloric acid (HCl) | 35 ± 2 | 36 ± 3 |
| Sulfuric acid ($H_2SO_4$) | 1.5 ± 2.5 | 1.7 ± 3.5 |
| Perchloric acid ($HClO_4$) | 73 ± 6 | 78 ± 4 |
| Phosphoric acid ($H_3PO_4$) | 0.7 ± 0.2 | 0.8 ± 0.2 |
| Lithium perchlorate ($LiClO_4$) | 68 ± 6 | 70 ± 3 |

Polyaniline conducting polymer films synthesized in sulfuric acid ($H_2SO_4$) and phosphoric acid ($H_3PO_4$) show low conductivity values in the range of 0.5 to 1.7 S/cm.

*4.2.3 Surface Morphology Study:*

The SEM images of polyaniline films synthesized by potentiodynamic and potentiostatic methods are presented in Figs. 4.8-4.12 Polyaniline films synthesized in HCl show a granular and highly porous microstructure (Fig. 4.8). The potentiodynamic method produces more uniform surface morphology (Fig. 4.8a) than the potentiostatic (Fig. 4.8b) method. Polyaniline films deposited in $H_2SO_4$ show very rough surface morphology (Fig. 4.9). Uniform granular microstructure is obtained for polyaniline films synthesized in $HClO_4$ by potentiodynamic method (Fig. 4.10a). The pore size increases in potentiostatic method (Fig. 4.10b). Polyaniline conducting polymer films synthesized in $H_3PO_4$ (Fig. 4.11) are very rough and flaky showing that the roughness is more in potentiostatically deposited films (Fig. 4.11b). A smoother film surface with regular pore size is obtained in $LiClO_4$ doped polyaniline films (Fig. 4.12a), in this case also the pore size increases in potentiostatic method (Fig. 4.12b).

From the studies of the SEM images, it has been observed that the film surface is rougher for the films deposited by potentiostatic method. This could be attributed to the fact that electropolymerization in the potentiostatic method takes place at a constant potential. The oxidation potential of monomers is higher than that of dimers, and trimers have lower oxidation potential than that of the dimers and so on. In the potentiostatic method the polymerization process nucleates at the monomer sites only at the applied potential and dimers, trimers etc. don't grow further due to the unfavourable potential resulting in the haphazard growth due to preferential oxidation at monomer sites. On the other hand in the potentiodynamic method since the potential keep changing and in the process becomes equal to the oxidation potentials of monomer, dimer, trimer etc. therefore the polymerization can occur at all sites making the polymer film dense, smooth and less porous.

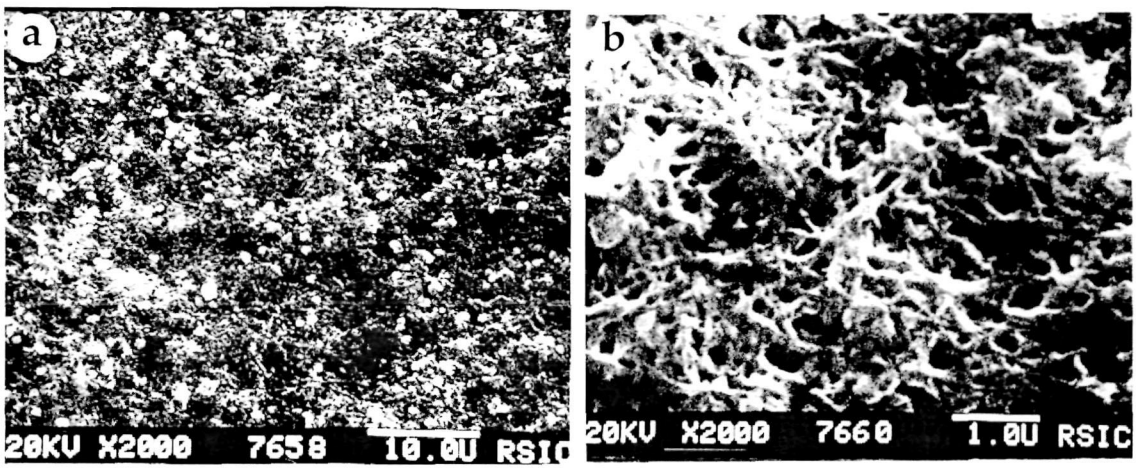


Figure 4.8: SEM images of polyaniline doped with HCl deposited by (a) potentiodynamic method and (b) potentiostatic method.

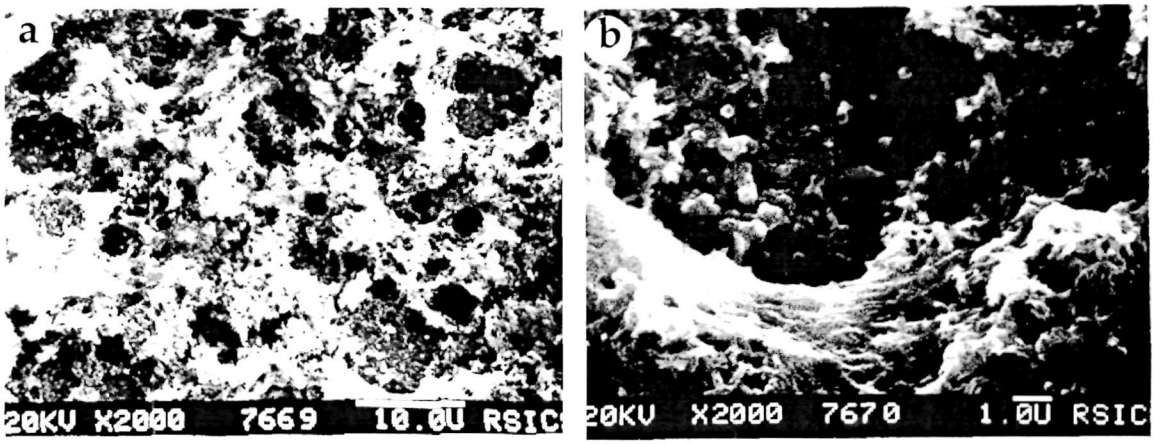


Figure 4.9: SEM images of polyaniline doped with $H_2SO_4$ deposited by (a) potentiodynamic method and (b) potentiostatic method.

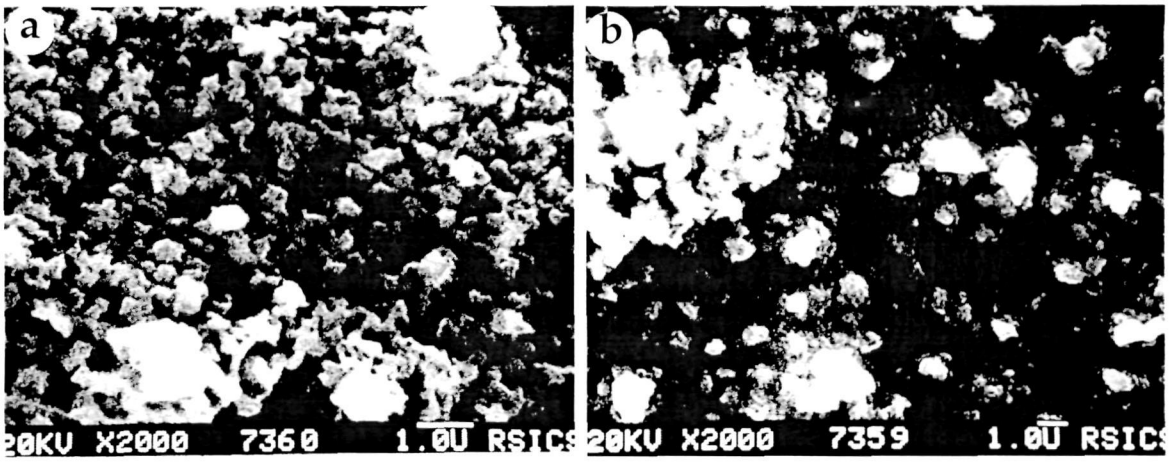


Figure 4.10: SEM images of polyaniline doped with $HClO_4$ deposited by (a) potentiodynamic method and (b) potentiostatic method.

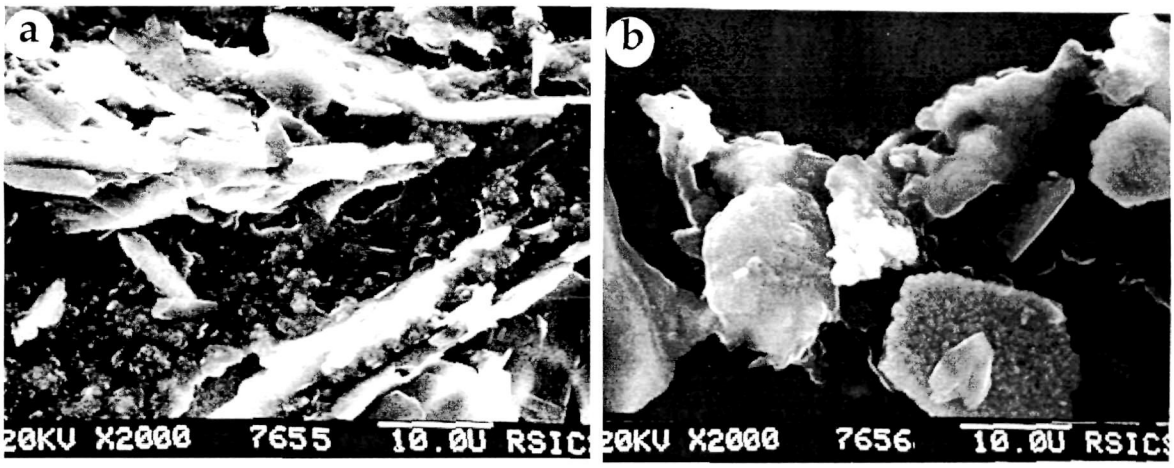


Figure 4.11: SEM images of polyaniline doped with $H_3PO_4$ deposited by (a) potentiodynamic method and (b) potentiostatic method.

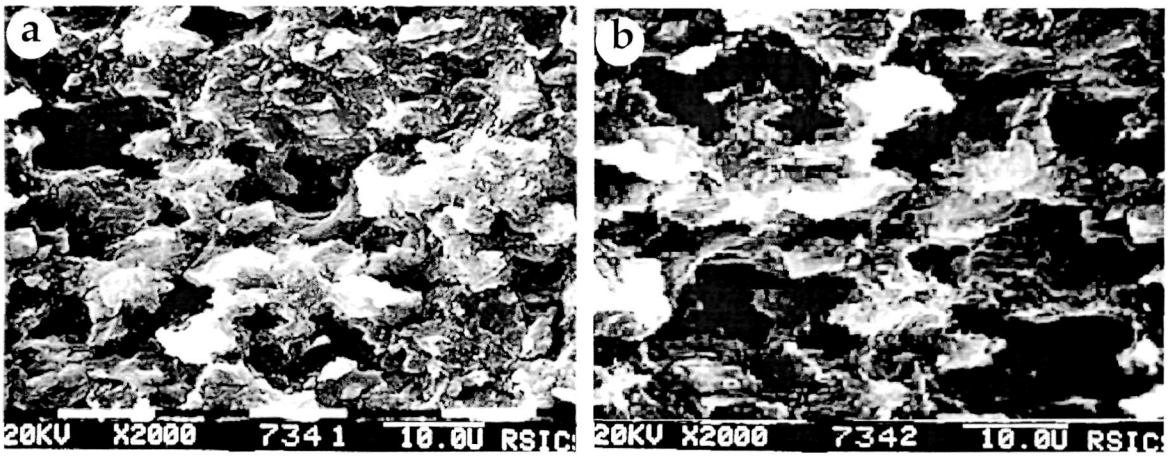


Figure 4.12: SEM images of polyaniline doped with $LiClO_4$ deposited by (a) potentiodynamic method and (b) potentiostatic method.

### *4.2.4 UV-Vis spectroscopy:*

UV-Vis spectroscopy is a versatile technique to investigate the electronic transitions and provide key information regarding the electronic structure of polymer films. The UV-Vis spectra of the polyaniline polymer films electrodeposited on ITO coated glass using different dopants are shown in Figs. 4.13a-e. In all the absorption spectra of doped polyaniline, absorption peaks near 300 nm (3.75 eV) is attributed to $\pi$–$\pi^*$ transition of benzenoid ring and the broad absorption band around 600 nm (1.96 eV) is attributed to $\pi$–$\pi^*$ transition of quinoid ring of polyaniline chain [247, 254, 255]. The absorption peak around 300 nm (3.75 eV) due to benzenoid absorption of the polymer chain occurs at

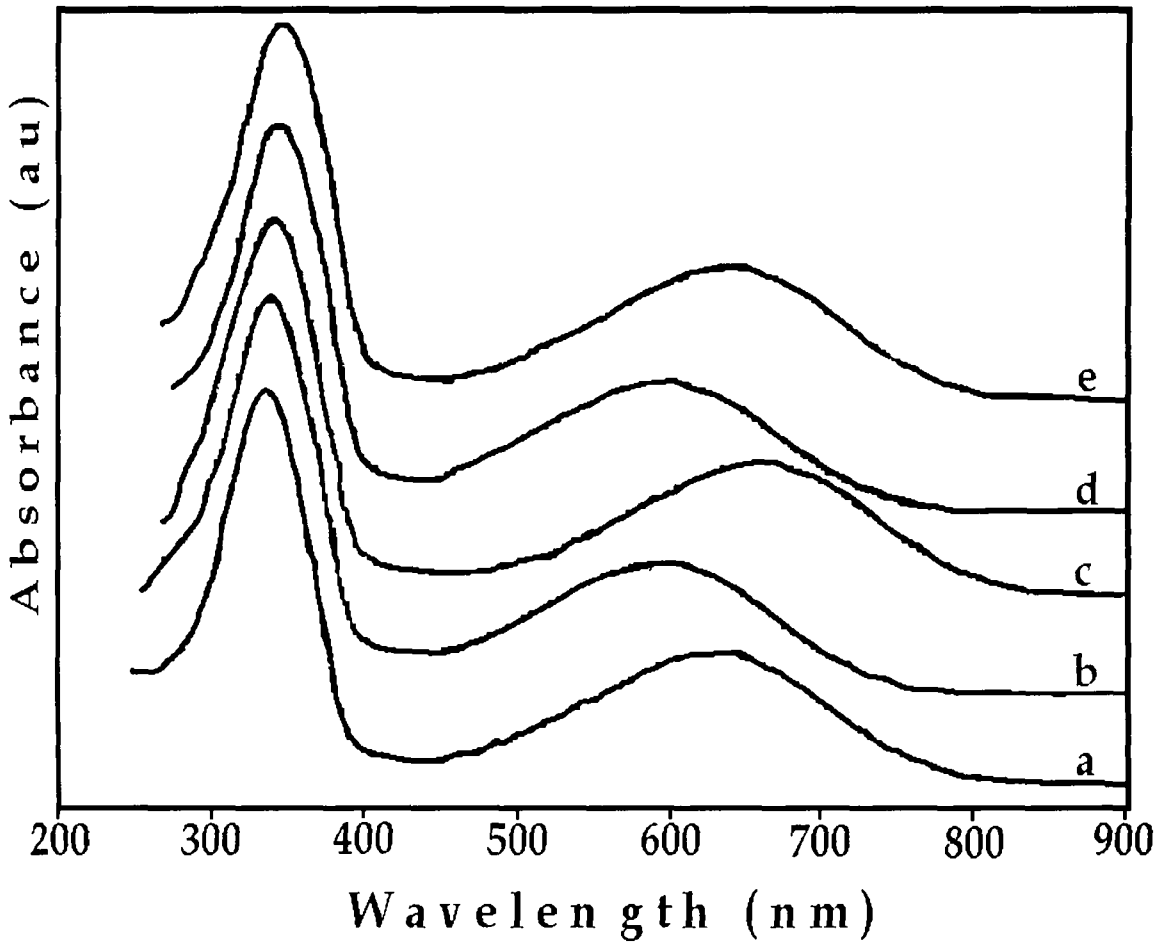


Figure 4.13: UV-Vis spectra of polyaniline doped with (a) HCl, (b) $H_2SO_4$, (c) $HClO_4$ (d) $H_3PO_4$ and (e) $LiClO_4$.

the same position for all the polyaniline films, but the absorption peak at around 600 nm occurs at different wavelengths for different dopants. The conductivity of the polymer films appears to depend on the position of this peak. A conducting polymer with the quinoid absorption peak at higher wavelength shows higher conductivity. The perchloric acid and lithium perchlorate doped polyaniline films (Figs. 4.13 c and d) showing the quinoid absorption peak at higher wavelength around 650 nm exhibit the higher conductivity values. This peak for hydrochloric acid doped polyaniline occurs at around 630 nm, whereas for sulfuric acid and phosphoric acid doped polyaniline the peak arises at around 600 nm showing the lowest conductivity. The quinoid absorption peak position can be related with the band gap of the polymer film, lower band gap causing the absorption at higher wavelength and

vice-versa. The change in absorption peak position with different dopants has been theoretically presented for conducting polymer in literature [256] and also observed with different sulfonic acid doped polyaniline conducting polymer [257]. The ratio of the $\pi \rightarrow \pi^*$ electronic transition absorption peak and the quinoid ring absorption peak gives the ratio of benzenoid and quinoid i.e., the degree of oxidation of the respective conducting polymer film.

*4.2.5 FTIR spectroscopy:*

The Fourier Transform Infra-Red (FTIR) spectroscopy studies of the polymer films have been carried out with a view to probe the presence of dopants in the electrochemically synthesized conducting polymer films. The FTIR spectra of undoped polyaniline are shown in Fig. 4.14 a [258]. The FTIR spectra of the polyaniline films electrodeposited in phosphoric acid, in hydrochloric acid, in sulfuric acid, in acetonitrile with lithium perchlorate salt dopant and in perchloric acid are presented in Figs. 4.14 b-f respectively. In all the spectra the broad peak around 3100 -3470 $cm^{-1}$ is attributed to the N-H stretching of the amine group of aniline, the peak near 1585 $cm^{-1}$ is attributed to quinoid ring C=C stretching and the peak in the range of 1450-1500 $cm^{-1}$ is due to the benzenoid ring C=C stretching of polyaniline [259]. The strong band observed near 1100 $cm^{-1}$ and the band at 1235 $cm^{-1}$ are due to C-C stretching and C-C twisting, respectively of the alkyl chain [260]. The peak at 1300 $cm^{-1}$ is due to the C-N stretching of the polymer. The peak near 800 $cm^{-1}$ is due to the N-H out-of- plane bending absorption. The C=C stretching absorption of aromatic compound occurs in the range of 1475-1600 $cm^{-1}$. In the present study, this peak is obtained at about 1477 $cm^{-1}$. The peak due to N-H bending can be seen in the range of 1560-1640 $cm^{-1}$. The peak near 3000 $cm^{-1}$ is due to the C-H stretching absorption. The stretching peak of N-H appears in the range of 3420-3450 $cm^{-1}$[261]. The peaks observed at 1592 and 1508 $cm^{-1}$ in the undoped polyaniline show change in position in the FTIR spectra of doped polyaniline is possibly due to quinoid rings in polyaniline being converted into benzenoid rings [258].

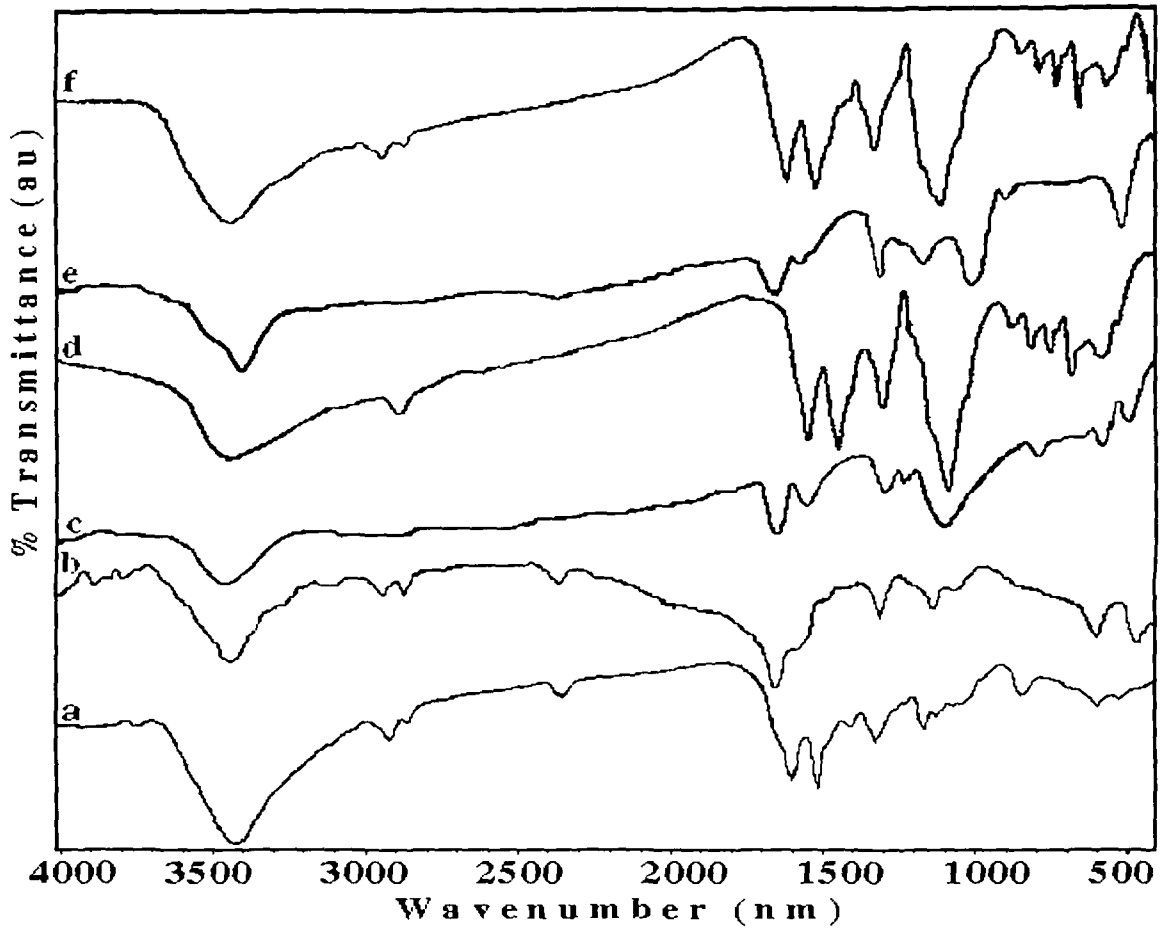


Figure 4.14: FTIR spectra of polyaniline (a) undoped and doped with (b) HCl, (c) $H_2SO_4$, (d) $HClO_4$, (e) $H_3PO_4$ and (f) $LiClO_4$.

The C-Cl stretching peak at 595 $cm^{-1}$ in Fig. 4.14a is clearly observed in chloride doped polyaniline films [261]. The absorption bands at 1100 $cm^{-1}$ in perchloric acid and lithium perchlorate doped polyaniline (Figs. 4.14 d and f) are assigned to the $ClO_4^-$ anion [262-264]. This peak at 1100 $cm^{-1}$ is a combination of ClO4- and C-C stretching (Fig. 4.14 d and f) and hence its intensity is high. A weak peak only due to C-C stretching occurs in the HCl doped polyaniline (Fig. 4.14 b). The absorption peak at 630 $cm^{-1}$ in the FTIR spectra of perchloric acid and lithium perchlorate doped polyaniline (Figs. 4.14 d and f) are assigned to the $ClO_4^-$ anion [265]. The peak at 1105 $cm^{-1}$ in Fig. 4.14c is attributed to $SO_4^{2-}$ indicating that the polyaniline films synthesized in sulfuric acid contained $SO_4^{2-}$ [266]. This peak, which is due to a combination of $SO_4^{2-}$ and C-C stretching absorption is broader as compared to that in HCl doped

polyaniline (Fig. 4.14 b), which occurs only due to C-C stretching. An intense $PO_4^{3-}$ peak at 1020 $cm^{-1}$ in the FTIR spectra of polyaniline doped with phosphoric acid (Fig. 4.14 e) confirms the presence of phosphate groups in the polyaniline conducting polymer film doped with phosphoric acid [267]. The formation of quinod and benzenoid rings confirmed the polymerization of the monomer aniline into polyaniline and oxidation of the polyaniline films. Also the presence of the absorption peaks of each dopant ion in the respective IR spectra confirms the doping of the polyaniline films during synthesis.

### *4.2.6 X-Ray Diffractogram study:*

The X-Ray diffraction is a powerful technique for the structural characterization of materials. In the case of polymeric materials XRD is used to determine the proportions of crystalline and amorphous phases in terms of degree of crystallinity. The X-Ray diffractograms of polyaniline films synthesized using different dopants are shown in Fig. 4.15.

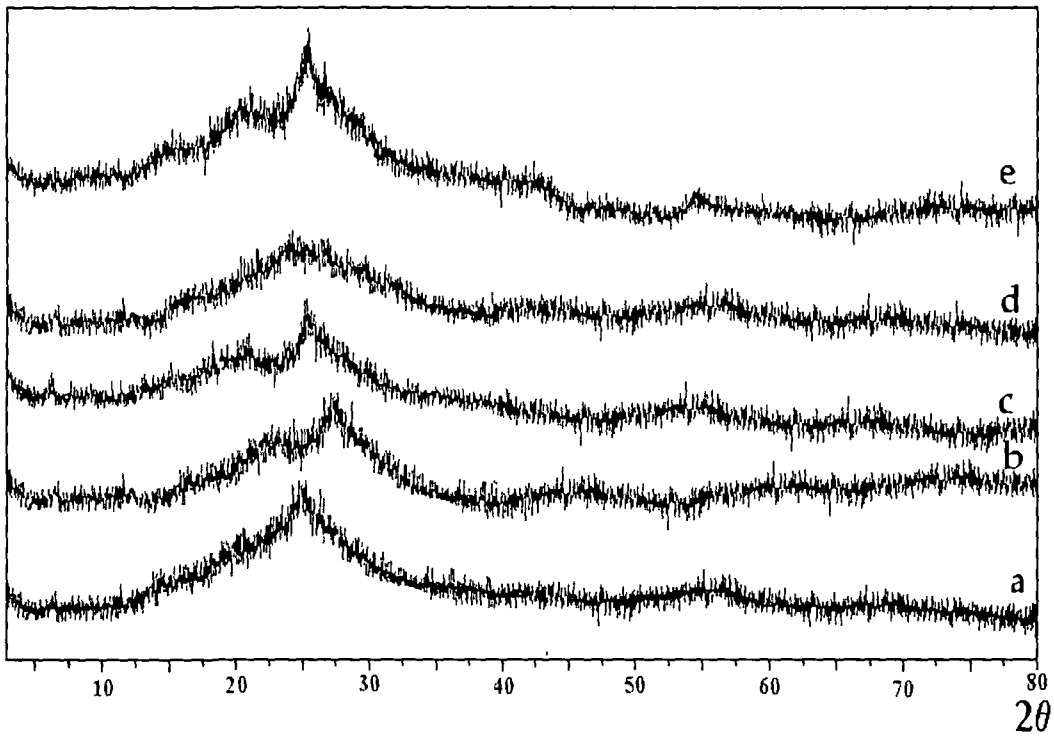


Figure 4.15: X-ray Diffractograms of polyaniline doped with (a) HCl, (b) $H_2SO_4$, (c) $HClO_4$ (d) $H_3PO_4$ and (e) $LiClO_4$

The XRD patterns show that the films are semi-crystalline in nature i.e., some portions of the film are amorphous with some crystalline regions. The crystallinity of the polymer films arises due to systematic alignment of polymer chains by chain folding or by formation of single or multiple helices for atleast part of their lengths [268]. The crystallinity of doped conducting polymer may also arise due to the dopant ion moieties entering into the polymer film [270] during electrochemical synthesis of the polymer films and the change in degree of crystallinity has also been reported with change of dopant concentration in conducting polymer films [271].

The degree of crystallinity (K) of the polymer films has been calculated using the relation as described in chapter III section 3.6.6

$$K = \frac{\text{Area under diffraction peak}}{\text{Total area under diffractogram}} x100\%$$

For visualizing the trend of change in crystallinity of the polymer films with change of dopant, the K values have been calculated by dividing the enlarged diffractogram into small square divisions of 0.5 mm X 0.5 mm and counting the total number of squares above the base line and number of squares under the peak using the above relation.

(a) For HCl doped polyaniline films the K value is:

$$K = \frac{279}{953} x100\% = 29.28\%$$

(b) For $H_2SO_4$ doped polyaniline, the K value is:

$$K = \frac{212}{821} X100\% = 25.82\%$$

(c) For perchloric acid doped polyaniline, the K value is:

$$K = \frac{203}{678} X100\% = 29.94\%$$

(d) For phosphoric acid doped polyaniline, the K value is

$$K = \frac{119}{634} X100\% = 18.77\%$$

(e) And for lithium perchlorate doped polyaniline, the K value is

$$K = \frac{236}{816} X100\% = 28.92\%$$

The polyaniline films doped with perchloric acid show highest crystallinity (29.94%) and the lowest crystallinity has been observed in phosphoric acid doped polyaniline films (18.77%). The degree of crystallinity shows linear relation with the conductivity of the polymer films. The polymer films with higher degree of crystallinity show higher conductivity values, which could be attributed to the decreased scattering of the charge conducting species and decrease in the interchain hopping resistance in the conducting polymer films.

### 4.3 SHI irradiation of polyaniline films:

The polyaniline conducting polymer films doped with hydrochloric acid and perchloric acid have been irradiated with 160 MeV $Ni^{12+}$ and 120 MeV $Si^{9+}$ ion beams respectively with three different ion fluences of $5x10^{10}$, $5x10^{11}$ and $3x10^{12}$ ions/$cm^2$. The irradiation of the conducting polymer films has been carried out in the high vacuum general purpose scattering chamber (GPSC) and materials science (MS) beam lines of Inter University Accelerator Center, New Delhi. The ion current is kept low (0.5 pna) to avoid sample burning. All the characterizations for unirradiated films have been carried out on the irradiated polyaniline polymer films.

### 4.4 Characterization of irradiated polyaniline films:

#### *4.4.1 Cyclic voltammetry:*

The cyclic voltammograms of the SHI irradiated HCl doped polyaniline films are shown in Fig. 4.15. The cyclic voltammogram (CV) of the polyaniline polymer films both unirradiated and irradiated, have been recorded at 50mV/sec scan rate in an electrochemical cell containing an aqueous electrolyte with 1.0 M HCl concentration which is the same as in synthesis. The CV is observed to be related with the electrochromism of the conducting polymer i.e.

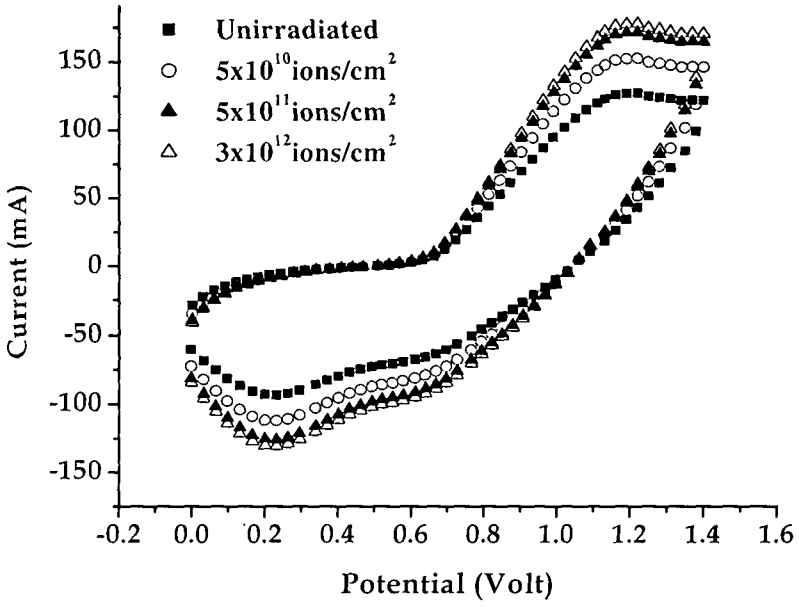


Figure 4.16: Cyclic voltammograms HCl doped polyaniline after SHI irradiation with 160 MeV $Ni^{12+}$ ion at different fluences.

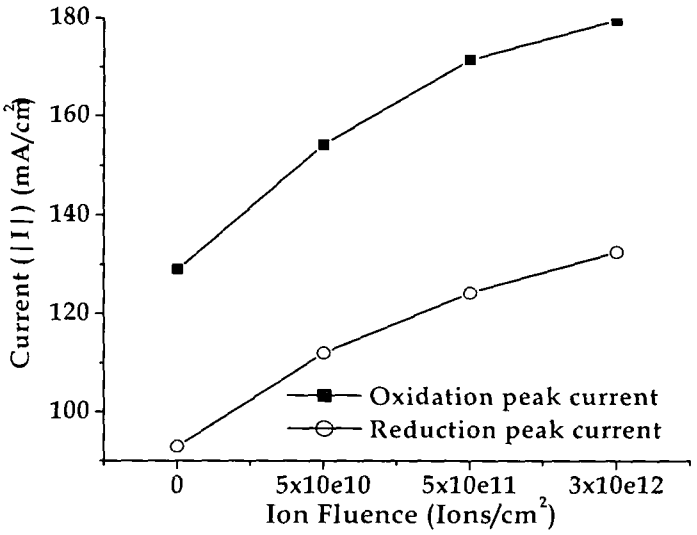


Figure 4.17: Oxidation and reduction peak current before and after irradiation of polyaniline doped with HCl.

the redox peaks observed in the CV coincide with colour change of the conducting polymers. The colour changes from bottle green to deep green on oxidation in the forward sweep of potential and again to bottle green on reduction in the reverse sweep. Like the unirradiated polyaniline films all the

irradiated polymer films show good electroactivity. The shape of the cyclic voltammograms of the unirradiated and irradiated polymer films are same with oxidation and reduction occurring at the same potential 830 mV and 380 mV respectively. The redox response of the irradiated polymer films remains same as that for unirradiated. However, there is an increase in the magnitude of oxidation and reduction peak currents, which could be attributed to enhanced charge carrier concentration in the polymer film upon SHI irradiation, as the electrolyte and other experimental conditions in which the cyclic voltammograms are carried out are kept same. A plot of oxidation and reduction peak current vs. ion fluence is drawn in Fig. 4.17, which shows that the peak current magnitude of oxidation and reduction increases with the increase of fluence.

Fig. 4.18 shows the cyclic voltammogram of $HClO_4$ doped polyaniline films after SHI irradiation with 120 MeV $Si^{9+}$ ion beams with three different fluences of $5x10^{10}$, $5x10^{11}$ and $3x10^{12}$ ions/cm$^2$. The cyclic voltammetry of the $HClO_4$ doped polyaniline films shows similar result i.e., increase in oxidation reduction peak current after SHI irradiation and increases with the increase in fluence.

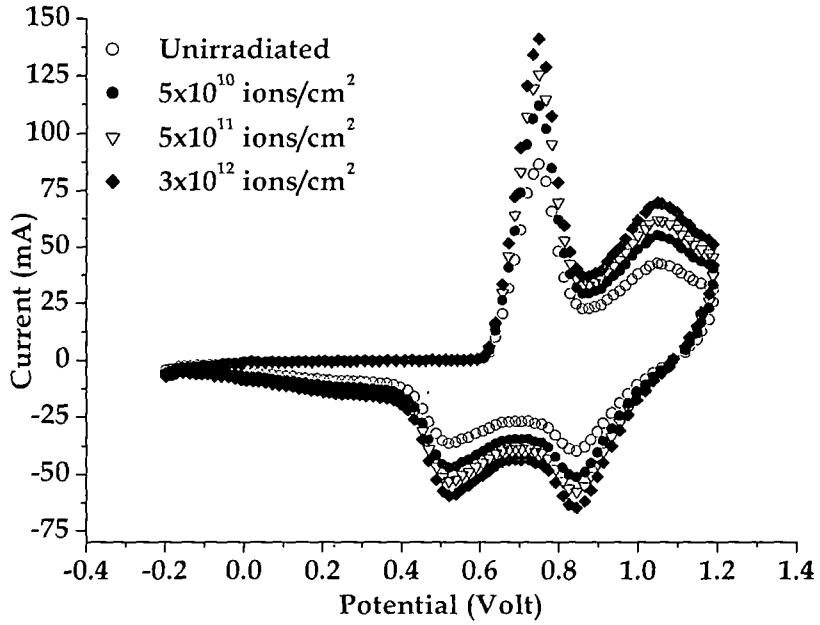


Figure 4.18: Cyclic voltammograms $HClO_4$ doped polyaniline after irradiation with 120 MeV $Si^{9+}$ ion at different.

### *4.4.2 Conductivity measurements:*

The conductivity of the polyaniline films shows an increasing trend with the increase in ion fluence. The dc conductivity of polyaniline unirradiated films has been measured to be ~36 $Scm^{-1}$, which after irradiation increases to ~61 $Scm^{-1}$ i.e., 70% increase in conductivity of polyaniline film is observed upon SHI irradiation. The $HClO_4$ doped polyaniline films upon irradiation with 120 MeV $Si^{9+}$ ion beam also show about 60% increase in conductivity. The increase has been observed to be less in case of $Si^{9+}$ ion irradiation as compared to $Ni^{12+}$ ion irradiation, which may be attributed to the lower value of electronic energy loss of $Si^{9+}$ ion than that of the $Ni^{12+}$ ion. The increase in conductivity of the polymer films after SHI irradiation can be attributed to electronic stopping of the irradiating ion beam in the polymer, which creates large number of active chemical species, cations, anions, radicals and electrons along the ion track in the target polymer.

Table 4.2: Conductivity of polyaniline films after SHI irradiation with 160 MeV $Ni^{12+}$ (HCl doped) and 120 MeV $Si^{9+}$ ($HClO_4$) ion at different fluences.

| Fluence | Conductivity (S/cm) | |
|---|---|---|
| | HCl doped | $HClO_4$ doped |
| Unirradiated | 36.5 ± 2.5 | 78.0 ± 4.0 |
| $5X10^{10}$ ions/$cm^2$ | 51.7 ± 1.8 | 114.2 ± 3.5 |
| $5X10^{11}$ ions/$cm^2$ | 57.3 ± 2.5 | 118.7 ± 2.1 |
| $3X10^{12}$ ions/$cm^2$ | 61.2 ± 2.15 | 124.0 ± 2.8 |

The coulombic interaction among these active species may lead to cross-linking as well as bond breaking, however at high energy irradiation above 100 MeV, cross-linking of the polymer chains dominates over bond breaking resulting in cross-linking in the polymer chains [196]. Inter chain electron hopping required for conduction between two chains, which obviously increases the resistance of the polymer, is reduced due the cross-linking of the polymer chains after irradiation. Defect sites in the molecular structure of the polymer chains created by the SHI irradiation also contributes to higher dc

conductivity as charge accumulation takes place, which produces charge carrier species. The increase of crystallinity of the polymer films also contributes to conductivity increase in SHI irradiation.

### *4.4.3 Surface Morphology Study:*

SEM images of the polyaniline films doped with HCl before and after irradiation with fluences $5x10^{10}$, $5x10^{11}$ and $3x10^{12}$ ions/cm$^2$ are shown in Figs. 4.19 a-d. The unirradiated films show granular porous microstructure (Fig. 4.19 a) with a comparatively smaller grains, which upon irradiation with $5X10^{10}$ ions/cm$^2$ (Fig. 4.19 b) show an increase in the grain size as well as the pore size. The grain size further increases at $5x10^{11}$ ions/cm$^2$ (Fig. 4.19 c) fluence and some large pores appeared in the micrograph, which increased at the highest fluence of $3x10^{12}$ ions/cm$^2$ (Fig. 4.19 d). Fig. 4.20 shows the SEM micrographs of $HClO_4$ doped polyaniline film before and after SHI irradiation with 120 MeV

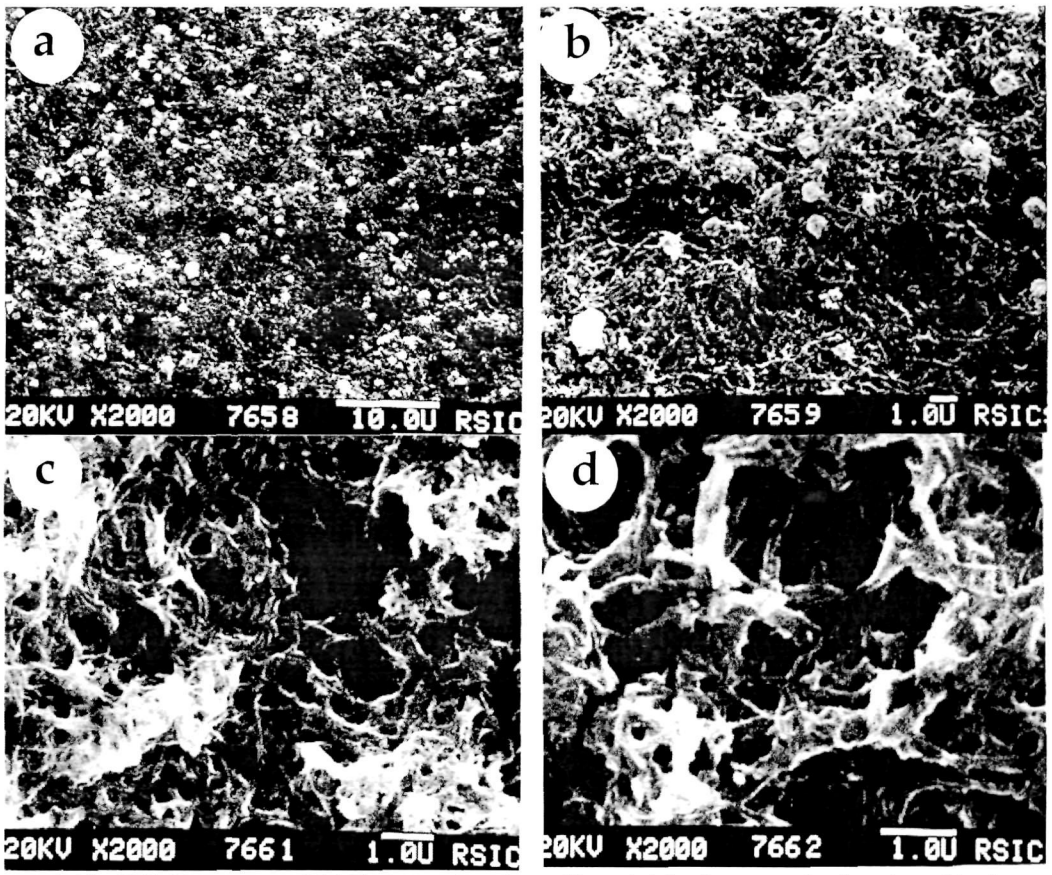


Figure 4.19: SEM images of HCl doped polyaniline (a) before, and after irradiation with 160 MeV $Ni^{12+}$ ion at fluences (b) $5x10^{10}$, (c) $5x10^{11}$ and (d) $3x10^{12}$ ions/cm$^2$.

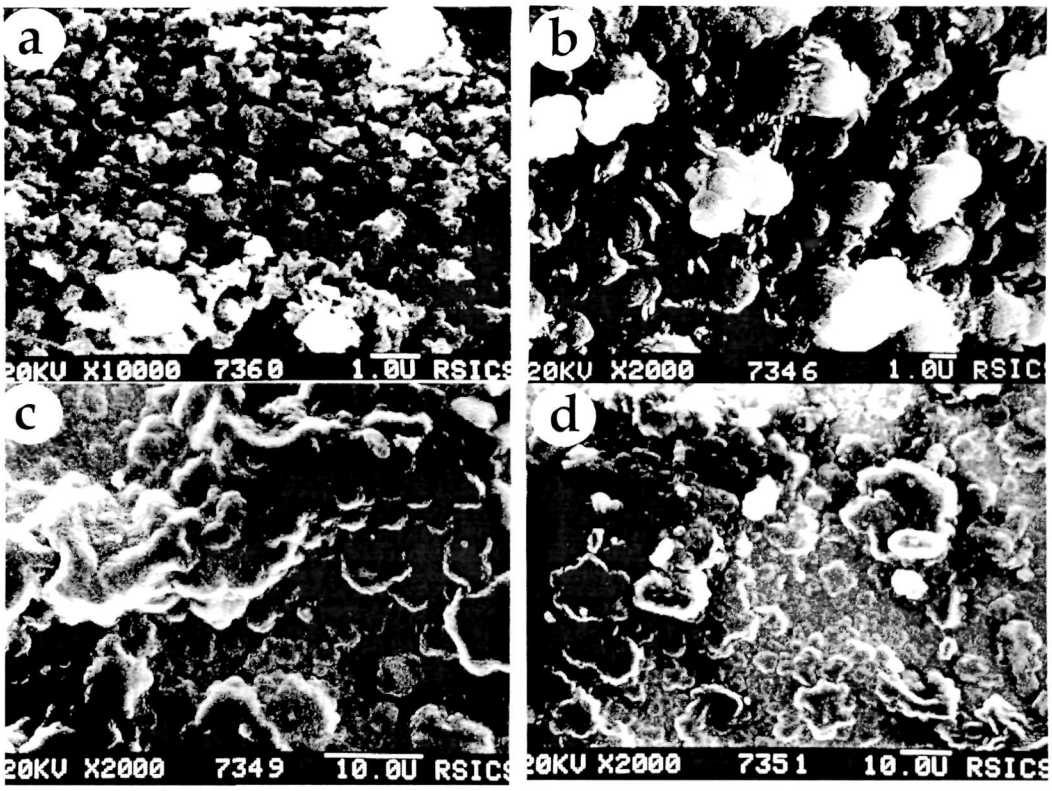


Figure 4.20: SEM images of $HClO_4$ doped polyaniline (a) before, and after irradiation with 120 MeV $Si^{9+}$ ion at fluences (b) $5x10^{10}$, (c) $5x10^{11}$ and (d) $3x10^{12}$ ions/cm$^2$.

$Si^{9+}$ ions at three different fluences of $5x10^{10}$, $5x10^{11}$ and $3x10^{12}$ ions/cm$^2$. The SEM images of $HClO_4$ doped polyaniline films also show grain growth and densification of the surface upon SHI irradiation. The grain growth could be attributed to occur due to the huge energy transfer due to electronic stopping mechanism upon SHI irradiation.

### *4.4.4 UV-Vis spectroscopy:*

The UV-Vis spectra of the conducting polymer films after irradiation with 160 MeV $Ni^{12+}$ ion are shown in Fig. 4.21. The characteristic $\pi \rightarrow \pi^*$ electronic transition of the benzenoid ring of polyaniline occurs at 310 nm [247]. The carrier absorption peak of unirradiated polyaniline appears at 600 nm which is also referred to as $\pi \rightarrow \pi^*$ transition of the quinoid ring of the oxidized polyaniline [247]. After SHI irradiation, the intensity of this carrier absorption peak increases with the increase in fluence, which is consistent with the conductivity results. This carrier absorption peak is also shifted towards higher

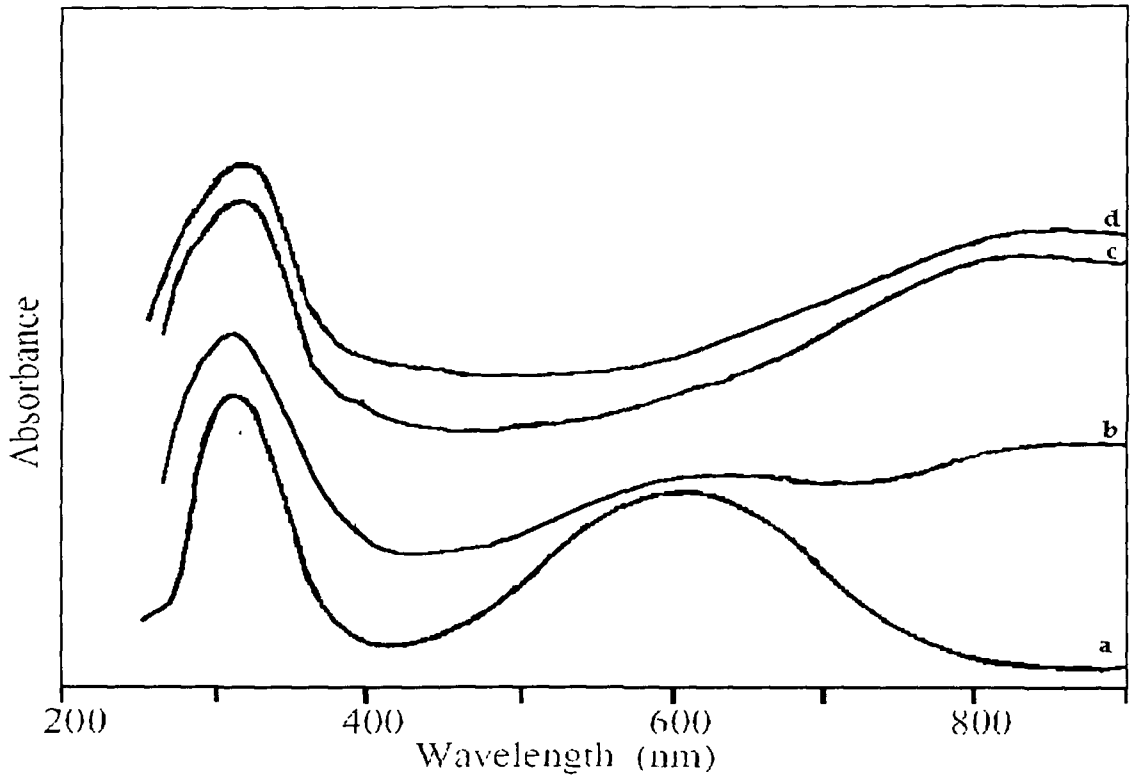


Figure 4.21: UV-Vis spectra of HCl doped polyaniline (a) before and after irradiation with 160 MeV $Ni^{12+}$ ion at fluences (b) $5x10^{10}$, (c) $5x10^{11}$ and (d) $3x10^{12}$ ions/$cm^2$.

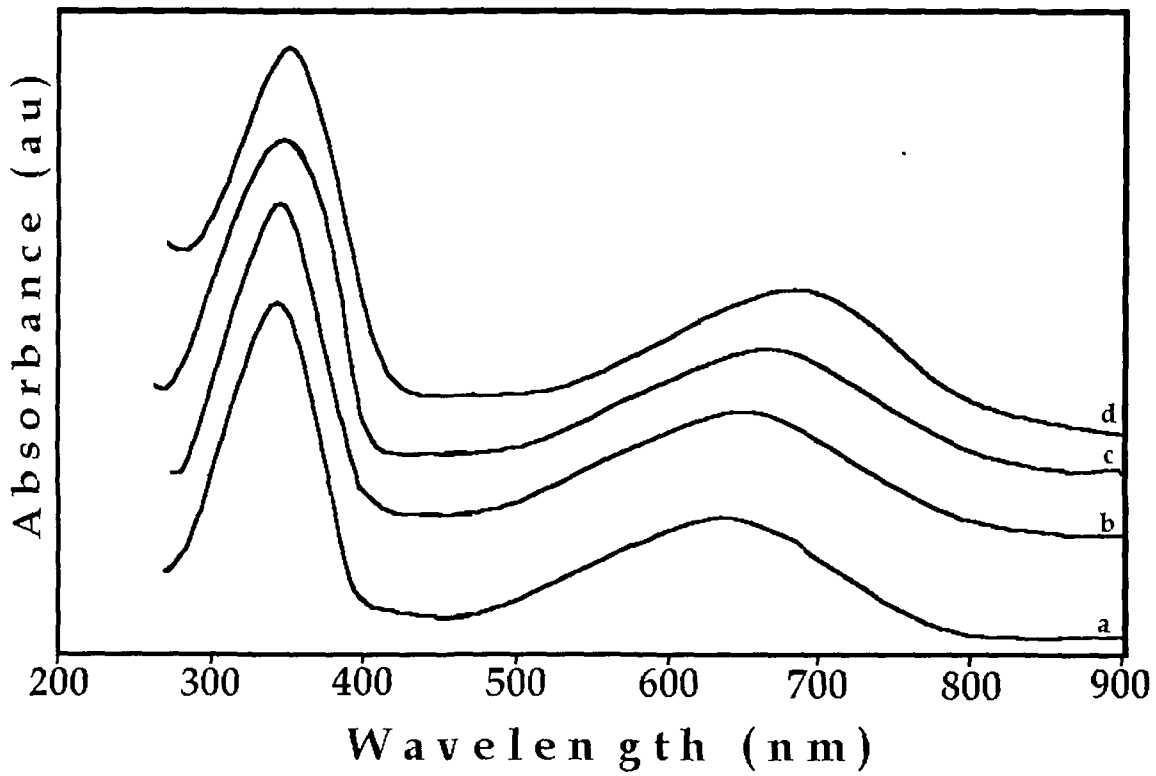


Figure 4.22: UV-Vis spectra of $HClO_4$ doped polyaniline (a) before and after irradiation with 120 MeV $Si^{9+}$ ion at fluences (b) $5x10^{10}$, (c) $5x10^{11}$ and (d) $3x10^{12}$ ions/$cm^2$.

wavelength region and becomes broader with the increase in fluence. The broadening of the carrier absorption peak may occur due to increase in defect sites of the polymer chain upon SHI irradiation, which causes absorption at different wavelengths giving rise to the broad absorption peak.

The UV-Vis spectra of the $HClO_4$ doped polyaniline conducting polymer films after irradiation with120 MeV $Si^{9+}$ ions at three different fluences of $5x10^{10}$, $5x10^{11}$ and $3x10^{12}$ ions/$cm^2$ are shown in Fig. 4.22. The UV-Vis spectra shows increase in absorption intensity at about 630 nm, which is attributed to the carrier absorption or quinoid absorption peak with shift of the peak towards higher wavelength with the increase in fluence. The increase in absorption towards higher wavelength and the peak shift indicates the lowering of energy band gap of the polymer film upon SHI irradiation, which is in consistent with the conductivity measurements. The decrease of band gap occurs due to broadening of polaron/bipolaron bands, which is attributed to increase in carrier concentration in the polymer films as large number of cations, anions, radicals and charged particles are created upon SHI irradiation.

### *4.4.5 FTIR spectroscopy:*

The FTIR spectra of HCl doped polyaniline films before and after irradiation with 160 MeV $Ni^{12+}$ ions are shown in Figs. 4.23 a-d respectively. The FTIR spectra of $HClO_4$ doped polyaniline irradiated with 120 MeV $Si^{9+}$ ions are shown in Figs. 4.24 a-d. Almost all the peaks observed in the unirradiated polyaniline film are present in the irradiated films indicating no change in the basic polymer chemical structure upon SHI irradiation. The stretching absorption peak [261] of N-H appeared in the range of 3420-3450 $cm^{-1}$. The peak near 3000 $cm^{-1}$ is due to the C-H stretching absorption. The peak at 1585 $cm^{-1}$ is attributed to quinod ring and the peak in the range of 1450-1500 $cm^{-1}$ is due to the benzenoid ring of polyaniline [258]. The peak due to N-H bending can be observed in the region of 1560-1640 $cm^{-1}$. The C=C stretching absorption of aromatic compound is obtained at about 1477 $cm^{-1}$. The peak at 1300 $cm^{-1}$ is due to the C-N stretching of the polymer. The strong band observed near 1100

$cm^{-1}$ and the band at 1235 $cm^{-1}$ is due to C-C stretching and C-C twisting, respectively of the alkyl chain [260]. The peak near 800 $cm^{-1}$ is due to the N-H out-of-plane bending absorption.

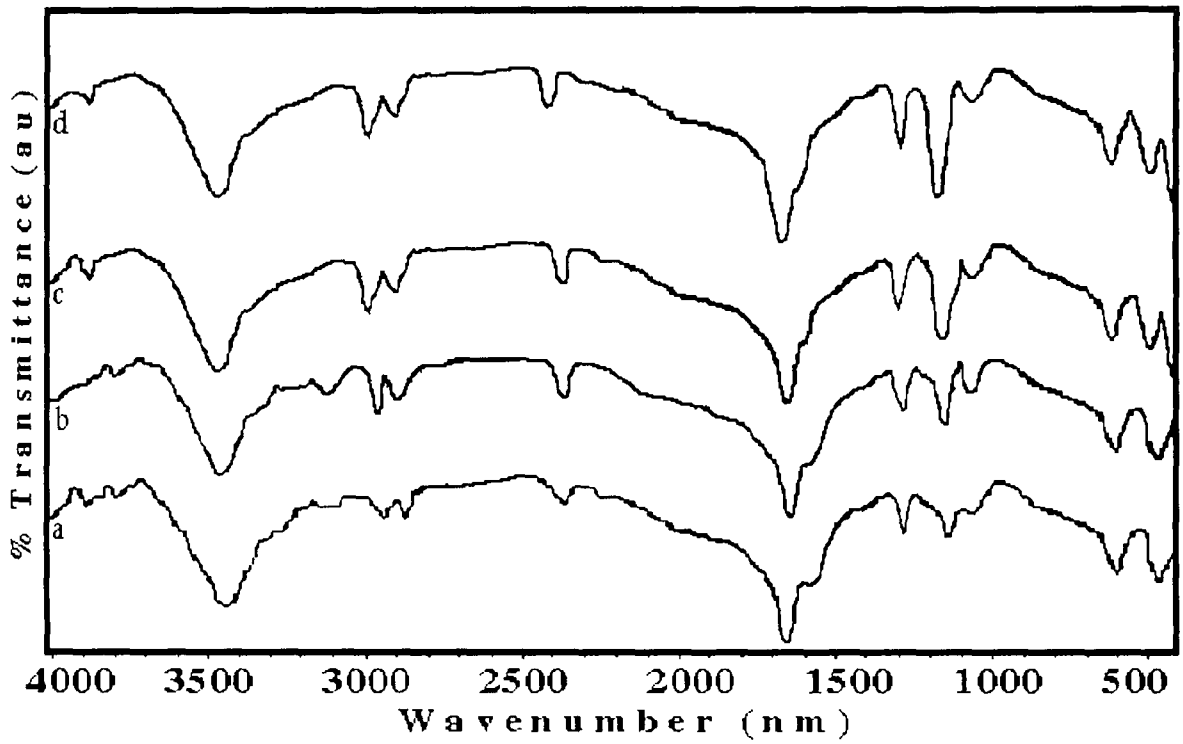


Figure 4.23: FTIR spectra of HCl doped polyaniline (a) before and after irradiation with 160 MeV $Ni^{12+}$ ions at fluences (b) $5x10^{10}$, (c) $5x10^{11}$ and (d) $3x10^{12}$ ions/$cm^2$.

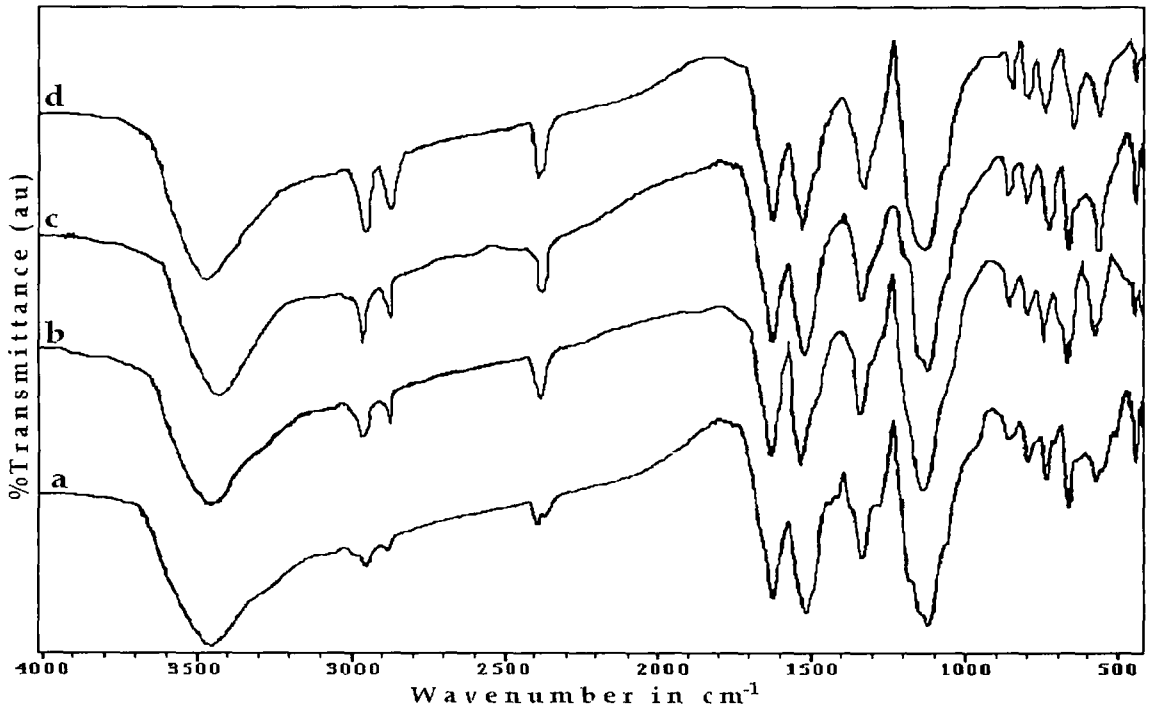


Figure 4.24: FTIR spectra of $HClO_4$ doped polyaniline (a) before and after irradiation with 120 MeV $Si^{9+}$ ions at fluences (b) $5x10^{10}$, (c) $5x10^{11}$ and (d) $3x10^{12}$ ions/$cm^2$.

After irradiation the peak intensity at 1150 $cm^{-1}$ is increased indicating possible cross linking in the polymer film occurring upon SHI irradiation. Moreover the intensity of C-H twisting vibration absorption peak at 1250 $cm^{-1}$ is decreased, this may also be an effect of cross-linking of the polymer chains, which binds the chain and hence twisting mode vibration is reduced and hence the peak intensity. The presence of absorption peak at 595 $cm^{-1}$ in the FTIR spectra of irradiated polyaniline film, which is attributed to C-Cl stretching confirms the presence of dopant in the polymer film. The absorption bands around 1100 $cm^{-1}$ in perchloric acid doped polyaniline have been assigned to the $ClO_4^-$ anion [262-264] confirming the presence of the dopant ion even after the SHI irradiation (Fig. 4.24).

### *4.4.6 X-Ray Diffractogram study:*

The XRD patterns of the HCl doped conducting polymer films before and after SHI irradiation with 160 MeV $Ni^{12}$ ions are presented in Figs. 4.25a-d. The XRD patterns of $HClO_4$ doped polyaniline films irradiated with 120 MeV $Si^{9+}$ ions are shown in Figs. 4.26a-d. The figures show that the polyaniline conducting polymer films before and after irradiation is semi-crystalline. The degree of crystallinity (K) calculated using the method described in chapter 3, section 3.6.6 of the polyaniline films are given in Table 4.3. The degree of crystallinity shows an increase with the increase in fluence. The crystallinity of polymer films arises due to systematic alignment of polymer chains by chain folding or by the formation of single or multiple helices, for at least part of their lengths [268]. These regions possess long range order and are therefore crystalline.

Upon SHI irradiation, collective excitations (plasmons) produces a large excited volume in which, the backbone bonds may rotate and adopt a variety of conformations. Upon cooling, the lower-energy configurations of bonds are preferred. Stereoregular chains then favour regular helical zigzag shapes. At the same time, these regular sections of chain may align together to form

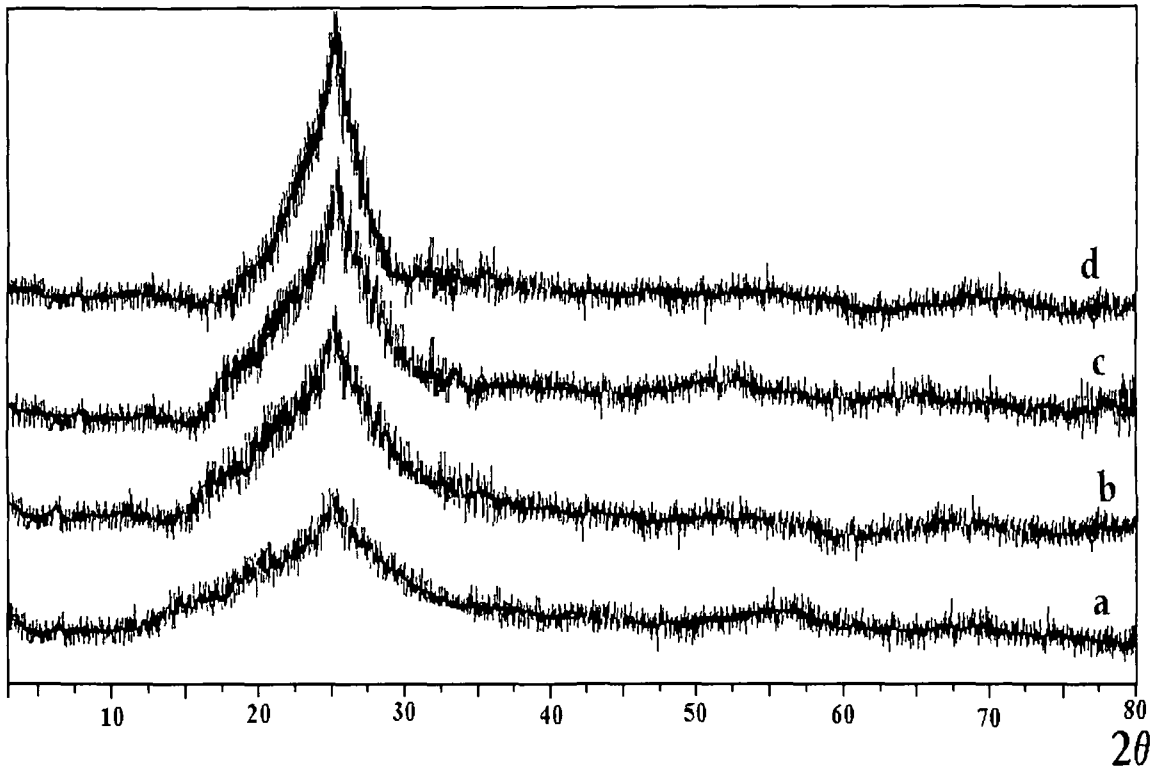


Figure 4.25: X-ray Diffractograms of HCl doped polyaniline films (a) before and after irradiation with 160 MeV $Ni^{12+}$ ion at fluences (b) $5x10^{10}$, (c) $5x10^{11}$ and (d) $3x10^{12}$ ions/$cm^2$.

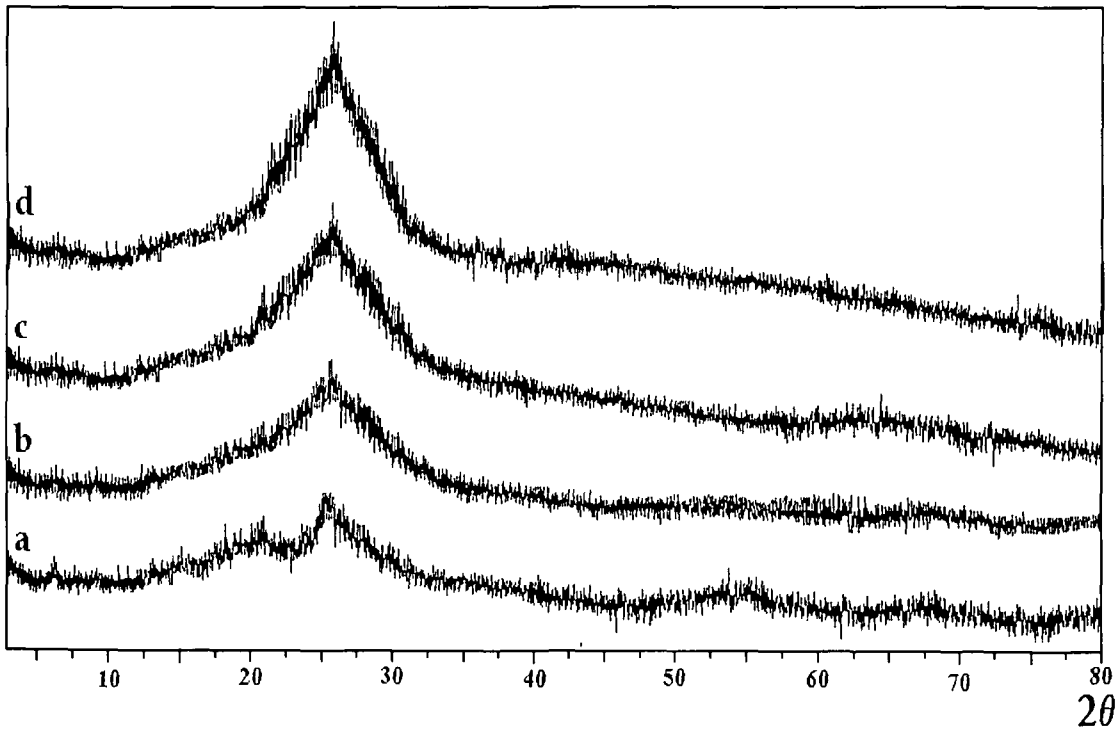


Figure 4.26: X-ray Diffractograms of $HClO_4$ doped polyaniline films (a) before and after irradiation with 120 MeV $Si^{9+}$ ion at fluences (b) $5x10^{10}$, (c) $5x10^{11}$ and (d) $3x10^{12}$ ions/$cm^2$.

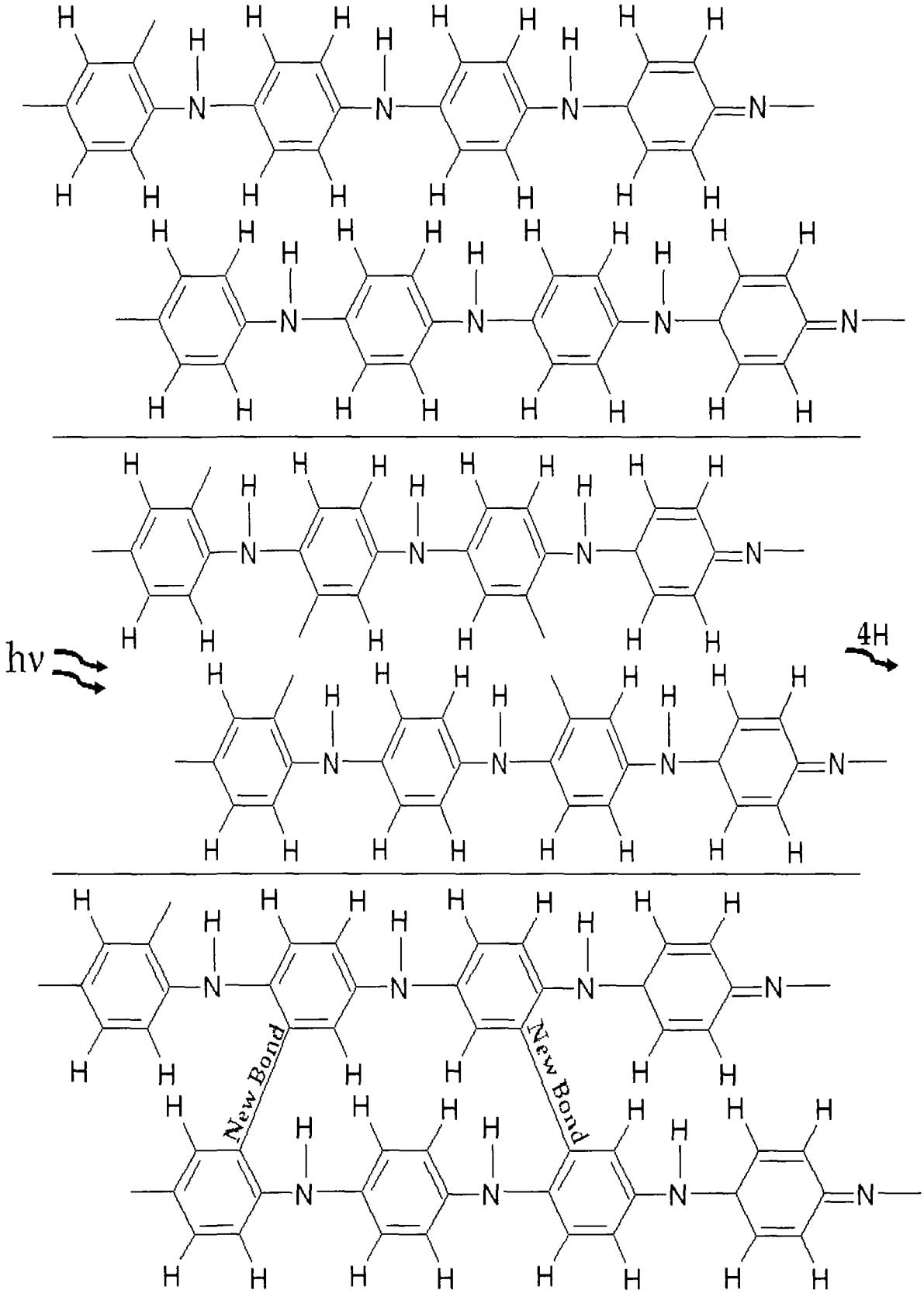


Figure 4.27: Schematic diagram for cross linking of polyaniline in SHI irradiation.

regions of crystallinity. The density of the polymer may increase upon SHI irradiation [269], this may have produced closely packed regions by chain folding, cross-linking of polymer chain or by the formation of single or multiple helices producing more crystalline regions in the polymer films resulting in the increase in degree of crystallinity. A possible mechanism of cross linking of polyaniline upon SHI irradiation is shown in Fig. 4.27. The degree of crystallinity is increased with the increase in ion fluence. The relative increase in the degree of crystallinity is less in case of $Si^{9+}$ ion irradiated polyaniline compared to $Ni^{12+}$ ion, which may be due to the difference in electronic energy loss ($S_e$) (Chapter III, Table 3.4).

Table 4.3: Degree of crystallinity of polyaniline films after SHI irradiation with 160 MeV $Ni^{12+}$ (HCl doped) and 120 MeV $Si^{9+}$ ($HClO_4$ doped) ion at different fluences.

| Fluence | Degree of crystallinity K (in %) | |
|---|---|---|
| | HCl doped | $HClO_4$ doped |
| Unirradiated | 29.3% | 29.9% |
| $5X10^{10}$ ions/cm$^2$ | 34.7% | 33.1% |
| $5X10^{11}$ ions/cm$^2$ | 40.2% | 38.9% |
| $3X10^{12}$ ions/cm$^2$ | 44.9% | 42.3% |

**4.5 Summary:**

The electropolymerization of polyaniline conducting polymer films has been carried out successfully on ITO coated glass substrates with different dopants. The polyaniline films synthesized in acetonitrile have been found to be dry and need not be dried for application as electrode unlike the films grown in aqueous electrolyte. The dopant concentration is required to be kept high for polymerization as well as to obtain good electronic conductivity, which has been consistent with earlier reported work [239]. The potentiodynamic method produces smoother and denser polymer films as compared to the potentiostatic method as observed in the surface morphological study. In potentiostatic method, the potential being fixed equal to the oxidation potential

of monomers, the dimers, trimers etc., near the working electrode grow haphazardly, which makes the surface of the film rough and more porous. The dc conductivity of the polymer films are dopant dependent [250] i.e., different dopants in the same medium in a particular conducting polymer show different conductivity. Cyclic voltammetry of the polyaniline conducting polymer films show good electroactivity with change in colour from bottle green in reduced polyaniline to deep green in the fully oxidized polyaniline film. The redox peak height i.e., the magnitude of oxidation and reduction current densities increases in the SHI irradiated polyaniline films, which is solely due to increase of conductivity of polymer films after irradiation as other experimental condition of cyclic voltammetry are kept exactly same. The FTIR spectroscopy of polyaniline films confirms the presence of the dopants in the polymer films. The presence of dopant ion after irradiation has also been confirmed from the studies of FTIR spectra of polyaniline films after irradiation. The conductivity of the polymer films is directly dependent of the band gap, which is observed in the UV-Vis spectra and the polymer absorbing at higher wavelength in the UV-Vis spectra (i.e., lower band gap) shows better conductivity. The degree of crystallinity of the polymer films also largely affects the electronic conductivity and this has been nicely observed in the X-Ray diffraction studies. The polymer with higher degree of crystallinity shows higher conductivity. In other words, it can be inferred that a conducting polymer film, which shows absorption in the higher wavelength region in the UV-Vis spectra and has higher degree of crystallinity would have high dc conductivity. The SHI irradiation of polyaniline films substantially increases the electronic conductivity. In the UV-Vis spectra of polyaniline after irradiation, it has been observed that the absorption in the higher wavelength region increases indicating lowering of band gap resulting in higher conductivity. The degree of crystallinity of the polyaniline conducting polymer films also increases upon SHI irradiation due to cross-linking of the polymer chains as a result of electronic stopping, which is a major effect at high energy ion irradiation of polymers. The more crystalline polymer morphology, i.e., the cross-linking of the polymer chains facilitates the

charge conduction between polymer chains resulting in increased conductivity. In the dc conductivity measurements and XRD studies of polyaniline films after irradiation with 160 MeV $Ni^{12+}$ and 120 MeV $Si^{9+}$ ion, a less increase in conductivity and degree of crystallinity has been observed in polyaniline conducting polymer films irradiated with $Si^{9+}$ ion beam, which may be due to less electronic energy transfer by the $Si^{9+}$ ion beam as compared to that by $Ni^{12+}$ ion beam (Chapter III, Table 3.4).

# CHAPTER V

# POLYPYRROLE: ELECTROPOLYMERIZATION, CHARACTERIZATION AND SHI IRRADIATION

Conducting polymers have been extensively explored as alternative materials to metals and inorganic semiconductors in the fabrication of microelectronic, optoelectronic and micromechanical devices [11,272-282]. One of the most interesting conducting polymers is polypyrrole (pPy), which has good environmental stability, high conductivity, high charge capacity, and easy synthesis. These properties are promising for application in sensors [283], actuators [284,285], molecular electronics [286,287], organic light emitting diodes (OLED) [288-290] and most significantly as electrodes in energy storage devices [218, 252, 291-293]. The oxidation potential of polypyrrole is lower than that of pyrrole monomer and hence polypyrrole prepared by both chemical and electrochemical methods produces polypyrrole in oxidized state and carries charges in the polymer [294]. The physical properties of polypyrrole conducting polymer films largely depend on methods of synthesis and nature of dopants. Recently it has been shown that a lower polymerization temperature of polypyrrole leads to higher electrical conductivity [295]. This increase in conductivity has been speculated to be due to improved ordering and morphology even though a direct evidence of ordering has not yet been provided [11]. Polypyrrole is known to have a coplanar structure of the heteroaromatic rings [31]. The doping process introduces positive holes (or polarons) along with the charge-balancing anions in the polymer chain. For polypyrrole a maximum of one dopant anion can be introduced for three monomer units. A recent study indicates that side reactions, including the introduction of free radicals by over-oxidation, can be minimized by electropolymerization at low temperatures [296]. One perceived disadvantage of polypyrrole is that it can only be p-doped, restricting the range of voltage available in symmetrical (type I) supercapacitors. Also the doping dependent conductivity limits the higher values of electrical conductivity of polypyrrole as

the increase of dopant concentration beyond a certain limit does not yield further increase in conductivity. Slow polymerization rate and low temperature produce more ordered polymer films with higher conductivity [295] due to increase of degree of crystallinity, which supports electronic conduction in the polymer film.

Most of research work reported on polypyrrole deals with cyclic voltammetry, conductivity, UV-Vis spectroscopy, device application such as sensors [283], artificial muscle [284, 285], organic electronics including organic light emitting diode (OLED) [286-290], electrodes in rechargeable batteries and supercapacitors[218, 252, 291-293] and material modification by adding side groups to the monomer or long chain dopants [274,275,279,297-299]. A few studies have been carried out on modification of the properties by swift heavy ion (SHI) irradiation. To the best our knowledge, SHI irradiation of polypyrrole conducting polymer above 100 MeV for electrode application is being reported in the present thesis for the first time. Moreover, few reports appeared with X-Ray diffraction and surface morphological studies on polypyrrole [271, 299-301].

In this chapter the electrochemical polymerization and characterization of polypyrrole is presented. The cyclic voltammetry of the polypyrrole films four probe measurements for dc conductivity, UV-Vis and FTIR spectroscopy, XRD and SEM studies of polypyrrole conducting polymer films have been carried out and presented in this chapter. Efforts have been made to enhance the properties like conductivity and crystallinity of the polypyrrole conducting polymer films 160 MeV $Ni^{12+}$ ion beam irradiation. All the characterizations of cyclic voltammetry, conductivity measurements, UV-Vis, FTIR spectroscopy, X-Ray diffraction and SEM, have been repeated on irradiated polymer films and the results and discussions thereof are presented in this chapter.

### 5.1 Electrochemical polymerization of polypyrrole film:

The electropolymerization of polypyrrole films have been carried out by potentiodynamic method in a three electrode electrochemical cell with stainless

steel counter electrode and saturated calomel electrode (SCE) as reference electrode on indium doped tin oxide (ITO) coated glass working electrodes as substrate. Lithium perchlorate ($LiClO_4$) and lithium trifluoromethanesulfonate ($LiCF_3SO_3$), tetrabutylammonium tetrafluoroborate ($[CH_3(CH_2)_3]_4NBF_4$), tetrabutylammonium hexafluorophosphate ($[CH_3(CH_2)_3]_4NPF_6$) and sodium perchlorate ($NaClO_4$) are used as dopants for preparation of polypyrrole conducting polymer films. For polypyrrole deposition by potentiodynamic method the potential is varied between -200 mV to 850 mV Vs SCE at a scan rate of 50 mV/s. High conducting blackish films of polypyrrole are obtained after about 75 cycles. Potentiostatic electropolymerization of polypyrrole films have been carried out at a constant potential of 850 mV against SCE reference electrode for 25 minutes. The films of polypyrrole synthesized in organic solvent are free standing, though brittle. Different concentrations of monomers (from 0.05 M to 0.15 M) and salt (from 0.2 M to 2.0 M) have been tried for optimizing the high conductivity of the polypyrrole films. The monomer concentration of 0.1M is observed to produce smoother surface films and above this concentration polymer films with rough flaky surface are produced. Below this concentration of monomer the rate of polymerization is slow and the yield of the polymer film is less. Lithium perchlorate salt concentration beyond 1.5 M does not increase the conductivity. Similarly for sodium perchlorate the saturation in dc conductivity is obtained at 1.5 M, 1.3 M for $LiCF_3SO_3$ and 1.7 M for ($[CH_3(CH_2)_3]_4NBF_4$) and ($[CH_3(CH_2)_3]_4NPF_6$). These optimum concentrations of monomers and salts have been maintained for preparation of all the electrolyte solutions for synthesis and cyclic voltammetry of the polypyrrole conducting polymer films.

## 5.2 Characterization of polypyrrole conducting polymer films:

### *5.2.1 Cyclic voltammetry:*

Cyclic voltammetry of conducting polymers is the most basic characterization technique to probe the redox response and to determine the electrochemical window within which the redox process is reversible. The

cyclic voltammograms (CVs) of polypyrrole films doped with $ClO_4^-$ ion in $LiClO_4$ on ITO coated glass substrate at different scan rates recorded with a potentiostate/galvanostate are shown in Fig. 5.1. The polypyrrole film doped with lithium perchlorate shows very good redox response with oxidation and reduction peaks. The magnitude of current in the oxidation and reduction process goes on increasing with the increase in scan rate. In the anodic sweep the current remains constant up to 0.5 V i.e., the polypyrrole film remains in reduced state. The oxidation of the polypyrrole film starts from 0.5 V and the oxidation peak occurs at 0.79 V. In the cathodic sweep i.e., reverse sweep the reduction of the polypyrrole films begins from 0.1 V and the reduction peak occurs at -0.35 V. In the oxidation process, perchlorate ion ($ClO_4^-$) moves into the polypyrrole polymer film and compensates for the electronic imbalance created in the polymer chain in the oxidation process so as to maintain the charge neutrality of the polymer chain. In the reverse sweep the dopant ion comes out of the polymer film as the polymer chain gets reduced. Complete expulsion of dopant ion, however, does not occur as some of the ions are trapped within the polymer chain.

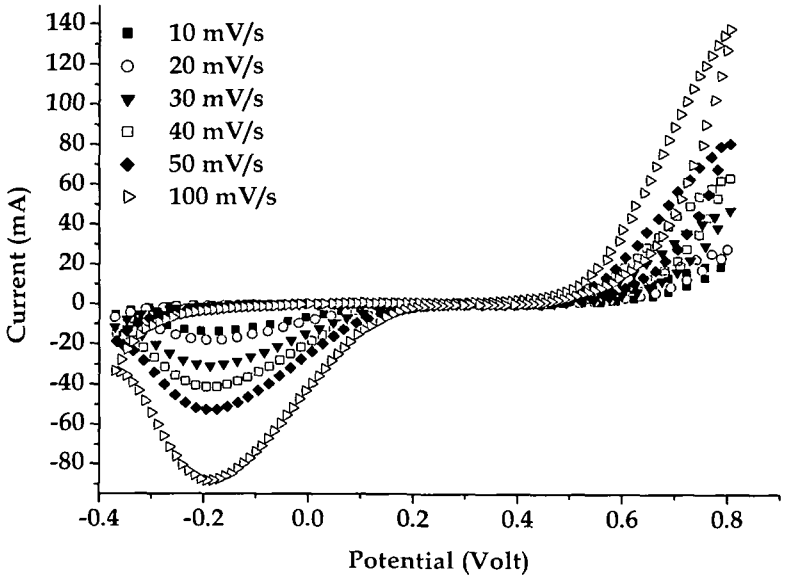


Figure 5.1: Cyclic voltammograms of polypyrrole doped with $LiClO_4$ at different scan rates.

The cyclic voltammograms (CVs) of $NaClO_4$ doped polypyrrole conducting polymer films are shown in Fig. 5.2. The oxidation and reduction peaks of $NaClO_4$ doped polypyrrole conducting polymer films occur at 850 mV and -190 mV in the forward and reverse sweep respectively. In the CVs of polypyrrole films doped with $ClO_4^-$ ion of $NaClO_4$ (Fig. 5.2) the oxidation and reduction peaks are broader as compared to those in the cyclic voltammogram of lithium perchlorate doped polypyrrole films (Fig. 5.1). This can be attributed to the larger size of the $Na^+$ ion, which has lower mobility. The peak current magnitude is also less in case of sodium perchlorate doped polypyrrole film for the same reason.

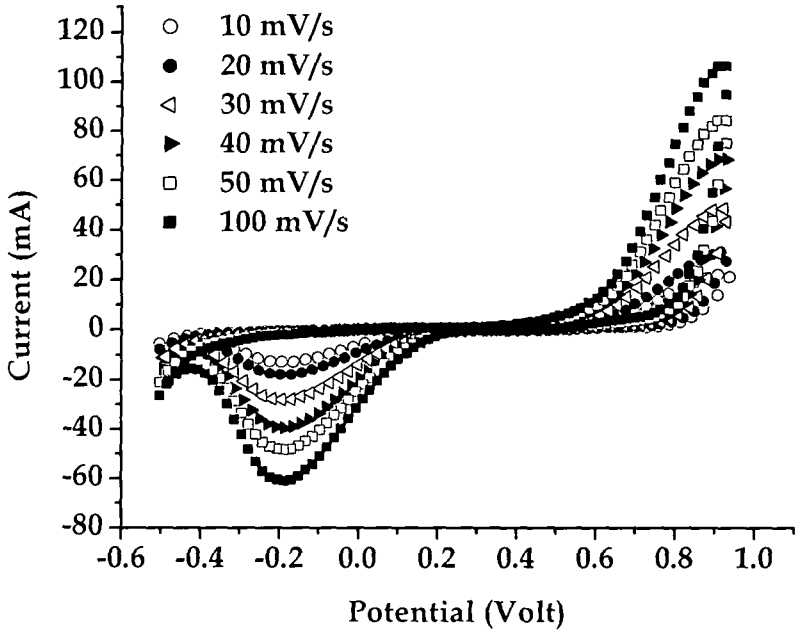


Figure 5.2: Cyclic voltammograms of polypyrrole doped with $NaClO_4$ at different scan rates.

The cyclic voltammograms of polypyrrole doped with lithium trifluoromethanesulfonate ($LiCF_3SO_3$) on ITO coated glass substrates are shown in Fig. 5.3. The cyclic voltammograms of $LiCF_3SO_3$ doped polypyrrole conducting polymer films show a broader oxidation peak. The oxidation peak for $LiCF_3SO_3$ doped polypyrrole occurs at 795 mV, which is 5 mV higher than that of the lithium perchlorate doped polypyrrole film. This may be attributed

to the larger dopant ion ($CF_3SO_3^-$) size. The reduction peak of $LiCF_3SO_3$ doped polypyrrole film has been observed at -210 mV, which is also broader compared to those with perchlorate ($ClO_4^-$) dopant ion. The polypyrrole conducting polymer films doped with lithium trifluoromethane sulfonate salt is observed to be in completely reduced state up to 0.35 V in the forward sweep and the oxidation of the film begins after this potential. In the reverse sweep, the reduction of the polymer film starts from 0.1 V and the process is completed at 0.4 V. In $CF_3SO_3^-$ ion doped polypyrrole, the trifluoro methane sulfonate ion moves into the polypyrrole conducting polymer film during oxidation and in the reverse sweep the dopant ion comes out of the polymer film, but due to the larger size of the dopant ion, larger quantity of dopant ions is trapped inside the polymer film as compared to that in the $ClO_4^-$ ion doped polypyrrole film, which again contributes to the oxidation process in the forward sweep. This could be the reason of increase of oxidation current at lower potential in the anodic sweep as compared to that of the perchlorate ion doped polypyrrole conducting polymer films.

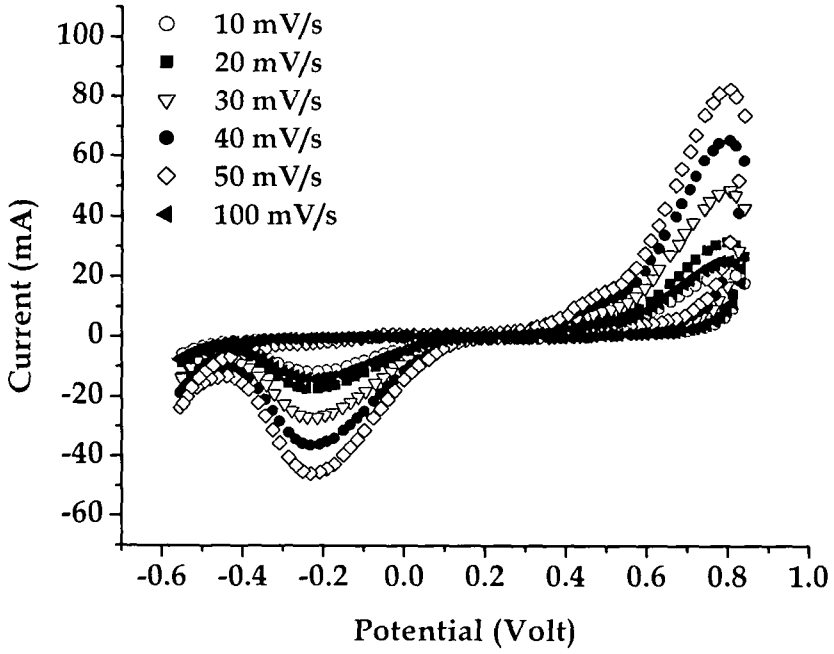


Figure 5.3: Cyclic voltammograms of polypyrrole doped with $LiCF_3SO_3$ at different scan rates.

The cyclic voltammograms of tetrabutylammonium tetrafluoroborate ($[CH_3(CH_2)_3]_4NBF_4$) doped polypyrrole films on ITO coated glass substrates recorded at different scan rates are shown in Fig. 5.4. The cyclic voltammograms show oxidation peak at potential 810 mV and the reduction peak at -280 mV. In tetrabutylammonium tetrafluoroborate doped polypyrrole, the tetrafluoro borate ($BF_4^-$) ion moves into the polypyrrole film during oxidation in the anodic or forward sweep of potential. Since $BF_4^-$ ion is smaller in size than $CF_3SO_3^-$ ion, hence most of the $BF_4^-$ ion comes out of the polymer film as against $CF_3SO_3^-$ during reverse sweep resulting in shift of oxidation peak towards higher potential in the $[CH_3(CH_2)_3]_4NBF_4$) doped polypyrrole films.

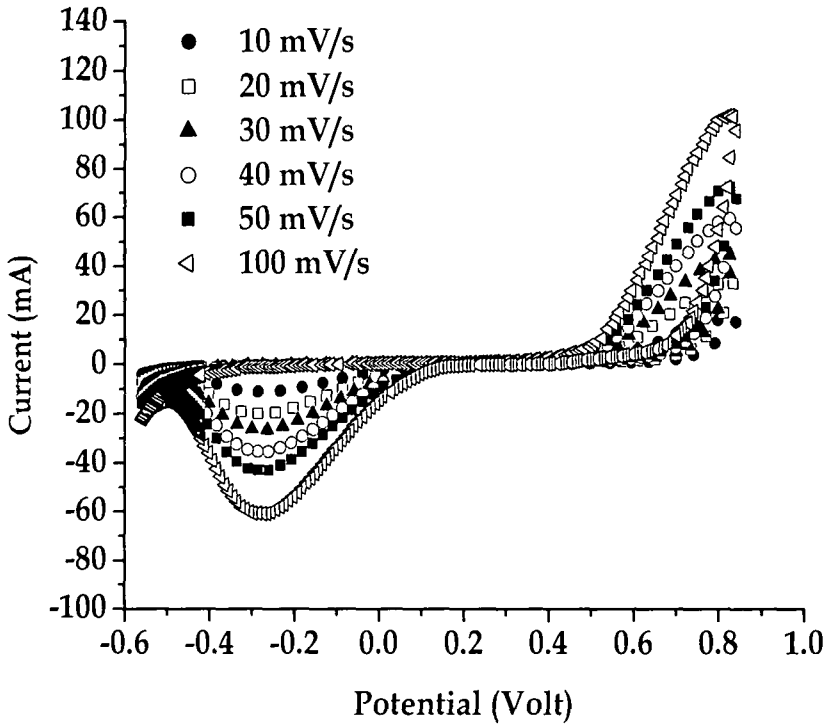


Figure 5.4: Cyclic voltammograms of polypyrrole doped with $[CH_3(CH_2)_3]_4NBF_4$ at different scan rates.

Cyclic voltammograms of polypyrrole conducting polymer films doped with tetrabutylammonium hexafluorophosphate ($[CH_3(CH_2)_3]_4NPF_6$) are shown in Fig. 5.5. The oxidation and reduction peaks of tetra butyl ammonium

hexafluoro phosphate doped polypyrrole films occur at 800 mV and -205 mV respectively but the oxidation current begins to rise from 0.3 V. This may be attributed to the trapped lower mobility and larger size dopant $PF_6^-$ ions inside the polymer film during synthesis and forward sweep of potential, which stimulates the oxidation process, occurs at relatively lower potential.

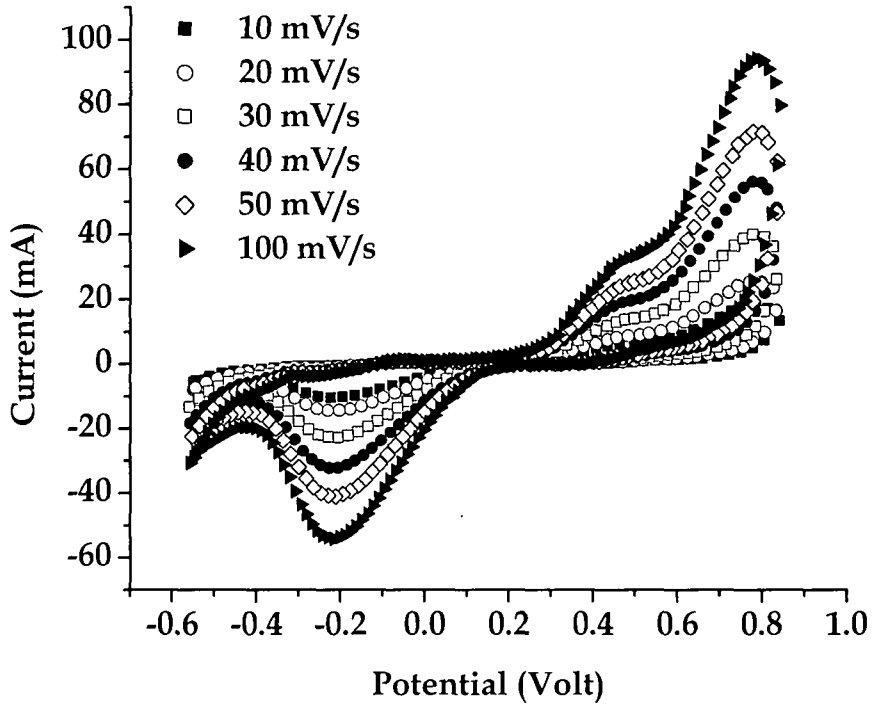


Figure 5.5: Cyclic voltammogram of polypyrrole doped with $[CH_3(CH_2)_3]_4NPF_6$ at different scan rate.

The oxidation reduction processes of polypyrrole conducting polymer films doped with different dopants are accompanied by change in colour. The deep brown polypyrrole film turns into black oxidized polypyrrole film in the forward sweep of potential, which again becomes deep brown in the reverse sweep. The oxidation reduction processes are reversible within the limit of potentials in which cyclic voltammetry is carried out. However, it is well known that polypyrrole is irreversibly damaged at potentials above 1.0 V versus SCE [302].

### 5.2.2 *Conductivity Studies:*

The dc conductivity of a material in thin film form can be measured with high accuracy using the four probe technique. The conductivity measurements of the polypyrrole polymer films have been carried out with laboratory standard four probe setup. The dc conductivity of polypyrrole films synthesized by potentiodynamic and potentiostatic method is measured for same dopant (Table 5.1) with slightly higher values of conductivity in polymer films synthesized by potentiodynamic method. The conductivity of polypyrrole films with different dopants does not vary much. The highest value of conductivity is obtained for polypyrrole films doped with tetrabutylammonium hexafluorophosphate (117 S/cm) and the lowest value of conductivity (86.9 S/cm) is obtained for sodium perchlorate doped polypyrrole conducting polymer films.

Table 5.1: The dc conductivity of polypyrrole conducting polymer films doped with different dopants measured by four probe method.

| Dopant | Conductivity (S/cm) | |
|---|---|---|
| | Potentiostatic | Potentiodynamic |
| Lithium perchlorate | 103 ± 2.7 | 107.4 ± 3.5 |
| Sodium perchlorate | 90 ± 3.1 | 92.7 ± 4.6 |
| Lithium trifluoro methane sulfonate | 97 ± 2.2 | 105.5 ± 3.5 |
| Tetra butyl ammonium tetrafluoro borate | 100.3 ± 2.9 | 112.5 ± 2.5 |
| Tetra butyl ammonium hexafluoro phosphate | 98.4 ± 3.1 | 113.5 ± 3.5 |

### 5.2.3 *Surface Morphology Study:*

Scanning electron microscopy is a versatile characterization technique to study the surface morphology of films. The SEM images of polypyrrole films doped with lithium perchlorate ($LiClO_4$), sodium perchlorate ($NaClO_4$), lithium trifluoromethanesulfonate ($LiCF_3SO_3$), tetrabutylammonium tetrafluoroborate ($[CH_3(CH_2)_3]_4NBF_4$) and tetrabutylammonium hexafluorophosphate ($[CH_3(CH_2)_3]_4NPF_6$) are presented in Figs. 5.6-5.10. Potentiodynamic synthesis of polypyrrole conducting polymer films doped with $LiClO_4$ shows globular

and fine granular surface morphology (Fig. 5.6), while polypyrrole films doped with $NaClO_4$ also show globular and granular morphology, in the latter the grain size is smaller and porosity is higher as compared to that of the former (Fig. 5.7). The lithium trifluoromethane sulfonate doped polypyrrole films show uniform granular surface morphology with less porosity (Fig. 5.8). The polypyrrole conducting polymer films doped with tetrabutylammonium tetrafluoroborate salt show dense surface morphology with fine grained structure (Fig. 5.9). In Fig. 5.10, tetra butyl ammonium hexafluoro phosphate doped polypyrrole film shows cauliflower like rough, flaky and porous surface morphology.

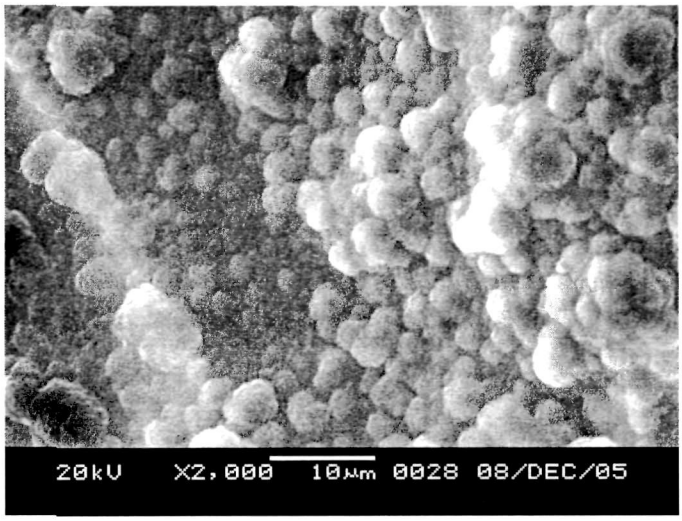


Figure 5.6: SEM image of polypyrrole doped with lithium perchlorate ($LiClO_4$).

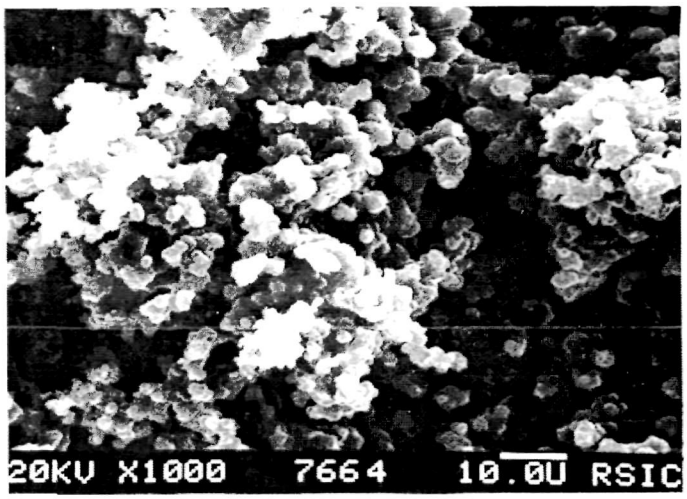


Figure 5.7: SEM image of polypyrrole doped with sodium perchlorate ($NaClO_4$).

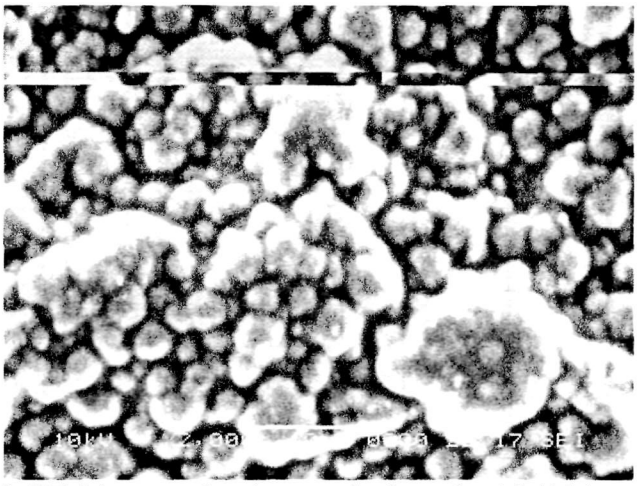

Figure 5.8: SEM image of polypyrrole doped with lithium trifluoro methane sulfonate ($LiCF_3SO_3$).

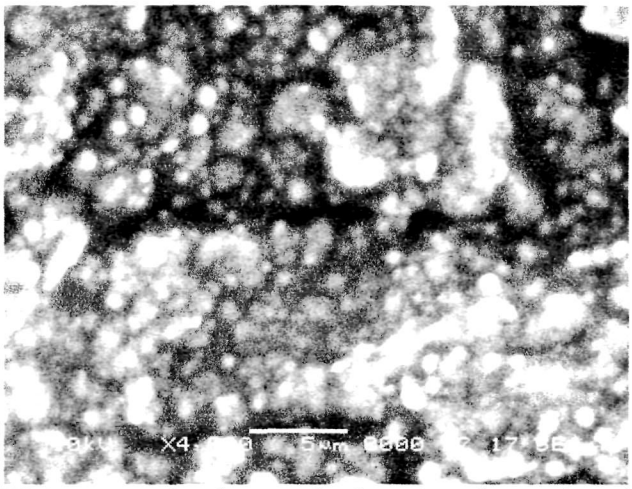

Figure 5.9: SEM image of polypyrrole doped with tetrabutylammonium tetrafluoroborate $[CH_3(CH_2)_3]_4NBF_4$.

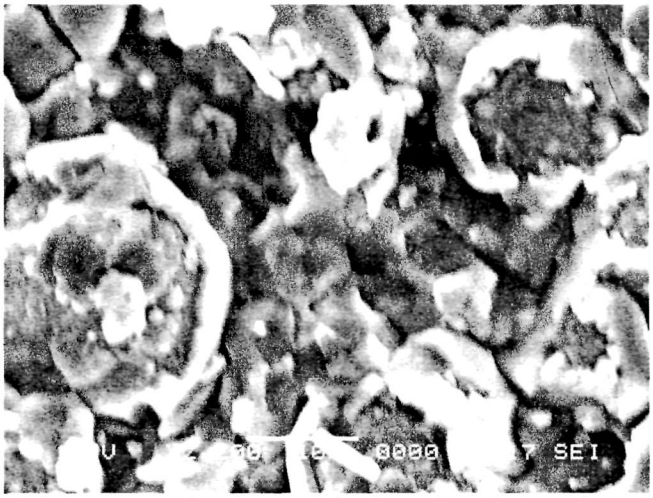

Figure 5.10: SEM image of polypyrrole doped with tetrabutylammonium hexafluorophosphate $[CH_3(CH_2)_3]_4NPF_6$.

### *5.2.4 UV-Vis spectroscopy:*

UV-Vis absorption spectroscopy is a versatile characterization technique, which directly reflects the electronic structure and band gap of a material as most of the electronic transitions between different energy levels take place in this energy region. The UV-Vis absorption spectra of the polymer films have been recorded to probe the electronic structure and determine the band gap on which the conductivity of the polymer films depends directly. The UV-Vis spectra of polypyrrole conducting polymer films doped with lithium perchlorate ($LiClO_4$), sodium perchlorate ($NaClO_4$), lithium trifluoromethane sulfonate ($LiCF_3SO_3$), tetrabutylammonium tetrafluoroborate ($[CH_3(CH_2)_3]_4NBF_4$) and tetrabutylammonium hexafluorophosphate ($[CH_3(CH_2)_3]_4NPF_6$) are presented in Fig. 5.11. The characteristic absorption peaks of polypyrrole at 320 nm corresponds to the characteristic $\pi \rightarrow \pi^*$ transition of the heteroaromatic pyrrole ring [303]. The absorption peak at 440 nm is the bipolaron absorption peak of polypyrrole conducting polymer [303].

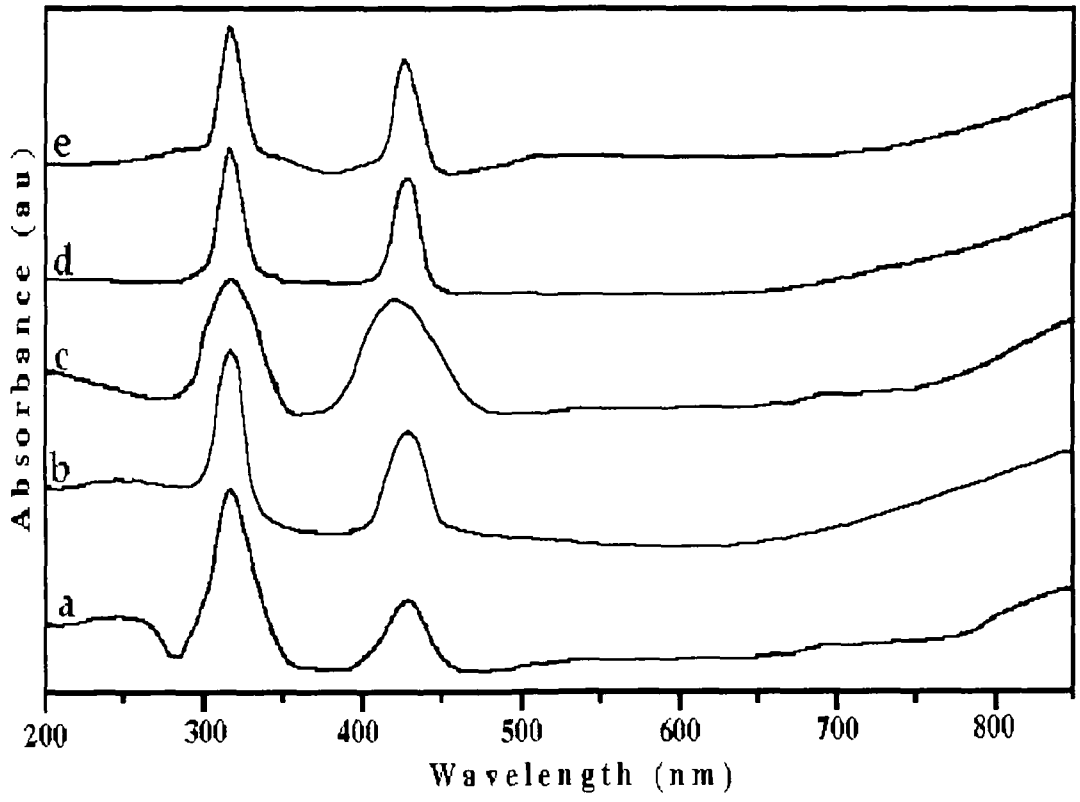


Figure 5.11: UV-VIS spectra of polypyrrole doped with (a) $LiClO_4$, (b) $NaClO_4$, (c) $LiCF_3SO_3$ (d) $[CH_3(CH_2)_3]_4NBF_4$ and (e) $[CH_3(CH_2)_3]_4NPF_6$.

The UV-Vis absorption spectra of all the polypyrrole conducting polymer films shows absorption in the higher wavelength (near IR) region, which indicates a low band gap of the polypyrrole conducting polymer films giving rise to possibility of obtaining higher conductivity, which has been observed in the conductivity studies.

*5.2.5 FTIR spectroscopy:*

Fourier transform infra-red (FTIR) spectroscopy provides a spectrum of large number of absorption bands due to stretching and bending modes of interactions between different atoms/groups of atoms in a molecule/polymer from which the chemical structure of the molecule/polymer can be visualized. The FTIR spectra of the polypyrrole conducting polymer films have been recorded to study the chemical structure of the polymer films and to probe the presence of dopants so as to ascertain the doping of the polymer films. The FTIR spectra of polypyrrole conducting polymer films undoped and doped with $LiClO_4$, $NaClO_4$, $LiCF_3SO_3$, $[CH_3(CH_2)_3]_4NBF_4$ and $[CH_3(CH_2)_3]_4NPF_6$ are presented in Figs. 5.12 a-f respectively. The N-H stretching peak appears at around 3400 $cm^{-1}$ in all the spectra. The conjugated peak at about 2800 $cm^{-1}$ is the C-H stretching vibration absorption of heteroaromatic pyrrole ring. The C=C stretching peak is obtained at 1600 $cm^{-1}$. N-H bending peak is obtained at 1500 $cm^{-1}$ and the C-N stretching absorption is obtained at 1250$cm^{-1}$. C-C stretching vibration absorption peaks for all the heteroaromatic pyrrole rings are observed at around 1100 $cm^{-1}$. N-H out of plane bending absorption peak occurs at 800 $cm^{-1}$. The C-Cl weak interaction peak is observed at 700 $cm^{-1}$ in the FTIR spectra of perchlorate ion doped polypyrrole conducting polymer films (Figs. 5.12 b and c).

The absorption bands at 1100 $cm^{-1}$ in lithium perchlorate and sodium perchlorate doped polypyrrole (Figs. 5.12 b and c) are attributed to the $ClO_4^-$ anion [263,264]. The absorption peak at 630 $cm^{-1}$ in the FTIR spectra of lithium

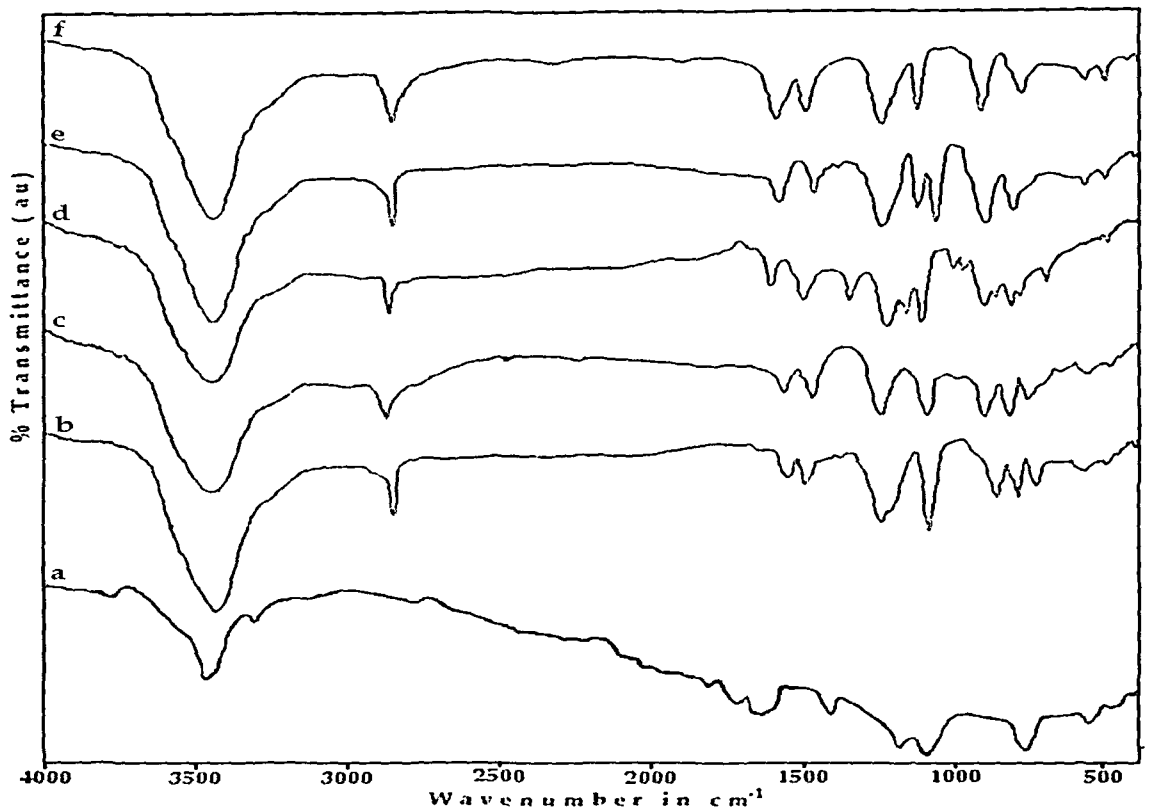


Figure 5.12: FTIR spectra of polypyrrole (a) undoped and doped with (b) $LiClO_4$, (c) $NaClO_4$, (d) $LiCF_3SO_3$, (e) $[CH_3(CH_2)_3]_4NBF_4$ and (f) $[CH_3(CH_2)_3]_4NPF_6$.

perchlorate and sodium perchlorate doped polypyrrole (Figs. 5.12 b and c) are assigned to the $ClO_4^-$ anion [265]. The strong absorption peak of S=O asymmetric stretching is observed at 1360 $cm^{-1}$ and the symmetric stretching vibration absorption for S=O is observed at 1180 $cm^{-1}$ in the trifluoromethanesulfonate doped polypyrrole film (Fig. 5.12 d). The S-O stretching vibration absorption in the $CF_3SO_3^-$ ion doped polypyrrole film shows several peaks in the absorption band of 1000- 750 $cm^{-1}$[265]. The band observed at 1089 $cm^{-1}$ (Fig. 5.12 e) in tetrabutylammonium tetrafluoroborate doped polypyrrole appears due to $BF_4^-$ dopant ion [304]. The sharp band at 842 $cm^{-1}$ (Fig. 5.12 f) is due to the incorporation of hexafluorophosphate ($PF_6^-$) ions [305]. The presence of dopant interaction absorption peaks in the FTIR spectra of respective salt doped polypyrrole conducting polymer films confirms the electrochemical doping of the polymer films during synthesis. Shifting of peaks, appearance of new absorption peaks and change in peak intensities in the lower

wavenumber region in the FTIR spectra of doped polypyrrole as compared to the undoped polypyrrole film could be attributed to the interaction of the dopant ions with the polymer chain.

### *5.2.6 X-Ray Diffractogram study:*

X-Ray diffraction is a most useful technique for the structural characterization of materials. For polymeric materials the proportion of crystalline region to that of amorphous region can be estimated in terms of the degree of crystallinity from the XRD patterns. The X-Ray diffractogram of polypyrrole conducting polymers doped with $LiClO_4$, $NaClO_4$, $LiCF_3SO_3$, $[CH_3(CH_2)_3]_4NBF_4$ and $[CH_3(CH_2)_3]_4NPF_6$ are presented in Figs. 5.13 a-e respectively.

The XRD patterns of polypyrrole conducting polymer films exhibit semicrystalline nature of the polymer films. Linear polymers are crystallisable if all the structural units are identical and will be inevitable for homopolymers for which the structural units are simple. Crystalline regions in polymer films are produced by systematic alignment of polymer chains by chain folding or by the formation of single or multiple helices, for at least part of their chain length [268].

The degree of crystallinity (K) of the polypyrrole films has been calculated using the relation

$$K = \frac{\text{Area under diffraction peak}}{\text{Total area under diffractogram}} x100\%$$

For visualizing the trend of change in crystallinity of the polymer films with change of dopant, the K values have been calculated by dividing the enlarged diffractogram into small square divisions of 0.5 mm X 0.5 mm and counting the total number of square division and number of square division under the peak using the above relation as described in chapter 3 section 3.6.6.1 and are presented in Table 5.2. The degree of crystallinity of polypyrrole films are almost identical i.e., about 25% of the polymer films are crystalline and the rest of the portion amorphous. The lithium trifluoromethanesulfonate doped

polypyrrole films exhibit the highest degree of crystallinity with K value of 26.70% and the tetrabutyl ammonium tetrafluoro borate doped polypyrrole conducting polymer films show lowest K value of 22.69%. the results are consistent with the conductivity results i.e., higher the degree of crystallinity, larger is the dc conductivity.

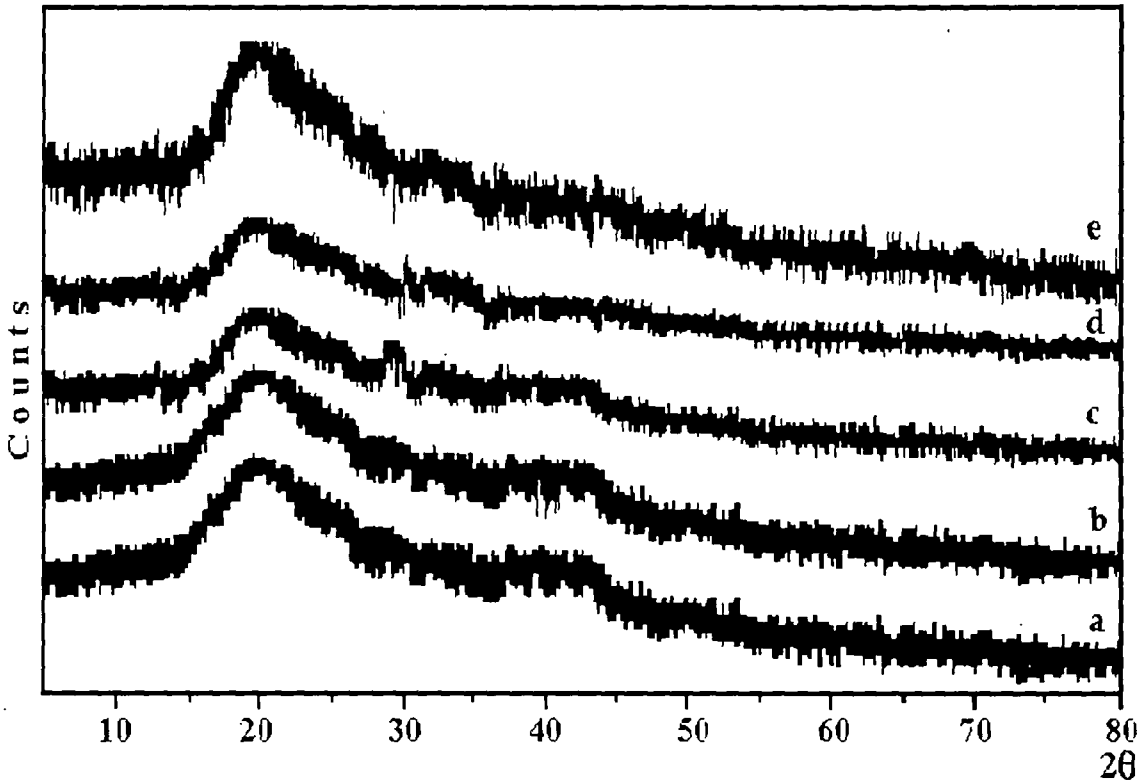


Figure 5.13: XRD patterns of polypyrrole doped with (a) $LiClO_4$, (a) $NaClO_4$, (c) $LiCF_3SO_3$, (d) $[CH_3(CH_2)_3]_4NBF_4$ and (e) $[CH_3(CH_2)_3]_4NPF_6$.

Table 5.2: Degree of crystallinity of polypyrrole conducting polymer films doped with different dopants.

| Dopant | Degree of crystallinity (K) |
|---|---|
| $LiClO_4$ | 25.35% |
| $NaClO_4$ | 24.82% |
| $LiCF_3SO_3$ | 26.70% |
| $[CH_3(CH_2)_3]_4NBF_4$ | 22.69% |
| $[CH_3(CH_2)_3]_4NPF_6$ | 25.68% |

## 5.3 SHI irradiation of polypyrrole conducting polymer films:

The polypyrrole conducting polymer films doped with $LiClO_4$, $LiCF_3SO_3$, ($[CH_3(CH_2)_3]_4NBF_4$) and ($[CH_3(CH_2)_3]_4NPF_6$) have been irradiated with 160 MeV $Ni^{12+}$ ion beam at three different ion fluences, $5x10^{10}$, $5x10^{11}$ and $3x10^{12}$ ions/$cm^2$. The irradiation of the conducting polymer films have been carried out in high vacuum in the general purpose scattering chamber (GPSC) of Inter University Accelerator Center, New Delhi. The ion current is kept low (0.5 pna) so as to avoid sample burning. All the characterizations on unirradiated polymer films have been repeated on the irradiated polypyrrole polymer films.

## 5.4 Characterization of irradiated polypyrrole films:

### *5.4.1 Cyclic voltammetry:*

The cyclic voltammograms of polypyrrole films doped with $LiClO_4$, $LiCF_3SO_3$, $[CH_3(CH_2)_3]_4NBF_4$ and $[CH_3(CH_2)_3]_4NPF_6$ recorded after irradiation with 160 MeV $Ni^{12+}$ ion at the scan rate of 50 mV/s are presented in the Figs. 5.14-5.17 respectively. All the conducting polypyrrole films show an electrochemical window within which the doping/dedoping (redox) processes are largely reproducible, beyond, which the oxidative or reductive decomposition of the conducting polymer occurs. The results obtained are consistent with the results reported on polypyrrole films [306, 307].

The CVs are related with the electrochromism of the conducting polymer films i.e., the redox peaks observed in the CVs coincide with colour change of the polymer films. All polymer films, unirradiated as well as irradiated, show large electroactivity in the organic electrolyte. Upon SHI irradiation the shape of the CVs of the unirradiated and irradiated polymer films remains same with oxidation and reduction occurring at the same potentials of 790 mV and -380 mV respectively, which shows that the redox property of the polypyrrole conducting polymer films remains same after SHI irradiation. However, there is an increase in the magnitude of oxidation and reduction current upon SHI irradiation, which can be attributed to the

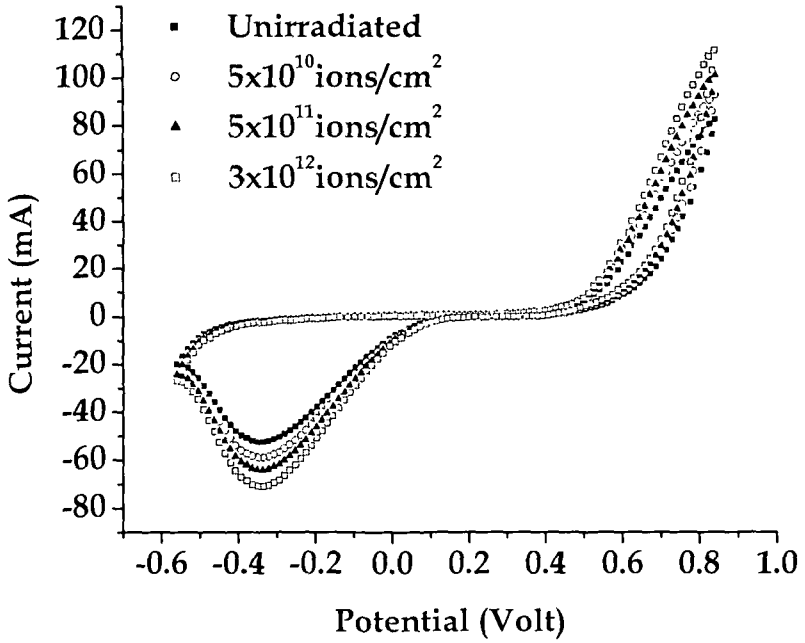


Figure 5.14: Cyclic voltammograms of polypyrrole films doped with $LiClO_4$ before and after irradiation at 50 mV/s scan rate.

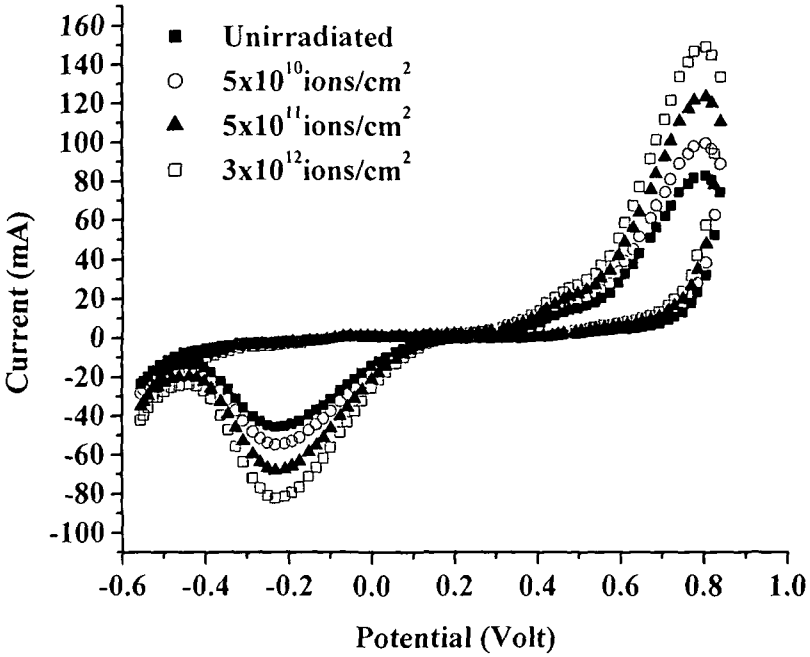


Figure 5.15: Cyclic voltammograms of polypyrrole doped with $LiCF_3SO_3$ before and after irradiation at 50 mV/s scan rate.

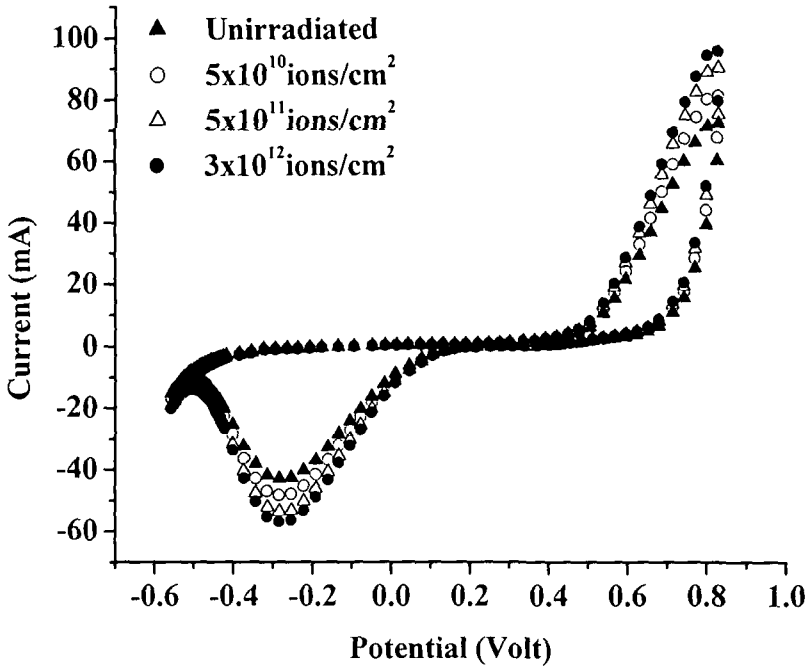


Figure 5.16: Cyclic voltammograms of polypyrrole doped with $[CH_3(CH_2)_3]_4NBF_4$ before and after irradiation at 50 mV/s scan rate.

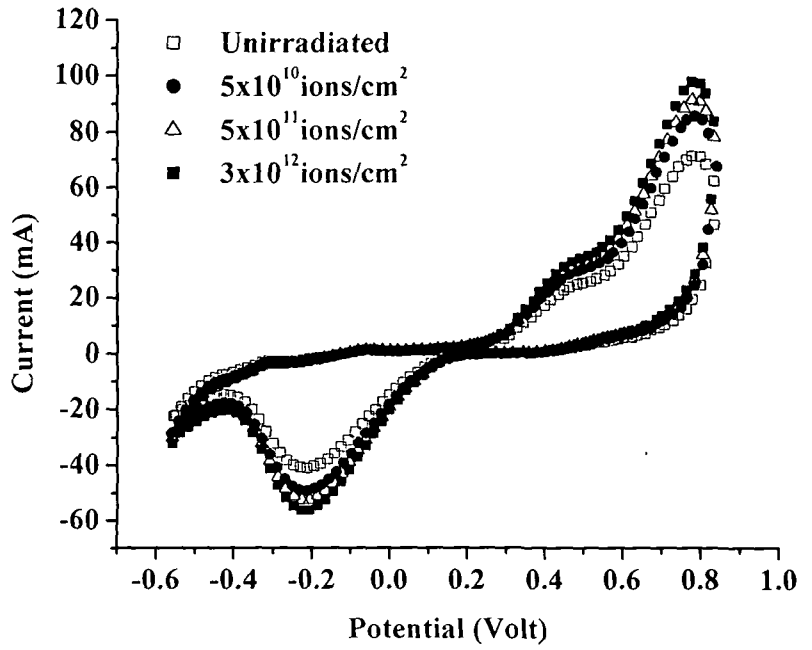


Figure 5.17: Cyclic voltammograms of polypyrrole doped with $[CH_3(CH_2)_3]_4NPF_6$ before and after irradiation at 50 mV/s scan rate.

increase in the charge carrier concentration in the polypyrrole films after SHI irradiation as the electrolyte and other experimental conditions in which the

CVs have been recorded, are kept unchanged. The oxidation and reduction peak currents have also been observed to increase with the increase of fluence, which is consistent with the conductivity results.

### *5.4.2 Conductivity measurements:*

The conductivity of the polymer films of the 160 MeV $Ni^{12+}$ ion irradiated polypyrrole conducting polymer films doped with $LiClO_4$, $LiCF_3SO_3$, $[CH_3(CH_2)_3]_4NBF_4$ and $[CH_3(CH_2)_3]_4NPF_6$ measured by using laboratory standard four-probe set-up at room temperature are presented in Table 5.3. The room temperature dc conductivity of unirradiated polypyrrole films is about 100 $Scm^{-1}$. The conductivity of the polypyrrole films has been observed to increase with the increase in irradiation fluence. The conductivity of the irradiated films has been measured to be around 160-170 S/cm. The increase in conductivity of the polymer films after 160 MeV $Ni^{12+}$ SHI irradiation may be ascribed to cross-linking occurring due to collective excitations (plasmons), which produce a large excited volume resulting in coercive interaction among the ions and radical pairs produced in the adjacent chains within the volume as a result of electron stopping mechanism [196]. These results are consistent with the effect of swift heavy ion irradiation of polymers [146.]. At high energy ion irradiation of polymer, cross-linking/recrystallization processes dominate over chain scission and bond-breaking processes [196], which increases the conductivity by enhancing the

Table 5.3: Conductivity of unirradiated and irradiated polypyrrole films.

| Dopant | Unirradiated (S/cm) | $5x10^{10}$ions/$m^2$ (S/cm) | $5x10^{11}$ions/$cm^2$ (S/cm) | $3x10^{12}$ions/$cm^2$ (S/cm) |
|---|---|---|---|---|
| $LiClO_4$ | 107.4 ± 3.5 | 152.4 ± 2.6 | 161.5 ± 3.5 | 167.5 ± 3.5 |
| $LiCF_3SO_3$ | 105.5 ± 3.5 | 155.5 ± 2.5 | 162.5 ± 4.5 | 169.5 ± 4.5 |
| $[CH_3(CH_2)_3]_4NBF_4$ | 112.5 ± 2.5 | 157 ± 3 | 162 ± 4.5 | 177.5 ± 3.5 |
| $[CH_3(CH_2)_3]_4NPF_6$ | 113.5 ± 3.5 | 153.5 ± 4.5 | 165 ± 5 | 176 ± 4 |

carrier mobility [196, 308] through the polymer chains, which otherwise occurs by the inter chain hopping mechanism required for conduction between the chains. The XRD results confirm that the crystallinity increases upon SHI irradiation.

### *5.4.3 Surface Morphology Study:*

The surface morphological studies of the polypyrrole conducting polymer films doped with $LiClO_4$, $LiCF_3SO_3$, $[CH_3(CH_2)_3]_4NBF_4$ and $[CH_3(CH_2)_3]_4NPF_6$ have been carried out by taking SEM images after irradiation with 160 MeV $Ni^{12+}$ ion at different fluences of $5x10^{10}$, $5x10^{11}$ and $3x10^{12}$ ions $cm^{-2}$ are presented in Figs. 5.18-5.21 respectively. Unirradiated polypyrrole films doped with $LiCF_3SO_3$ (Fig. 5.19a) show cauliflower like flaky and rough surface morphology. As the fluence of SHI irradiation increases the grain size decreases

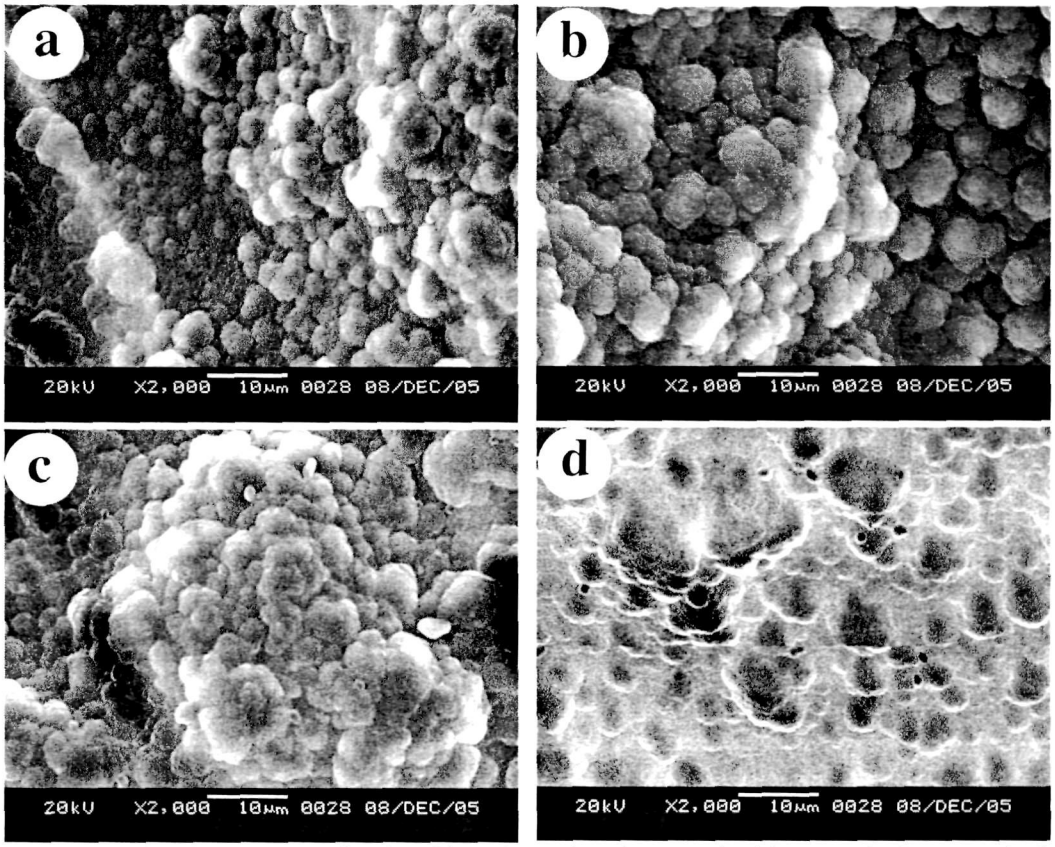


Figure 5.18: SEM micrograph of $LiClO_4$ doped polypyrrole films (a) before, and after irradiation with fluence (b) $5x10^{10}$, (c) $5x10^{11}$ and (d) $3x10^{12}$ ions/$cm^2$.

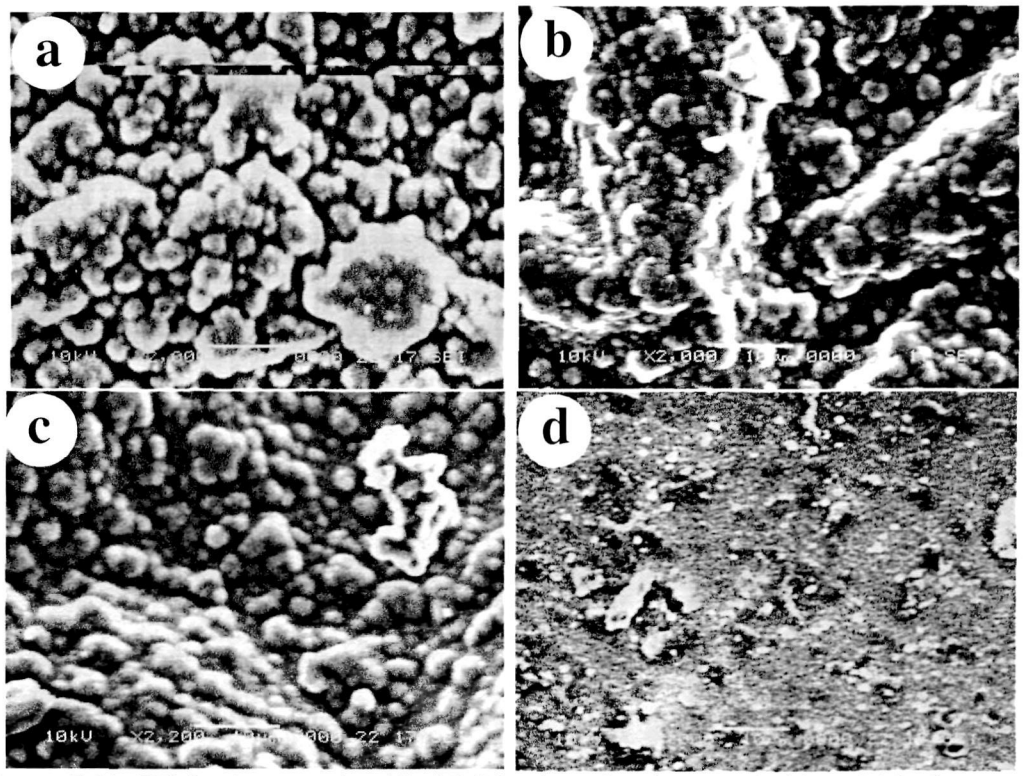


Figure 5.19: SEM micrograph of $LiCF_3SO_3$ doped polypyrrole films (a) before, and after irradiation with fluence (b) $5x10^{10}$, (c) $5x10^{11}$ and (d) $3x10^{12}$ ions/$cm^2$.

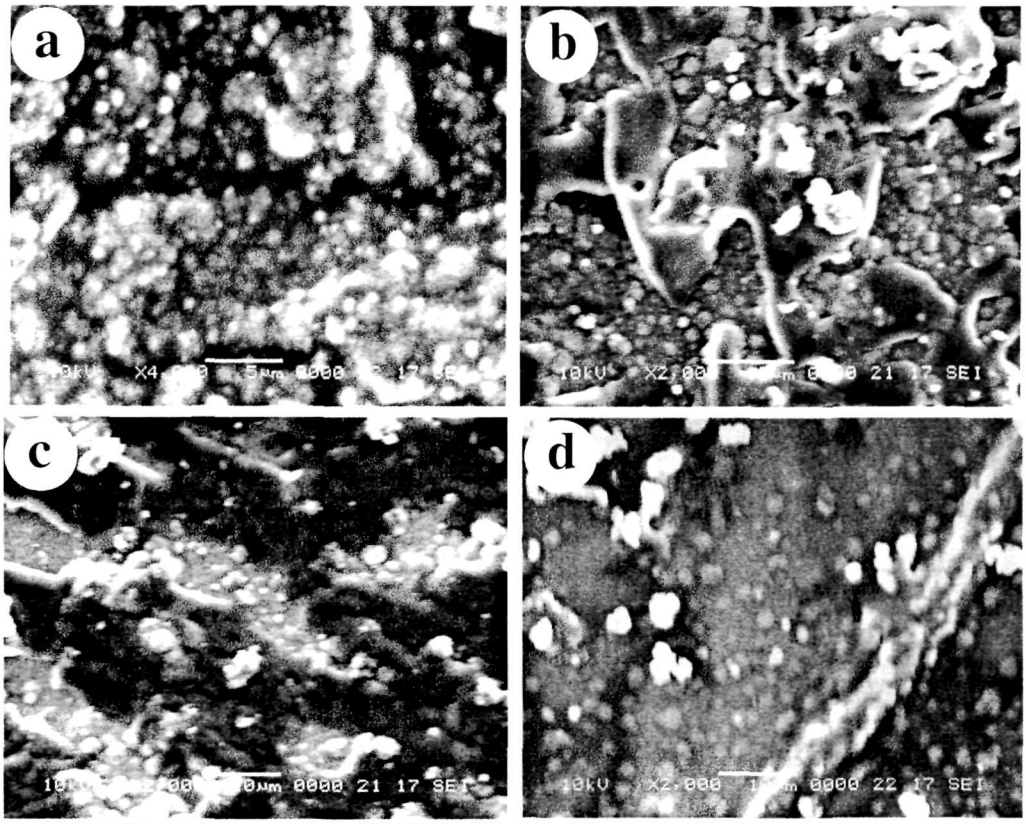


Figure 5.20: SEM micrograph of $[CH_3(CH_2)_3]_4NBF_4$ doped polypyrrole films (a) before, and after irradiation with fluence (b) $5x10^{10}$, (c) $5x10^{11}$ and (d) $3x10^{12}$ ions/$cm^2$.

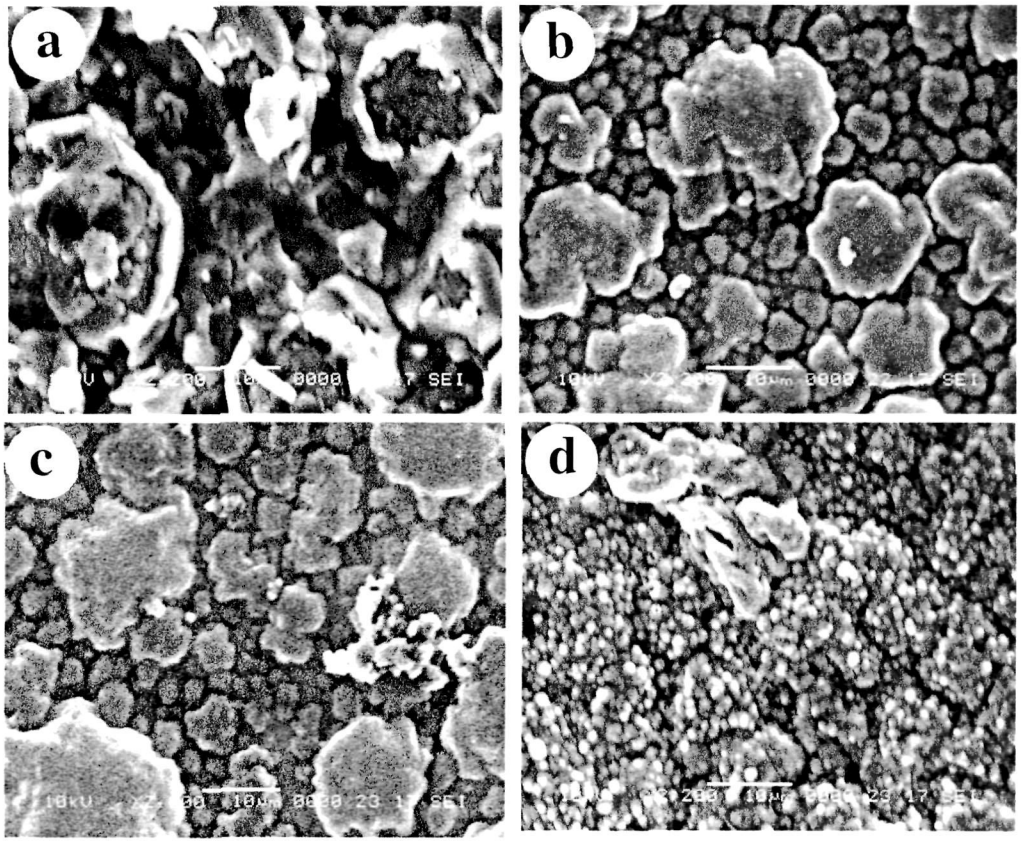


Figure 5.21: SEM micrograph of $[CH_3(CH_2)_3]_4NPF_6$ doped polypyrrole films (a) before, and after irradiation with fluence (b) $5x10^{10}$, (c) $5x10^{11}$ and (d) $3x10^{12}$ ions/$cm^2$.

and at the fluence of $3x10^{12}$ ions/$cm^2$, the surface of the polymer films becomes smooth and dense (Fig. 5.19d). Similar effects are observed in polypyrrole films doped with $[CH_3(CH_2)_3]_4NBF_4$ (Fig. 5.20) and $[CH_3(CH_2)_3]_4NPF_6$ (Fig. 5.21). The changes observed in the morphology of the polymer films may be ascribed to the displacement of the polymer chains from hilly to valley regions under the impact of the incident swift heavy ions making the film surface dense and smooth [196].

### *5.4.4 UV-Vis spectroscopy:*

The electronic structure and carrier density can be visualized from the study of UV-Vis spectra. The UV-Vis spectra of the conducting polypyrrole films doped with $LiClO_4$, $LiCF_3SO_3$, $[CH_3(CH_2)_3]_4NBF_4$ and $[CH_3(CH_2)_3]_4NPF_6$ recorded after SHI irradiation with 160 MeV $Ni^{12+}$ ion at each fluence and are presented in Figs. 5.22-5.25 respectively. The characteristic absorption peak

corresponding to $\pi$–$\pi^*$ transition of the heteroaromatic pyrrole ring of unirradiated polypyrrole film has been observed at around 320 nm [303]. The absorption peak at around 440 nm is the absorption peak of bipolaron band of polypyrrole conducting polymer [303]. After SHI irradiation, the intensity of the carrier absorption peak increases with the increase in fluence, which indicates an increase in the bipolaron concentration in polymer films upon ion irradiation, which could be attributed to the electronic linear energy transfer due to the incident heavy ion producing active chemical species, cations, anions, radicals and electrons along the ion track [196]. The increase in absorption intensities and shift of absorption peaks towards higher wavelength observed in SHI irradiated polypyrrole films indicating lowering of band gap [309] are consistent with the conductivity results, which increases with fluence upon SHI irradiation. The decrease of band gap occurs due to broadening of polaron/bipolaron bands, which is attributed to the increase in carrier concentration in the polymer films as large number of cations, anions, radicals and charged particles are created upon SHI irradiation.

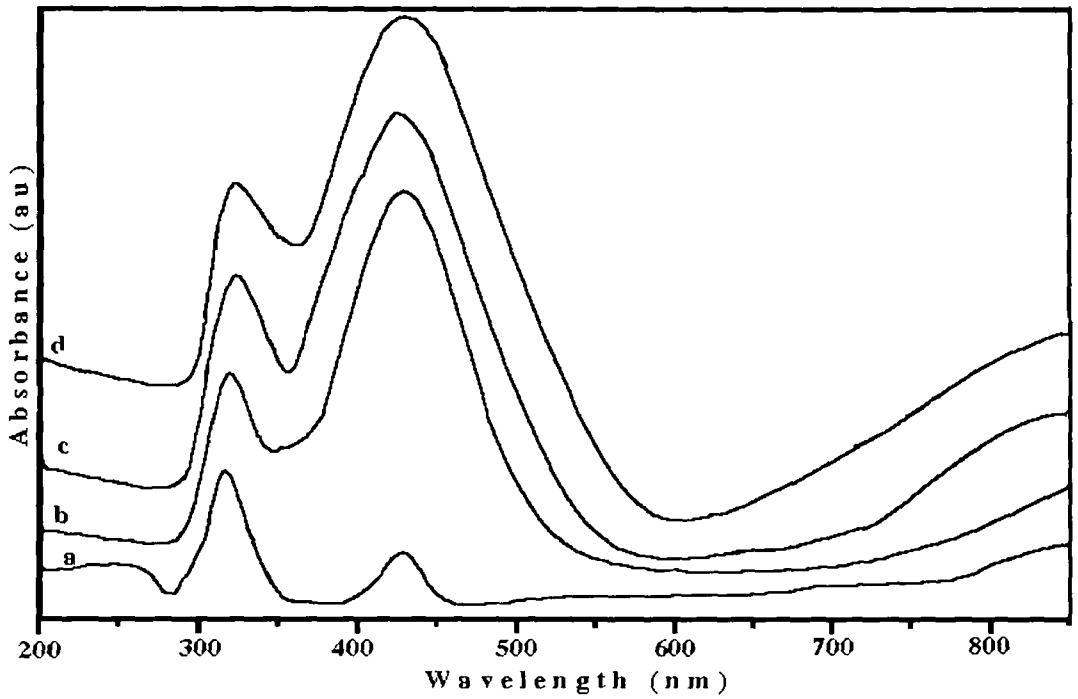


Figure 5.22: UV-Vis spectra of $LiClO_4$ doped polypyrrole films (a) before, and after irradiation with fluence (b) $5x10^{10}$, (c) $5x10^{11}$ and (d) $3x10^{12}$ ions/cm$^2$.

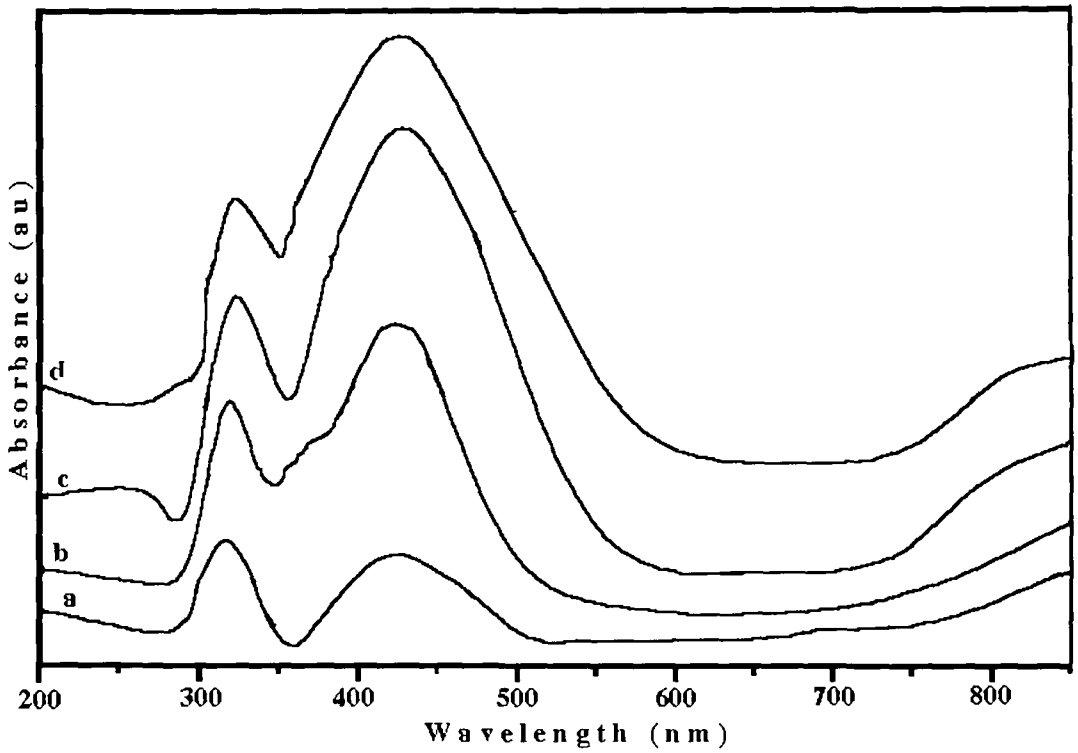


Figure 5.23: UV-Vis spectra of $LiCF_3SO_3$ doped polypyrrole films (a) before, and after irradiation with fluence (b) $5x10^{10}$, (c) $5x10^{11}$ and (d) $3x10^{12}$ ions/cm$^2$.

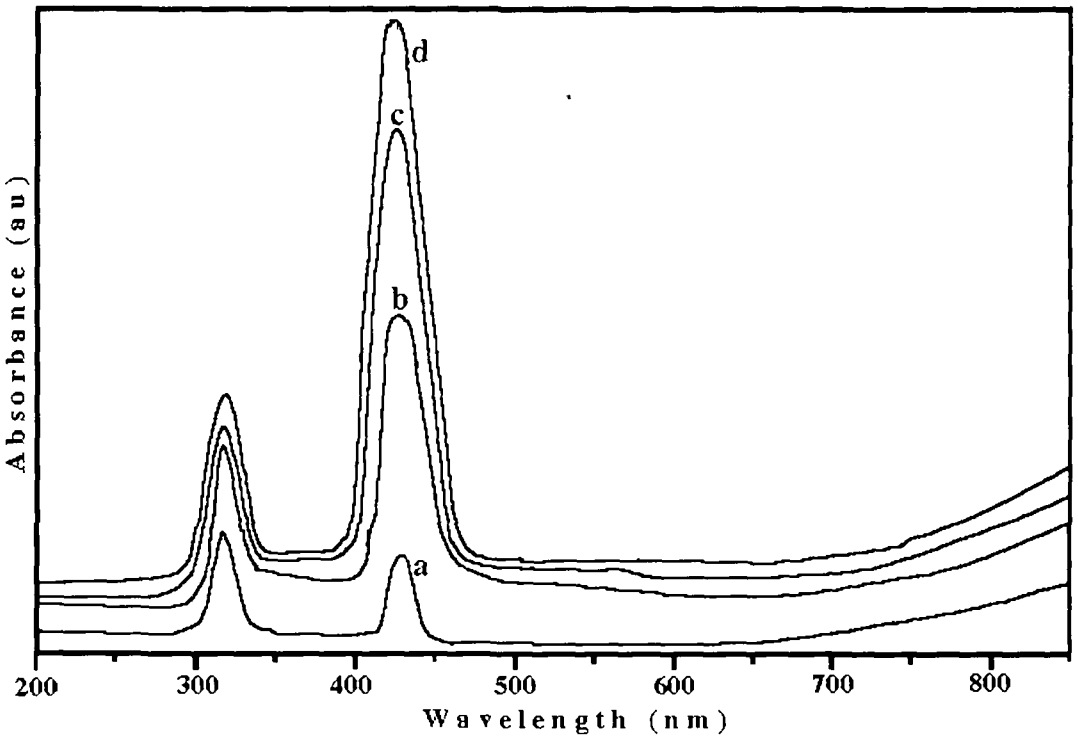


Figure 5.24: UV-Vis spectra of $[CH_3(CH_2)_3]_4NBF_4$ doped polypyrrole films (a) before, and after irradiation with fluence (b) $5x10^{10}$, (c) $5x10^{11}$ and (d) $3x10^{12}$ ions/cm$^2$.

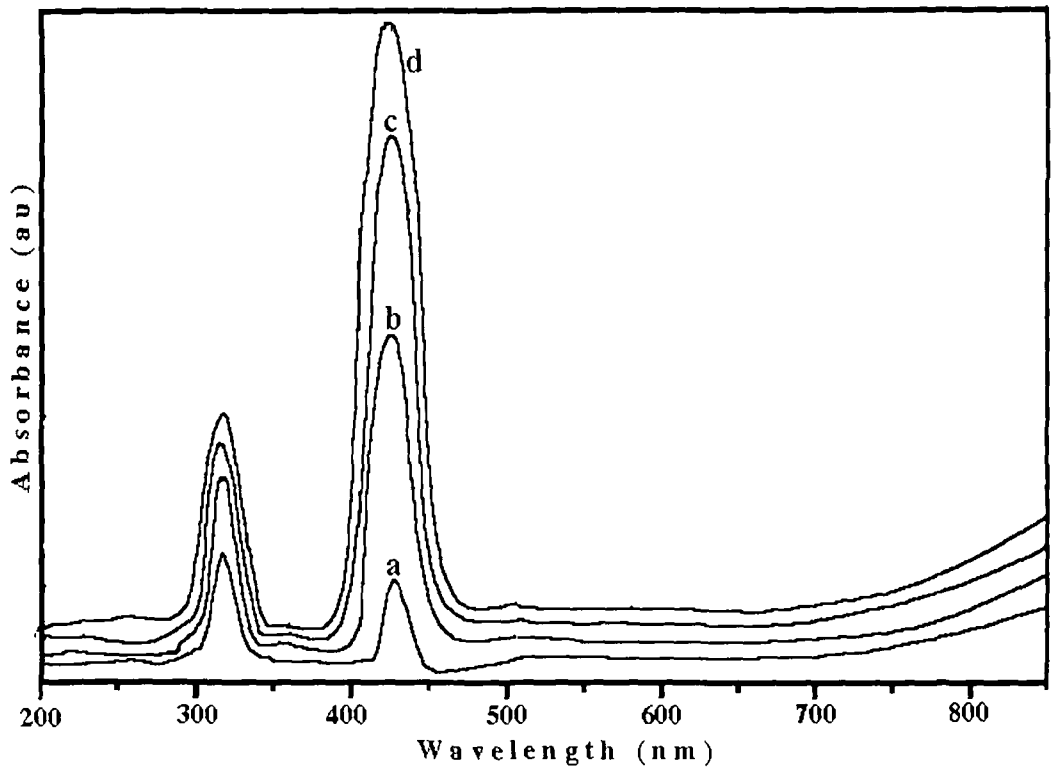


Figure 5.25: UV-Vis spectra of $[CH_3(CH_2)_3]_4NPF_6$ doped polypyrrole films (a) before, and after irradiation with fluence (b) $5x10^{10}$, (c) $5x10^{11}$ and (d) $3x10^{12}$ ions/cm$^2$.

### 5.4.5 *FTIR spectroscopy:*

The FTIR spectra of the polypyrrole conducting polymer films doped with $LiClO_4$, $LiCF_3SO_3$, $[CH_3(CH_2)_3]_4NBF_4$ and $[CH_3(CH_2)_3]_4NPF_6$ recorded after SHI irradiation with 160 MeV $Ni^{12+}$ ion with fluence $3X10^{12}$ ions/cm$^2$ are presented in Fig. 5.26. There is no major change in the FTIR spectra have been observed in the SHI irradiation, only some peak intensity and slight change in absorption peak position are found to occur in the spectra of irradiated polypyrrole film samples.

Absorption peaks at around 3400 cm$^{-1}$ in all the FTIR spectra are attributed to the N-H stretching vibration. The C-H stretching vibration absorption peak of heteroaromatic pyrrole ring occurs around 2800 cm$^{-1}$. The C=C stretching absorption peak is obtained at 1600 cm$^{-1}$. The N-H bending vibration absorption peak occurs at 1500 cm$^{-1}$ whose intensity is observed to decrease after SHI irradiation (Figs. 5.26 b, d, f and h). N-H out of plane bending

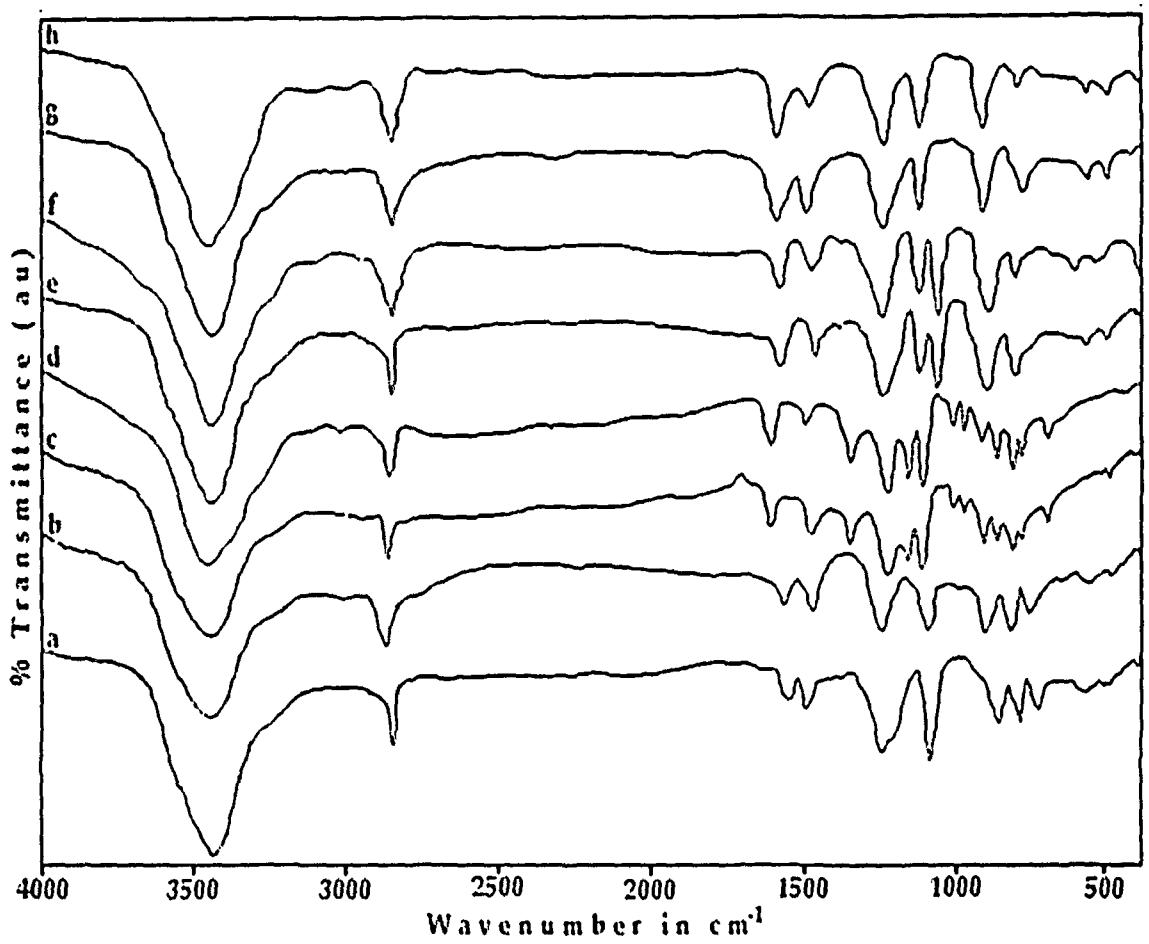


Figure 5.26: FTIR spectra of $LiClO_4$ doped (a) before and (b) after irradiation, $LiCF_3SO_3$ doped (c) before and (d) after irradiation, $[CH_3(CH_2)_3]_4NBF_4$ doped (e) before and (f) after irradiation and $[CH_3(CH_2)_3]_4NPF_6$ doped (g) before and (h) after irradiation of polypyrrole films.

absorption peak occurs at 800 $cm^{-1}$, which is also found to decrease upon irradiation. The decrease in intensities of N-H bending absorption peaks suggests breaking of N-H bonds upon SHI irradiation. The sites where hydrogen atoms are lost upon SHI irradiation may be the possible cross-linking sites. Schematic diagram of possible cross-linking in polypyrrole upon SHI irradiation is presented in Fig. 5.31. The C-N stretching absorption is obtained at 1250 $cm^{-1}$. The C-Cl weak interaction peak is observed at 700 $cm^{-1}$ in the FTIR spectra of perchlorate ion doped polypyrrole conducting polymer films (Figs. 5.26 a and b). The strong absorption symmetric and asymmetric stretching peaks of S=O are observed at 1180 $cm^{-1}$ and 1360 $cm^{-1}$ respectively in the trifluoromethanesulfonate doped polypyrrole film (Figs. 5.26 c and d). Several

peaks observed in the region of 1000 - 750 $cm^{-1}$ are of the S-O stretching vibration absorption in the $CF_3SO_3^-$ ion doped polypyrrole film. In FTIR spectra of tetrabutylammonium tetrafluoroborate doped polypyrrole the band observed at 1089 $cm^{-1}$ (Fig. 5.12 d) is due to $BF_4^-$ dopant ion [304]. The absorption band at 842 $cm^{-1}$ in the tetrabutylammonium hexafluorophosphate doped polypyrrole film (Fig. 5.12 e) is due to the $PF_6^-$ ions [305]. The presence of absorption peaks in the FTIR spectra of respective salt doped polypyrrole conducting polymer films confirms the electrochemical doping of the polymer films during electropolymerization.

### *5.4.6 X-Ray Diffractogram study:*

The XRD spectra of the polymer films after SHI irradiation with 160 MeV $Ni^{12+}$ ion are presented in Figs. 5.27-5.30. The unirradiated polypyrrole conducting polymer films are semi-crystalline. Significant increase in the degree of crystallinity of the polymer films has been observed upon SHI irradiation. The degree of crystallinity (K) of the polypyrrole films are shown in Table 5.4. Collective excitations (plasmons) produced upon SHI irradiation produces a large excited volume causing the backbone bonds to rotate and adopt a variety of conformations. Upon cooling the backbone chains prefer the lower-energy positions. Stereoregular chains will then favour regular helical shapes. These regular sections of chain may align together to form regions of crystallinity. Upon SHI irradiation the density of the polymer increases [269] making the polymer more compact, which may have produced closely packed regions by chain folding, cross-linking of polymer chain or by the formation of single or multiple helices producing more crystalline regions in the polymer films resulting in the increase in degree of crystallinity. The possible mechanism of cross linking after ejection of hydrogen atoms from the polypyrrole conducting polymer chain upon SHI irradiation is shown in Fig. 5.31. The degree of crystallinity increases with the increase in ion fluence. These

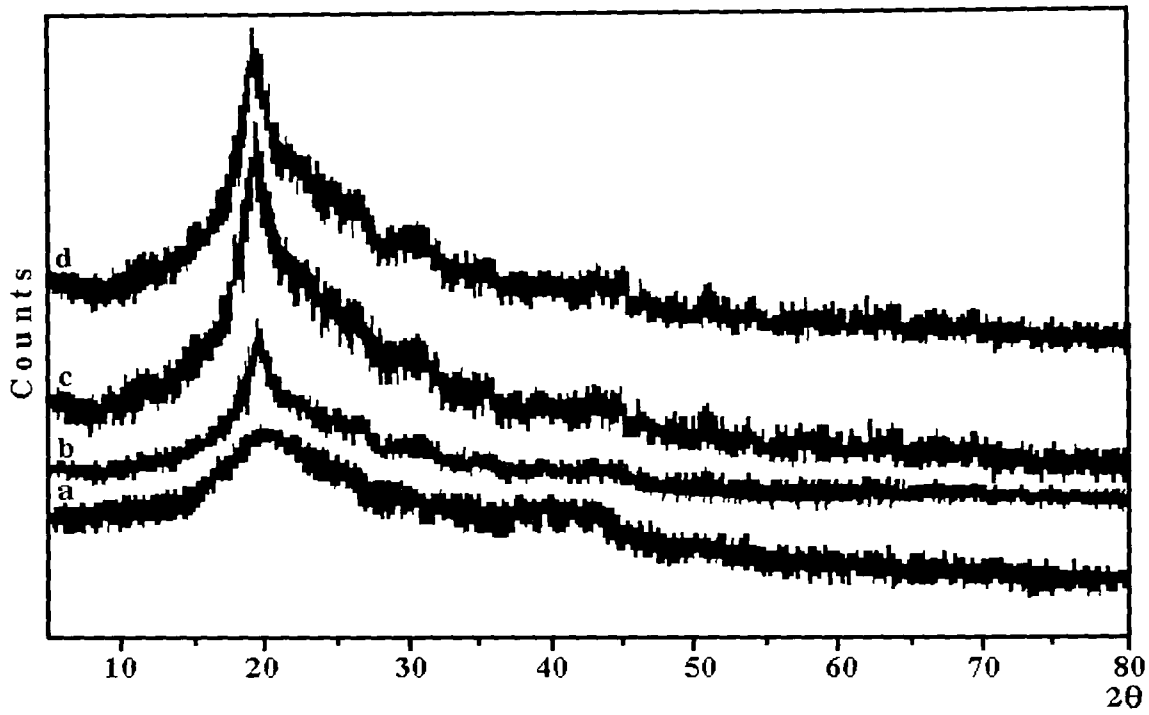


Figure 5.27: X-Ray diffractograms of $LiClO_4$ doped polypyrrole films (a) before, and after irradiation with fluence (b) $5x10^{10}$, (c) $5x10^{11}$ and (d) $3x10^{12}$ ions/cm$^2$.

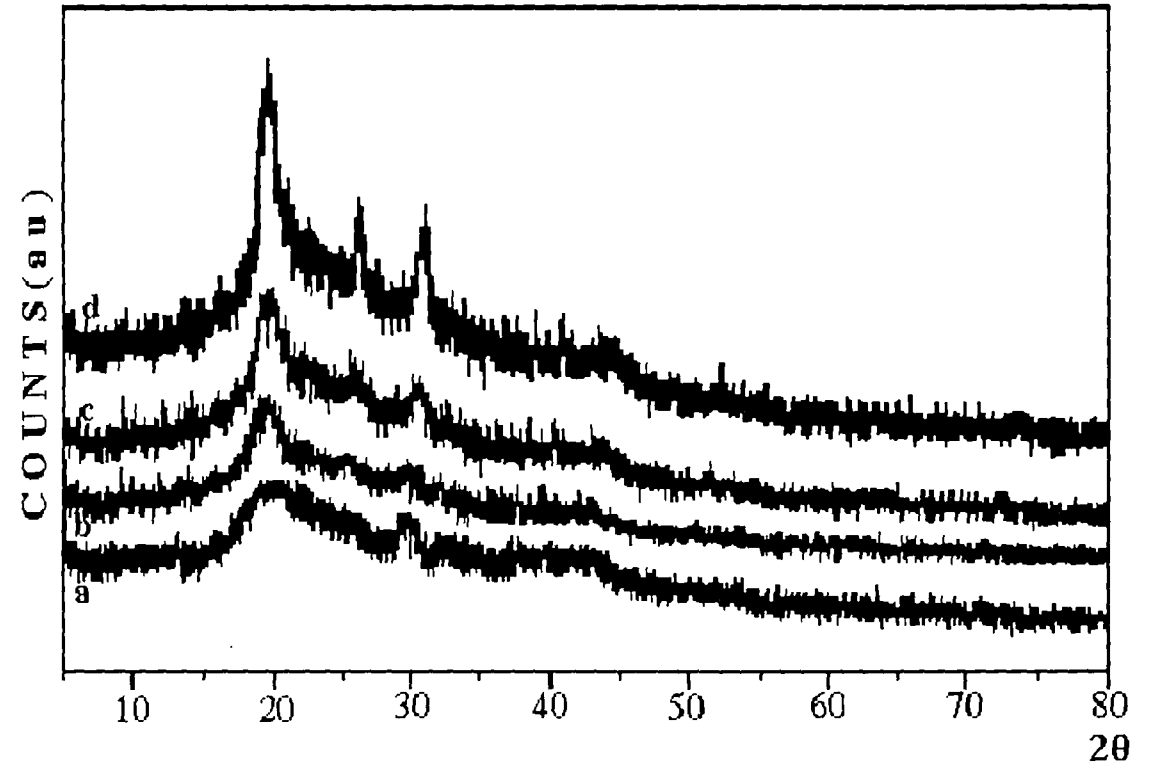


Figure 5.28: X-Ray diffractograms of $LiCF_3SO_3$ doped polypyrrole films (a) before, and after irradiation with fluence (b) $5x10^{10}$, (c) $5x10^{11}$ and (d) $3x10^{12}$ ions/cm$^2$.

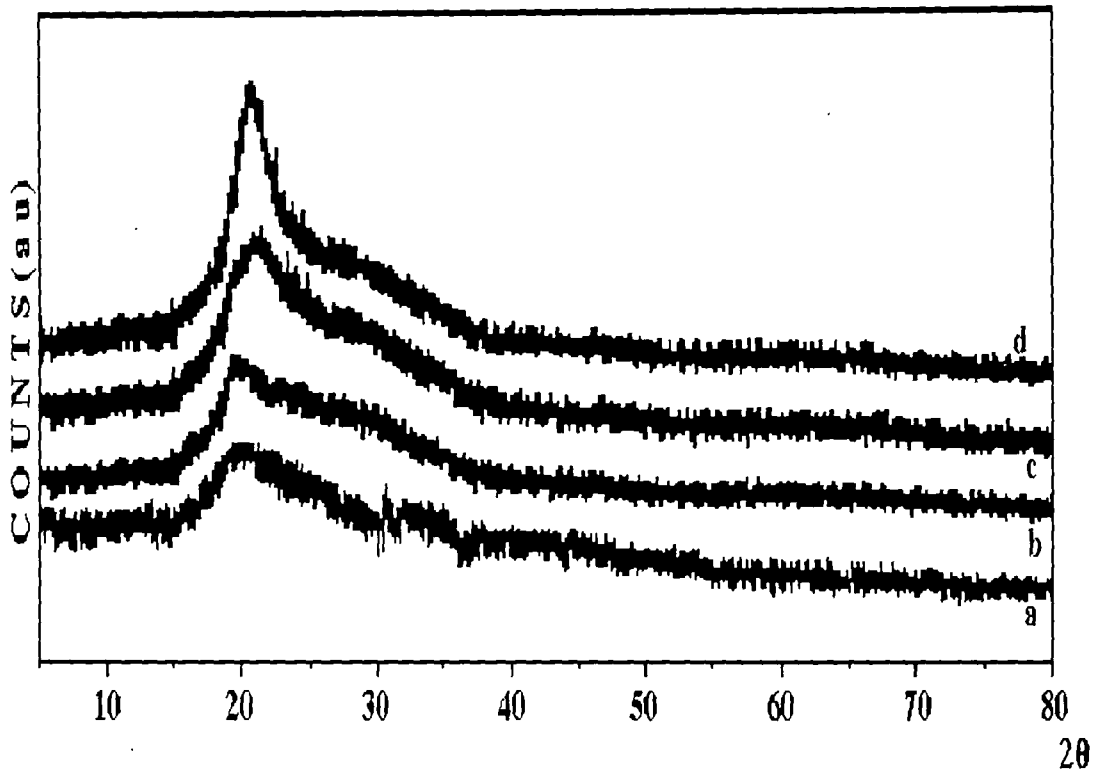


Figure 5.29: X-Ray diffractograms of $[CH_3(CH_2)_3]_4NBF_4$ doped polypyrrole films (a) before, and after irradiation with fluence (b) $5x10^{10}$, (c) $5x10^{11}$ and (d) $3x10^{12}$ ions/cm$^2$.

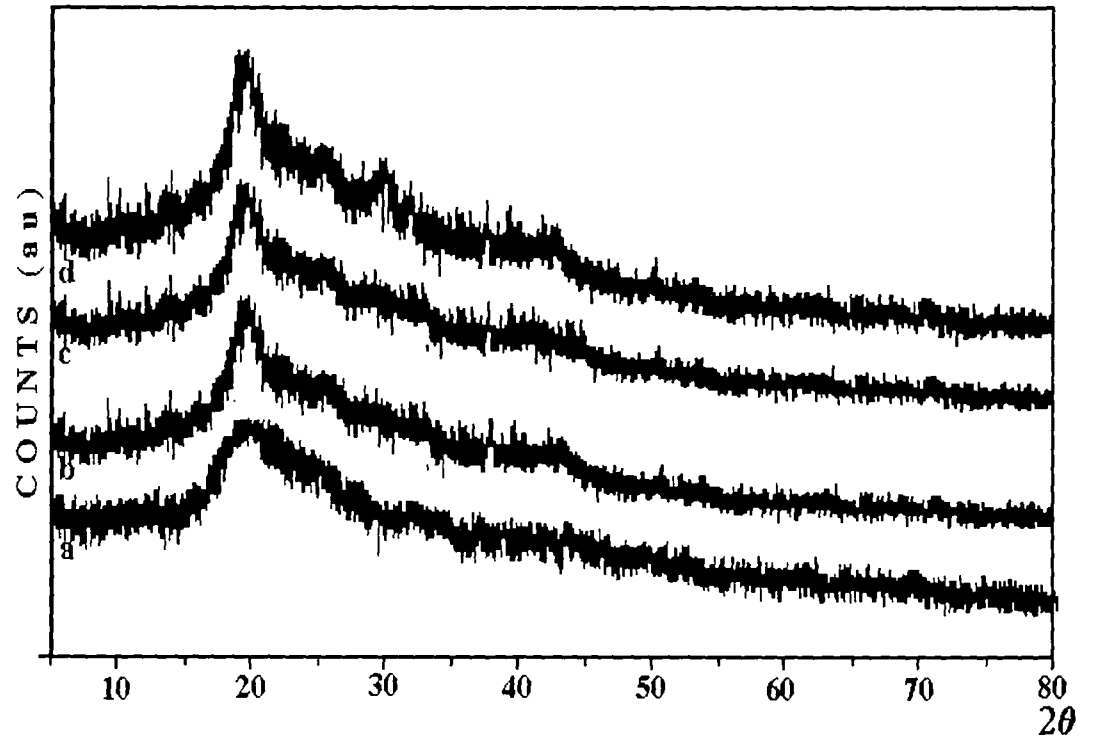


Figure 5.30: X-Ray diffractograms of $[CH_3(CH_2)_3]_4NPF_6$ doped polypyrrole (a) before, and after irradiation with fluence (b) $5x10^{10}$, (c) $5x10^{11}$ and (d) $3x10^{12}$ ions/cm$^2$.

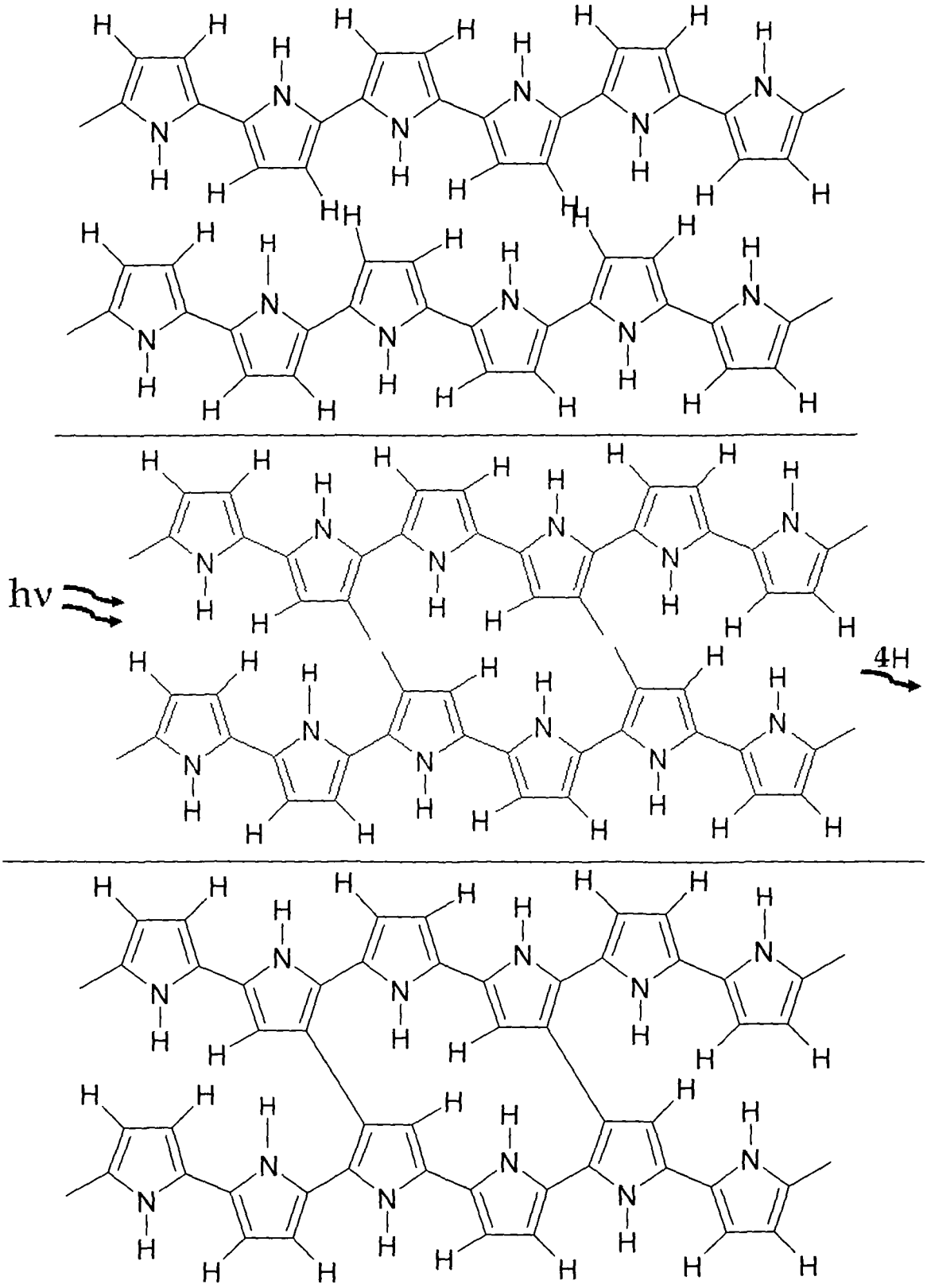


Figure 5.31: Schematic diagram of possible cross linking in polypyrrole conducting polymer upon SHI irradiation.

crystalline regions produce faster charge conduction in the polymer films resulting in higher conductivity, which is consistent with the dc conductivity measurements. The degree of crystallinity (K) of the polypyrrole conducting polymer films calculated using the method as described in details in chapter 3 section 3.6.6.1 are presented in Table 5.4. About 75% increase in crystallinity in the polypyrrole conducting polymer films have been obtained after SHI irradiation.

Table5.4: Degree of crystallinity of polypyrrole films after SHI irradiation with 160 MeV $Ni^{12+}$ ion at different fluences.

| Dopant | Unirradiated | $5x10^{10}$ ions/cm$^2$ | $5x10^{11}$ ions/cm$^2$ | $3x10^{12}$ ions/cm$^2$ |
|---|---|---|---|---|
| $LiClO_4$ | 25.35% | 30.24% | 36.89% | 45.64% |
| $LiCF_3SO_3$ | 26.70% | 30.82% | 34.00% | 46.38% |
| $[CH_3(CH_2)_3]_4NBF_4$ | 22.69% | 25.74% | 32.55% | 43.10% |
| $[CH_3(CH_2)_3]_4NPF_6$ | 25.68% | 28.32% | 34.48% | 40.20% |

**5.5 Summary:**

The pyrrole monomers have been successfully electropolymerized by oxidative polymerization on ITO coated glass substrate. The cyclic voltammogram of the polypyrrole films doped with lithium perchlorate ($LiClO_4$), sodium perchlorate ($NaClO_4$), lithium trifluoromethane sulfonate ($LiCF_3SO_3$), tetrabutylammonium tetrafluoroborate ($[CH_3(CH_2)_3]_4NBF_4$) and tetrabutylammonium hexafluorophosphate ($[CH_3(CH_2)_3]_4NPF_6$) shows very good redox response with electrochromism. The redox response of the polypyrrole conducting polymer films remains same upon SHI irradiation with 160 MeV $Ni^{12+}$ ion. The redox peak height i.e., the magnitude of oxidation and reduction current density increases in the SHI irradiated polypyrrole films, which is solely due to increase of conductivity of polymer film after irradiation as other experimental conditions of cyclic voltammetry are kept unchanged. The electrical conductivity measurements show that the unirradiated

polypyrrole films have dc conductivity of about 100 S/cm (Table 5.1), which after irradiation increases to 181 S/cm (Table 5.3). The UV-Vis spectroscopy shows the characteristic absorption peaks of polypyrrole films at 320 nm and 440 nm corresponding to $\pi \rightarrow \pi^*$ transition and bipolaron absorption respectively. The carrier absorption peak intensity has been observed to increase after SHI irradiation, which is attributed to the increase of carrier concentration in the polymer films after irradiation as large number of cations, anions, radicals and charged particles are created upon SHI irradiation. The FTIR spectroscopy confirms the presence of dopant ions inside the polypyrrole films. The possibility of cross-linking at N-H bond breaking sites of polymer chains after SHI irradiation is also suggested by the FTIR spectra. Surface morphological study by SEM shows formation of uniform and dense morphology of the polymer films after SHI irradiation due to the huge energy transfer. The XRD patterns of the unirradiated polymer films show semi-crystalline nature of the polypyrrole conducting polymer films, which upon SHI irradiation show upto 75% increase in the degree of crystallinity. From the SHI irradiation study of polypyrrole conducting polymer films it can be concluded that the electrical conductivity of conducting polymer films is not only doping dependent but depends on the crystallinity of the polymer films also.

# CHAPTER VI

# POLY(3-METHYLTHIOPHENE): ELECTROPOLYMERIZATION, CHARACTERIZATION AND SHI IRRADIATION

Polythiophene and its derivatives are some of the most important conducting polymers for their possible potential applications in various devices and also for their n-dopability [282,289, 310-322]. While the early application prospects of these materials mostly involved the highly-conducting doped states, it recently appeared that conjugated polymers also represent a promising new class of organic semiconductors and found applications in fabrication of semiconducting devices [66]. Polythiophene conducting polymers found potential applications in field effect transistors [282,289, 310], light-emitting diodes [311], solar cells [312-314], electrochromic devices [315,316], electronic circuits [317, 318], and other devices sensors [321, 322]. Among those polymers, poly(3-methylthiophene) has attracted special interest since 1980s as a cathode material for rechargeable batteries [323]. More recently, other substituted polythiophenes have been proposed as suitable active materials for supercapacitor electrodes [324]. This is mainly due to their high specific capacitance, fast doping-dedoping kinetics, and their ability to undergo both n- and p-doping, making them usable in a symmetric configuration. Poly(3-methylthiophene) of high quality can be directly prepared by electrochemical synthesis of the inexpensive monomer, yielding a lower cost and higher purity polymer. Most of the existing work in literature deals with the UV-Vis, FTIR, cyclic voltammetry [325-329]. A few studies have been reported for characterizations like XRD, SEM and Raman spectroscopy [283, 330, 331] of poly(3-methylthiophene). Modification and improvement of the quality of poly(3-methylthiophene) are achieved with different techniques such as formation of blend [332], co-polymerization [333] etc.

In the present study a sincere effort has been made to study the electrodeposited poly(3-methylthiophene) conducting polymer films by cyclic

voltammetry, four probe measurement, UV-Vis, FTIR, XRD and SEM techniques. Modification of fundamental characteristics like crystallinity, electronic conductivity, density etc. of polymeric materials can be achieved by swift heavy ion [73-100]. SHI irradiation of poly(3-methylthiophene) films has been carried out with 120 MeV $Si^{9+}$ ion beam with fluences $5x10^{10}$, $5x10^{11}$ and $3x10^{12}$ ions/$cm^2$. The characterizations on the unirradiated films have been repeated on the irradiated polymer films to investigate the effects of SHI irradiation.

**6.1 Electrochemical polymerization of poly(3-methylthiophene) film:**

The electropolymerization of poly(3-methylthiophene) thin films has been carried out by potentiodynamic method on indium doped tin oxide (ITO) coated glass substrates in a three electrode electrochemical cell with stainless steel counter electrode and saturated calomel electrode (SCE) as reference electrode. Salts lithium perchlorate ($LiClO_4$), lithium trifluoro methane sulfonate ($LiCF_3SO_3$), tetrabutylammonium tetrafluoroborate ($[CH_3(CH_2)_3]_4NBF_4$), tetrabutylammonium hexafluorophosphate ($[CH_3(CH_2)_3]_4NPF_6$) are used as dopants for poly(3-methylthiophene) conducting polymer films. The potential is varied between -200mV to 1600 mV Vs SCE at a scan rate of 50mV/sec for poly(3-methylthiophene) deposition by potentiodynamic method. High conducting blackish films of poly(3-methylthiophene) are obtained after about 80 cycles. Different concentrations of monomer (from 0.05 to 0.2) and salt (from 0.2 M to 2.0 M) have been tried for obtaining higher conductivity of the poly(3-methylthiophene) films. It is observed that monomer concentration of 0.15M produces films with smooth surface and above this concentration films with rough and flaky surface are produced. Below 0.15 M concentration of monomer the rate of polymerization is slow, the polymer yield is less and irregular broken films are produced. Lithium perchlorate salt concentration beyond 1.8M does not increase the conductivity. Similarly for sodium perchlorate the saturation in dc conductivity has been obtained at 1.8M, 1.5M for $LiCF_3SO_3$ and 1.3M for $[CH_3(CH_2)_3]_4NBF_4$

and $[CH_3(CH_2)_3]_4NPF_6$. These optimum concentrations of monomers and salt are maintained for preparation of all electrolyte solution for synthesis and cyclic voltammetry of the poly(3-methylthiophene) conducting polymer films. The n-doping of the poly(3-methylthiophene) conducting polymer films are done with $Li^+$ ion by applying a potential of -2V to the polymer film for about 8 hrs in potentiostatic mode in an organic solution of acetonitrile and $LiClO_4$.

## 6.2 Characterization of poly(3-methylthiophene) films:

### *6.2.1 Cyclic voltammetry:*

Cyclic voltammetry is a versatile electrochemical characterization technique for studying the redox behaviour of conducting polymers. The cyclic voltammograms (CVs) at different scan rate of poly(3-methylthiophene) conducting polymer films doped with $LiClO_4$ on ITO coated glass substrate against stainless steel counter electrode and SCE reference electrode are shown in Fig. 6.1. The cyclic voltammograms show broad anodic peak at 1060 mV in the forward sweep of potential and one broad cathodic peak at 600 mV in the reverse sweep. In the $LiClO_4$ doped poly(3-methylthiophene) conducting polymer the perchlorate ion ($ClO_4^-$) enters into the polymer film in the forward

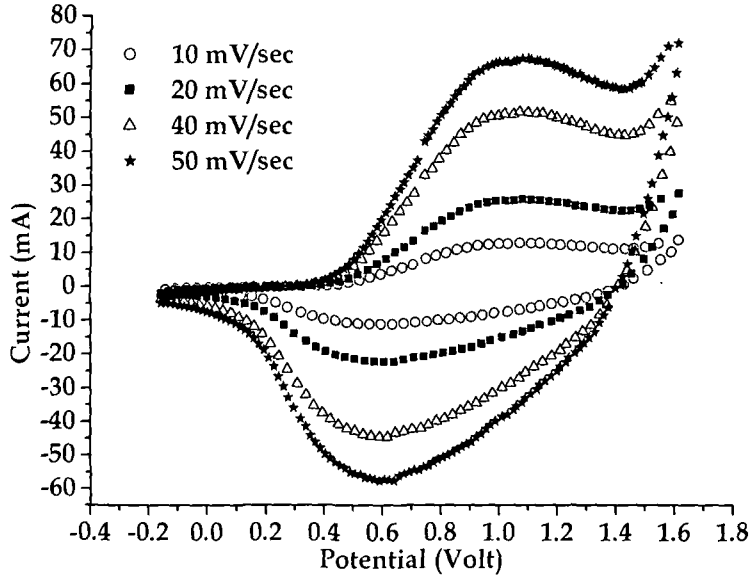


Figure 6.1: Cyclic voltammogram of poly(3-methylthiophene) doped with $LiClO_4$ at different scan rates.

sweep and in the reverse sweep the dopant ion comes out of the polymer film into the electrolyte solution.

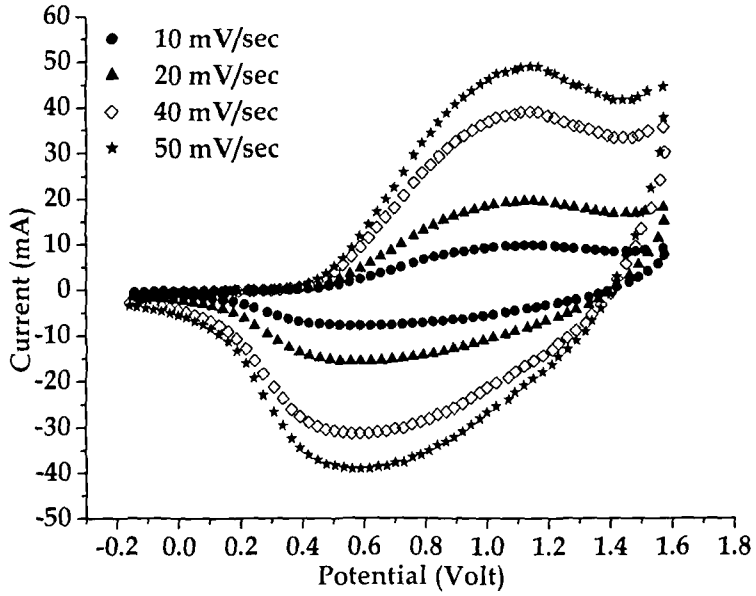


Figure 6.2: Cyclic voltammograms of poly(3-methylthiophene) doped with $LiCF_3SO_3$ at different scan rates.

The cyclic voltammograms of poly(3-methylthiophene) doped with $LiCF_3SO_3$ against stainless steel counter electrode and SCE reference electrode in organic solvent acetonitrile recorded at different scan rates are presented in Fig. 6.2. The oxidation of the poly(3-methylthiophene) conducting polymer films starts from 415 mV in the forward sweep and the peak occurs at 1100 mV. In the reverse sweep the broad reduction peak occurs centered at around 600 mV, same as that of lithium perchlorate doped poly(3-methylthiophene). The occurrence of oxidation peak at higher potential as compared to those of lithium perchlorate doped poly(3-methylthiophene) can be attributed to the larger size of the dopant ion ($CF_3SO_3^-$), which has lower mobility than the perchlorate ion ($ClO_4^-$).

The cyclic voltammograms of poly(3-methylthiophene) doped with tetrabutyl ammonium tetrafluoro borate ($[CH_3(CH_2)_3]_4NBF_4$) carried out in a single compartment three electrode electrochemical cell at different scan rates

are shown in Fig. 6.3. The oxidation of the poly(3-methylthiophene) conducting polymer films doped with $[CH_3(CH_2)_3]_4NBF_4$ starts at 7.8 V in the anodic sweep and the peak is reached at 1.18 V, which is much higher, due to the low-mobility of the large sized dopant ion as compared to $CF_3SO_3^-$ and $ClO_4^-$ dopant ions . Similarly the reduction peak in the cathodic sweep also occurs at lower potential 0.42 V, which can be ascribed to the size effect of the dopant ion.

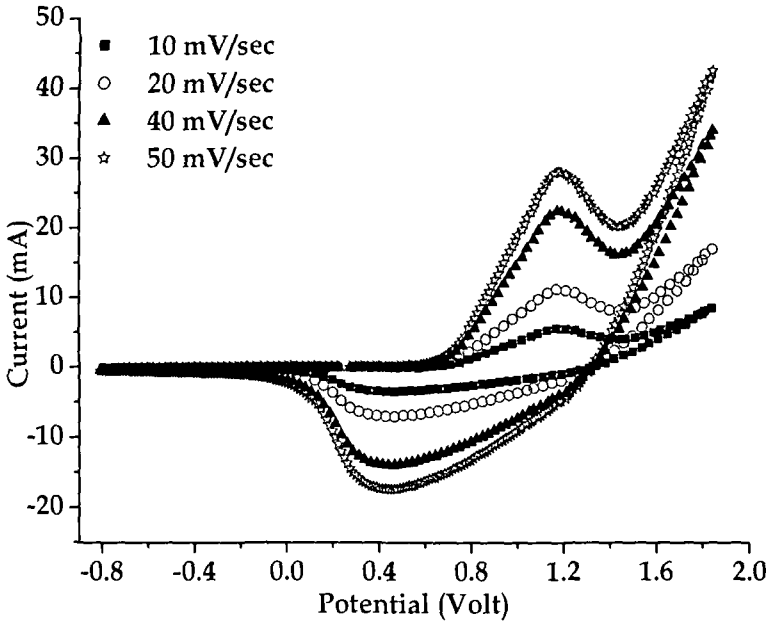


Figure 6.3: Cyclic voltammogram of poly(3-methylthiophene) doped with $[CH_3(CH_2)_3]_4NBF_4$ at different scan rates.

The cyclic voltammograms of the tetrabutylammonium hexafluorophosphate ($[CH_3(CH_2)_3]_4NPF_6$) doped poly(3-methylthiophene) conducting polymer films recorded at different scan rates are presented in Fig. 6.4. The oxidation peak of the $[CH_3(CH_2)_3]_4NPF_6$ doped poly(3-methylthiophene) films starts at 0.8 V and attains peak value at 1.2 V in the forward sweep of potential. The reduction peak is observed to occur at 0.4 V in the reverse sweep. The oxidation and reduction peak potential values for $[CH_3(CH_2)_3]_4NPF_6$ salt are compareable to $[CH_3(CH_2)_3]_4NBF_4$ salt, which confirms that oxidation and reduction potentials depend on the size of the dopant ion, which enters into and comes out of the film during oxidation and reduction respectively.

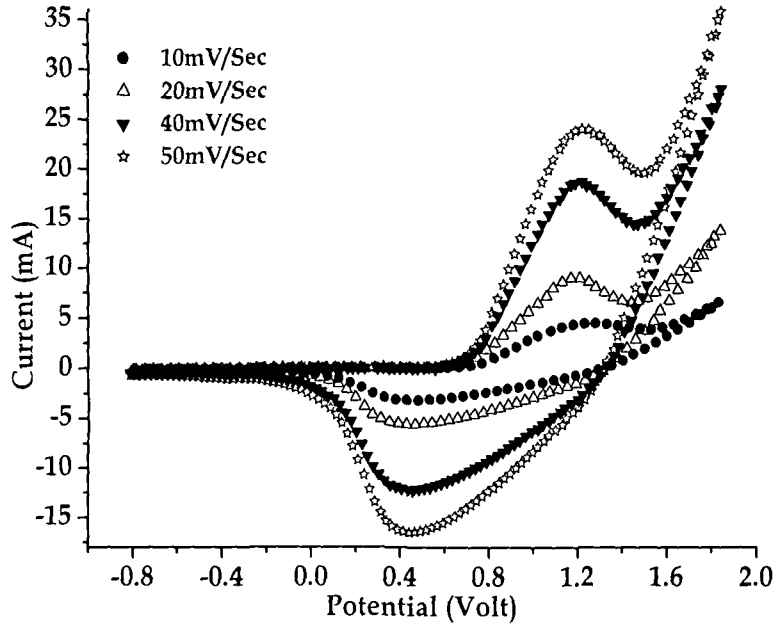


Figure 6.4: Cyclic voltammogram of poly(3-methylthiophene) doped with $[CH_3(CH_2)_3]_4NPF_6$ at different scan rates.

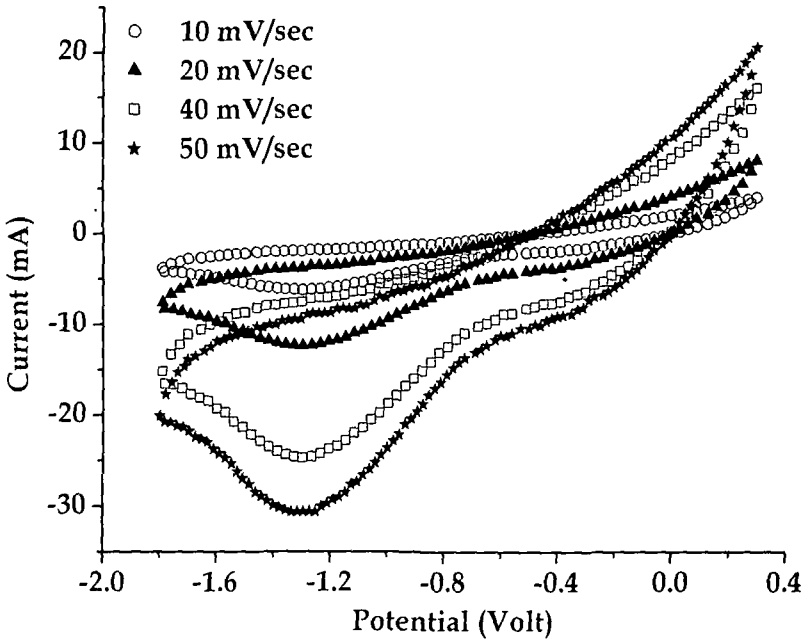


Figure 6.5: Cyclic voltammogram of n-doped poly(3-methylthiophene) with $LiClO_4$ at different scan rates.

The cyclic voltammograms of the n-doped poly(3-methylthiophene) conducting polymer films with $LiClO_4$ salt in acetonitrile against stainless steel

counter electrode and SCE reference electrode recorded at different scan rates are presented in Fig. 6.5. In case of n-doped poly(3-methylthiophene) the potential is first varied from +ve to -ve value, called the cathodic sweep and then back to +ve potential the anodic sweep. The broad reduction peak of the n-doped poly(3-methylthiophene) conducting polymer films is observed at -1.3 V in the cathodic sweep. The current in the +ve direction increases in the anodic sweep but no distinct oxidation peaks are observed in the scanned potential region of -1.8 V to +0.3 V as the oxidation of poly(3-methylthiophene) occurs at potential above +0.3V.

All the poly(3-methylthiophene) conducting polymer films show redox electroactivity in organic medium and good electrochromism of the films are observed. The colour of the p-doped poly(3-methylthiophene) film changes from deep violet to black in the forward sweep on oxidation, which again turns back to deep violet on reduction in the reverse sweep. The scan rate dependence of the cyclic voltammogram i.e., the increase in oxidation-reduction peak current with increase in scan rate is observed in all the poly(3-methylthiophene) conducting polymer films doped with different dopants.

### 6.2.2 *Conductivity measurements:*

Four probe technique is an accurate method to measure the dc conductivity of a material in thin film form. The dc conductivity of the synthesized polymer films have been measured to confirm whether the prepared films are conducting. The conductivity of the doped polyaniline films measured by the four probe technique at room temperature is presented in Table 6.1. The highest conductivity of 125 S/cm has been obtained for $LiClO_4$ doped poly(3-methylthiophene) polymer films. The lowest conductivity value of 105 S/cm has been obtained for $[CH_3(CH_2)_3]_4NPF_6$ doped poly(3-methylthiophene) conducting polymer films. The n-doped poly(3-methylthiophene) conducting polymer films incorporating $Li^+$ ion as dopant show a conductivity value of 76-84 S/cm. The measured conductivity values are consistent with those reported in the literature [325-329].

Table 6.1: The dc conductivity of poly(3-methylthiophene) films doped with different dopants.

| Dopant (ion) | Conductivity (S/cm) |
|---|---|
| $LiClO_4$ ($ClO_4^-$) | 120 ± 5 |
| $LiCF_3SO_3$($CF_3SO_3^-$) | 112 ± 4 |
| $[CH_3(CH_2)_3]_4NBF_4$($BF_4^-$) | 108 ± 7 |
| $[CH_3(CH_2)_3]_4NPF_6$ ($PF_6^-$) | 105 ± 6 |
| $LiClO_4$ ($Li^+$) | 80 ± 4 |

### *6.2.3 Surface Morphology Study:*

Scanning electron microscopy is a most effective characterization technique to study the surface morphology of films. The SEM images of poly(3-methylthiophene) films doped with lithium perchlorate ($LiClO_4$), lithium trifluoro methane sulfonate ($LiCF_3SO_3$), tetra butyl ammonium tetrafluoro borate ($[CH_3(CH_2)_3]_4NBF_4$), tetra butyl ammonium hexafluoro phosphate ($[CH_3(CH_2)_3]_4NPF_6$) and n-doped poly(3-methylthiophene) with $LiClO_4$ are presented in Fig. 6.6a-e. Potentiodynamic synthesis of poly(3-methylthiophene) conducting polymer films doped with $LiClO_4$ show porous surface structure with globular grains forming clusters (Fig. 6.6a). The lithium trifluoro methane sulfonate doped poly(3-methylthiophene) films show uneven sized globular surface morphology with less porosity (Fig. 6.6b). The poly(3-methylthiophene) conducting polymer films doped with tetra butyl ammonium tetrafluoro borate salt show dense surface morphology with granular structure (Fig. 6.6c). In Fig. 6.6d, the surface morphology of tetra butyl ammonium hexafluoro phosphate doped poly(3-methylthiophene) film shows rough and porous surface morphology. The SEM micrograph of n-doped poly(3-methylthiophene) conducting polymer films show uneven granular morphology with smaller pores as compared to that in the $LiClO_4$ p-doped poly(3-methylthiophene) conducting polymer film (Fig. 6.6e).

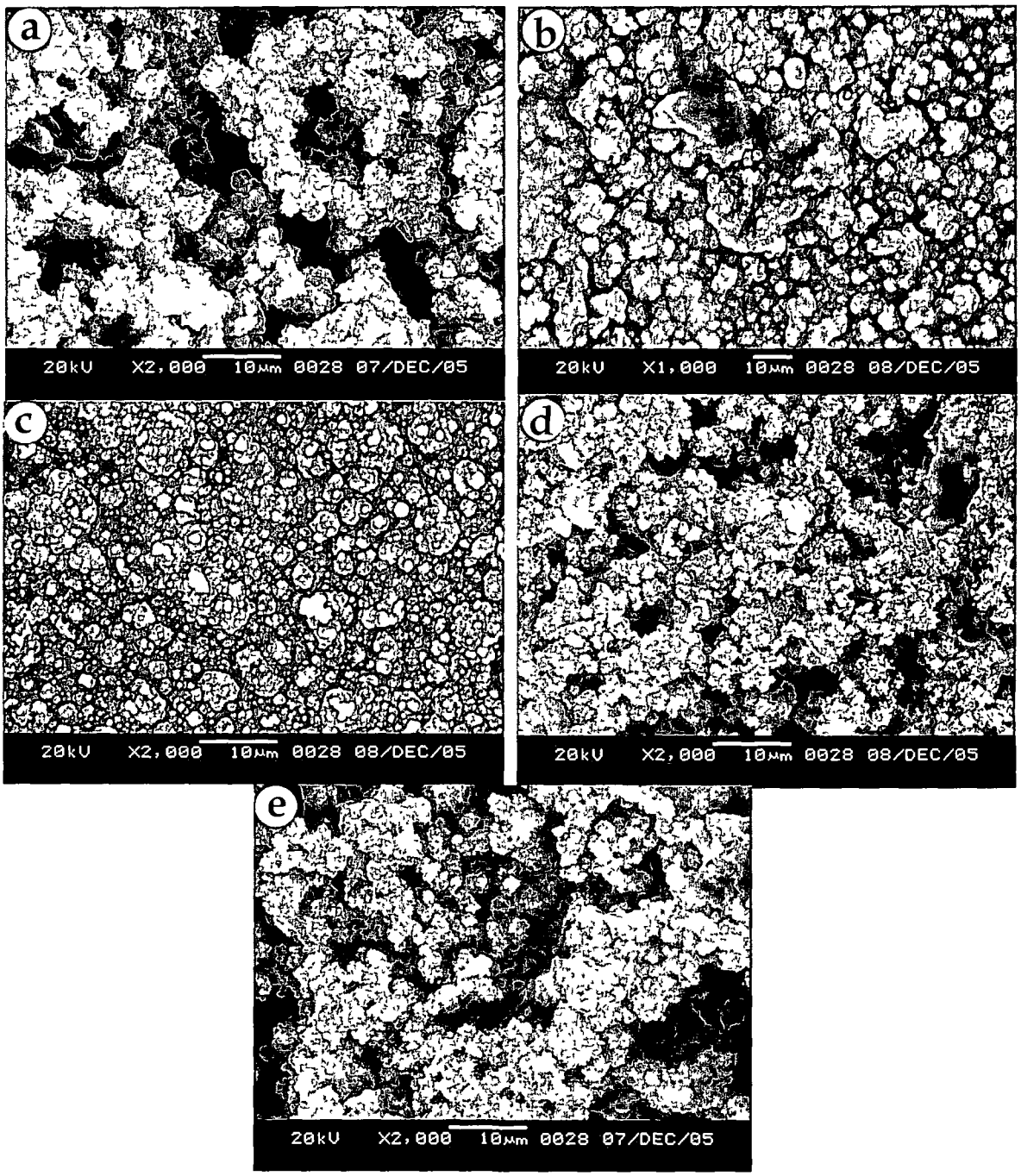


Figure 6.6: SEM images of poly(3-methylthiophene) conducting polymer films doped with (a) $LiClO_4$, (b) $LiCF_3SO_3$, (c) $[CH_3(CH_2)_3]_4NBF_4$, (d) $[CH_3(CH_2)_3]_4NPF_6$ and (e) n-doped with $LiClO_4$.

### *6.2.4 UV-Vis spectroscopy:*

UV-Vis spectroscopy is a common technique to study the electronic transitions and provides the key information regarding the electronic energy structure of the material. UV-Vis spectra of the $LiClO_4$, $LiCF_3SO_3$,

$[CH_3(CH_2)_3]_4NBF_4$ and $[CH_3(CH_2)_3]_4NPF_6$ doped poly(3-methylthiophene) polymer films have been recorded to study the electronic structure i.e., the band gap and electronic transition taking place within the UV-Vis range of energy and are shown in Figs. 6.7 a-d. The characteristic absorption peak at 450nm corresponding to $\pi \rightarrow \pi^*$ transition of the poly(3-methylthiophene) conducting polymer appears in all the four UV-Vis spectra. The polaron/bipolaron absorption peak of the polymer in oxidized state appears at around 730nm [327]. The slight rising of absorbance extending towards the near IR region of the spectrum indicates that the polymer films are in doped state [327]. The peak around 730nm shows a small shift in its position in the spectrum with change in dopant. The spectrum of poly(3-methylthiophene) doped with $LiClO_4$ and $LiCF_3SO_3$ shows peaks at higher wavelength compared to those doped with $[CH_3(CH_2)_3]_4NBF_4$ and $[CH_3(CH_2)_3]_4NPF_6$, which leads to higher value of conductivity of the respective polymer films (Table 6.1).

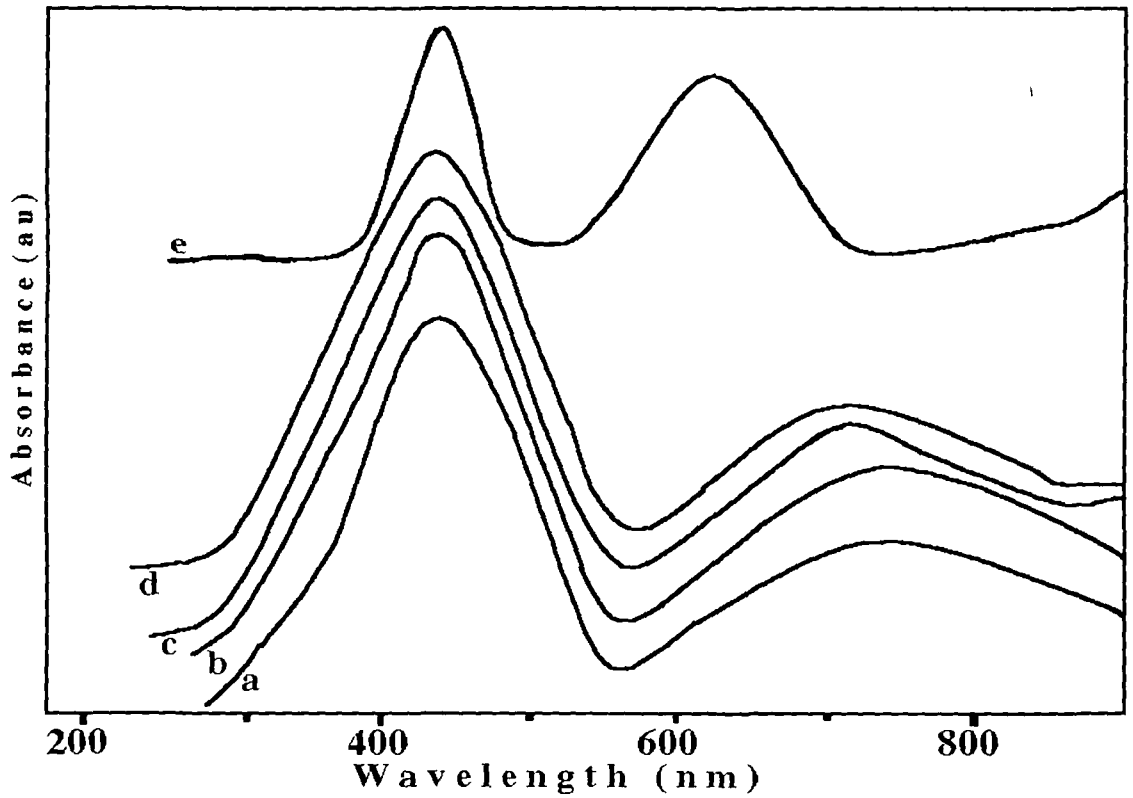


Figure 6.7: UV-Vis spectra of polythiophene conducting polymer films doped with (a) $LiClO_4$, (b) $LiCF_3SO_3$, (c) $[CH_3(CH_2)_3]_4NBF_4$, (d) $[CH_3(CH_2)_3]_4NPF_6$ and (e) n-doped with $LiClO_4$.

The UV-Vis spectra of n-doped poly(3-methylthiophene) conducting polymer films doped with $LiClO_4$ is shown in Fig. 6.7e. The characteristic absorption of the 3-methylthiophene ring due to the $\pi \rightarrow \pi^*$ transition of electrons occurs at 450 nm. In the n-doped poly(3-methylthiophene) the polaron are the dominant carriers and the absorption peak due to the polaron occurs at 620 nm giving rise to higher band gap, which is reflected in the lower conductivity values of the n-doped poly(3-methylthiophene) conducting polymer films.

### *6.2.5 FTIR spectroscopy:*

FTIR spectroscopy provides absorption spectra of vibrating bonds, which enables to identify the characteristic bond interactions and functional groups present in the materials. The FTIR spectroscopic study of the poly(3-methylthiophene) conducting polymer films have been carried out for understanding the bond structure of the polymer films as well as to examine the presence of the dopant ions in the conducting polymer films. The FTIR spectra of poly(3-methylthiophene) conducting polymer films undoped and doped with $LiClO_4$, $LiCF_3SO_3$, $[CH_3(CH_2)_3]_4NBF_4$ and $[CH_3(CH_2)_3]4NPF6$ are presented in Figs. 6.8 a-e respectively. The FTIR spectra of n-doped poly(3-methylthiophene) conducting polymer films is shown in Fig. 6.8 f.

The absorption peak observed at around 670 $cm^{-1}$ appeared in all the FTIR spectra are attributed to the C-S stretching vibration of poly(3-methylthiophene). The peaks at ~700 $cm^{-1}$ and ~800 $cm^{-1}$ are attributed to the C-H out-of-plane vibration and C-H ring vibration of the thiophene monomer [334]. C-H in-plane deformation vibration peaks are observed in all the four FTIR spectra at about 1050 $cm^{-1}$. The C-C ring stretching of the heteroaromatic ring vibration absorption occurs around 1440 $cm^{-1}$ [335]. The C=C aromatic ring stretching vibration absorption peak appears at about 1635 $cm^{-1}$ in all the four spectra [335, 336]. The =C-H stretching vibration absorption peak of the heteroaromatic ring occurs at about 3045 $cm^{-1}$. The presence of methyl group in the poly(3-methylthiophene) conducting polymer films can be assured from the

absorption peaks at 2960 $cm^{-1}$, 2865 $cm^{-1}$ and 1370 $cm^{-1}$, which are attributed to the asymmetric C-H stretching, symmetric C-H stretching and bending mode C-H vibration of the methyl group respectively.

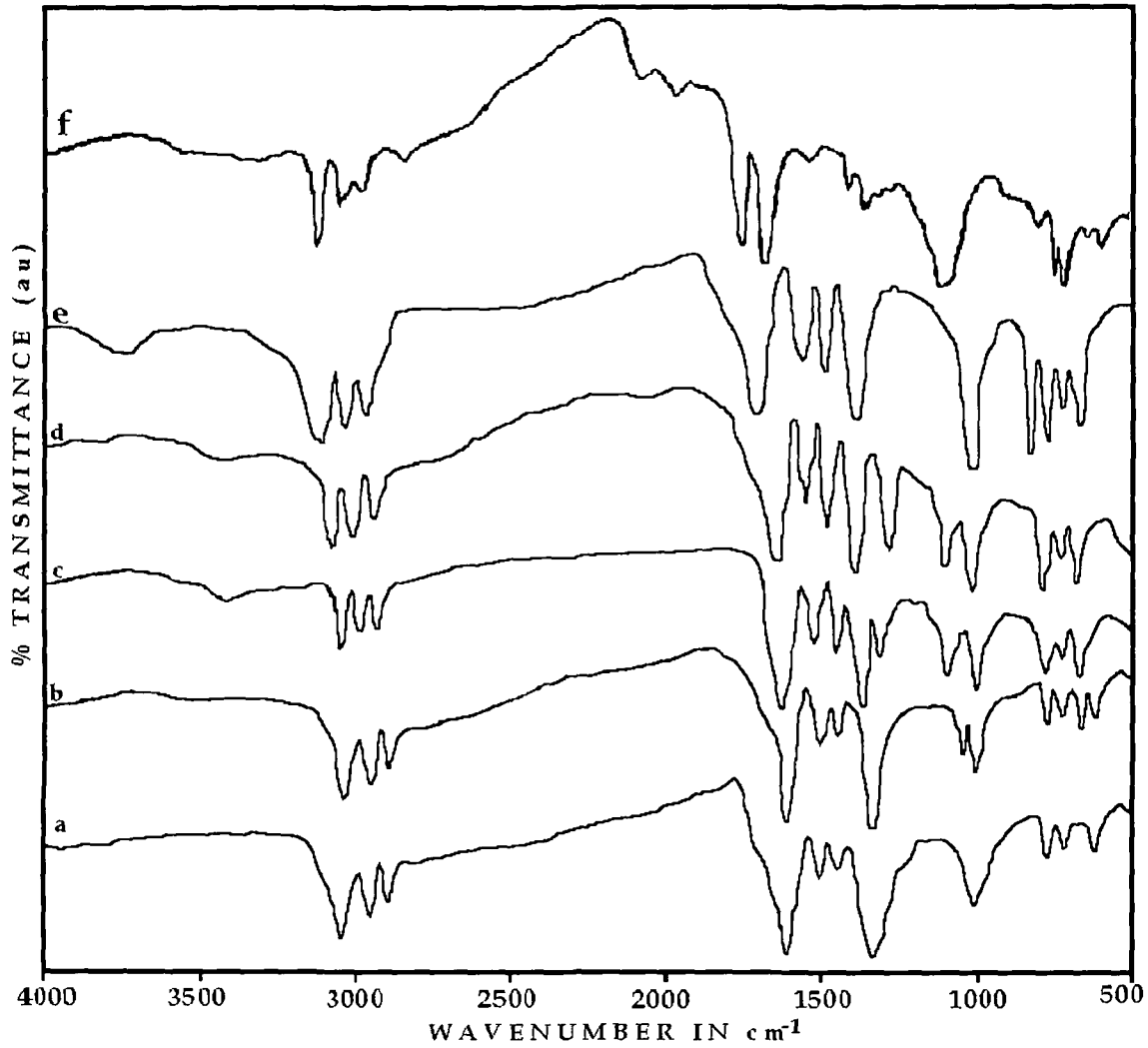


Figure 6.8: FTIR spectra of poly(3-methylthiophene) (a) undoped and doped with (b) $LiClO_4$, (c) $LiCF_3SO_3$, (d) $[CH_3(CH_2)_3]_4NBF_4$, (e) $[CH_3(CH_2)_3]_4NPF_6$ and(f) $LiClO_4$ n-doped.

The absorption peak due to the presence of $ClO_4^-$ ion in the poly(3-methylthiophene) conducting polymer film doped with $LiClO_4$ appears at 1100 $cm^{-1}$ and 630 $cm^{-1}$ [263-265] (Fig. 6.8 b), which is not observed in the FTIR spectra of undoped poly(3-methylthiophene) (Fig. 6.8 a). The absorption peak appeared at around 1360 $cm^{-1}$ and 1180 $cm^{-1}$ in the FTIR spectra of $LiCF_3SO_3$ doped poly(3-methylthiophene) are attributed to the S=O asymmetric and symmetric vibration of the dopant $CF_3SO_3^-$ ion present in the polymer film

[265]. Two absorption peaks at 1340 $cm^{-1}$ and 1136 $cm^{-1}$ in the FTIR spectra of $[CH_3(CH_2)_3]_4NBF_4$ doped poly(3-methylthiophene) (Fig. 6.8 d) are attributed to the $BF_4^-$ dopant ion present in the polymer film. The absorption peak due to the $PF_6^-$ ion in the spectra of $[CH_3(CH_2)_3]_4NPF_6$ doped poly(3-methylthiophene) (Fig. 6.8 e) conducting polymer films appeared at 845 $cm^{-1}$, which confirms the presence of the dopant ions in the polymer film. Shifting of peaks and appearance of new peaks observed in the FTIR spectra of doped poly(3-methylthiophene) as compared to the FTIR spectra of undoped poly(3-methylthiophene) confirms the interaction of the dopant ions with the polymer chain.

### *6.2.6 X-Ray Diffractogram study:*

The X-Ray diffraction is a prominent technique for the structural characterization. In case of polymeric materials XRD is used to determine the proportion of crystalline and amorphous phases in terms of the degree of crystallinity. The X-Ray diffractogram of poly(3-methylthiophene) conducting polymer films synthesized using different dopants $LiClO_4$, $LiCF_3SO_3$, $[CH_3(CH_2)_3]_4NBF_4$, $[CH_3(CH_2)_3]_4NPF_6$ and n-doped with $LiClO_4$ are shown in Figs. 6.9 a-e respectively.

The XRD patterns of the poly(3-methylthiophene) conducting polymer films show that the polymer films are semicrystalline in nature i.e., certain portions of the film are amorphous and certain portions are crystalline. The crystallinity of the polymer films arises due to systematic alignment of polymer chain by chain folding or by formation of single or multiple helices for atleast part of their length [268]. The crystallinity of doped conducting polymer may also arise due to the dopant ion moieties entering into the polymer film during electrochemical synthesis of the polymer films [270]. Change in degree of crystallinity is also observed with change of dopant concentration in conducting polymer films [271].

The degree of crystallinity (K) of the polymer films has been calculated using the relation described in details in chapter III, section 3.6.6, given below:

$$K = \frac{\text{Area under diffraction peak}}{\text{Total area under diffractogram}} x100\%$$

For visualizing the trend of change in crystallinity of the polymer films with change of dopant, the K values are calculated by dividing the enlarged diffractogram into small square divisions of 0.5 mm X 0.5 mm and counting the total number of square division and number of square division under the peak using the above relation and are presented in table 6.2. The degree of crystallinity of poly(3-methylthiophene) conducting polymer films are found to be less as compared to that of polyaniline and polypyrrole conducting polymer films, which is due to the presence of the methyl group attached to the polythiophene, which provides steric hindrance to the linear arrangement of the polymer chains.

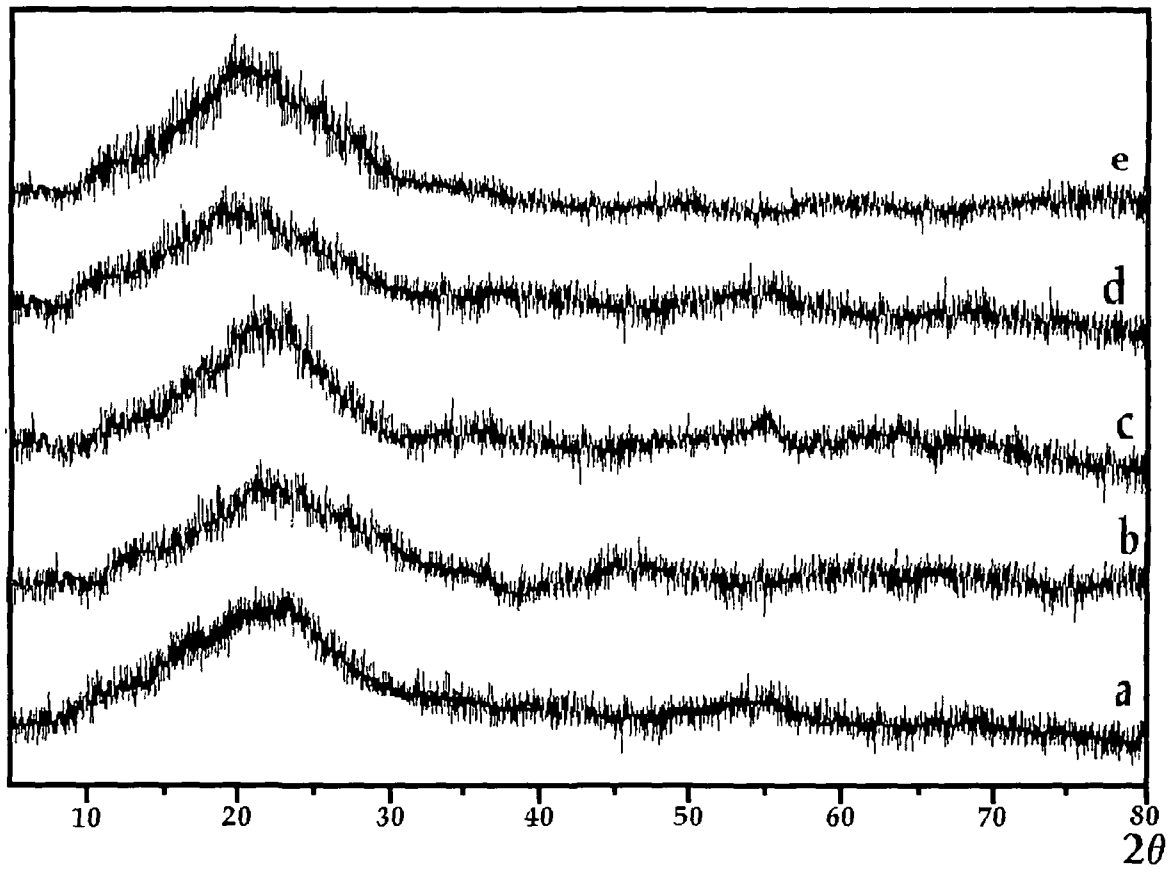


Figure 6.9: X-Ray diffractogram of poly(3-methylthiophene) doped with (a) $LiClO_4$, (b) $LiCF_3SO_3$, (c) $[CH_3(CH_2)_3]_4NBF_4$, (d) $[CH_3(CH_2)_3]_4NPF_6$ and (e) $LiClO_4$ n-doped.

Table 6.2: Degree of crystallinity (K) of poly(3-methylthiophene) films.

Table 6.2: Degree of crystallinity (K) of poly(3-methylthiophene) films doped with different dopants.

| Dopants | Degree of Crystallinity (K) |
|---|---|
| $LiClO_4$ | 17.82% |
| $LiCF_3SO_3$ | 16.67% |
| $[CH_3(CH_2)_3]_4NBF_4$ | 18.09% |
| $[CH_3(CH_2)_3]_4NPF_6$ | 17.52% |
| $LiClO_4$ (n-doping) | 17.64% |

### 6.3 SHI irradiation of poly(3-methylthiophene) films:

The poly(3-methylthiophene) conducting polymer films doped with $LiClO_4$, $LiCF_3SO_3$, $[CH_3(CH_2)_3]_4NBF_4$ and $[CH_3(CH_2)_3]_4NPF_6$ are irradiated with 120 MeV $Si^{9+}$ ion beams at three different ion fluence of $5x10^{10}$, $5x10^{11}$ and $3x10^{12}$ ions/cm$^2$. The irradiation of the conducting polymer films has been carried out in high vacuum in the Materials Science (MS) beam line of Inter University Accelerator Center, New Delhi. The ion current has been kept low (0.3-0.5 pna) to avoid sample burning. All the characterizations for unirradiated films have been carried out on the irradiated polymer films to study the swift heavy ion irradiation effects.

### 6.4 Characterization of irradiated poly(3-methylthiophene) films:

#### *6.4.1 Cyclic voltammetry:*

The cyclic voltammograms of poly(3-methylthiophene) films doped with $LiClO_4$, $LiCF_3SO_3$, $[CH_3(CH_2)_3]_4NBF_4$, $[CH_3(CH_2)_3]_4NPF_6$ and n-doped with $LiClO_4$ recorded after irradiation with 120 MeV $Si^{9+}$ ion beam at the scan rate of 50 mV/s are presented in the Figs. 6.10-6.14 respectively. All the conducting poly(3-methylthiophene) films show an electrochemical window within which the doping/dedoping (redox) processes are largely reproducible, beyond which oxidative or reductive decomposition of the conducting polymer occurs The cyclic voltammograms are related with the electrochromism of the conducting polymer i.e. the redox peaks observed in the CV usually coincide with colour changes of the polymer. The colour of the poly(3-methylthiophene) film changes

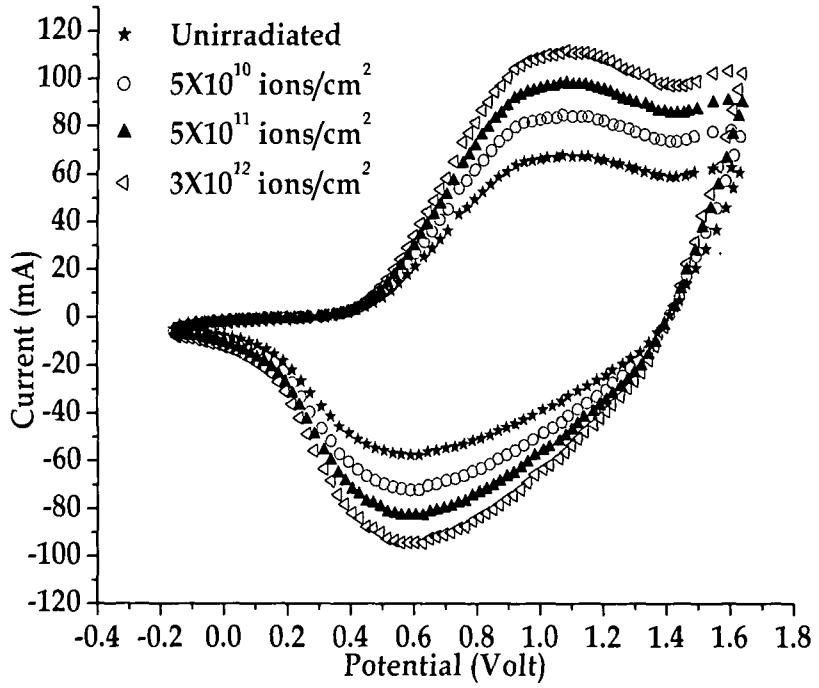


Figure 6.10: Cyclic voltammograms of poly(3-methylthiophene) films doped with $LiClO_4$ at 50 mV/sec scan rate before and after irradiation with different fluences.

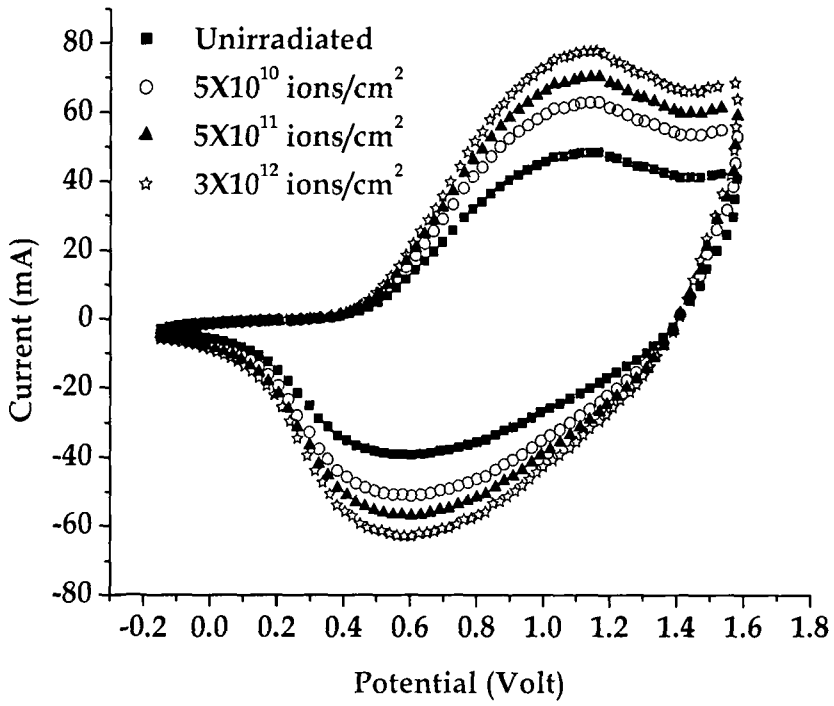


Figure 6.11: Cyclic voltammograms of poly(3-methylthiophene) films doped with $LiCF_3SO_3$ at 50 mV/sec scan rate before and after irradiation with different fluences.

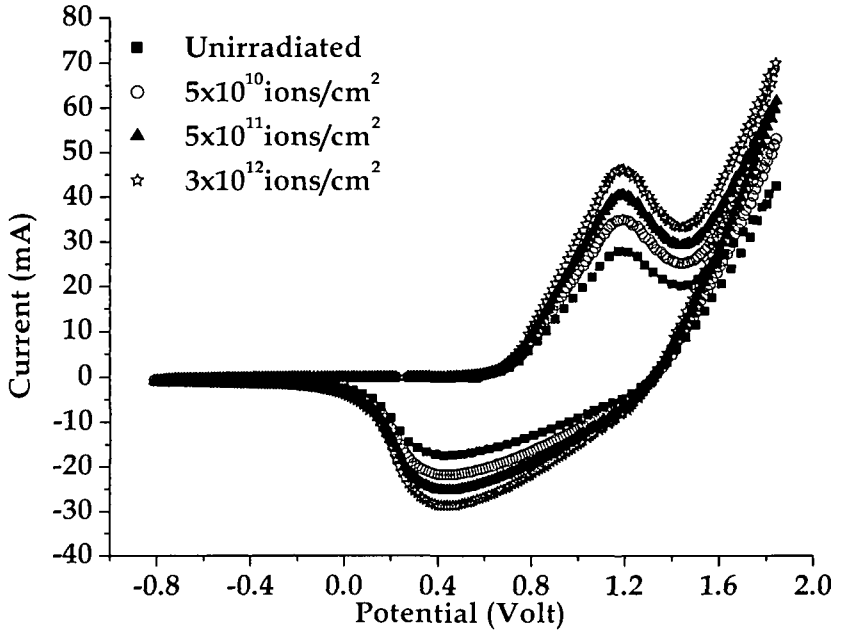


Figure 6.12: Cyclic voltammograms of poly(3-methylthiophene) films doped with $[CH_3(CH_2)_3]_4NBF_4$ at 50 mV/sec scan rate before and after irradiation with different fluences.

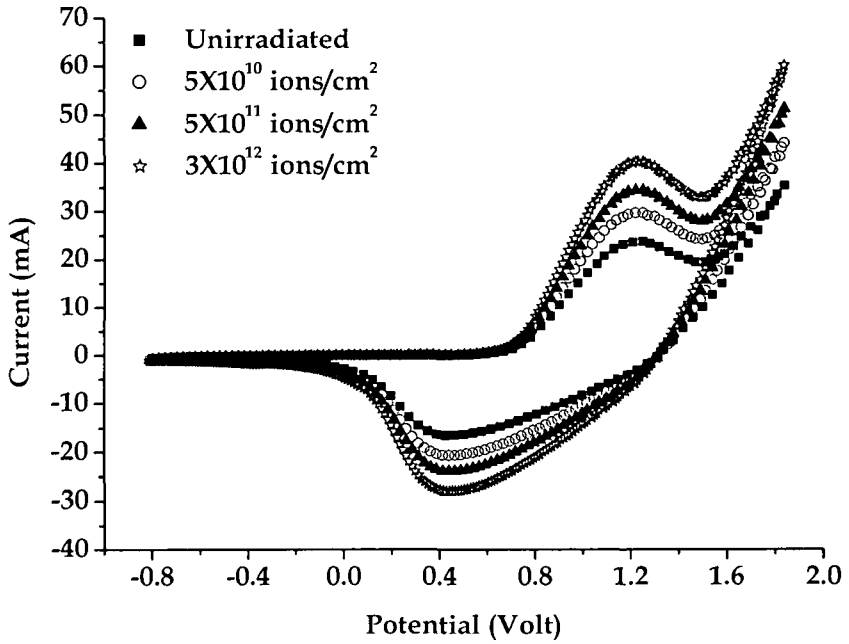


Figure 6.13: Cyclic voltammograms of poly(3-methylthiophene) films doped with $[CH_3(CH_2)_3]_4NPF_6$ at 50 mV/sec scan rate before and after irradiation with different fluences.

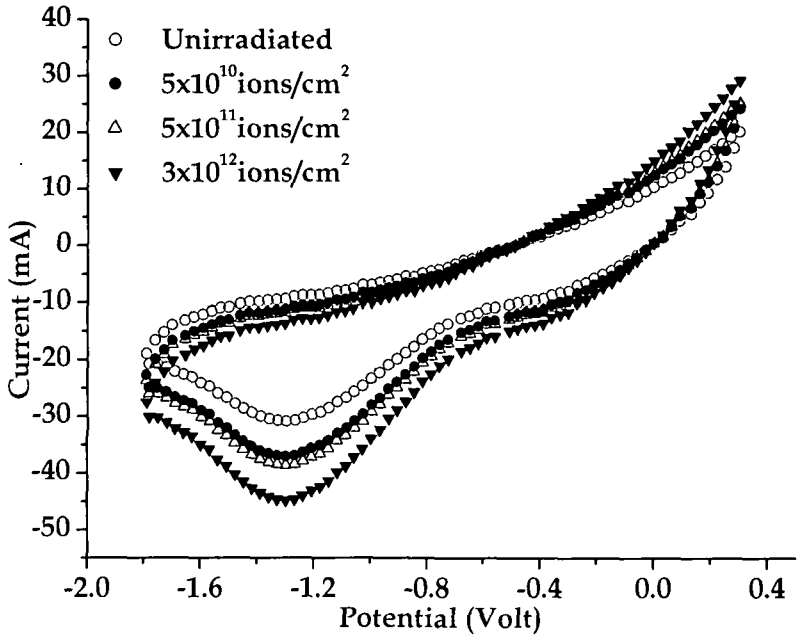


Figure 6.14: Cyclic voltammogram of n-doped poly(3-methylthiophene) films doped with $LiClO_4$ at 50 mV/sec scan rate before and after irradiation with different fluences.

from deep violet to black in the forward sweep on oxidation, which again turns back to deep violet on reduction in the reverse sweep. All polymer films, unirradiated and irradiated, show large electroactivity in the organic electrolyte. It is observed from the CV that upon SHI irradiation the shapes of the CV of the irradiated polymer films remain same with oxidation and reduction occurring at the same potential as that of unirradiated film, which shows that the redox property of the poly(3-methylthiophene) conducting polymer films remains almost similar after SHI irradiation. However there is an increase in magnitude of oxidation and reduction currents upon SHI irradiation, which can be attributed to the increase in the charge carrier concentration in the poly(3-methylthiophene) films upon SHI irradiation. The electrolyte and other experimental conditions in which the cyclic voltammograms are taken are kept unchanged for unirradiated and irradiated samples. The oxidation and reduction peak currents are also observed to increase with the increase of fluence, which is consistent with the conductivity results.

### 6.4.2 *Conductivity measurements:*

The conductivity of the poly(3-methylthiophene) films shows an increasing trend with increase in ion fluence upon SHI irradiation. The dc conductivity of poly(3-methylthiophene) unirradiated films show about 70% increase upon SHI irradiation (Table 6.3). The increase in conductivity of the conducting polymer films after SHI irradiation is mainly due to electronic stopping mechanism, which produces large number of charged and active chemical species, cations, anions, radicals and electrons along the ion track. Coulombic interaction among these active charged species leads to cross-linking as well as bond breaking, however, at high energy (above 100 MeV) irradiation, cross-linking of the polymer chains dominates over bond breaking resulting in cross-linking in the polymer chains [196]. Inter chain electron hopping required for conduction between two chains, which obviously increases the resistance of the polymer is reduced due the cross-linking of the polymer chains after irradiation. Defect sites in the molecular structure of the polymer chains created by SHI irradiation also contributes to higher dc conductivity as charge accumulation takes place, which produces charge carrier species. The increase of crystallinity of the polymer films also contributes to the increase in conductivity upon SHI irradiation.

Table 6.3: Conductivity of poly(3-methylthiophene) conducting polymer films doped with different dopants before and after SHI irradiation with different fluences.

| Dopant (ion) | Unirradiated | $5X10^{10}$ ions/cm$^2$ | $5X10^{11}$ ions/cm$^2$ | $3X10^{12}$ ions/cm$^2$ |
|---|---|---|---|---|
| $LiClO_4$ ($ClO_4^-$) | 120 ± 5 | 172 ± 4 | 185 ± 3 | 198 ± 5 |
| $LiCF_3SO_3$($CF_3SO_3^-$) | 112 ± 4 | 168 ± 3 | 181 ± 5 | 194 ± 3 |
| $[CH_3(CH_2)_3]_4NBF_4$($BF_4^-$) | 108 ± 7 | 154 ± 4 | 168 ± 3 | 172 ± 4 |
| $[CH_3(CH_2)_3]_4NPF_6$ ($PF_6^-$) | 105 ± 6 | 152 ± 3 | 165 ± 5 | 170 ± 3 |
| $LiClO_4$ ($Li^+$) | 80 ± 4 | 113 ± 5 | 125 ± 4 | 134 ± 5 |

### *6.4.3 Surface Morphology Study:*

The surface morphological studies of the poly(3-methylthiophene) conducting polymer films p-doped with $LiClO_4$, $LiCF_3SO_3$, $[CH_3(CH_2)_3]_4NBF_4$, $[CH_3(CH_2)_3]_4NPF_6$ and n-doped with $LiClO_4$ carried out by taking SEM images after irradiation with 120 MeV $Si^{9+}$ ion at different fluences of $5x10^{10}$, $5x10^{11}$ and $3x10^{12}$ ions/$cm^2$ are presented in Figs. 6.15-5.19 respectively. The porous surface structure with globular grains forming clusters before irradiation of $LiClO_4$ doped poly(3-methylthiophene) conducting polymer film (Fig. 6.15 a) shows grain growth and agglomeration after SHI irradiation (Fig. 6.15 b-d). The grain growth occurs due to huge energy deposition in the conducting polymer film as a result of electronic energy loss mechanism. Unirradiated poly(3-methylthiophene) films doped with $LiCF_3SO_3$ (Fig. 6.16a) show globular dense surface morphology also exhibit grain growth after irradiation. As the fluence of SHI irradiation increases the grain size increases and at the fluence of $3x10^{12}$ ions/$cm^2$, the grains become largest and also agglomeration is nicely observed

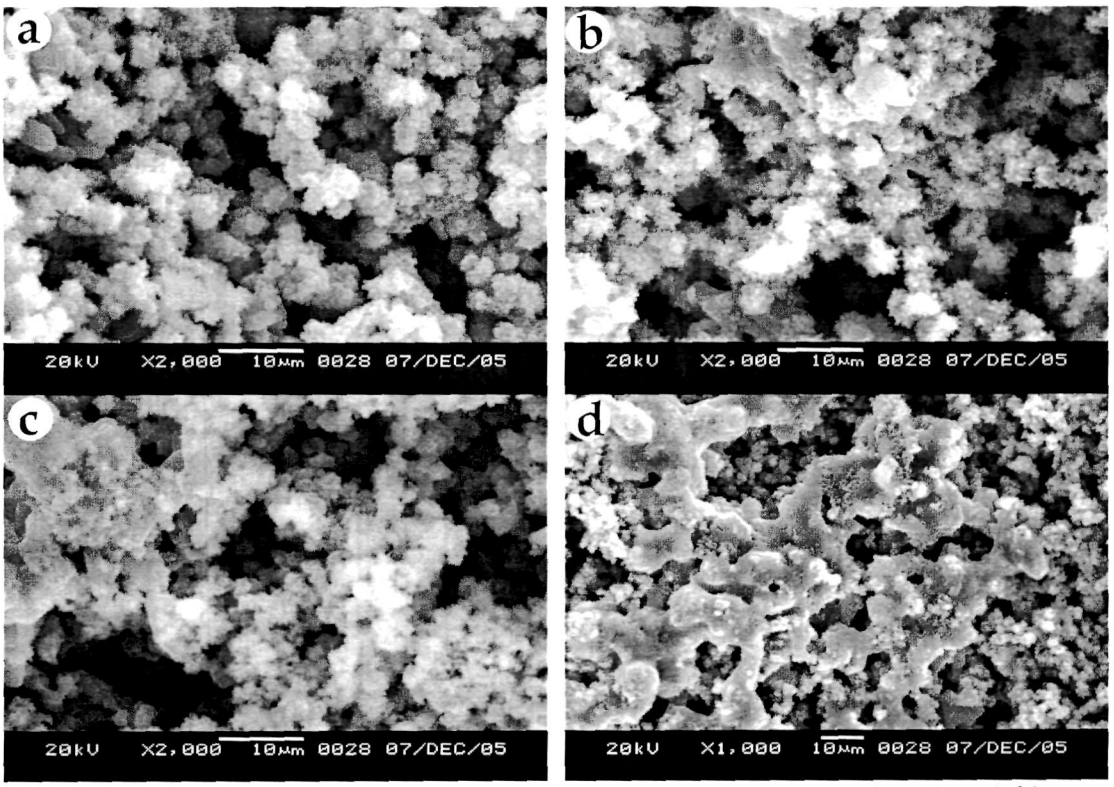


Figure 6.15: SEM micrographs of $LiClO_4$ p-doped poly(3-methylthiophene) films (a) before, and after irradiation with fluence (b) $5x10^{10}$, (c) $5x10^{11}$ and (d) $3x10^{12}$ ions/$cm^2$.

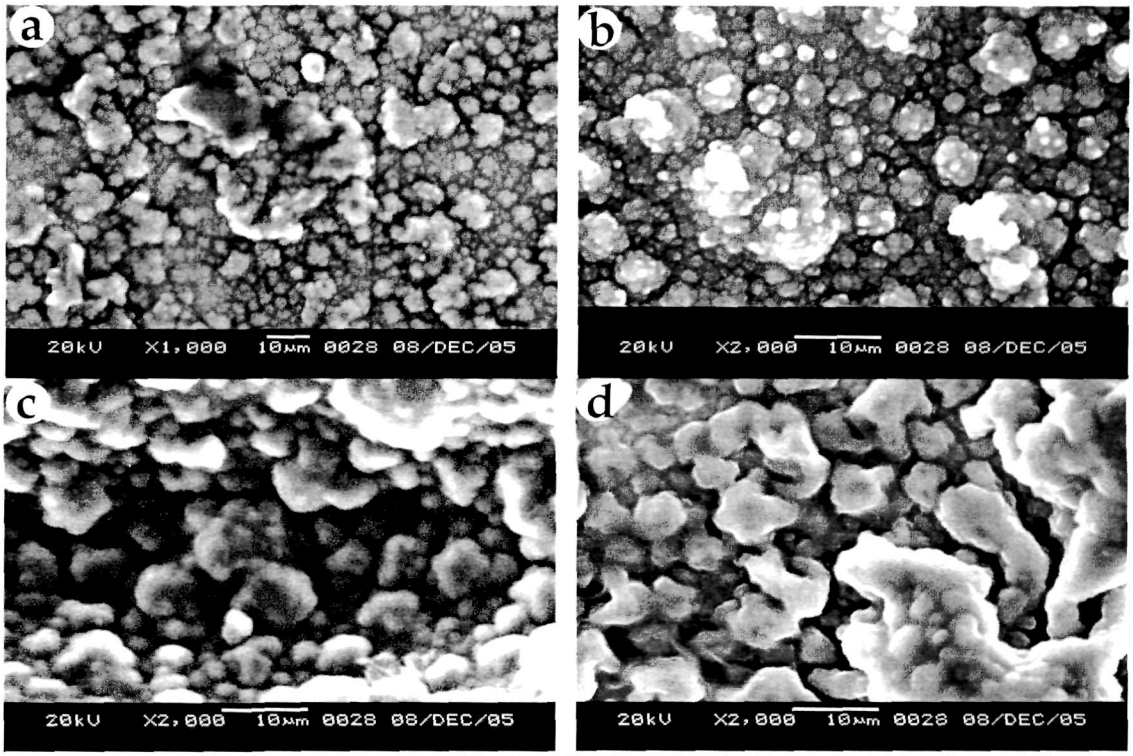


Figure 6.16: SEM micrographs of $LiCF_3SO_3$ doped poly(3-methylthiophene) films (a) before, and after irradiation with fluence (b) $5x10^{10}$, (c) $5x10^{11}$ and (d) $3x10^{12}$ ions/cm$^2$.

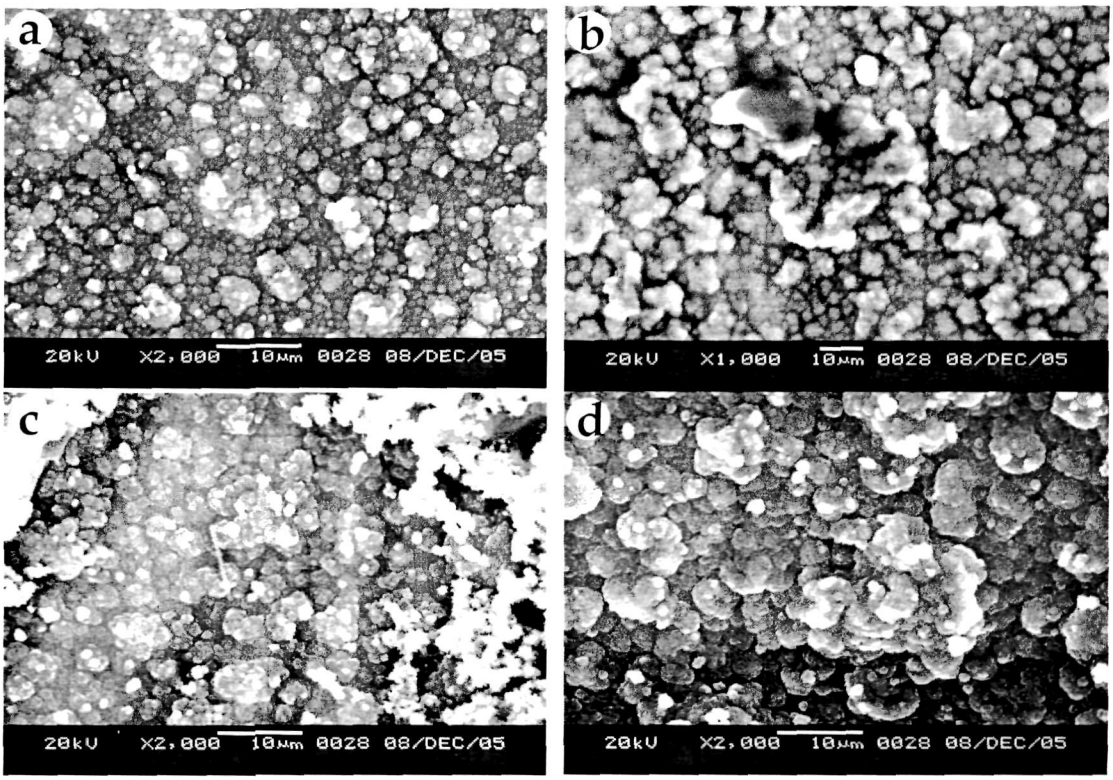


Figure 6.17: SEM micrographs of $[CH_3(CH_2)_3]_4NBF_4$ doped poly(3-methylthiophene) films (a) before, and after irradiation with fluence (b) $5x10^{10}$, (c) $5x10^{11}$ and (d) $3x10^{12}$ ions/cm$^2$.

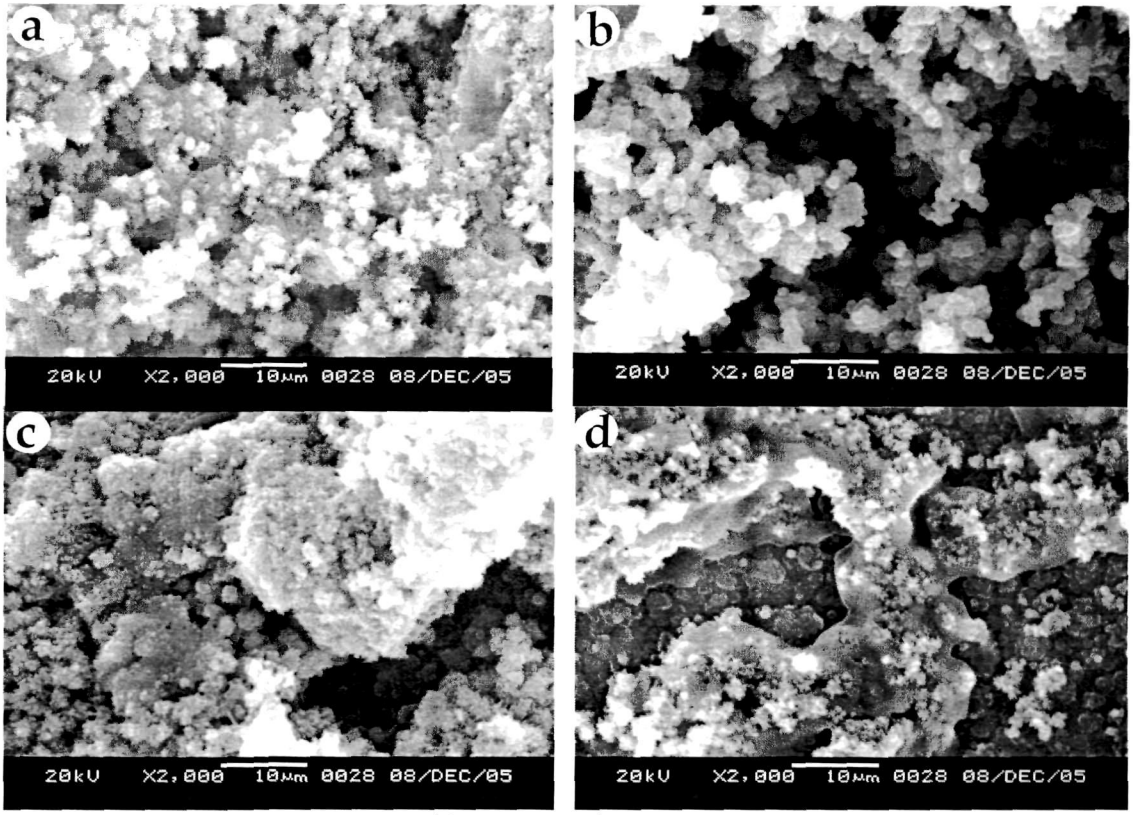


Figure 6.18: SEM micrographs of $[CH_3(CH_2)_3]_4NPF_6$ doped poly(3-methylthiophene) films (a) before, and after irradiation with fluence (b) $5x10^{10}$, (c) $5x10^{11}$ and (d) $3x10^{12}$ ions/cm$^2$.

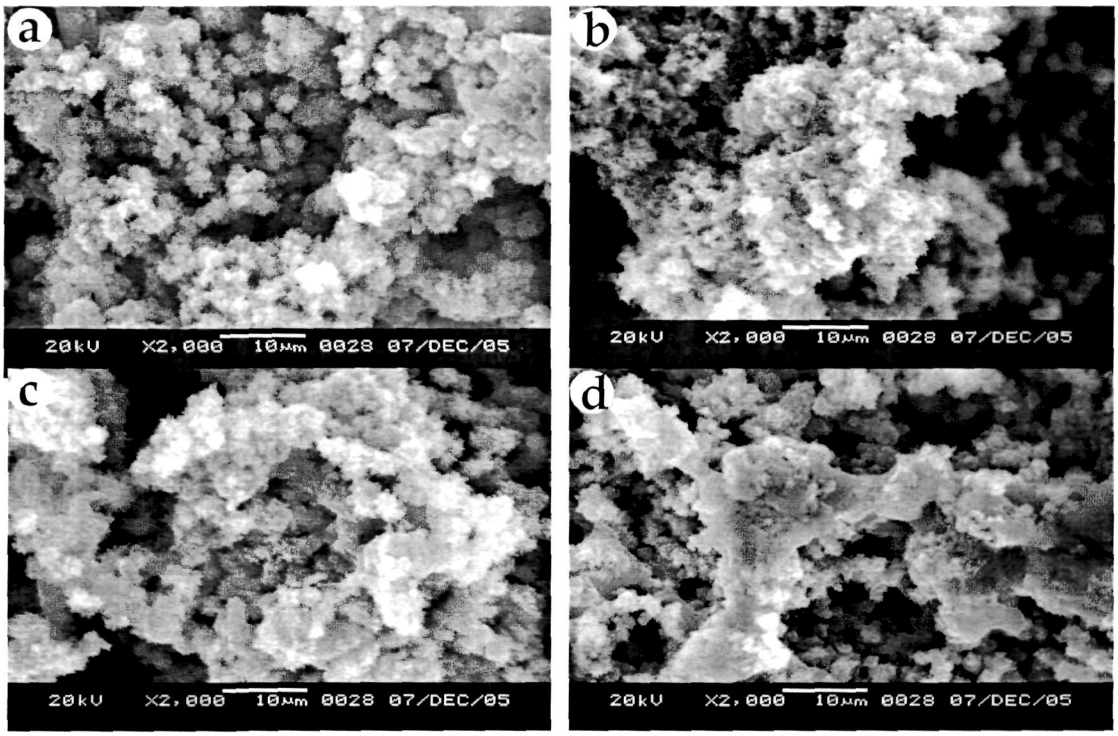


Figure 6.19: SEM micrographs of $LiClO_4$ n-doped poly(3-methylthiophene) films (a) before, and after irradiation with fluence (b) $5x10^{10}$, (c) $5x10^{11}$ and (d) $3x10^{12}$ ions/cm$^2$.

after irradiation (Fig. 6.16d). Similar effects are observed in poly(3-methylthiophene) films doped with $[CH_3(CH_2)_3]_4NBF_4$ (Fig. 6.17) and $[CH_3(CH_2)_3]_4NPF_6$ (Fig. 6.18). The fine grains observed in the unirradiated $LiClO_4$ n-doped poly(3-methylthiophene), after SHI irradiation the grain growth occur and as a result of agglomeration larger grains are observed on the surface (Fig. 6.19). The changes observed in the morphology of the polymer films may be ascribed to the grain growth, agglomeration and displacement of the polymer molecules from hilly to valley regions under the impact of the incident swift heavy ions making the film surface dense and smooth. A decrease in porosity of the polymer films is observed after SHI irradiation due to densification owing to the displacement of polymer molecules.

### *6.4.4 UV-Vis spectroscopy:*

The UV-Vis spectra of the conducting poly(3-methylthiophene) films doped with $LiClO_4$, $LiCF_3SO_3$, $[CH_3(CH_2)_3]_4NBF_4$, $[CH_3(CH_2)_3]_4NPF_6$ and n-doped with $LiClO_4$ recorded after SHI irradiation with 120 MeV $Si^{9+}$ ion at each fluence are presented in Figs. 6.20 a-e respectively. The electronic structure and carrier density can be visualized from the study of UV-Vis spectra. The absorption peak at 450nm appears in all the four UV-Vis spectra, which is the characteristic $\pi \rightarrow \pi^*$ transition absorption of the poly(3-methylthiophene) conducting polymer. The polaron/bipolaron absorption peak of the polymer in oxidized form appears at around 830nm [327]. The increase in intensity of the absorption peak at 830 nm is clearly observed in all the poly(3-methylthiophene) conducting polymer films, which could be attributed to the increase in carrier (polaron/bipolaron) concentration in the polymer film after SHI irradiation. These results are consistent with the increase in conductivity after SHI irradiation.

The UV-Vis absorption spectrum of the n-doped poly(3-methylthiophene) conducting polymer film is shown in Fig. 6.20e. The characteristic absorption peak after irradiation occurs at the same position, 450

nm as that for unirradiated film. The carrier absorption peak, which appears at 620 nm in unirradiated n-doped poly(3-methylthiophene), shifts towards higher wavelength and is found to appear at 650 nm in the polymer films irradiated with the highest fluence of $3X10^{12}$ ions/cm$^2$. The peak shift towards higher wavelength is also accompanied by broadening of the peak depicting increase in conductivity, which is experimentally observed in conductivity measurement. The decrease of band gap occurs due to broadening of polaron/bipolaron bands, which is attributed to the increase in carrier concentration in the polymer films as large number of cations, anions, radicals and charged particles are created upon SHI irradiation.

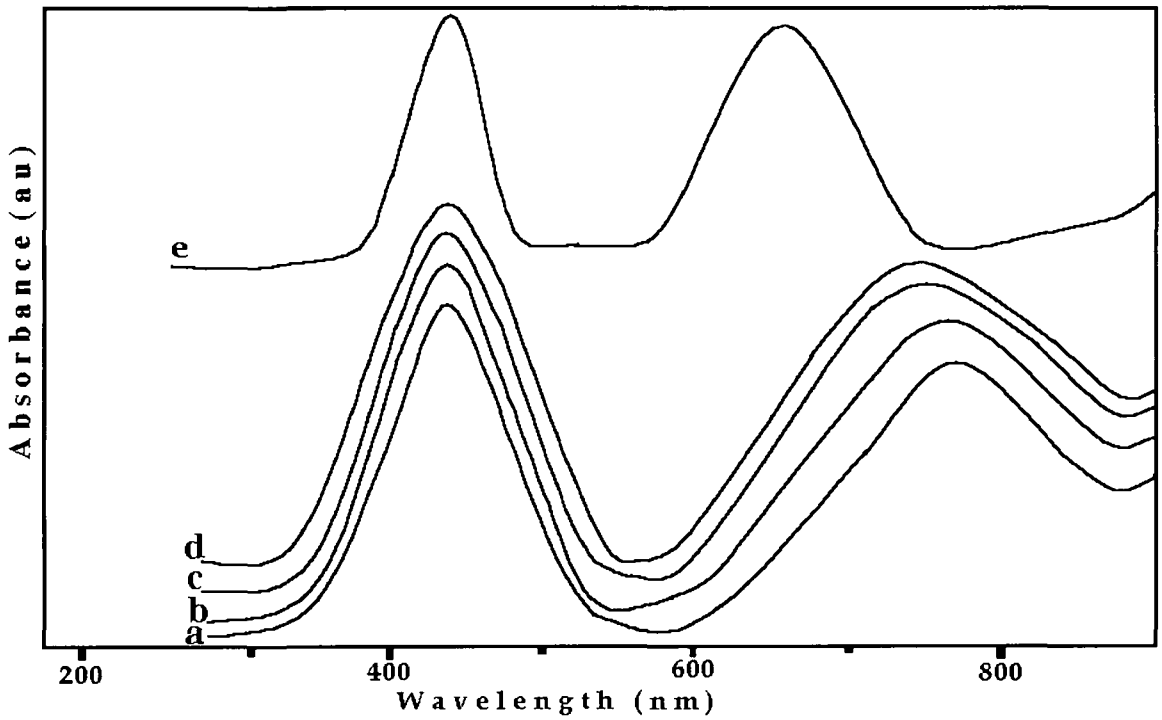


Figure 6.20: UV-Vis spectra of irradiated poly(3-methylthiophene) films p-doped with (a) $LiClO_4$, (b) $LiCF_3SO_3$, (c) $[CH_3(CH_2)_3]_4NBF_4$, (d) $[CH_3(CH_2)_3]_4NPF_6$ and n-doped with (e) $LiClO_4$.

### *6.4.5 FTIR spectroscopy:*

The FTIR spectra of 120 MeV $Si^{9+}$ ion irradiated poly(3-methylthiophene) conducting polymer films p-doped with $LiClO_4$, $LiCF_3SO_3$, $[CH_3(CH_2)_3]_4NBF_4$, $[CH_3(CH_2)_3]_4NPF_6$ and n-doped with $LiClO_4$ are presented in Figs. 6.21 a-e. The C-S stretching vibration absorption peak of poly(3-methylthiophene) is observed at around 670 cm$^{-1}$ in all the four FTIR spectra after irradiation. The

peak at ~700 $cm^{-1}$ is attributed to the C-H out of plane vibration and the peak at ~800 $cm^{-1}$ is due to C-H ring vibration of the thiophene monomer [334]. The C-H in-plane deformation vibration absorption peak is observed at 1050 $cm^{-1}$. The C-C ring stretching of the heteroaromatic ring vibration absorption occurs at 1440 $cm^{-1}$ [335]. The C=C aromatic ring stretching vibration absorption peak is observed at 1635 $cm^{-1}$ [335, 336]. The =C-H stretching vibration absorption peak of the heteroaromatic ring occurs at about 3045 $cm^{-1}$. The absorption peaks at 2965 $cm^{-1}$ and 2868 $cm^{-1}$ are attributed to the asymmetric and symmetric C-H stretching vibration absorptions respectively of the methyl group in the poly(3-methylthiophene) conducting polymer films. The bending mode C-H vibration absorption of the methyl group occurs at 1370 $cm^{-1}$. The peak intensity of the absorption peaks at 2965 $cm^{-1}$, 2868 $cm^{-1}$ and 1370 $cm^{-1}$ decrease upon SHI irradiation, which indicate the decrease in the methyl group concentration in the poly(3-methylthiophene) conducting polymer after SHI irradiation.

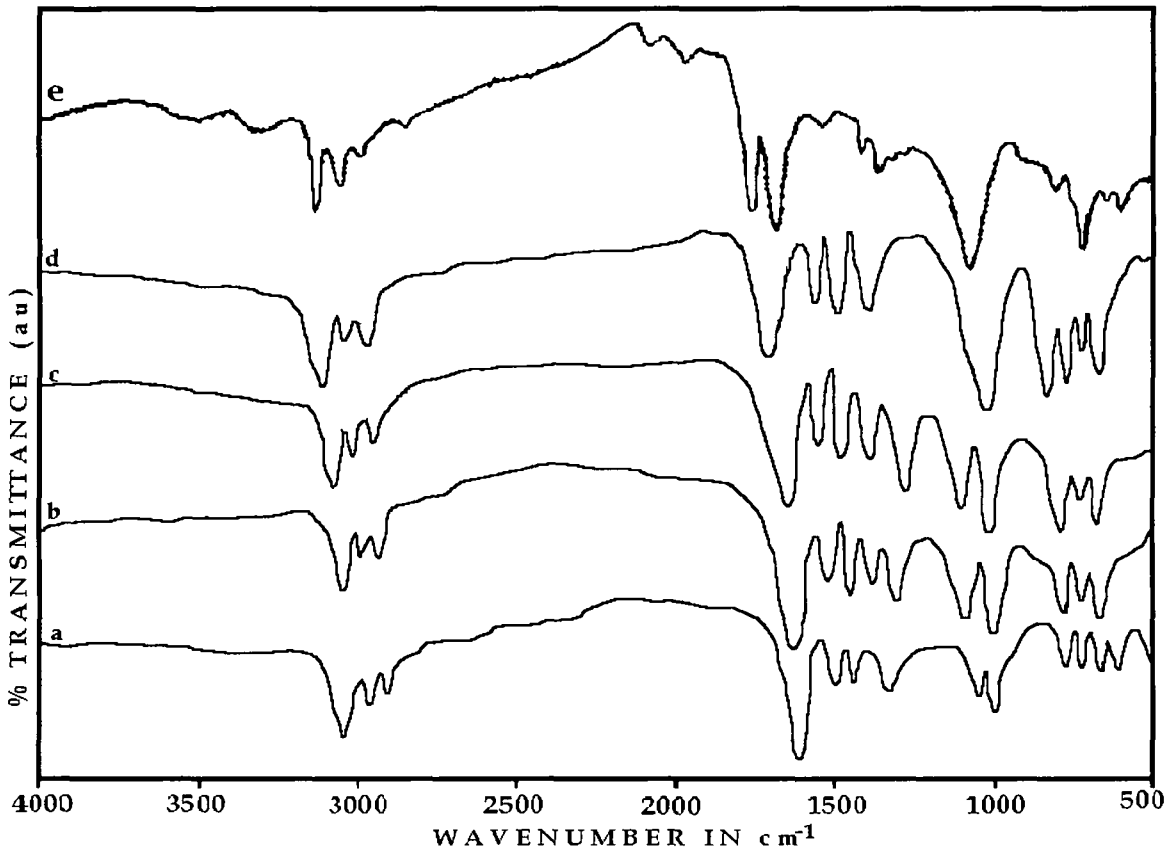


Figure 6.21: FTIR spectra of irradiated poly(3-methylthiophene) films p-doped with (a) $LiClO_4$, (b) $LiCF_3SO_3$, (c) $[CH_3(CH_2)_3]_4NBF_4$, (d) $[CH_3(CH_2)_3]_4NPF_6$ and n-doped with (e) $LiClO_4$.

The $ClO_4^-$ ion in the poly(3-methylthiophene) film doped with $LiClO_4$ (Fig. 6.21 a) shows two absorption peaks at 1100 $cm^{-1}$ and 630 $cm^{-1}$ [263-265]. The absorption peak at 1360 $cm^{-1}$ is attributed to the S=O asymmetric vibration and 1180 $cm^{-1}$ is attributed to S=O symmetric vibration of the dopant ion $CF_3SO_3^-$ ion in the FTIR spectra of $LiCF_3SO_3$ doped poly(3-methylthiophene) (Fig. 6.21 b) [265]. Two absorption peak at 1340 $cm^{-1}$ and 1136 $cm^{-1}$ are attributed to the $BF_4^-$ ion in the FTIR spectra of $[CH_3(CH_2)_3]_4NBF_4$ doped poly(3-methylthiophene) (Fig. 6.21 c). The absorption peak at 845 $cm^{-1}$ appears due to the presence of $PF_6^-$ ion in the spectra of $[CH_3(CH_2)_3]_4NPF_6$ doped poly(3-methylthiophene) conducting polymer films (Fig. 6.21 d). The presence of the dopant ions induced vibrational absorption peaks in the respective FTIR spectra confirm the presence of dopant ions in the conducting polymer films after SHI irradiation.

### *6.4.6 X-Ray Diffractogram study:*

The XRD spectra of the poly(3-methylthiophene) conducting polymer films p-doped with $LiClO_4$, $LiCF_3SO_3$, $[CH_3(CH_2)_3]_4NBF_4$, $[CH_3(CH_2)_3]_4NPF_6$ and n-doped with $LiClO_4$ recorded after SHI irradiation with 120 MeV $Si^{9+}$ ion

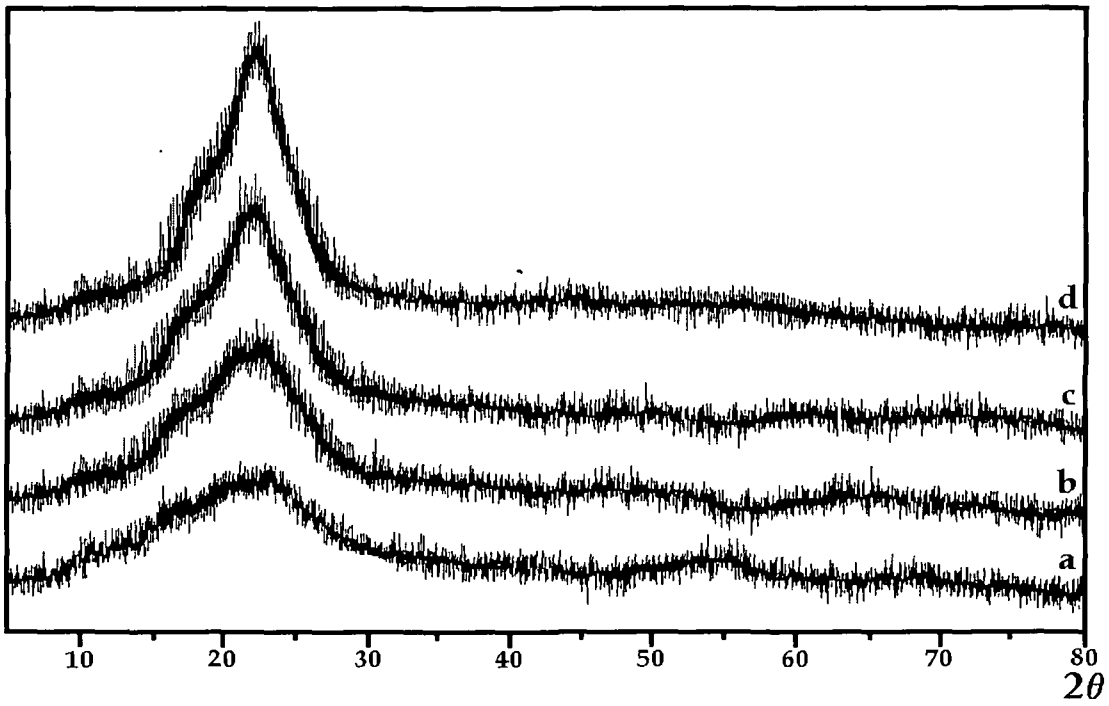


Figure 6.22: X-Ray diffractogram of $LiClO_4$ doped poly(3-methylthiophene) (a) before and after irradiation with fluence (b) $5x10^{10}$, (c) $5x10^{11}$ and (d) $3x10^{12}$ ions/$cm^2$.

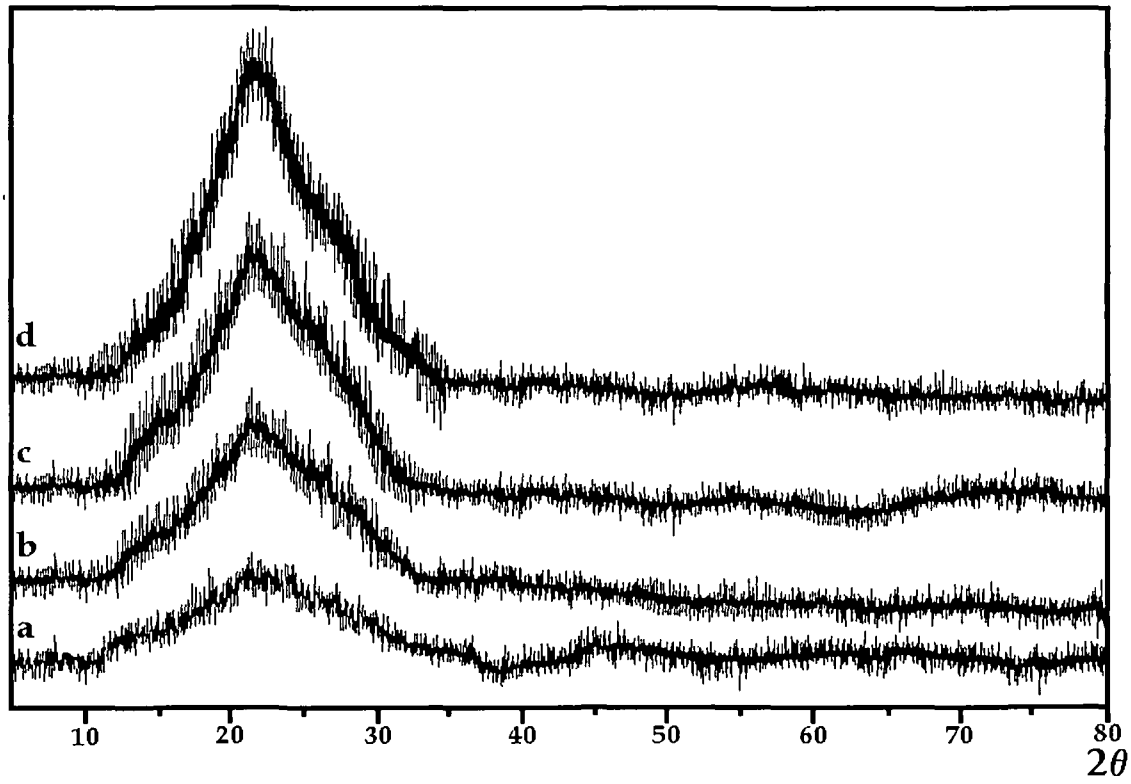


Figure 6.23: X-Ray diffractogram of $LiCF_3SO_3$ doped poly(3-methylthiophene) (a) before and after irradiation with fluence (b) $5x10^{10}$, (c) $5x10^{11}$ and (d) $3x10^{12}$ ions/$cm^2$.

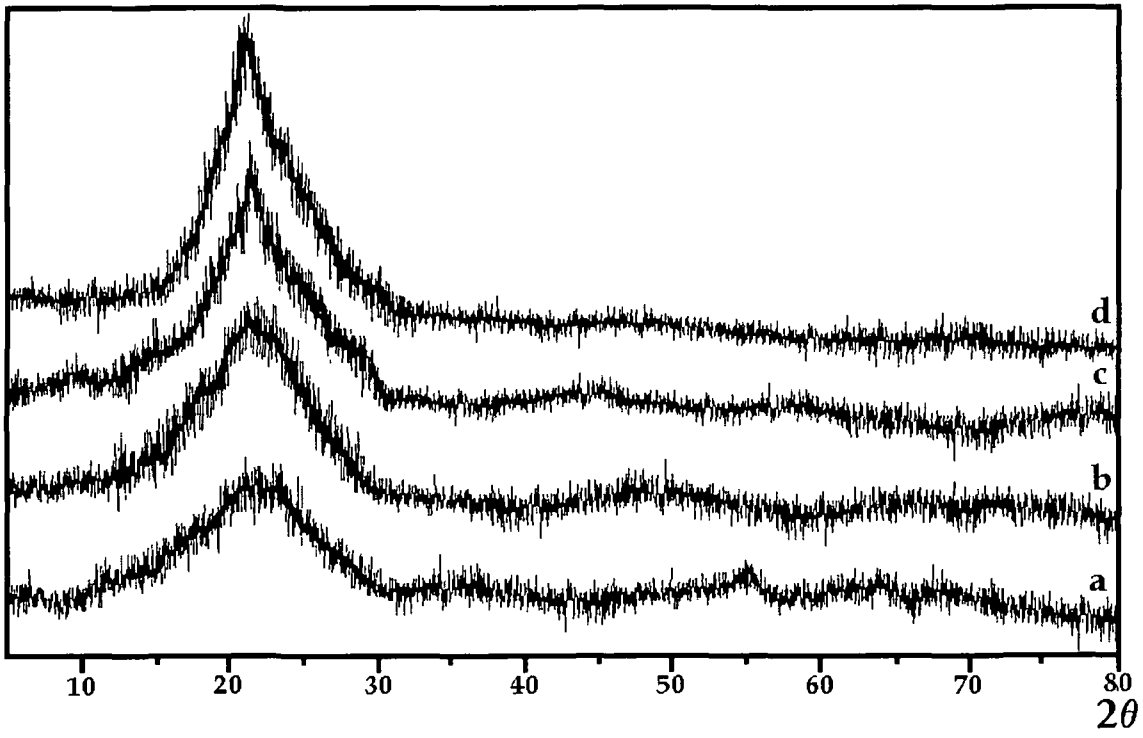


Figure 6.24: X-Ray diffractogram of $[CH_3(CH_2)_3]_4NBF_4$ doped poly(3-methylthiophene) (a) before and after irradiation with fluence (b)$5x10^{10}$, (c) $5x10^{11}$ and (d) $3x10^{12}$ ions/$cm^2$.

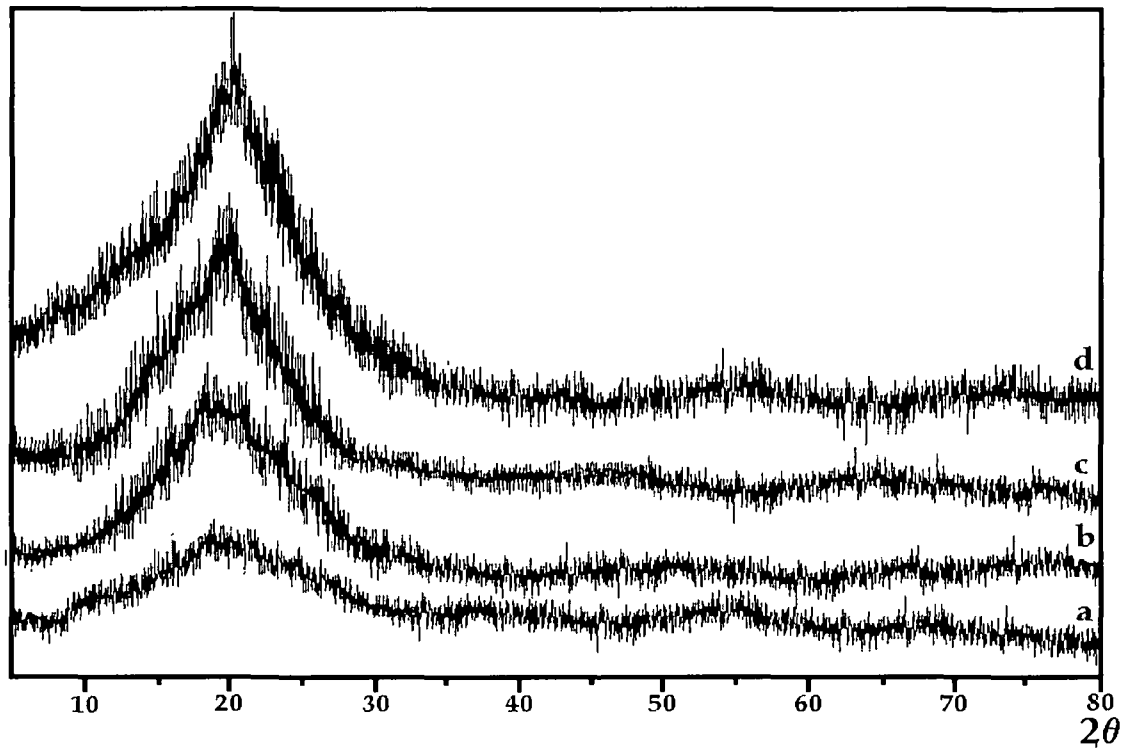


Figure 6.25: X-Ray diffractogram of $[CH_3(CH_2)_3]_4NPF_6$ doped poly(3-methylthiophene) before (a) and after irradiation with fluence $5x10^{10}$(b), $5x10^{11}$ (c) and $3x10^{12}$ (d) ions/$cm^2$.

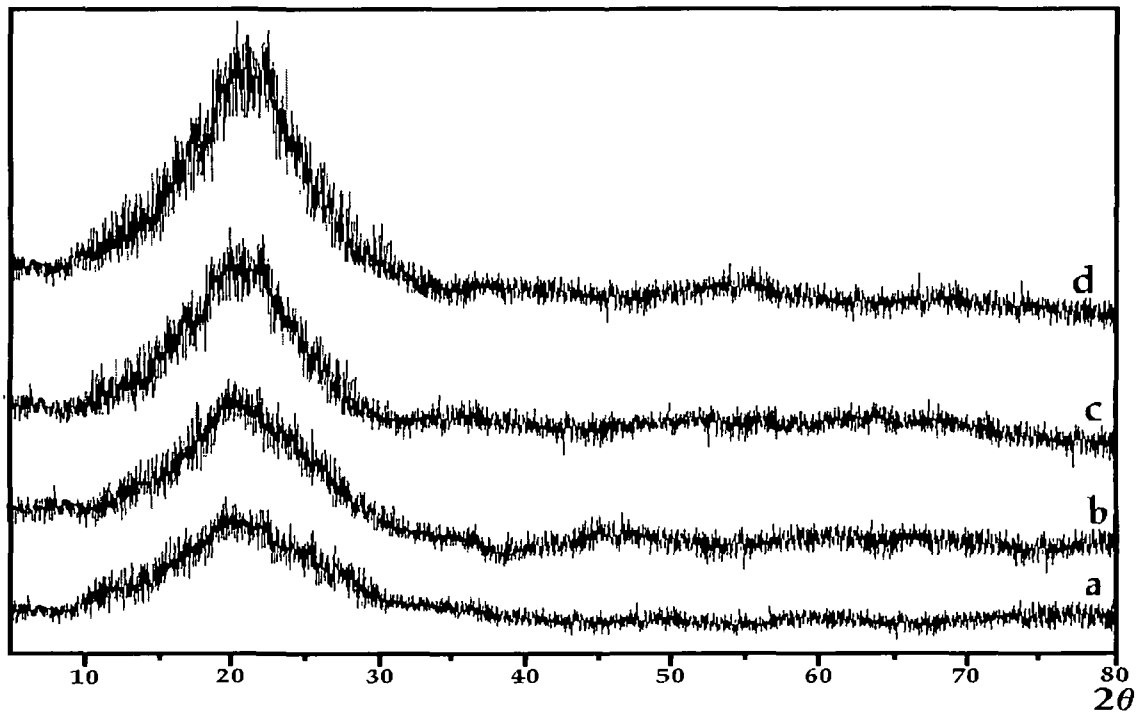


Figure 6.26: X-Ray diffractogram of $LiClO_4$ n-doped poly(3-methylthiophene) before (a) and after irradiation with fluence $5x10^{10}$(b), $5x10^{11}$ (c) and $3x10^{12}$ (d) ions/$cm^2$.

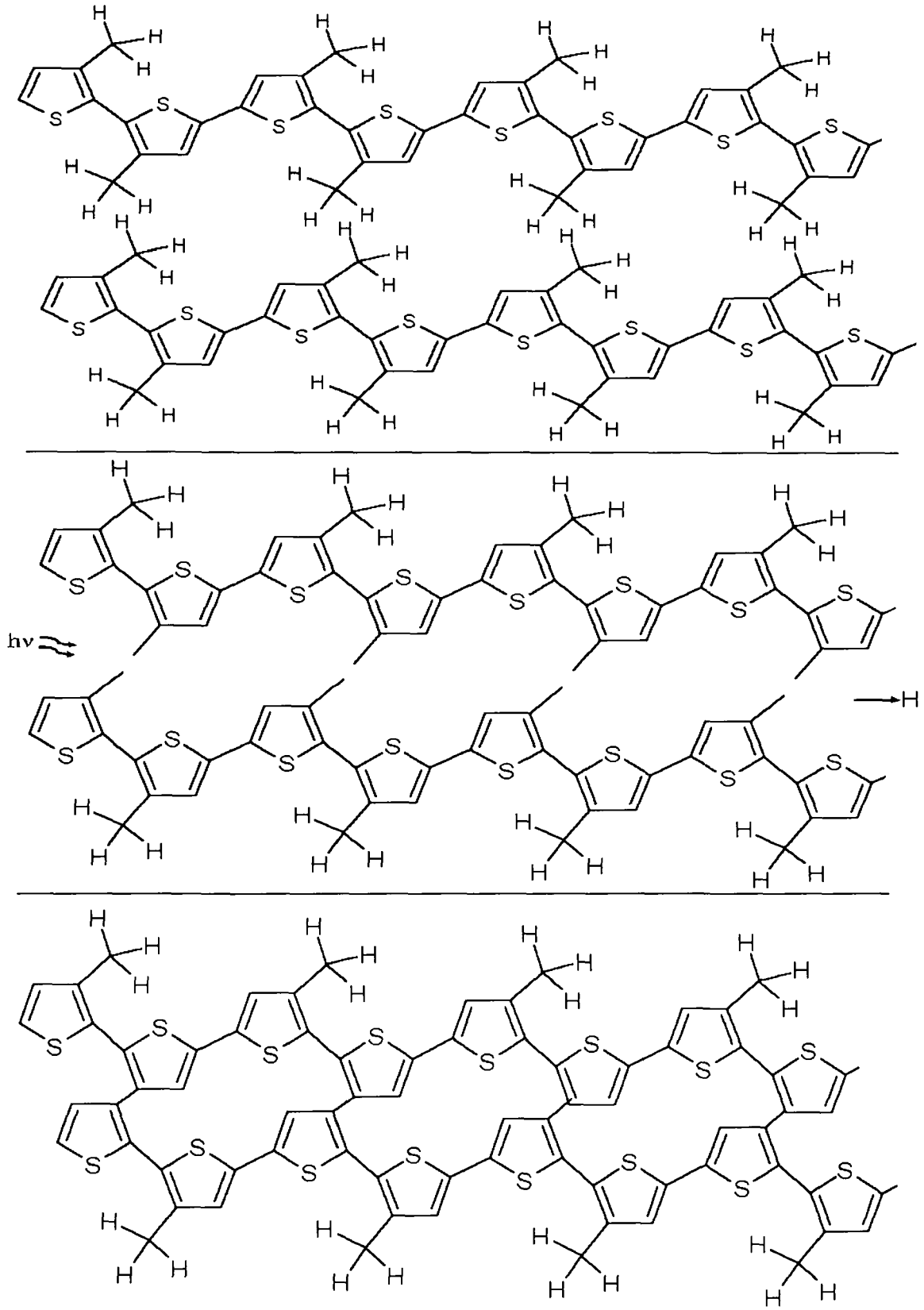


Figure 6.27: Schematic diagram of cross linking for poly(3-methylthiophene) upon SHI irradiation.

at three different fluence of $5X10^{10}$, $5X10^{11}$ and $3X10^{12}$ ions/cm$^2$ are presented in Figs. 6.22-6.26. The unirradiated poly(3-methylthiophene) conducting polymer films are semi-crystalline. Significant increase in the degree of crystallinity of the polymer films is observed after SHI irradiation as shown in Table 6.4. Collective excitations (plasmons) produced upon SHI irradiation, which produces a large excited volume, the backbone bonds may rotate and adopt a variety of conformations. As they cool, the lower-energy positions come to be preferred. Stereo-regular chains will then favour regular helical shapes. At the same time, these regular sections of chain may pack together to form regions of crystallinity. Upon SHI irradiation the density of the polymer increases [269] making the polymer more compact, which may have produced closely packed regions by chain folding, cross linking of polymer chain or by the formation of single or multiple helices, which produces more crystalline regions in the polymer films resulting in increase in degree of crystallinity. The schematic diagram of possible cross linking for poly(3-methylthiophene) upon SHI irradiation and ejection of hydrogen atoms from the polymer chain is shown in Fig. 6.27. The degree of crystallinity increases with increase in ion fluence.

Table6.4: Degree of crystallinity (K) of poly(3-methylthiophene) films after SHI irradiation with 120 MeV $Si^{9+}$ ion at different fluences.

| Dopant | Unirradiated | 5x10$^{10}$ions/cm$^2$ | 5x10$^{11}$ions/cm$^2$ | 3x10$^{12}$ions/cm$^2$ |
|---|---|---|---|---|
| $LiClO_4$ | 17.82% | 31.28% | 37.92% | 46.86% |
| $LiCF_3SO_3$ | 16.67% | 30.92% | 38.52% | 46.21% |
| $[CH_3(CH_2)_3]_4NBF_4$ | 18.09% | 29.34% | 36.68% | 45.52% |
| $[CH_3(CH_2)_3]_4NPF_6$ | 17.52% | 29.68% | 35.90% | 45.36% |
| $LiClO_4$ (n-doping) | 17.64% | 29.22% | 34.85% | 44.86% |

The degree of crystallinity (K) of the poly(3-methylthiophene) conducting polymer films have been calculated using the method as described in details in chapter 3 section 3.6.6.1 and are presented in Table 6.4. About 75% increase in the degree of crystallinity of the poly(3-methylthiophene)

conducting polymer films are obtained after SHI irradiation. The crystalline portions of the polymer films provide easy path for charge carrier conduction decreasing the resistivity, which is consistent with the conductivity measurements.

**6.5 Summary:**

The poly(3-methylthiophene) conducting polymer films have been successfully synthesized by electrochemical oxidative polymerization of 3-methylthiophene monomer with different dopants in organic media acetonitrile on ITO coated glass. The n-doping of the poly(3-methylthiophene) film has also been successfully carried out with $LiClO_4$ salt by applying a potential of -2V for about 8 hrs. The cyclic voltammograms of the poly(3-methylthiophene) films doped with lithium perchlorate ($LiClO_4$), lithium trifluoro methane sulfonate ($LiCF_3SO_3$), tetrabutylammonium tetrafluoroborate ($[CH_3(CH_2)_3]_4NBF_4$) and tetrabutylammonium hexafluorophosphate ($[CH_3(CH_2)_3]_4NPF_6$) show very good redox response with electrochromism. The redox response of the poly(3-methylthiophene) conducting polymer films remains unchanged upon SHI irradiation with 120 MeV $Si^{9+}$ ion beam. The magnitude of oxidation and reduction current density of the SHI irradiated poly(3-methylthiophene) films increases, which could be attributed to the increase in conductivity of polymer film after SHI irradiation as other experimental condition of cyclic voltammetry are kept same. The electrical conductivity measurement shows up to 70% increase in the dc conductivity of the polymer films upon SHI irradiation (Table 6.3). The UV-Vis spectroscopy shows the regular characteristic absorption peaks of poly(3-methylthiophene) films at 450 nm and 730 nm due to $\pi \rightarrow \pi^*$ transition and polaron/bipolaron absorption respectively. The n-doped poly(3-methylthiophene) conducting polymer films show UV-Vis absorption peaks at 440 nm and 620 nm. The carrier absorption peak intensities are observed to increase after SHI irradiation, which could be attributed to the increase of carrier concentration in the polymer films after irradiation as large number of cations, anions, radicals and charged

particles are created upon SHI irradiation. The doping of the poly(3-methylthiophene) films are confirmed by the dopant ion interaction absorption peaks in the FTIR spectra. The XRD patterns show semi-crystalline nature of the poly(3-methylthiophene) conducting polymer films. Upon SHI irradiation up to 75% increase in crystallinity has been observed and also the loss of the methyl group is predicted from the FTIR spectroscopy, which leads to the possible inference that the presence of the methyl group attached to the thiophene ring prevents the systematic linear alignment of the poly(3-methylthiophene) polymer chains making the unirradiated poly(3-methylthiophene) conducting polymer films more amorphous. The increase in the degree of crystallinity with the increase of fluence upon SHI irradiation gives rise to increase in the electrical conductivity, which is consistent with the conductivity measurements.

# CHAPTER VII

## FABRICATION AND CHARACTERIZATION OF ALL-POLYMER REDOX SUPERCAPACITORS

There is an increasing interest in the electrochemical systems under conditions in which the electrical power demand is highly time dependent, often in the form of short term pulses. This has led to efforts to develop electrical devices that are optimized in terms of their short-term power output, rather than total energy content. Because of the general observation that capacitors can be used to provide short electrical pulses, attention has been focused upon the concept of electrochemical systems that exhibit capacitor-like characteristics. There are two general categories of energy storage mechanisms in electrochemical systems. One of these involves the charge storage in the double layer at or near the electrode/electrolyte interface, and the other is related to the reversible absorption of atomic species into the crystal structure of bulk solid electrodes. An important feature of double layer supercapacitors is that the amount of charge stored is a linear function of the voltage. The voltages therefore, falls linearly with the amount of charge extracted. Thus voltage-dependent applications can only utilize a fraction of the total energy stored in such systems. Due to the characteristics of the electrode/electrolyte surface structure and its related thermodynamics, it is often found that modest amount of Faradic electrodeposition can occur at potentials somewhat removed from those needed for the bulk deposition of a new phase. This results in the occupation of specific crystallographic surface sites. This mechanism typically results in only partial surface coverage, and thus the production of an 'adsorption pseudocapacitance' of some 200-400 mF/cm$^2$ at the interface. The possibility of the development of $RuO_2$-type materials as commercial capacitors began in 1975 [337]. Since the amount of energy stored is proportional to the amount of the electroactive species that can be absorbed by the electrode, this bulk storage mechanism can lead to much higher values of energy storage per

unit volume of electrode structure than any surface related process. This new mechanism has been called redox pseudocapacitance by the Conway group [338] who later renamed it introducing the new term 'supercapacitors' to describe the devices utilizing this type of charge storage.

Redox supercapacitors are attracting increasing attention as high power devices [339]. Supercapacitors can be used as uninterrupted power sources, can be coupled with batteries to provide peak power and can replace batteries for memory back-up [340]. Conducting polymers are very promising electrode materials for redox capacitors as they are less expensive than other alternating electrode materials e.g., noble metal oxides, may be easily synthesized in the form of extended surface thin films and can store charge throughout their entire volume [115]. The noble metal oxide $RuO_2$ can give capacitance up to 380 F/gm, whereas conducting polymer electrodes can go up to 500 F/gm [337] providing a clear advantage of using conducting polymer as electrode materials. Other advantages of the conducting polymers include light weight, easy synthesis and the cheaper cost.

**7.1 Fabrication of all-polymer redox supercapacitors:**

An electrochemical capacitor with both its electrodes and electrolytes made up of polymer is referred to as all-polymer supercapacitor. All-polymer redox solid state supercapacitors have been fabricated using the conducting polymer films on ITO coated glass as electrodes as shown in Fig. 7.1. The ITO coating of the substrate acts as current collectors on both side of the capacitors. Unirradiated and irradiated conducting polymer films of polyaniline, polypyrrole and poly(3-methylthiophene) are used as electrodes. The PVDF-HFP(20w/o)-PMMA(10w/o)-LiCF3SO3(10w/o)-PC+DEC(57w/o)-SiO2(3w/o) gel polymer electrolyte has been prepared by solution casting technique as mentioned in chapter 3, section 3.3. All three types of supercapacitors, type I, type II and type III as described in chapter I, section 1.5.2, have been designed and characterized.

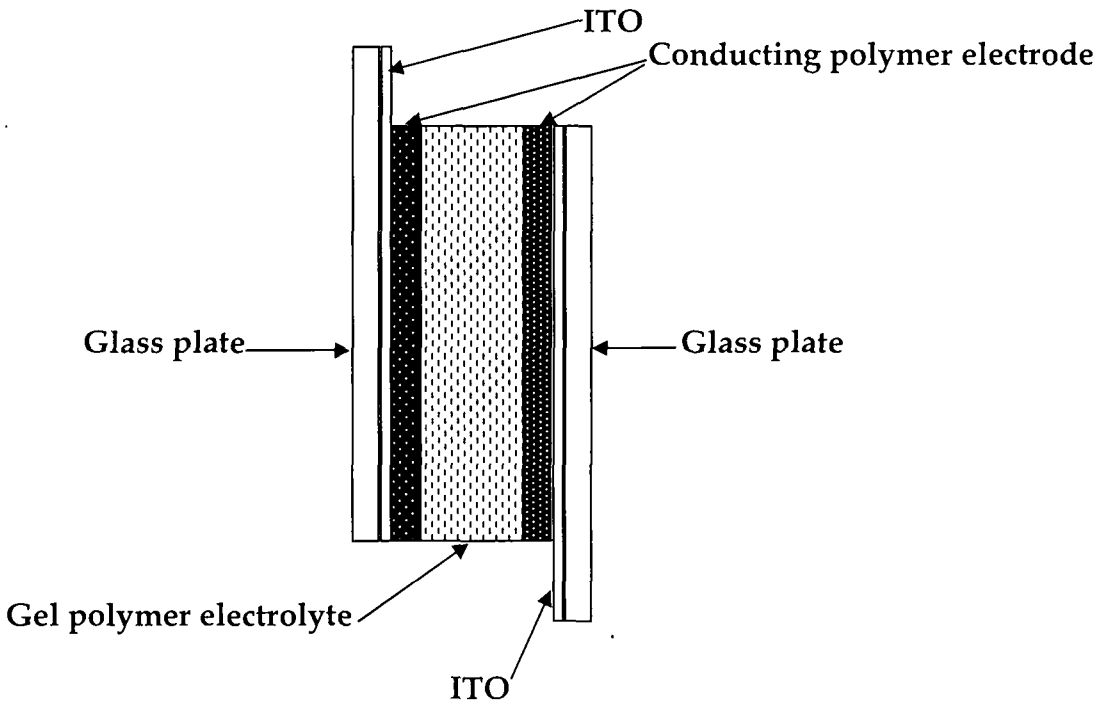


Figure 7.1: Geometrical structure of supercapacitor fabricated.

### 7.2 Supercapacitors with polyaniline electrodes:

The cyclic voltammetry of type I supercapacitor with polyaniline conducting polymer electrodes doped with HCl, $H_2SO_4$, $HClO_4$, $H_3PO_4$ and $LiClO_4$ have been carried out at different scan rates and are shown in Fig. 7.2. The capacitance of the supercapacitors has been calculated from the cyclic voltammograms using the relation:

$$C = i/s \qquad (7.1)$$

where 'i' is the current and 's' is the scan rate.

The cyclic voltammograms of the type I supercapacitors with p-doped polyaniline electrodes on both sides show ideal capacitance characteristics at lower scan rates but deviates from the ideal rectangular form at higher scan rates (100 mV/Sec). Small increase of current with rise of potential in either direction of potential sweep due to the redox property of the conducting polymer electrodes causes the deviation from the ideal capacitance behaviour. The scan rate dependency of current i.e., the increase of current with increase in scan rate is also observed in the cyclic voltammograms of all supercapacitors.

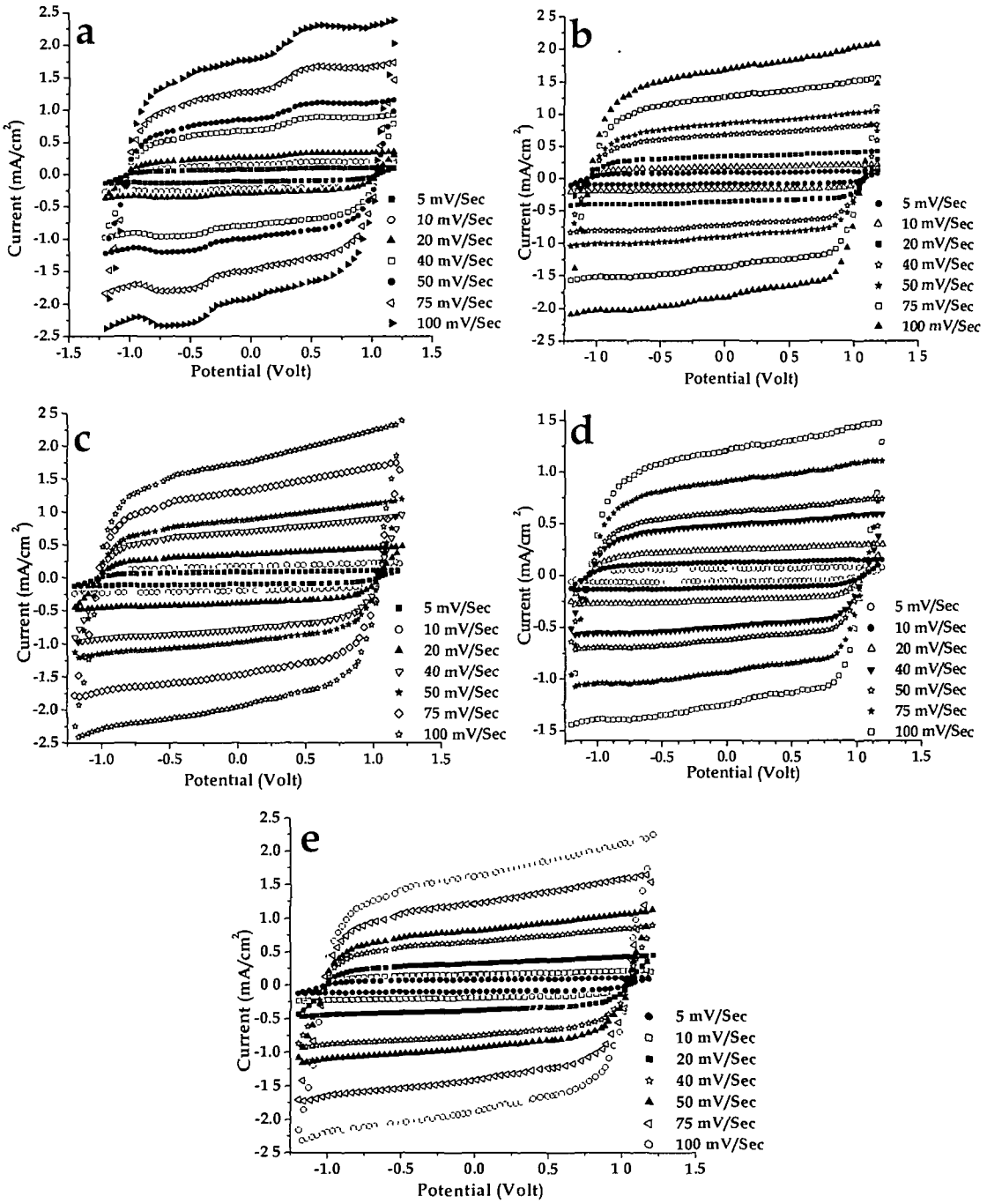


Figure 7.2: Cyclic voltammograms of type I supercapacitor with polyaniline electrodes doped with (a) HCl, (b) $H_2SO_4$, (c) $HClO_4$, (d) $H_3PO_4$ and (e) $LiClO_4$.

The characteristic properties of the supercapacitors with polyaniline electrodes doped with different dopants are presented in Table 7.1. The initial decrease of capacitance of the supercapacitors may be attributed to the charge

loss due to some irreversible Faradic reactions with volatile surface groups e.g., $OH^-$, $CN^-$, $CH_3^+$ etc. at the surface of the electrodes.

The Coulombic efficiency $\eta$ can be calculated easily from the galvanostatic charge-discharge plot from the relation:

$$\eta = \frac{\Delta t_D}{\Delta t_C} \times 100\% \qquad (7.2)$$

where $\Delta t_D$ and $\Delta t_C$ are times of charging and discharging respectively.

The galvanostatic charge-discharge plots of the type I supercapacitors with polyaniline electrodes at 100 μA are shown in Fig. 7.3. The discharge capacitance ($mF/cm^2$) of the individual supercapacitor cells (Table 7.1) has been calculated from the charge-discharge plot using the relation [341]:

$$C = \frac{i\Delta t}{\Delta V} \qquad (7.3)$$

where 'i' is the galvanostatic charging/discharging current, $\Delta t$ is the time interval in which a fall in potential $\Delta V$ occurs. From the discharge capacitance value obtained from the charge-discharge plot, the specific capacitance value of the individual electrode has been calculated in F/gm (Table 7.1). The initial sudden rise/fall of potential in the charging/discharging occurs due to the ohmic loss occurring in the internal resistance of the capacitor.

The internal resistance (Table 7.1) or the equivalent series resistance (ESR) of the supercapacitors has been calculated from the steep rise in potential of the charge-discharge plot using the relation:

$$R = V/i \qquad (7.4)$$

where 'i' is the charging current and 'V' is the magnitude of vertical rise in or fall of potential during charging or discharging respectively. The internal resistance of the supercapacitors has been found to be on the order of 1-2 $k\Omega cm^2$.

The energy density of the supercapacitors with polyaniline conducting polymer electrodes doped with different dopants has been calculated using the relation:

$$E_d = \tfrac{1}{2} CV^2 \qquad (7.5)$$

where C is the discharge capacitance of the electrode material (in F/gm) and V is the working potential i.e., the highest potential upto which the supercapacitor exhibit capacitive behaviour.

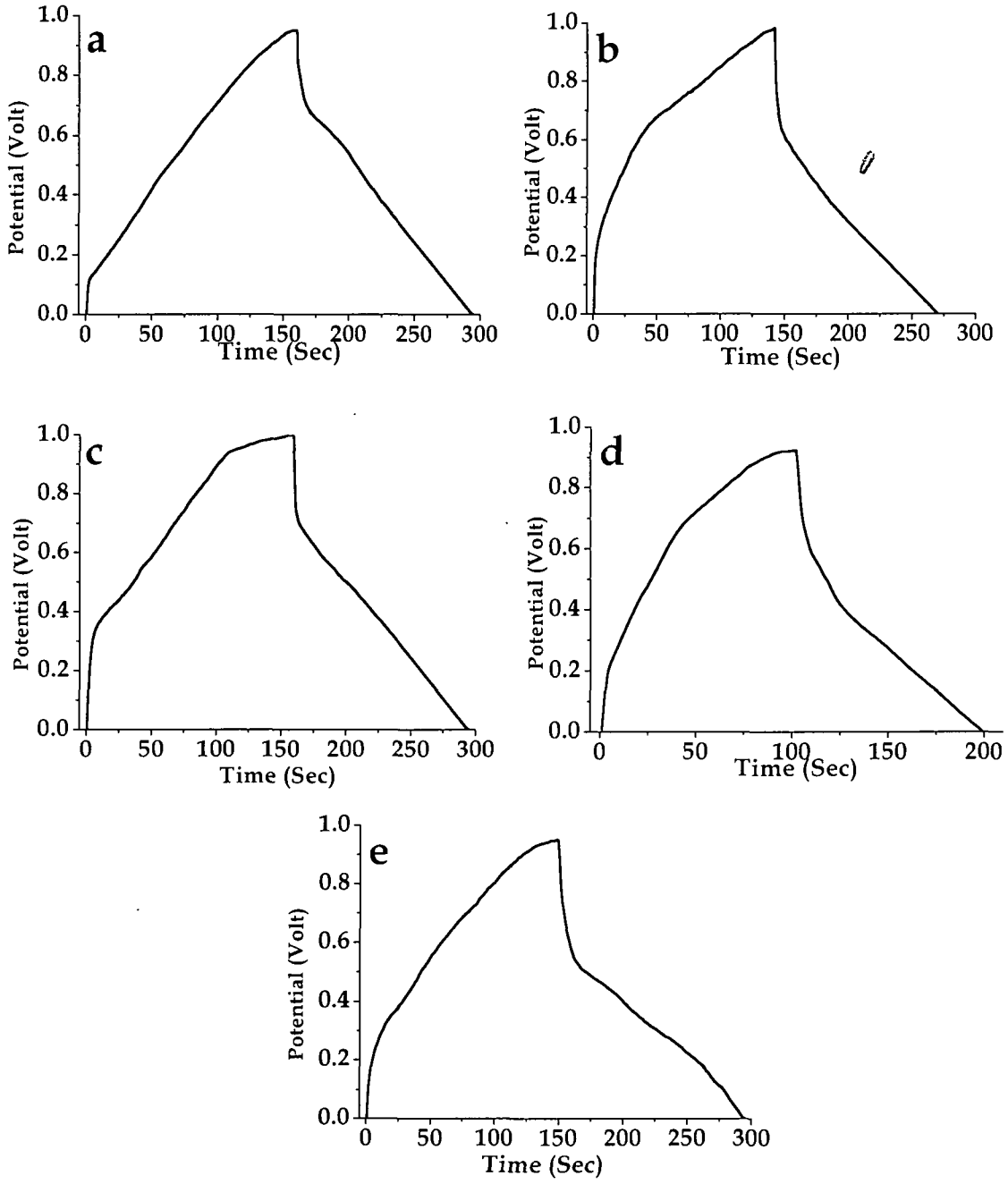


Figure 7.3: Charge-discharge plots of supercapacitor with polyaniline electrodes doped with (a) HCl, (b) $H_2SO_4$, (c) $HClO_4$, (d) $H_3PO_4$ and (e) $LiClO_4$.

Table 7.1: Characteristic properties of supercapacitors with polyaniline electrodes doped with different dopants.

| Dopant | Capacitance (F/gm) | | Discharge Capacitance | | Internal Resistance | Coulombic efficiency | Energy Density |
|---|---|---|---|---|---|---|---|
| | Initial | Final | (mF/cm²) | (F/gm) | $R_i$ (kΩ cm²) | η(%) | (Wh/kg) |
| HCl | 259.2 | 210.38 | 42.44 | 212.2 | 1.08 | 83.23 | 29.47 |
| $H_2SO_4$ | 195.6 | 149.2 | 38.12 | 190.6 | 1.72 | 88.81 | 26.47 |
| $HClO_4$ | 217.5 | 171.4 | 42.14 | 210.7 | 2.69 | 81.99 | 29.26 |
| $H_3PO_4$ | 134.75 | 98.7 | 26.30 | 131.5 | 2.11 | 93.20 | 18.26 |
| $LiClO_4$ | 206.7 | 169.8 | 39.16 | 195.8 | 2.15 | 96.00 | 27.19 |

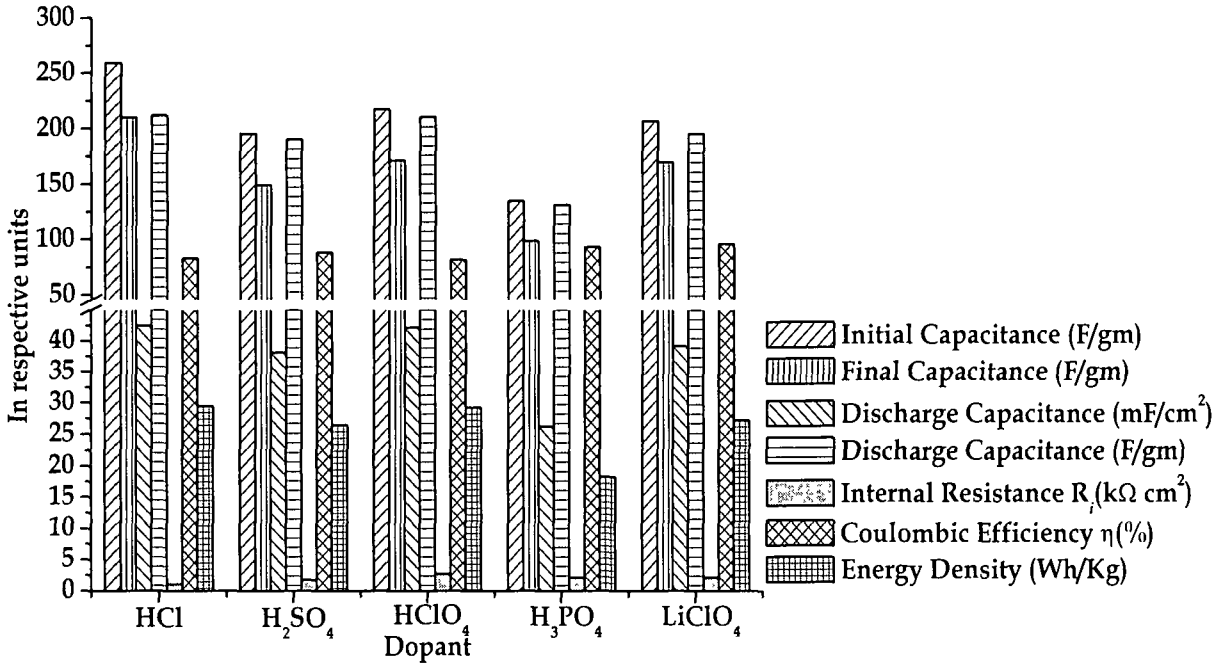


Figure 7.4: Characteristic properties of supercapacitors with polyaniline electrodes doped with different dopants.

Fig. 7.4 graphically represents the characteristic values of the supercapacitors with polyaniline electrodes doped with different dopants. The capacitance calculated from the cyclic voltammograms shows a slightly higher value than the discharge capacitance. This may be attributed to the fact that in the cyclic voltammogram the current contains a part from the leakage electronic current passing through the electrolyte as the polarity of the potential keeps on reversing. On the other hand in the charge-discharge process initially the

leakage current contributes, but as the polarity of applied potential remains same, the electronic current through the electrolyte diminishes and the contribution from the electronic current through the electrolyte becomes zero.

### *7.2.1 Supercapacitors with SHI irradiated HCl doped polyaniline electrodes:*

The cyclic voltammograms of the supercapacitors with 160 MeV $Ni^{12+}$ ion irradiated HCl doped polyaniline electrodes are shown in Figs. 7.5. The stability plots of the SHI irradiated polyaniline electrodes are shown in Fig. 7.6a. The charge-discharge plots of the supercapacitors with irradiated as well as the unirradiated electrodes are shown in Fig. 7.6b. The cyclic voltammograms of the supercapacitors with 160 MeV $Ni^{12+}$ ion irradiated polyaniline conducting polymer electrodes show reasonably good capacitive behavior up to a scan rate of 75 mV/Sec. At higher scan rate the cyclic voltammograms deviate from the ideal rectangular shape. At a given scan rate, the increase in current towards higher potential observed in the cyclic voltammograms occur due to the redox nature of the polyaniline electrodes which remains unchanged as observed in the cyclic voltammetry of the polyaniline films after irradiation (Chapter 4, section 4.4.1).

The electrochemical stability plots of the supercapacitors with unirradiated as well as irradiated polyaniline electrodes show initial sharp decrease in capacitance values, which may be attributed to the irreversible Faradic reaction of the highly reactive surface groups like etc. This initial decrease in capacitance of the supercapacitors with irradiated polyaniline electrodes is less as compared to that of the supercapacitors with unirradiated electrode. This may be due to the fact that the loosely bound volatile surface groups such as $OH^-$ etc. are stabilized or removed upon SHI irradiation from the polymer electrode. The decrease of capacitance in initial charge-discharge cycles is less with the increase in the fluence. The charge-discharge plots of the supercapacitors with irradiated electrodes are shown in Fig. 7.6b. Decrease in the total charge-discharge time of the supercapacitors with irradiated electrodes

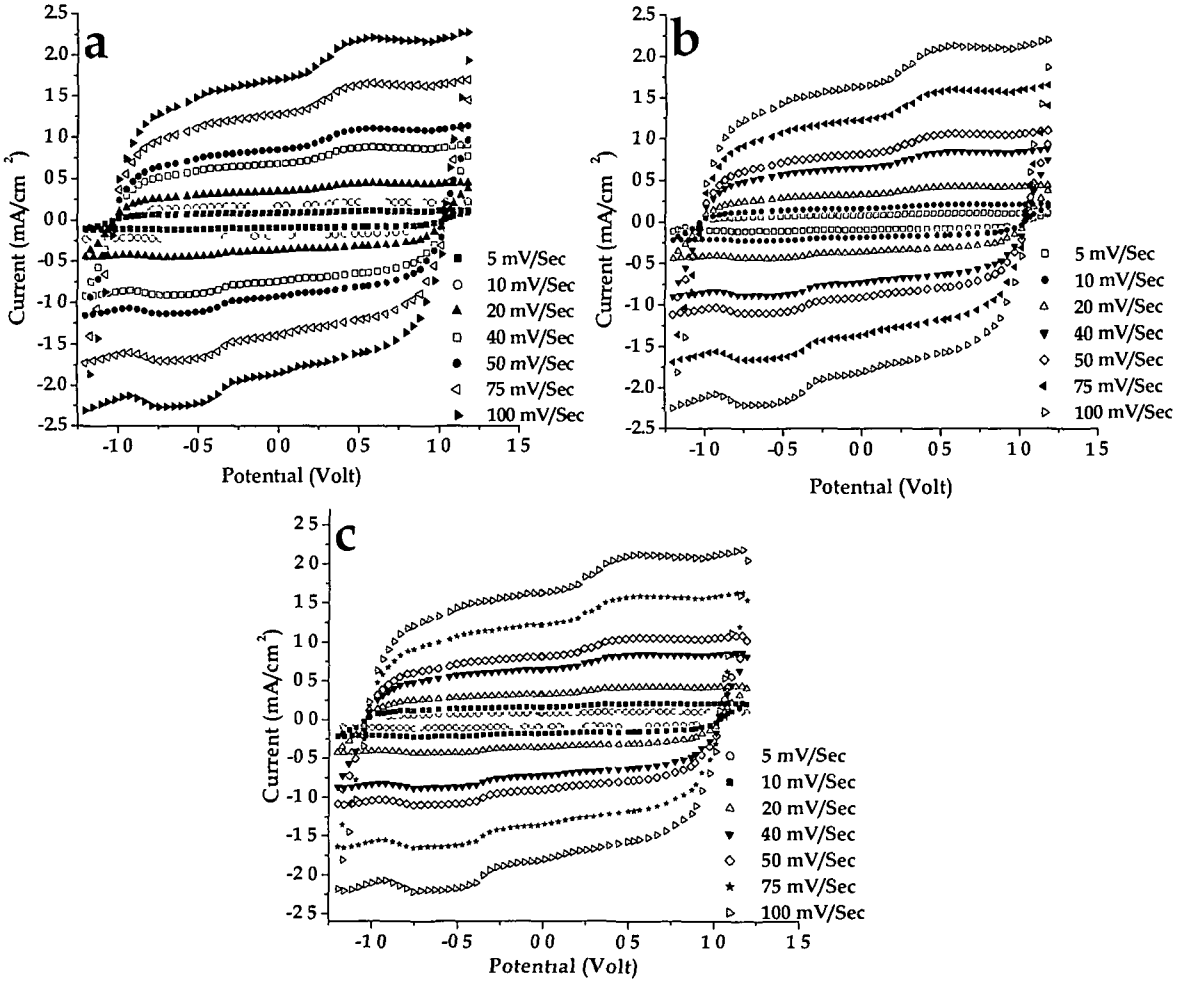


Figure 7 5 Cyclic voltammogram of supercapacitors with HCl doped polyaniline irradiated electrodes with fluence (a) $5X10^{10}$, (b) $5X10^{11}$ and (c) $3X10^{12}$ ions/cm$^2$

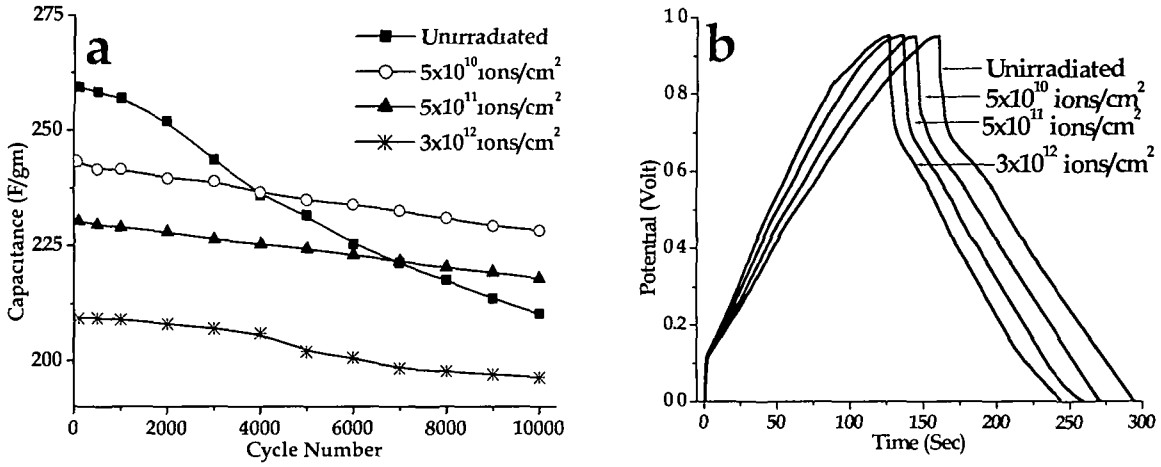


Figure 7 6 (a) Stability and (b) charge-discharge plot of supercapacitors with HCl doped polyaniline electrodes before and after SHI irradiation with different fluences

Table 7.2: Characteristic properties of supercapacitors with HCl doped polyaniline electrodes irradiated with different fluence.

| Fluence (Ions/cm$^2$) | Capacitance (F/gm) Initial | Final | Discharge Capacitance (mF/cm$^2$) | (F/gm) | Internal Resistance $R_i$ (kΩ cm$^2$) | Coulombic efficiency (η) | Energy Density (Wh/kg) |
|---|---|---|---|---|---|---|---|
| 0 | 259.2 | 210.38 | 42.44 | 212.2 | 1.08 | 83.23% | 29.47 |
| $5x10^{10}$ | 243.26 | 228.40 | 43.18 | 215.9 | 1.08 | 86.21% | 29.99 |
| $5x10^{11}$ | 230.38 | 218.04 | 40.54 | 202.7 | 1.09 | 89.78% | 28.15 |
| $3x10^{12}$ | 209.35 | 196.17 | 38.06 | 190.3 | 1.09 | 91.34% | 26.43 |

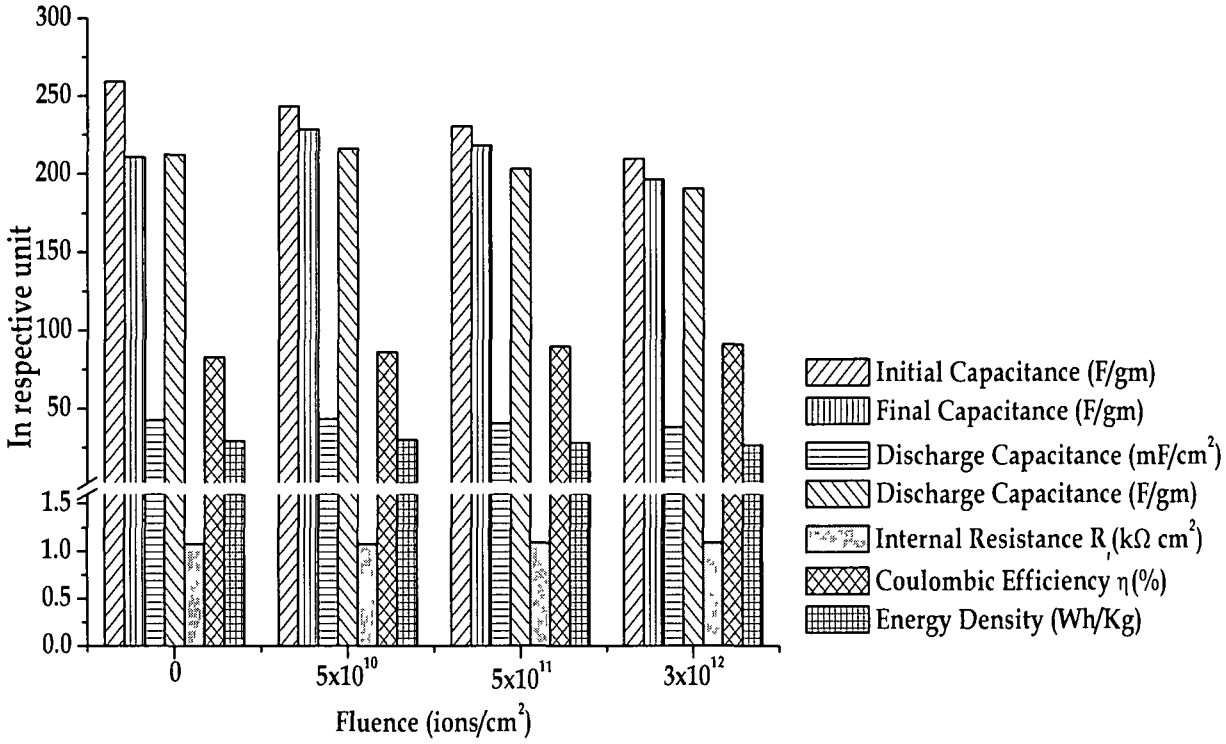


Figure 7.7: Characteristic properties of supercapacitors with HCl doped polyaniline electrodes irradiated with different fluences.

is observed with small increase in the coulombic efficiency. The decrease of charge-discharge time may be attributed to the increase in conductivity of the polymer electrodes after irradiation, which supports faster electron transport in the electrodes. The characteristic properties of the supercapacitors with irradiated HCl doped polyaniline electrodes are presented in table 7.2. The graphical representation of the characteristic values of the properties of the

supercapacitors with 160MeV $Ni^{12+}$ ion irradiated HCl doped polyaniline electrodes are shown in Fig. 7.7.

### *7.2.2 Supercapacitors with SHI irradiated $HClO_4$ doped polyaniline electrodes:*

The cyclic voltammograms of the supercapacitor with $HClO_4$ doped 120 MeV $Si^{9+}$ ion irradiated polyaniline electrodes recorded at different scan rates are shown in Fig. 7.8. The cyclic voltammograms of the supercapacitors show ideal capacitive behaviour at lower scan rates but at higher scan rates, the current increases towards higher potential and cyclic voltammograms deviate from the ideal rectangular shape. This is attributed to the redox property of the polyaniline electrodes, which causes the increase of current towards higher potential due to the oxidation of the conducting polymers. The characteristic

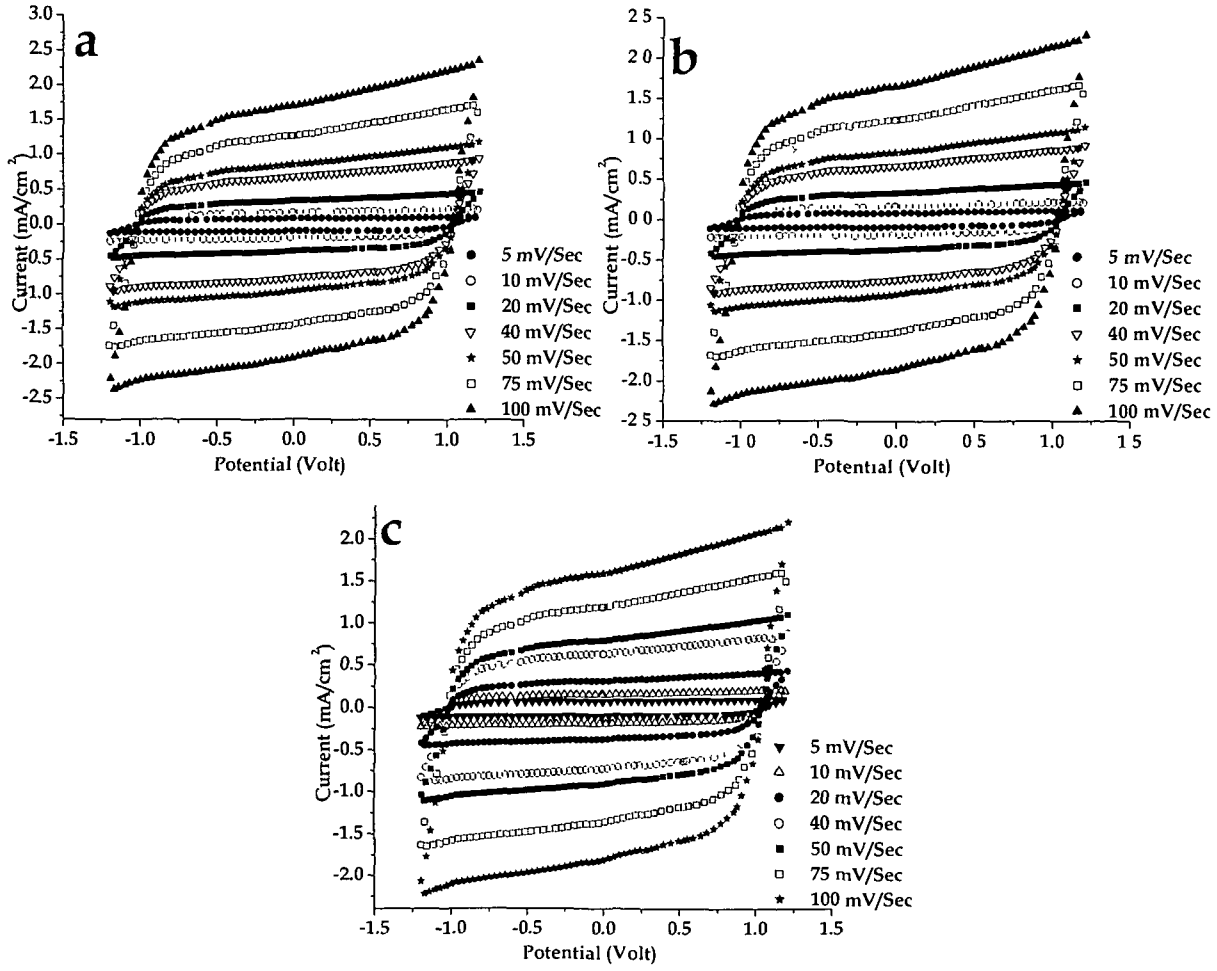


Figure 7.8: Cyclic voltammograms of supercapacitors with $HClO_4$ doped polyaniline irradiated electrodes with fluence (a) $5X10^{10}$, (b) $5X10^{11}$ and (c) $3X10^{12}$ ions/cm$^2$.

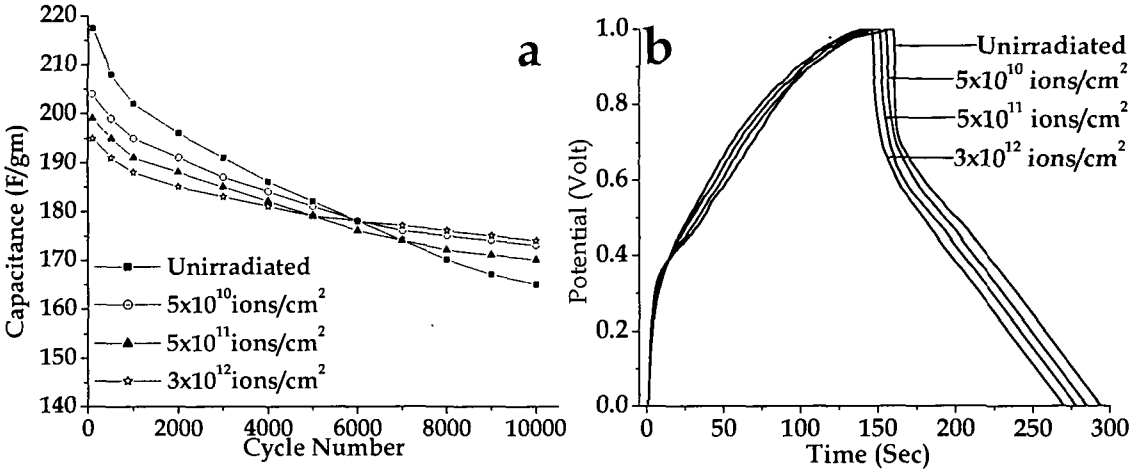


Figure 7.9: (a) Stability and (b) charge-discharge plots of supercapacitors with $HClO_4$ doped polyaniline electrodes before and after SHI irradiation with different fluences.

Table 7.3: Characteristic properties of supercapacitors with $HClO_4$ doped polyaniline electrodes irradiated with different fluence.

| Fluence (ions/cm$^2$) | Capacitance (F/gm) | | Discharge Capacitance | | Internal Resistance | Coulombic efficiency | Energy Density |
|---|---|---|---|---|---|---|---|
| | Initial | Final | (mF/cm$^2$) | (F/gm) | $R_i$ (kΩ cm$^2$) | η(%) | (Wh/kg) |
| 0 | 217.5 | 165.4 | 42.14 | 210.7 | 2.69 | 81.99 | 29.26 |
| $5x10^{10}$ | 204 | 173.2 | 40.50 | 202.5 | 2.12 | 84.52 | 28.13 |
| $5x10^{11}$ | 199 | 170.8 | 39.24 | 196.2 | 1.94 | 86.68 | 27.25 |
| $3x10^{12}$ | 195 | 174.5 | 38.56 | 192.8 | 1.67 | 89.87 | 26.78 |

values of the supercapacitors with $HClO_4$ doped polyaniline conducting polymer electrodes are presented in Table 7.3. The electrochemical stability of the supercapacitors has been tested for 10,000 charge-discharge cycles. The capacitance values have been calculated after every 1000 cycles and are presented in the stability plots in Fig. 7.9a. The charge-discharge plots of the supercapacitors with $HClO_4$ doped polyaniline electrodes recorded galvanostatically at 100 μA are presented in Fig. 7.9b. The internal resistance of the supercapacitors are found to be small (~2 kΩ cm$^2$) and a small decrease is observed with the increase in fluence of SHI irradiation. The characteristic values of properties are presented graphically in Fig. 7.10.

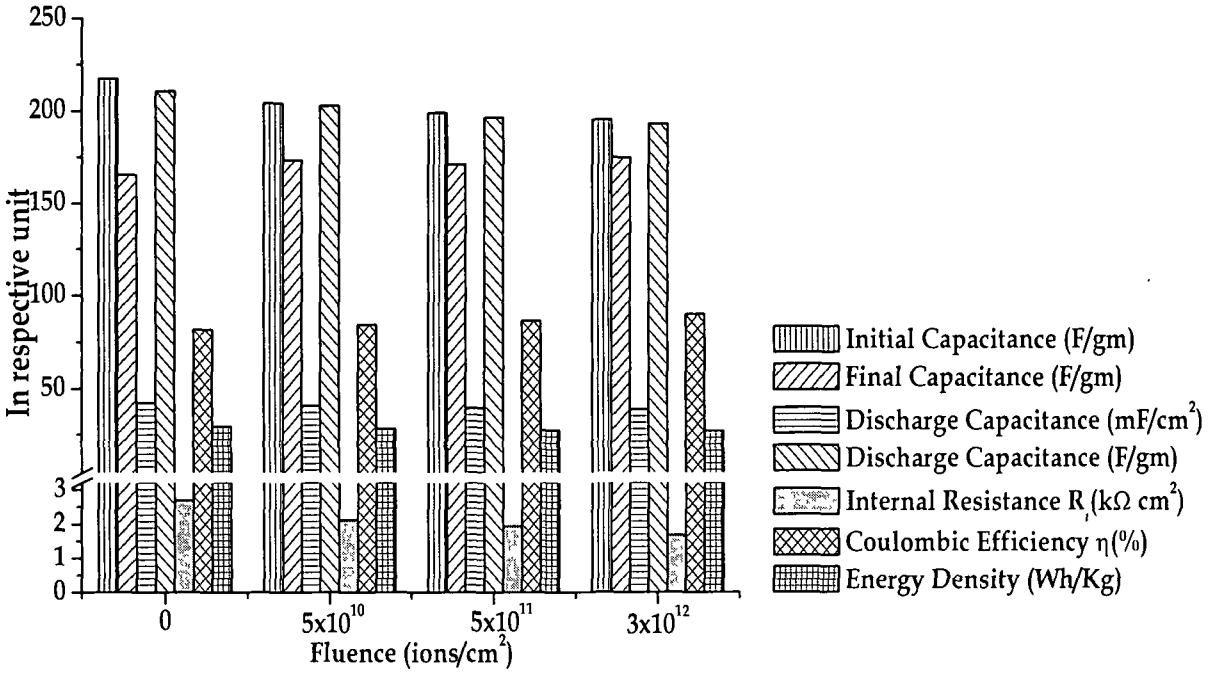


Figure 7.10: Characteristic properties of supercapacitors with $HClO_4$ doped polyaniline electrodes irradiated with different fluences.

### 7.3 Supercapacitors with polypyrrole electrodes:

The cyclic voltammograms of the supercapacitors with polypyrrole conducting polymer doped with $LiClO_4$, $NaClO_4$, $LiCF_3SO_3$, $[CH_3(CH_2)_3]_4NBF_4$ and $[CH_3(CH_2)_3]_4NPF_6$ are shown in Figs. 7.11a-e respectively. The cyclic voltammograms show good capacitive behaviour at lower scan rates but at higher scan rates (100 mV/Sec) the cyclic voltammograms slightly deviate from the ideal capacitive rectangular shapes. The redox property of the polypyrrole conducting polymer electrodes causes the increase in current towards higher potential, which results in deviation of the capacitive characteristics of the cyclic voltammograms from ideal one. In all the cyclic voltammograms of the supercapacitors with different salt doped polypyrrole electrodes, the scan rate dependence of current i.e., increase of current with increase in scan rate is observed. The charge-discharge plots of type I supercapacitors with polypyrrole conducting polymer electrodes are shown in Fig. 7.12. The galvanostatic charge-discharge of the supercapacitors carried out at a constant current of 100 μA upto

a potential of 1.0 Volt shows good charge-discharge characteristics with comparatively low internal resistance (~2 kΩ cm²)

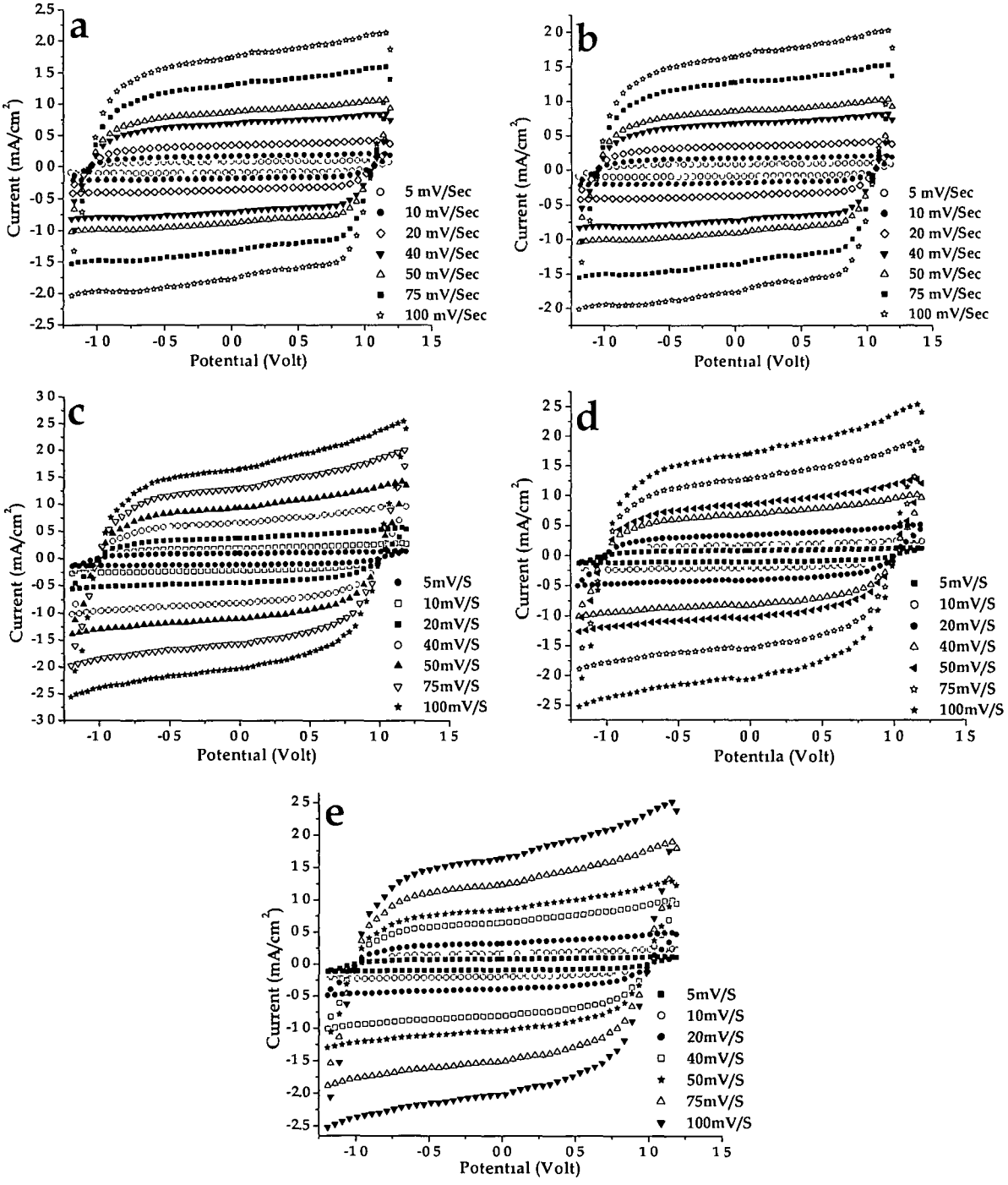


Figure 7.11: Cyclic voltammograms of type I supercapacitors with polypyrrole electrodes doped with (a) $LiClO_4$, (b) $NaClO_4$, (c) $LiCF_3SO_3$, (d) $[CH_3(CH_2)_3]_4NBF_4$ and (e) $[CH_3(CH_2)_3]_4NPF_6$

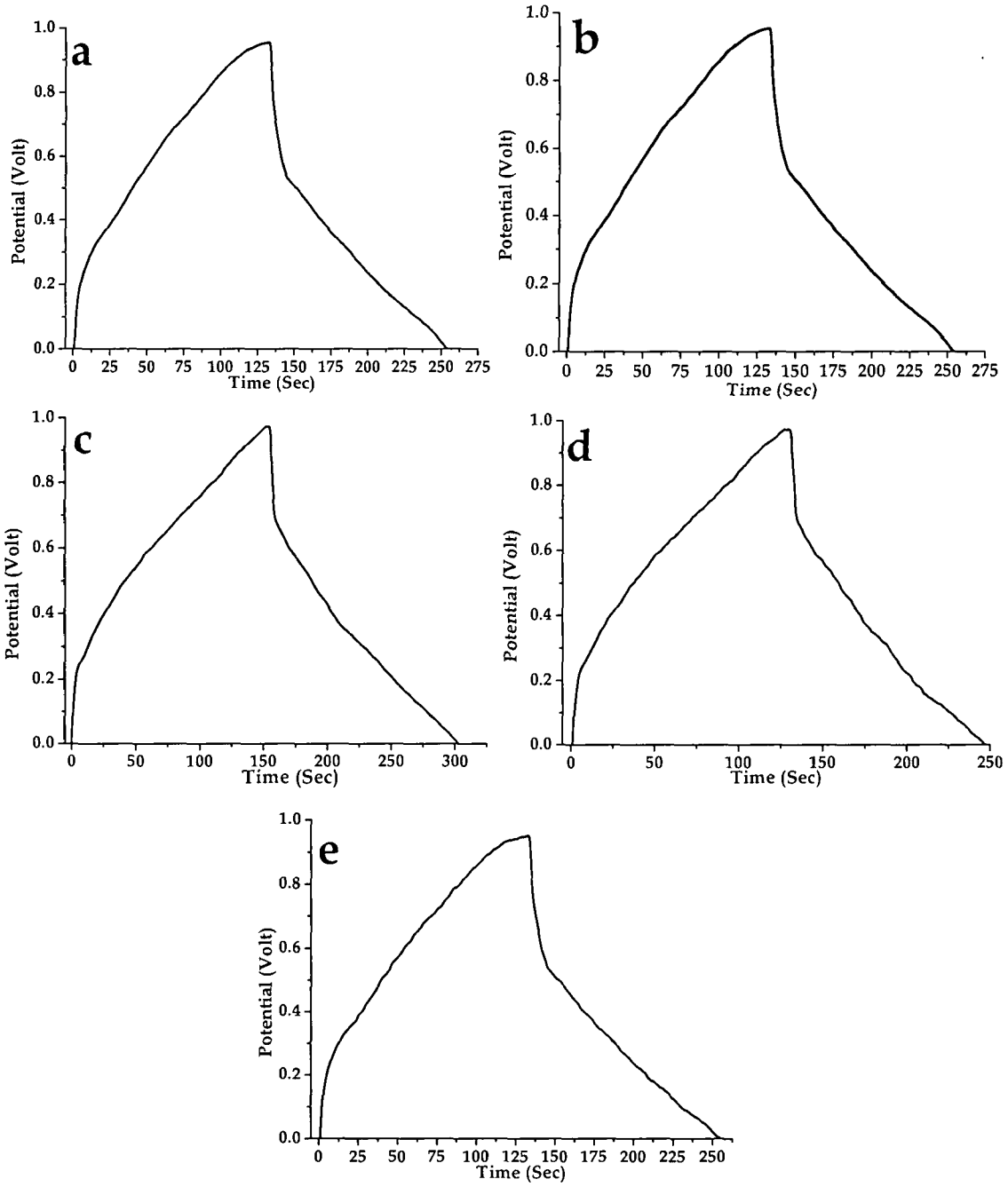


Figure 7.12: Charge-discharge plots of supercapacitors with polypyrrole electrodes doped with (a) $LiClO_4$, (b) $NaClO_4$, (c) $LiCF_3SO_3$, (d) $[CH_3(CH_2)_3]_4NBF_4$ and (e) $[CH_3(CH_2)_3]_4NPF_6$.

The characteristic values of capacitances, internal resistance, Coulombic efficiency and energy density are shown in Table 7.4 and are graphically represented in Fig. 7.13. The capacitance values calculated from the cyclic voltammograms are found to be slightly higher than those calculated from the

charge-discharge plot. This may be attributed to the fact that the total current in cyclic voltammogram constitutes a part from the electronic current passing through the electrolyte which due to alternation of polarity of potential in the potential sweep never gets stabilized, resulting in higher current value giving rise to higher capacitance value. However in the charge-discharge process, the polarity of the potential remains same and after a few charge-discharges cycles, the contribution from the electronic current through the electrolyte becomes zero.

Table 7.4: Characteristic properties of supercapacitors with polypyrrole electrodes doped with different dopants.

| Dopant | Capacitance (F/gm) | | Discharge Capacitance | | Internal Resistance | Coulombic efficiency | Energy Density |
|---|---|---|---|---|---|---|---|
| | Initial | Final | (mF/cm) | (F/gm) | $R_i$ (kΩ/cm) | η(%) | (Wh/kg) |
| $LiClO_4$ | 205.5 | 136.8 | 36.06 | 180.3 | 2.31 | 88.81 | 25.04 |
| $NaClO_4$ | 188.8 | 121.4 | 35.98 | 179.9 | 2.20 | 90.98 | 24.99 |
| $LiCF_3SO_3$ | 225.2 | 122.0 | 39.24 | 196.2 | 2.18 | 92.03 | 27.25 |
| $[CH_3(CH_2)_3]_4NBF_4$ | 204.7 | 126.9 | 36.64 | 183.2 | 2.15 | 88.46 | 25.44 |
| $[CH_3(CH_2)_3]_4NPF_6$ | 212.6 | 146.7 | 36.28 | 181.4 | 2.42 | 90.29 | 25.19 |

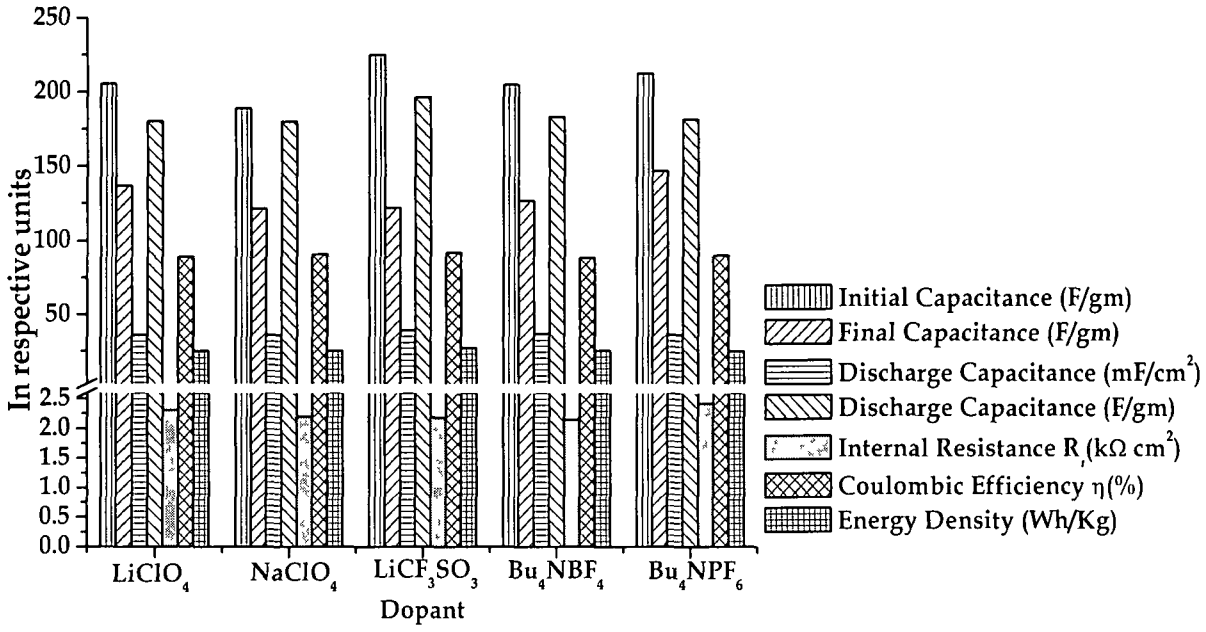


Figure 7.10: Characteristic properties of supercapacitors with polypyrrole electrodes doped with different dopants.

### *7.3.1 Supercapacitors with $LiClO_4$ doped polypyrrole irradiated electrodes:*

The lithium perchlorate ($LiClO_4$) salt p-doped polypyrrole conducting polymer electrodes irradiated with 160 MeV $Ni^{12+}$ ion beams at three different fluences of $5x10^{10}$, $5x10^{11}$ and $3x10^{12}$ ions/$cm^2$ are used as electrodes to fabricate type I supercapacitor. The cyclic voltammograms of the supercapacitors with $LiClO_4$ doped irradiated polypyrrole conducting polymer electrodes recorded at different scan rates are presented in Fig. 7.14. The cyclic voltammograms show good capacitive characteristics upto a scan rate of 100 mV/Sec. A small increase in the current towards higher potential observed in the cyclic voltammograms of the supercapacitors is due to the redox property of the conducting polymer electrodes. The capacitance values calculated from the cyclic voltammograms are presented in Table 7.5. The electrochemical stability of the supercapacitors with $LiClO_4$ doped irradiated polypyrrole electrode has been tested for 10,000 cycles of charging and discharging and the stability plots are presented in Fig. 7.15a. The initial decrease in the capacitance values observed in the stability plots may be attributed to the irreversible faradic reaction occurring at the electrode surface due to the presence of volatile surface groups e.g., $OH^-$, $CN^-$, $CH_3^+$ etc., which cause loss of charge at the electrode. After SHI irradiation, the decrease of initial capacitance is observed to be less as compared to the capacitance of unirradiated polymer electrode, which may be attributed to the reactive volatile surface groups, which are either stabilized or removed from the electrode surface upon SHI irradiation. Thus the electrochemical stability of the supercapacitors with irradiated electrode gets enhanced though the initial capacitance value is slightly less. The decrease of capacitance values after SHI irradiation may be attributed to possible surface modification due to cross linking induced by huge electronic energy loss mechanism and decrease in the concentration of the surface groups on the electrode surface, which decreases with the increase of fluence of SHI irradiation. The charge-discharge plots of the supercapacitors recorded galvanostatically at 100 μA are shown in Fig. 7.15b. The discharge capacitance values of the supercapacitors calculated from the

charge-discharge plots using relation 7 2 are presented in Table 7 5 The characteristic values of the supercapacitors with unirradiated and irradiated

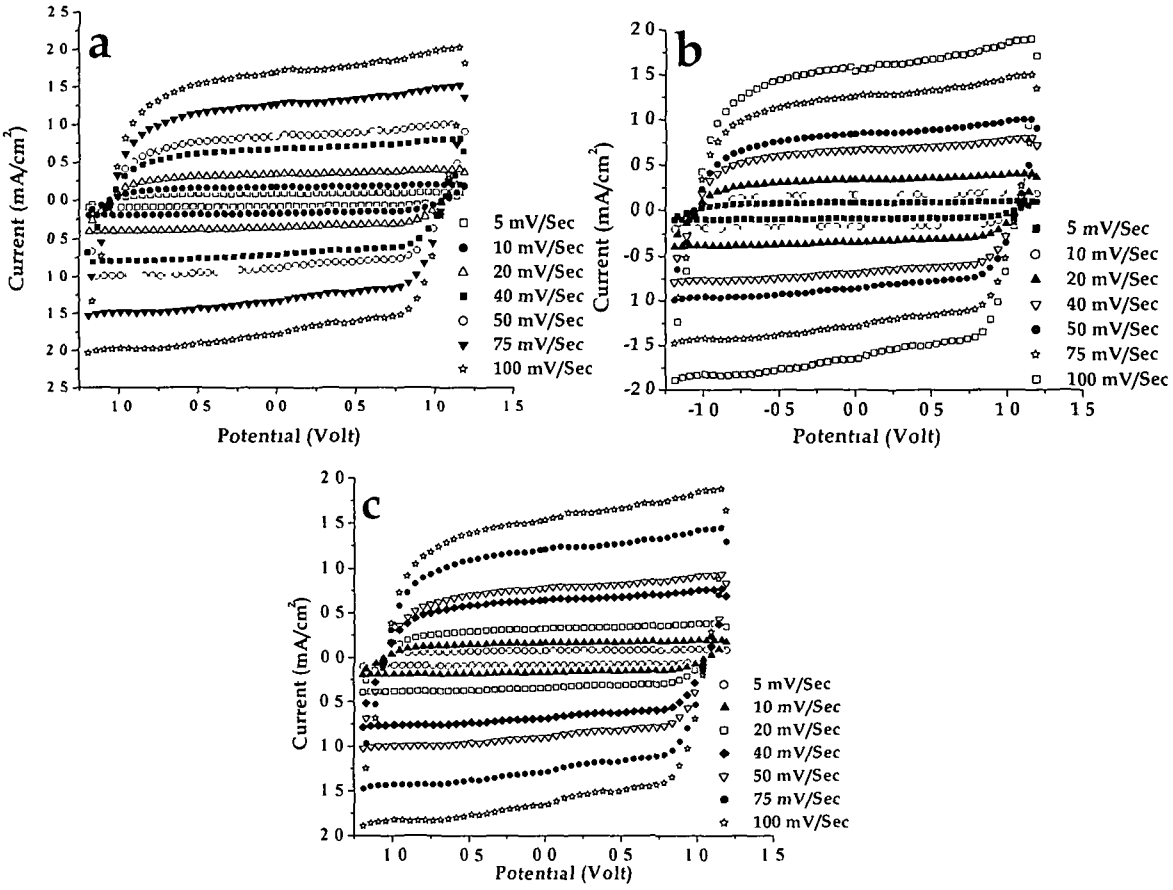


Figure 7 14 Cyclic voltammograms of supercapacitors with $LiClO_4$ doped polypyrrole irradiated electrodes with fluence of (a) $5X10^{10}$, (b) $5X10^{11}$ and (c) $3X10^{12}$ ions/cm²

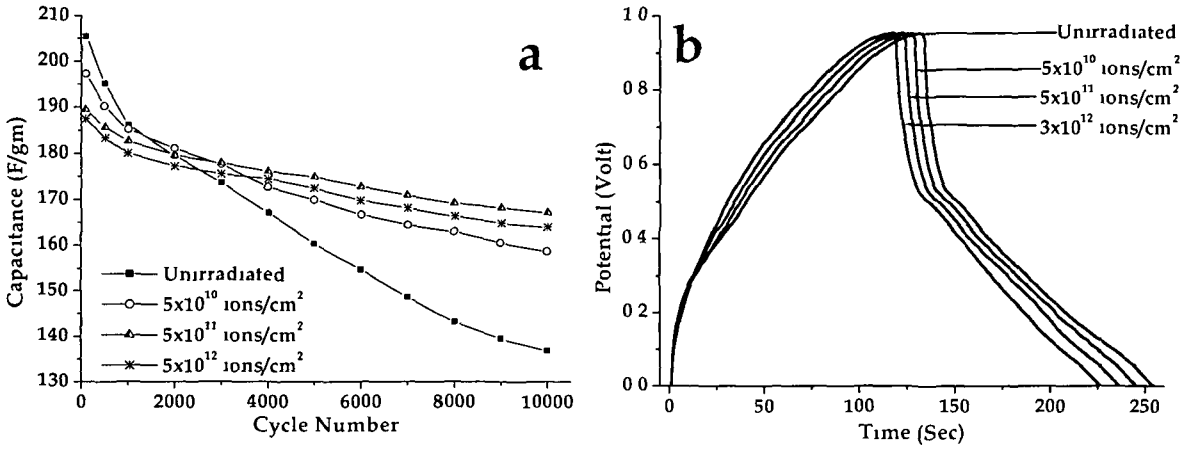


Figure 7 15 (a) Stability and (b) charge-discharge plots of supercapacitors with $LiClO_4$ doped polypyrrole electrodes before and after irradiation at different fluences

Table 7.5: Characteristic properties of supercapacitors with $LiClO_4$ doped polypyrrole irradiated electrodes.

| Fluence (Ions/cm²) | Capacitance (F/gm) | | Discharge Capacitance | | Internal Resistance | Coulombic efficiency | Energy Density |
|---|---|---|---|---|---|---|---|
| | Initial | Final | (mF/cm²) | (F/gm) | $R_i$ (kΩ cm²) | η(%) | (Wh/kg) |
| 0 | 205.5 | 136.8 | 36.06 | 180.3 | 2.31 | 88.81 | 25.04 |
| $5x10^{10}$ | 197.1 | 156.5 | 35.61 | 178.05 | 2.22 | 91.23 | 24.73 |
| $5x10^{11}$ | 189.2 | 167.2 | 34.82 | 174.10 | 1.92 | 92.14 | 24.18 |
| $3x10^{12}$ | 187.3 | 162.2 | 34.12 | 170.60 | 1.74 | 94.87 | 23.69 |

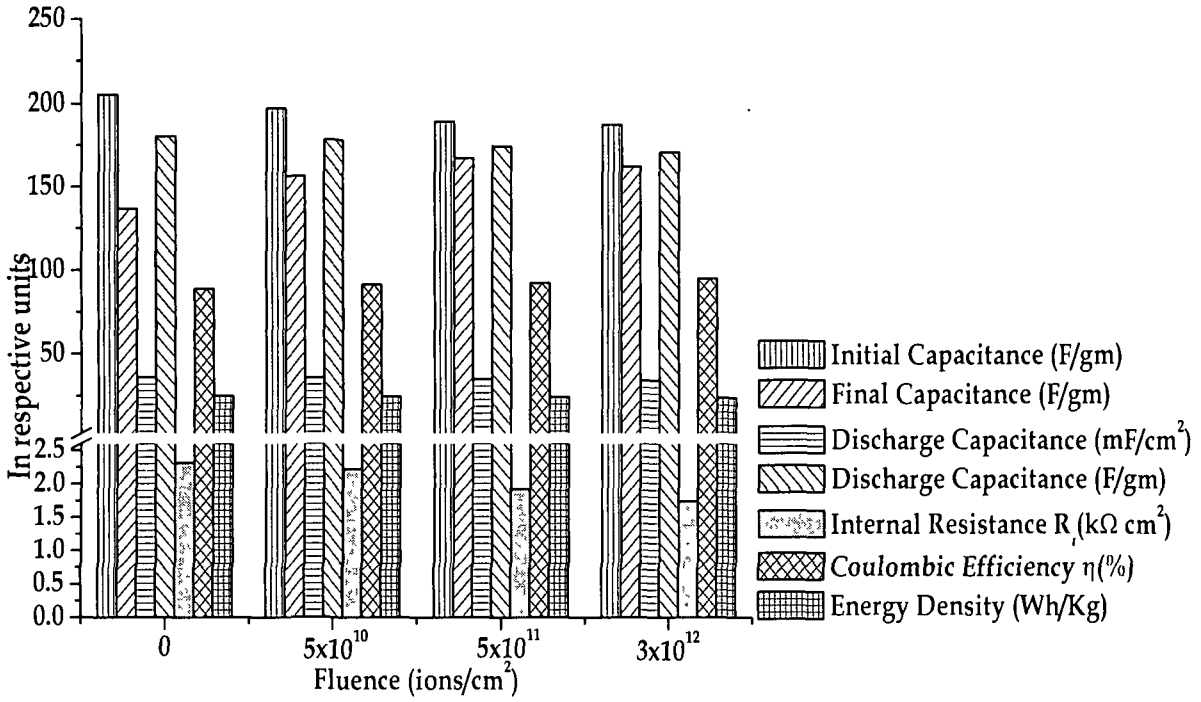


Figure 7.16: Characteristic properties of supercapacitors with $LiClO_4$ doped polypyrrole irradiated electrodes.

$LiClO_4$ doped polypyrrole conducting polymer electrodes are presented graphically in Fig. 7.16. The values of discharge capacitance of the supercapacitors from charge-discharge plots are found to be slightly less than that of calculated from the cyclic voltammograms, which may be due to the fact that the current in cyclic voltammograms constitutes in part due to the electronic current through the electrolyte due to continuous sweep of polarity of potential. The internal resistance of the supercapacitors with $LiClO_4$ doped polypyrrole electrode is small, of the order of 1-2 kΩ cm².

### 7.3.2 *Supercapacitors with $LiCF_3SO_3$ doped polypyrrole irradiated electrodes:*

The cyclic voltammograms of supercapacitors with $LiCF_3SO_3$ doped polypyrrole electrodes irradiated with 160 MeV $Ni^{12+}$ ions with three different fluences of $5x10^{10}$, $5x10^{11}$ and $3x10^{12}$ ions/cm$^2$, recorded at different scan rates are shown in Fig. 7.17. The cyclic voltammograms show ideal capacitive behaviour of the supercapacitors at lower scan rates but deviate from the ideal rectangular shape and an increase in current towards higher potential at higher scan rate is observed. This may be due to the redox property of the conducting polymer electrodes, which remains unchanged upon SHI irradiation. The capacitance values of the supercapacitors have been calculated from the cyclic voltammograms using relation 7.1 and are presented in Table 7.6. The electrochemical stability of the supercapacitors has been tested for 10,000 cycles and the stability plots are presented in Fig. 7.18a. The initial decrease of capacitance values for the supercapacitors occurs due to the faradic reactions taking place on the surface of the electrode due to the presence of volatile surface groups e.g., $OH^-$,$CN^-$, $CH_3^+$ etc., causing loss of charge at the electrode. The SHI irradiation causes stabilization or removal of the reactive surface groups, which results in less initial decrease of capacitance and the decrease in capacitance becomes lesser with the increase in fluence of SHI irradiation. The charge-discharge plots of the supercapacitors with unirradiated as well as irradiated electrodes are recorded galvanostatically at 100 μA and are presented in Fig. 7.18b. The characteristic values of the supercapacitor with $LiCF_3SO_3$ doped irradiated polypyrrole conducting polymer electrodes are presented in Table 7.6 and are graphically shown in Fig. 7.19. The internal resistance of the supercapacitors with $LiCF_3SO_3$ doped irradiated polypyrrole electrodes are found to be in the range of 2kΩ cm$^2$ and a small decrease in the internal resistance is observed upon SHI irradiation, which may be due to the increase in conductivity of the polypyrrole conducting polymer films after irradiation.

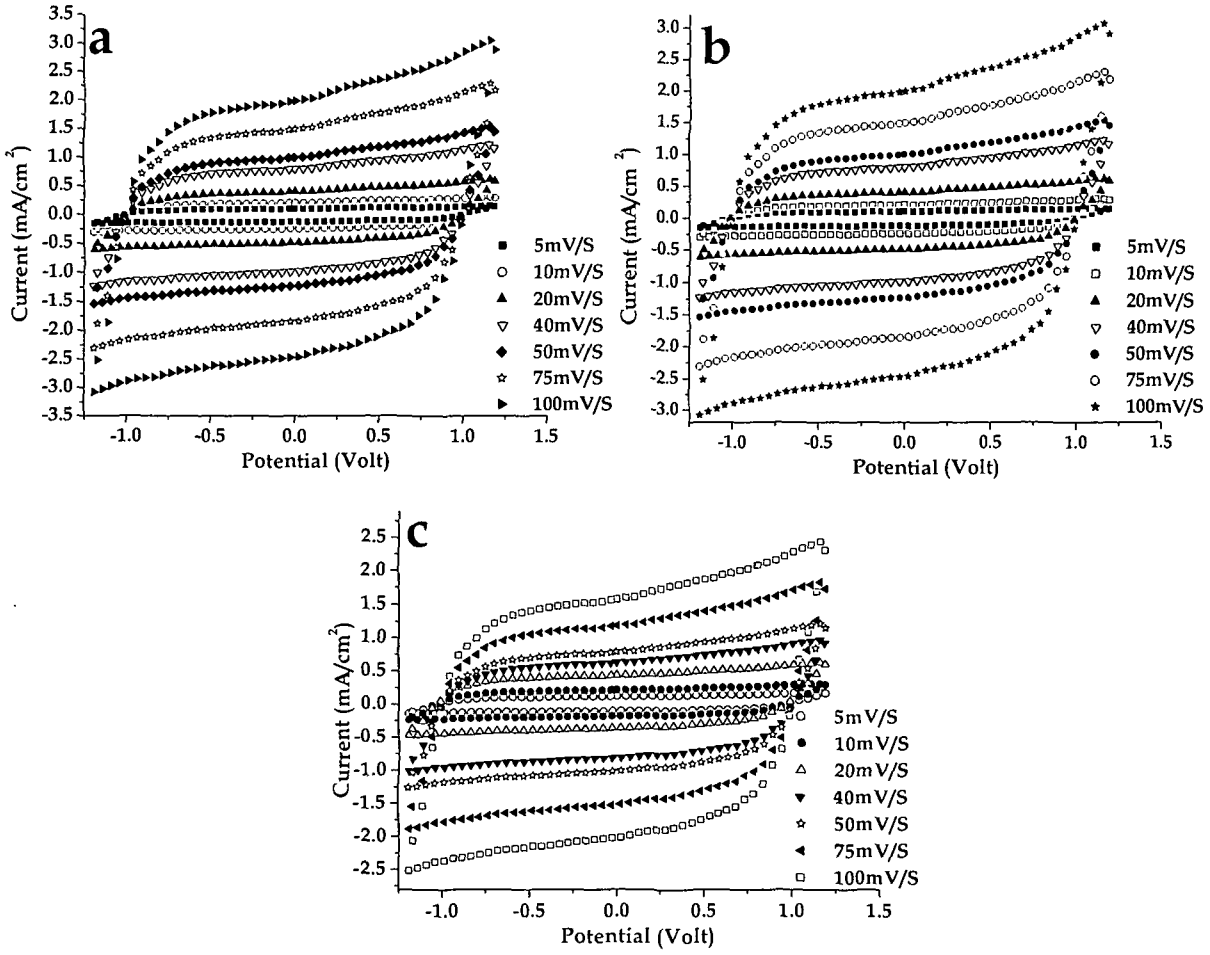


Figure 7.17: Cyclic voltammograms of supercapacitors with $LiCF_3SO_3$ doped polypyrrole irradiated electrodes with fluence (a) $5X10^{10}$, (b) $5X10^{11}$ and (c) $3X10^{12}$ ions/$cm^2$.

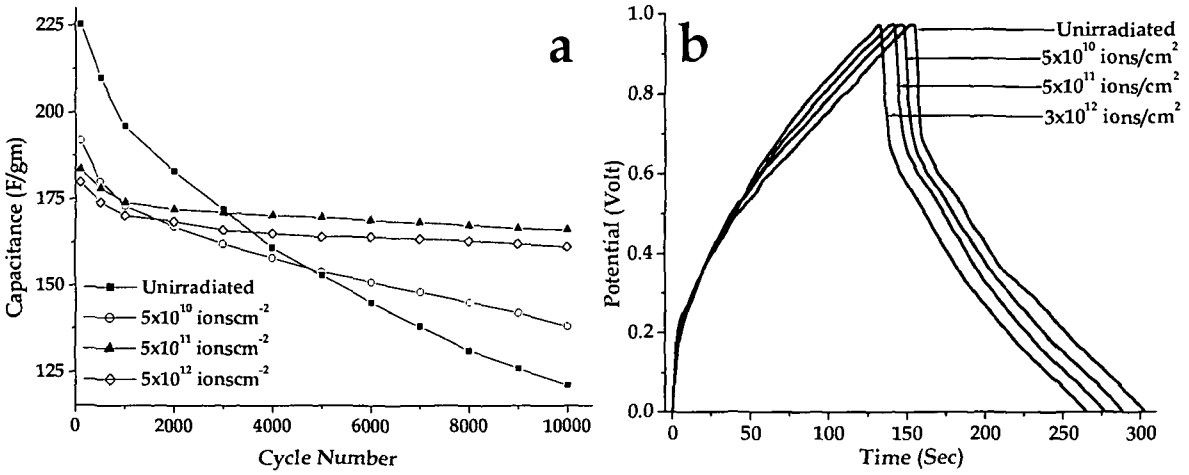


Figure 7.18: (a) Stability and (b) charge-discharge plots of supercapacitors with $LiCF_3SO_3$ doped polypyrrole electrodes before and after irradiation.

Table 7.6: Characteristic properties of supercapacitors with irradiated $LiCF_3SO_3$ doped polypyrrole electrodes.

| Fluence (Ions/cm²) | Capacitance (F/gm) | | Discharge Capacitance | | Internal Resistance | Coulombic efficiency | Energy Density |
|---|---|---|---|---|---|---|---|
| | Initial | Final | (mF/cm²) | (F/gm) | $R_i$ (kΩ cm²) | η(%) | (Wh/kg) |
| 0 | 225.2 | 122.0 | 39.24 | 196.2 | 2.18 | 92.03 | 27.25 |
| $5x10^{10}$ | 191.9 | 138.2 | 38.54 | 192.7 | 2.16 | 95.23 | 26.67 |
| $5x10^{11}$ | 183.5 | 166.1 | 36.19 | 180.95 | 2.11 | 95.74 | 25.13 |
| $3x10^{12}$ | 179.8 | 161.7 | 34.89 | 174.45 | 2.07 | 98.24 | 24.23 |

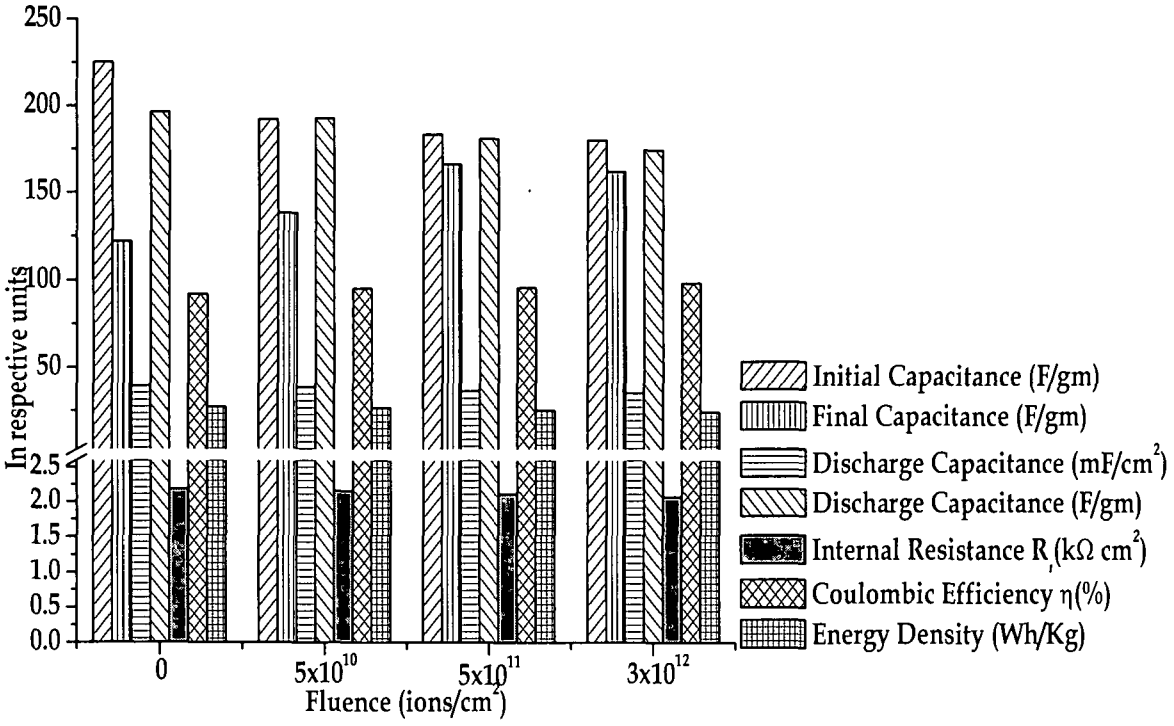


Figure 7.19: Characteristics of supercapacitors with irradiated $LiCF_3SO_3$ doped polypyrrole electrodes.

### 7.3.3 *Supercapacitors with $[CH_3(CH_2)_3]_4NBF_4$ doped polypyrrole irradiated electrodes:*

The cyclic voltammograms of the supercapacitors with 160 MeV $Ni^{12+}$ ion irradiated $[CH_3(CH_2)_3]_4NBF_4$ doped polypyrrole electrodes are shown in Fig. 7.20. The cyclic voltammograms of the supercapacitors with 160 MeV $Ni^{12+}$ ion

irradiated polypyrrole conducting polymer electrodes show good capacitive behavior upto a scan rate of 75 mV/Sec. At higher scan rates the cyclic voltammograms slightly deviate from the ideal rectangular shape. The increase in current towards higher potential at higher scan rates observed in the cyclic voltammograms occurs due to the redox nature of the polypyrrole electrodes, which remains unchanged upon SHI irradiation as observed in the cyclic voltammetry of the polypyrrole films after irradiation (Chapter 5, section 5.5.1).

The stability plots of the supercapacitors with SHI irradiated polypyrrole electrodes are shown in Fig. 7.21a. The electrochemical stability plots of the supercapacitors with unirradiated as well as irradiated polypyrrole electrodes show initial sharp decrease in capacitance values, which may be attributed to the irreversible Faradic reaction of the highly reactive surface groups like $CN^-$, $CH_3^+$ etc. This initial decrease of capacitance of the supercapacitors with irradiated polypyrrole electrodes is less as compared to the capacitance of the supercapacitor with unirradiated electrode. This may be due to the fact that the loosely bound volatile surface groups are stabilized or removed upon SHI irradiation from the polymer electrode and hence the decrease of capacitance in initial charge-discharge cycles becomes lesser with the increase in fluence. The charge-discharge plots of the supercapacitors with irradiated electrodes are shown in Fig. 7.21b. The characteristic values of supercapacitors with 160 MeV $Ni^{12+}$ ion irradiated $[CH_3(CH_2)_3]_4NBF_4$ doped polypyrrole electrodes calculated using relations 7.1-7.7.4 are presented in Table 7.7. Decrease in the total charge-discharge time of the supercapacitors with irradiated electrodes is observed in the charge-discharge plots with small increase in coulombic efficiency. The decrease of charge-discharge time may be attributed to the increase in conductivity of the polymer electrodes after SHI irradiation, which supports faster electron transport in the electrodes. The graphical representation of the characteristic values of the supercapacitor with 160MeV $Ni^{12+}$ ion irradiated $[CH_3(CH_2)_3]_4NBF_4$ doped polypyrrole electrodes are shown in Fig. 7.22.

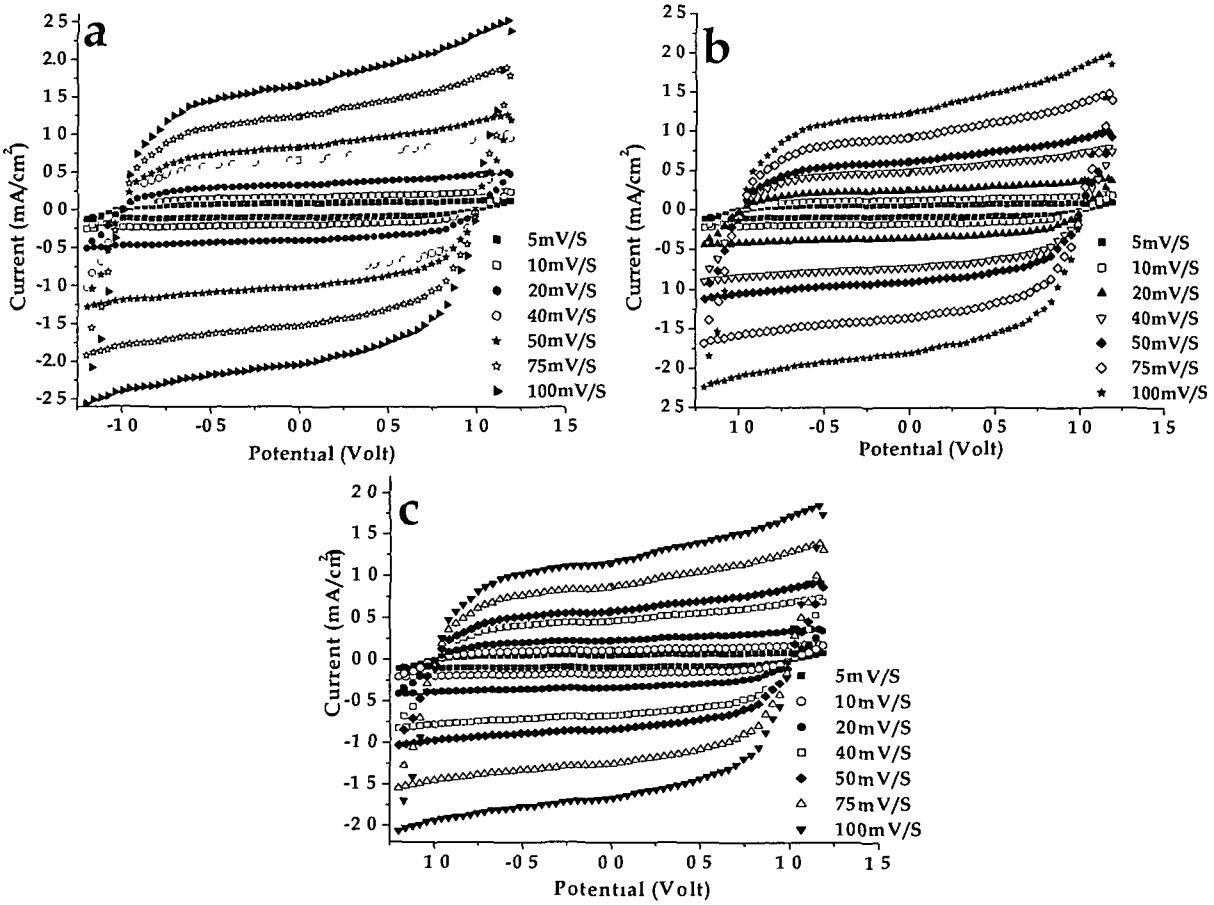


Figure 7 20 Cyclic voltammograms of supercapacitors with $[CH_3(CH_2)_3]_4NBF_4$ doped polypyrrole irradiated electrodes with fluence (a) $5X10^{10}$, (b) $5X10^{11}$ and (c) $3X10^{12}$ ions/cm²

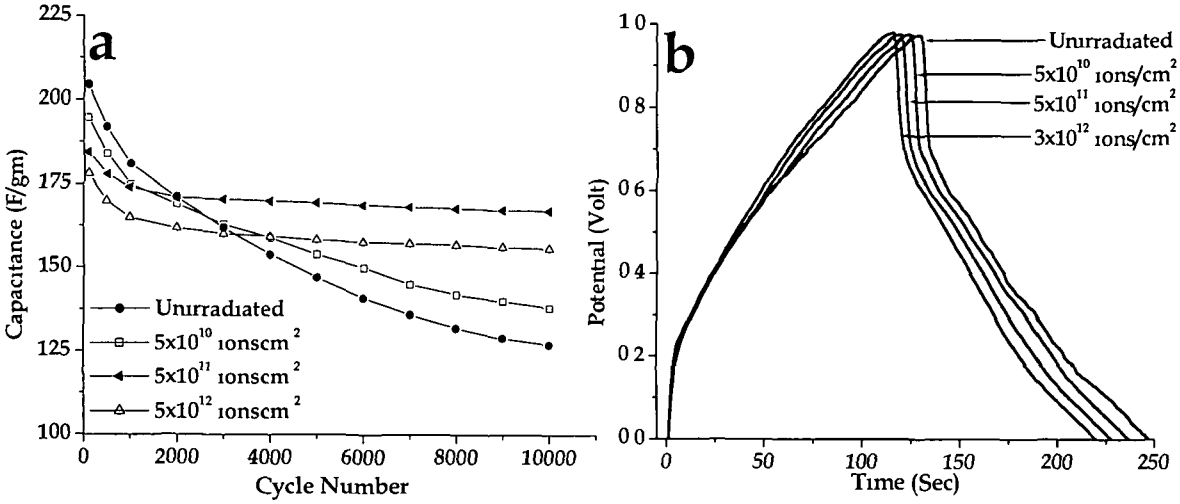


Figure 7 21 (a) Stability and (b) charge-discharge plots of supercapacitors with $[CH_3(CH_2)_3]_4NBF_4$ doped polypyrrole electrodes before and after

Table 7.7: Characteristic properties of supercapacitors with $[CH_3(CH_2)_3]_4NBF_4$ doped polypyrrole irradiated electrodes.

| Fluence (Ions/cm²) | Capacitance (F/gm) Initial | Final | Discharge Capacitance (mF/cm²) | (F/gm) | Internal Resistance $R_i$ (kΩ cm²) | Coulombic efficiency η(%) | Energy Density (Wh/kg) |
|---|---|---|---|---|---|---|---|
| 0 | 204.7 | 126.9 | 36.64 | 183.2 | 2.15 | 88.46 | 25.44 |
| $5x10^{10}$ | 194.81 | 138.5 | 35.82 | 179.1 | 2.07 | 88.80 | 24.88 |
| $5x10^{11}$ | 185.4 | 167.3 | 35.08 | 175.4 | 1.98 | 89.17 | 24.36 |
| $3x10^{12}$ | 178.2 | 155.7 | 34.49 | 172.5 | 1.95 | 89.57 | 23.96 |

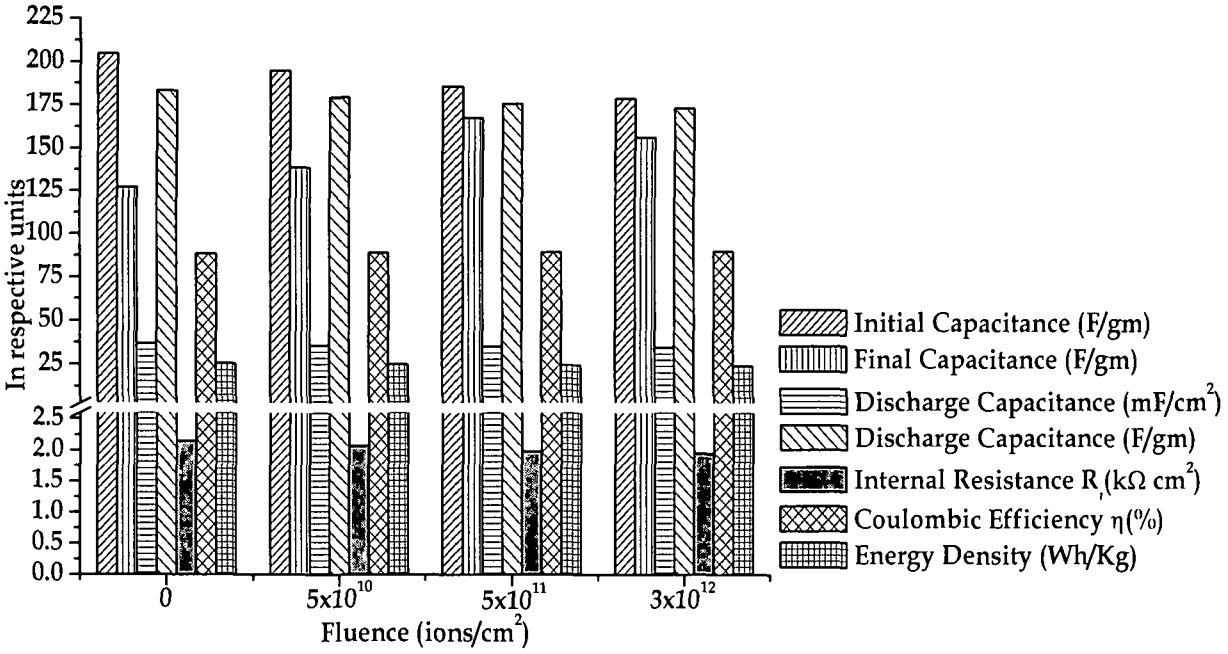


Figure 7.22: Characteristic properties of supercapacitors with $[CH_3(CH_2)_3]_4NBF_4$ doped polypyrrole irradiated electrodes.

### *7.3.4 Supercapacitors with $[CH_3(CH_2)_3]_4NPF_6$ doped polypyrrole irradiated electrodes:*

The cyclic voltammograms of the supercapacitor with $[CH_3(CH_2)_3]_4NPF_6$ doped 160 MeV $Ni^{12+}$ ion irradiated polypyrrole electrodes recorded at different scan rates are shown in Fig. 7.23. The cyclic voltammograms of the supercapacitors show ideal capacitive behaviour at lower scan rates but at higher scan rates the current increased towards higher potential and cyclic voltammograms deviated from the ideal rectangular shape. This is attributed to the redox property of the polypyrrole electrodes which causes the increase of

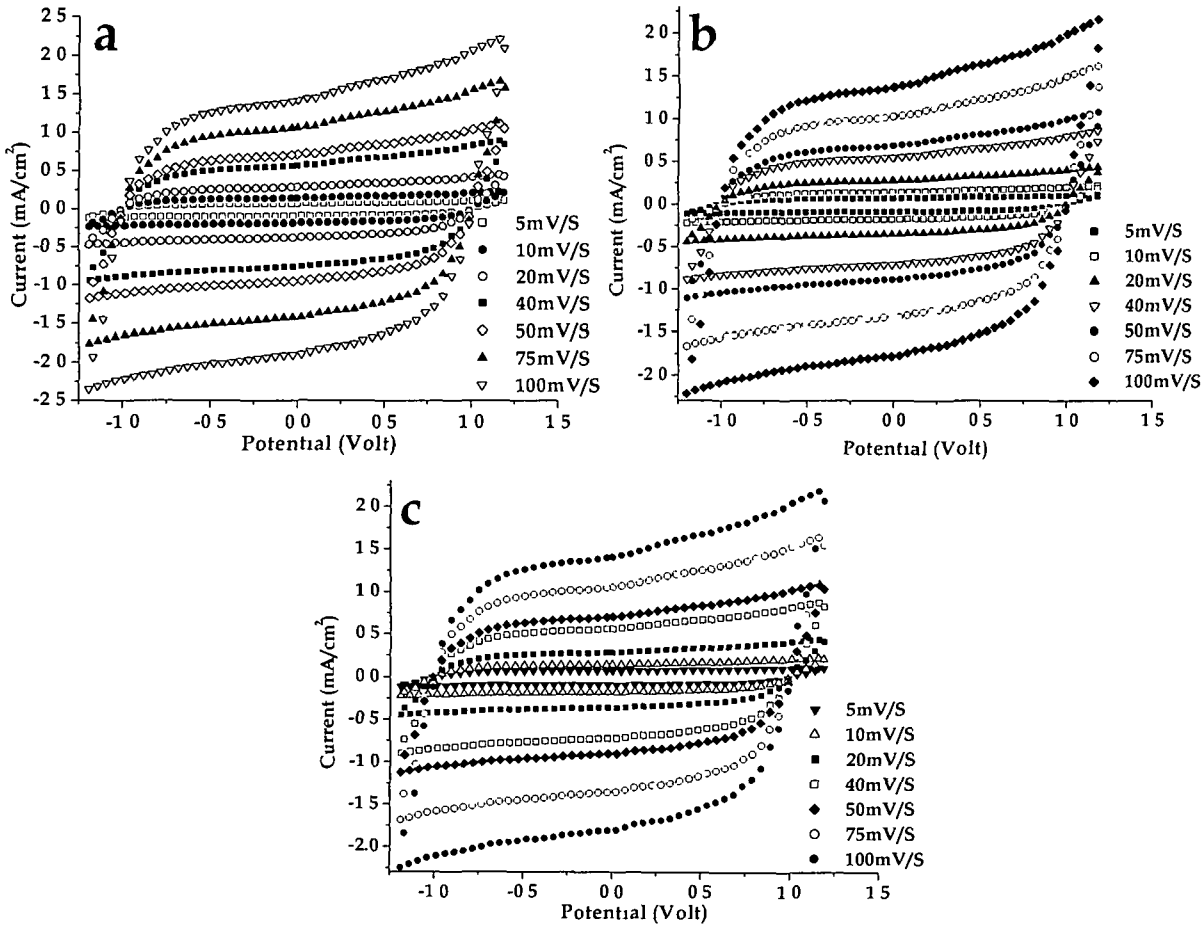


Figure 7.23 Cyclic voltammograms of supercapacitors with $[CH_3(CH_2)_3]_4NPF_6$ doped polypyrrole irradiated electrodes with fluence (a) $5X10^{10}$, (b) $5X10^{11}$ and (c) $3X10^{12}$ ions/cm$^2$

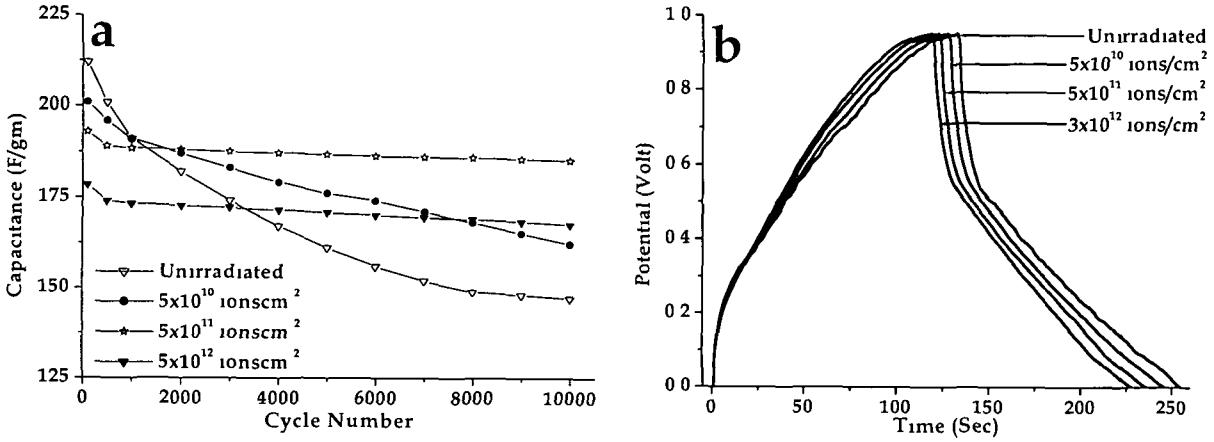


Figure 7 24 (a) Stability and (b) charge-discharge plots of $[CH_3(CH_2)_3]_4NPF_6$ doped polypyrrole electrodes before and after irradiation

Table 7.8: Characteristic properties of supercapacitors with $[CH_3(CH_2)_3]_4NPF_6$ doped polypyrrole irradiated electrodes.

| Fluence (Ions/cm²) | Capacitance (F/gm) | | Discharge Capacitance | | Internal Resistance $R_i$ (kΩ cm²) | Coulombic efficiency η(%) | Energy Density (Wh/kg) |
|---|---|---|---|---|---|---|---|
| | Initial | Final | (mF/cm²) | (F/gm) | | | |
| 0 | 212.6 | 146.7 | 36.28 | 181.4 | 2.42 | 90.29 | 25.19 |
| $5x10^{10}$ | 201.5 | 162.3 | 35.87 | 179.4 | 2.40 | 91.41 | 24.92 |
| $5x10^{11}$ | 193.2 | 185.8 | 34.98 | 174.9 | 2.38 | 90.24 | 24.29 |
| $3x10^{12}$ | 178.7 | 167.4 | 34.12 | 170.6 | 2.36 | 89.33 | 23.69 |

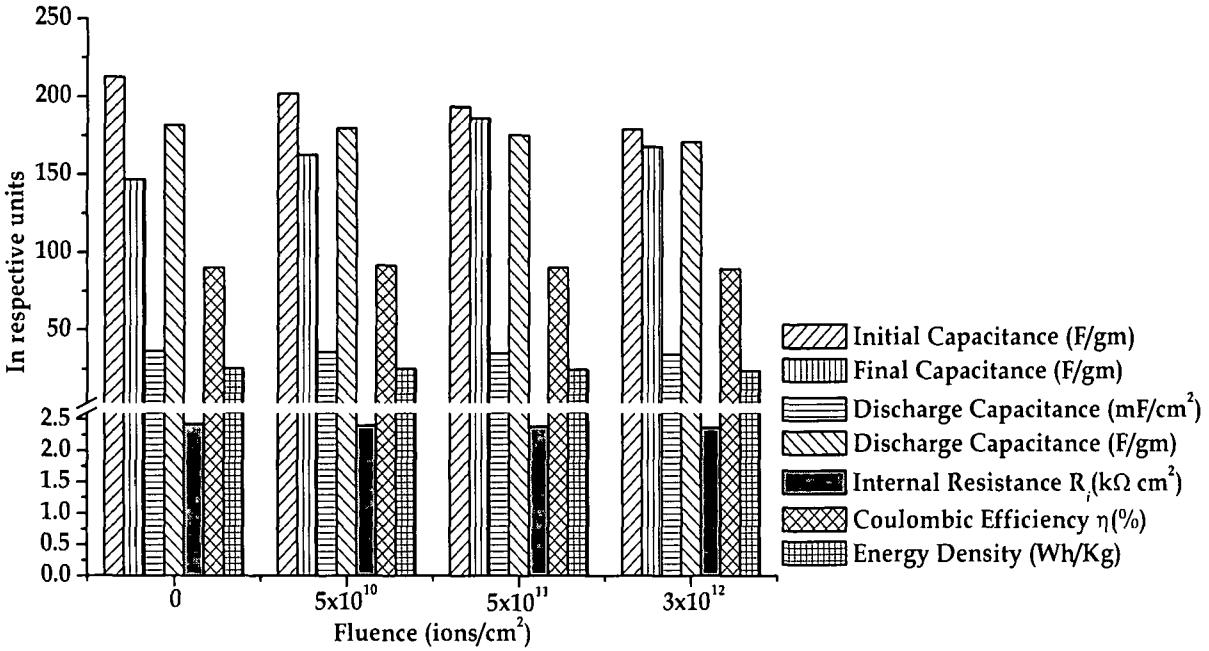


Figure 7.25: Characteristics of supercapacitors with $[CH_3(CH_2)_3]_4NPF_6$ doped polypyrrole irradiated electrodes.

current towards higher potential due to the oxidation of the conducting polymers. The characteristic values of the supercapacitors with $[CH_3(CH_2)_3]_4NPF_6$ doped polypyrrole conducting polymer electrodes are presented in Table 7.8. The electrochemical stability of the supercapacitors has been tested for 10,000 charge-discharge cycles, the capacitance values have been calculated after every 1000 cycles and are presented in the stability plots in Fig. 7.24 a. The decrease of capacitance values is found to be similar with the results

obtained for $LiClO_4$, $LiCF_3SO_3$ and $[CH_3(CH_2)_3]_4NBF_4$ doped polypyrrole electrodes. The charge-discharge plots of the supercapacitors with $[CH_3(CH_2)_3]_4NPF_6$ doped polypyrrole electrodes recorded galvanostatically at 100 μA are presented in Fig. 7.24b. The internal resistance of the supercapacitors are found to be small (~2 kΩ $cm^2$) and a small decrease is observed with the increase in fluence of SHI irradiation. The characteristic values of properties are presented graphically in Fig. 7.25.

**7.4 Type II supercapacitors with polyaniline and polypyrrole electrodes:**

Type II supercapacitors have been fabricated with unirradiated and SHI irradiated HCl doped polyaniline and $LiClO_4$ doped polypyrrole electrodes. The cyclic voltammograms of the type II supercapacitor recorded at different scan rates are presented in Fig. 7.26. The cyclic voltammograms show ideal capacitive shape at lower scan rates but at higher scan rates deviate from the ideal rectangular shape due to the redox property of the electrode materials.

Fig. 7.27a shows the stability plots of the type II supercapacitors with unirradiated and irradiated polyaniline and polypyrrole p-doped electrodes. The electrochemical stability test of the supercapacitors has been carried out for 10,000 cycles and the capacitance values have been calculated after every 1000 cycles. The stability plots of the supercapacitors show a sharp initial decrease of capacitance values and the decrease is less with irradiated electrodes. The decrease of initial capacitance value may be attributed to the irreversible faradic reaction due to the presence of highly reactive surface groups e.g., $OH^-$, $CN^-$, $CH_3^+$ etc., which get attached to the electrode surface from the solvent and atmosphere causing loss of charge. Upon SHI irradiation the loosely bound volatile surface groups are stabilized or removed from the electrode surface leading to markedly less decrease of capacitance during initial charge-discharge cycles. Upon SHI irradiation, possible surface modifications due to cross-linking induced by huge electronic energy loss mechanism and decrease in the concentration of the surface groups on the electrode surface, which decreases

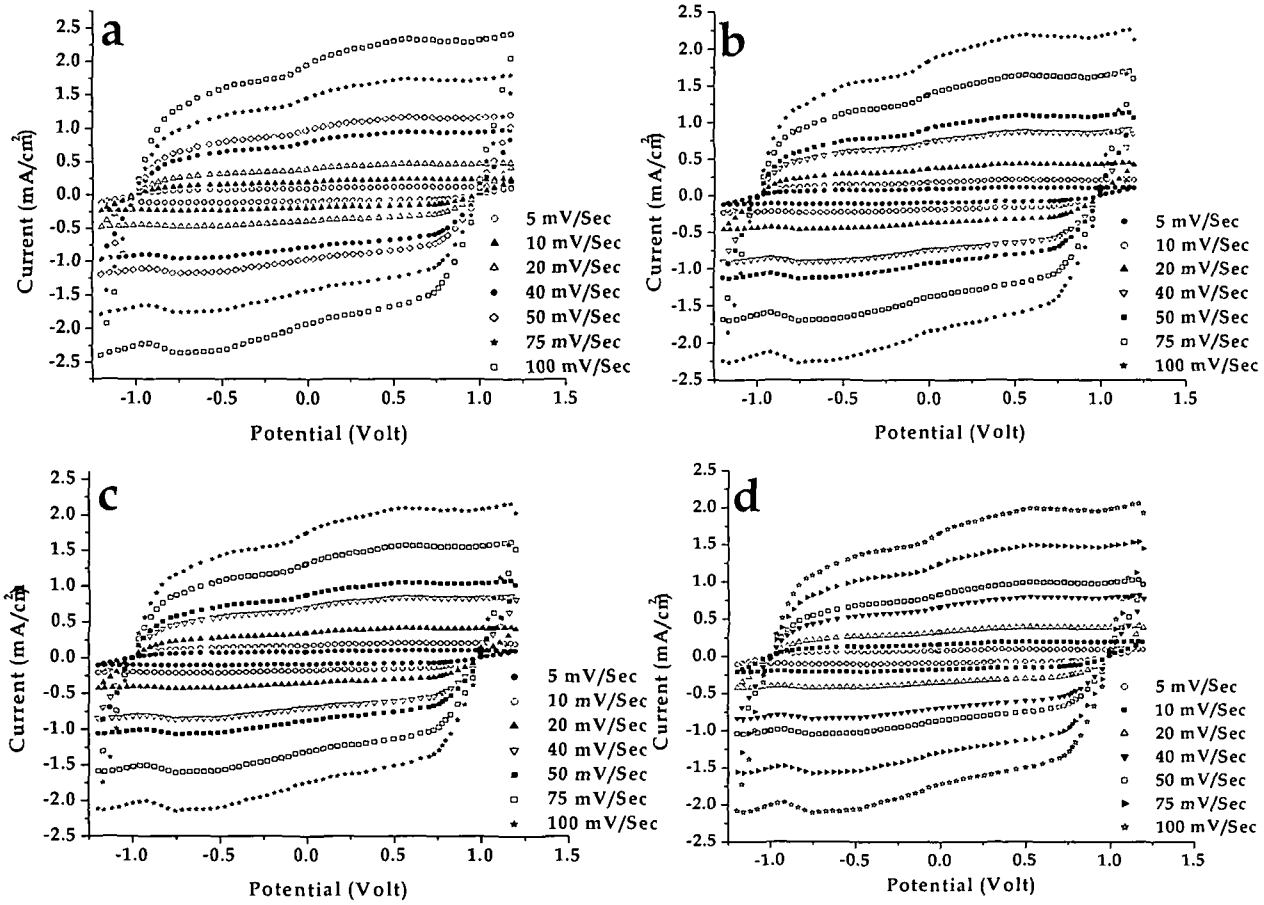


*Figure 7.26: Cyclic voltammograms of type II supercapacitors with HCl doped polyaniline and $LiClO_4$ doped polypyrrole (a) unirradiated and irradiated electrodes with fluences (b) $5X10^{10}$, (c) $5X10^{11}$ and (d) $3X10^{12}$ ions/cm².*

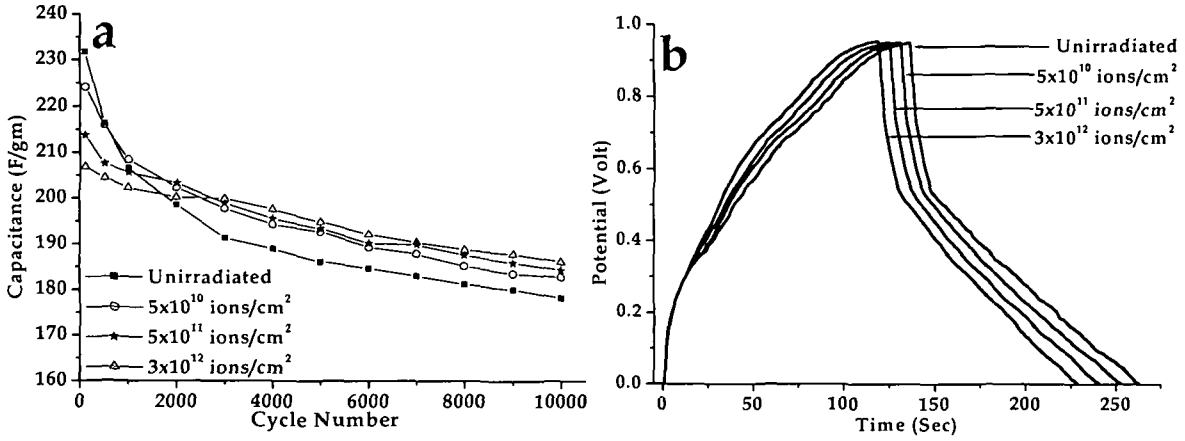


Figure 7.27: (a) Stability and (b) charge-discharge plots of type II supercapacitors with HCl doped polyaniline and $LiClO_4$ doped polypyrrole electrodes before and after SHI irradiation with different fluence.

Table 7.9: Characteristic properties of type II supercapacitors with HCl doped polyaniline and $LiClO_4$ doped polypyrrole electrodes before and after SHI irradiation with different fluences.

| Fluence (ions/cm²) | Capacitance (F/gm) | | Discharge Capacitance | | Internal Resistance | Coulombic efficiency | Energy Density |
|---|---|---|---|---|---|---|---|
| | Initial | Final | (mF/cm²) | (F/gm) | Ri (kΩ cm²) | η(%) | (Wh/kg) |
| 0 | 231.75 | 178.25 | 42.14 | 210.7 | 2.31 | 91.97 | 42.14 |
| $5x10^{10}$ | 224.17 | 182.72 | 40.72 | 203.6 | 2.31 | 91.60 | 40.72 |
| $5x10^{11}$ | 213.72 | 184.23 | 39.68 | 198.4 | 2.32 | 91.20 | 39.68 |
| $3x10^{12}$ | 206.88 | 186.04 | 38.58 | 192.9 | 2.32 | 90.76 | 38.58 |

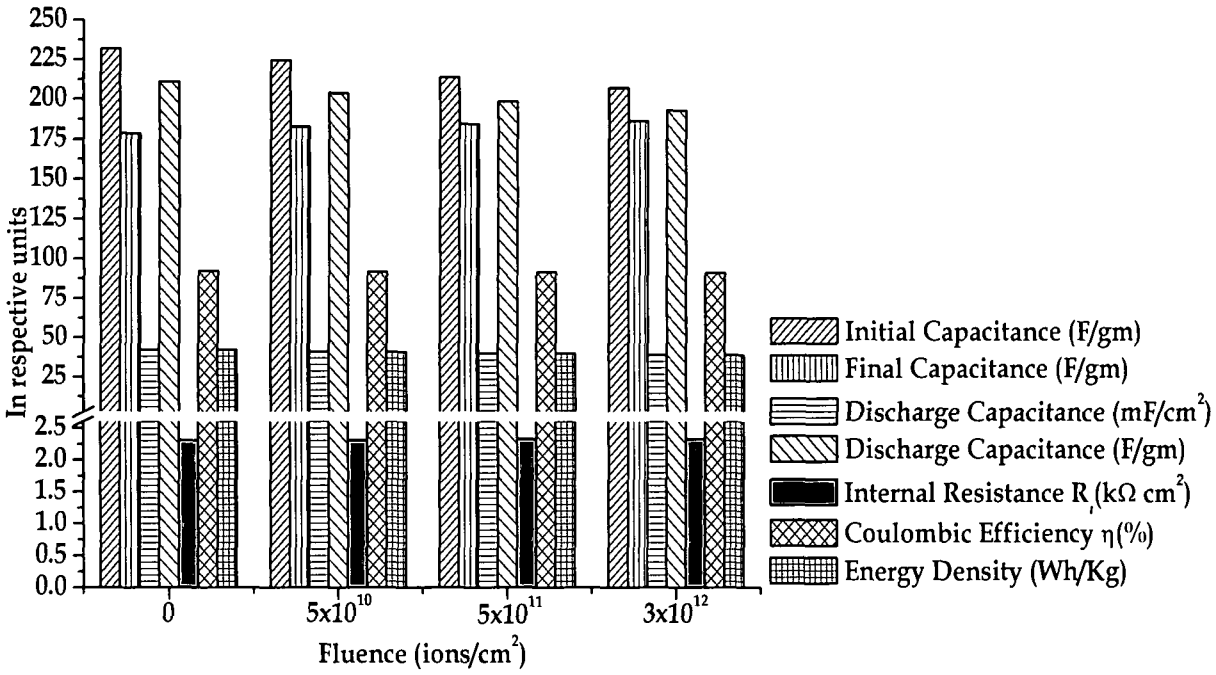


Figure 7.28: Characteristics of type II supercapacitors with HCl doped polyaniline and $LiClO_4$ doped polypyrrole electrodes before and after SHI irradiation with different fluences.

with the increase of fluence, result in less decrease in the capacitance values during initial charge-discharge cycles.

The charge-discharge plots of the type II supercapacitors with polyaniline and polypyrrole p-doped electrodes carried out galvanostatically at 100 μA using a battery testing unit are presented in Fig. 7.27b. The discharge

capacitance of the supercapacitor, capacitance of individual electrode, internal resistance, Coulombic efficiency calculated from the charge-discharge plot are presented in Table 7.9 and graphically shown in Fig. 7.28 for better comparison. The decrease of total charge-discharge time of the supercapacitors with irradiated electrodes is observed in the charge-discharge study, which may be attributed to the increase in conductivity of the polymer films after irradiation.

**7.5 Type I supercapacitors with poly(3-methylthiophene) p-doped electrodes:**

Type I supercapacitors with p-doped poly(3-methylthiophene) electrodes doped $LiClO_4$, $LiCF_3SO_3$, $[CH_3(CH_2)_3]_4NBF_4$ and $[CH_3(CH_2)_3]_4NPF_6$ dopants have been fabricated and characterized. The cyclic voltammograms of the supercapacitors recorded at different scan rates are presented in Fig. 7.29. The cyclic voltammograms show good capacitive behaviour of the fabricated supercapacitor at lower scan rates, but at scan rates above 75 mV/sec the shape of the cyclic voltammograms deviate from rectangular shape and current shows an increase towards higher potential. This may be attributed to the redox property of the poly(3-methylthiophene) electrodes. The capacitance values of the supercapacitors have been calculated from the cyclic voltammograms using the relation eqn. 7.1 and are presented in Table 7.10. Galvanostatic charge-discharge studies of the type I supercapacitor with poly(3-methylthiophene) electrodes carried out at constant current of 100 μA are shown in Fig. 7.30. The charge-discharge study shows good capacitive charge-discharge behaviour of the supercapacitors with very small internal resistance (~ 1.5 kΩ $cm^2$). The discharge capacitance of the individual capacitor cell from the charge-discharge plots, the capacitance of the single electrode from the cyclic voltammograms have been calculated and are presented in Table 7.10. The graphical presentation of the characteristic values of different properties of the type I supercapacitors with poly(3-methylthiophene) p-doped electrodes are shown in Fig. 7.31 for comparison of the values. The capacitance values obtained from the cyclic voltammograms are slightly higher than those calculated from the charge-

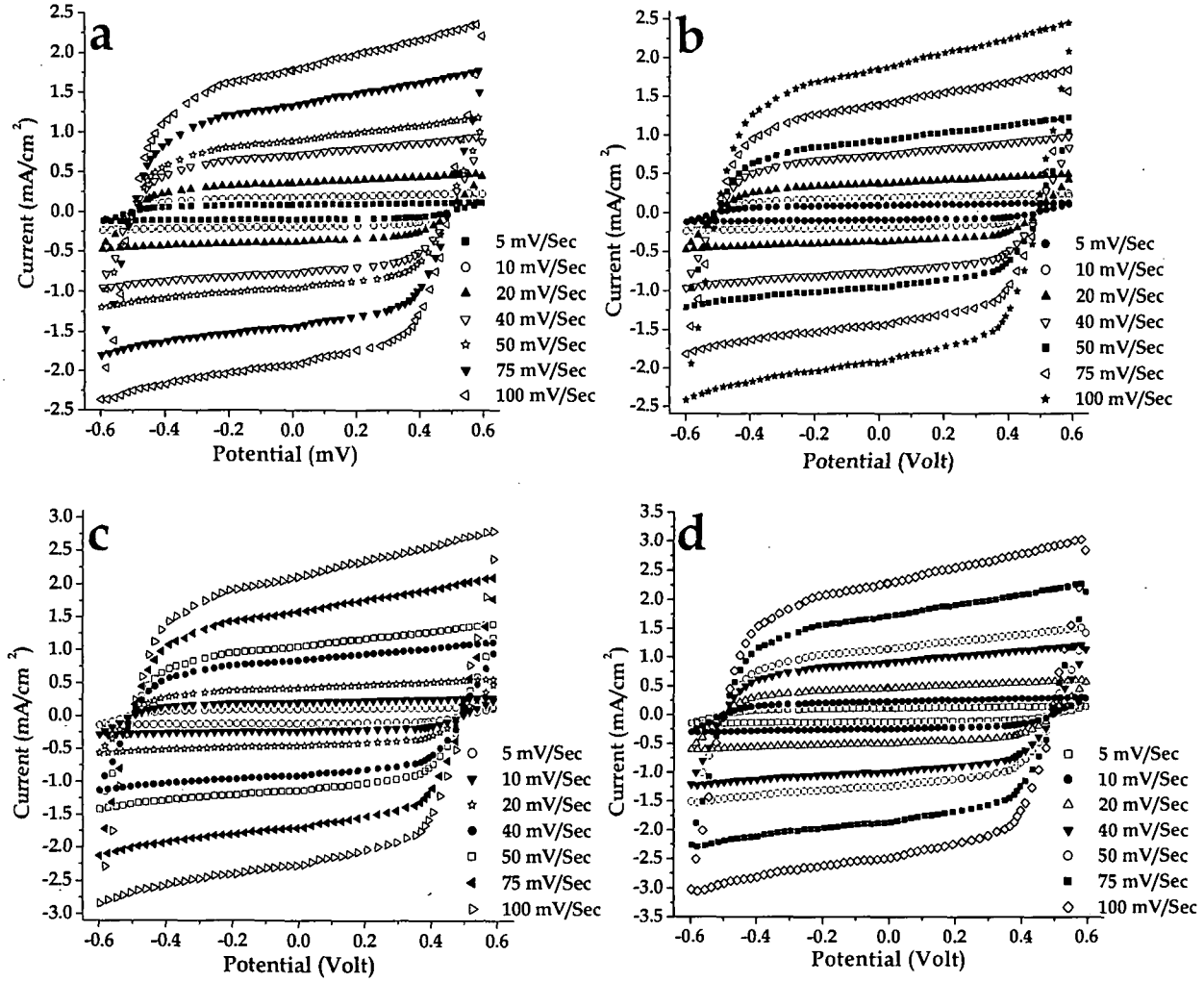


Figure 7.29: Cyclic voltammograms of supercapacitors with poly(3-methylthiophene) electrodes doped with (a) $LiClO_4$, (b) $LiCF_3SO_3$, (c) $[CH_3(CH_2)_3]_4NBF_4$ and (d) $[CH_3(CH_2)_3]_4NPF_6$.

discharge plots. This may be attributed to the electronic current passing through the electrolyte in the cyclic voltammetry, where the polarity of potential keeps changing and the electronic current do not get stabilized. The internal resistance for all the supercapacitors with poly(3-methylthiophene) electrode is found to be very small (~ 1.5 kΩ $cm^2$) as shown in Table 7.10 and Fig. 7.31. The value of energy density of supercapacitors with the poly(3-methylthiophene) electrodes is found to be small compared to those with the polyaniline and polypyrrole electrodes due to the lower working potential of the poly(3-methylthiophene) electrodes (~0.6 Volt).

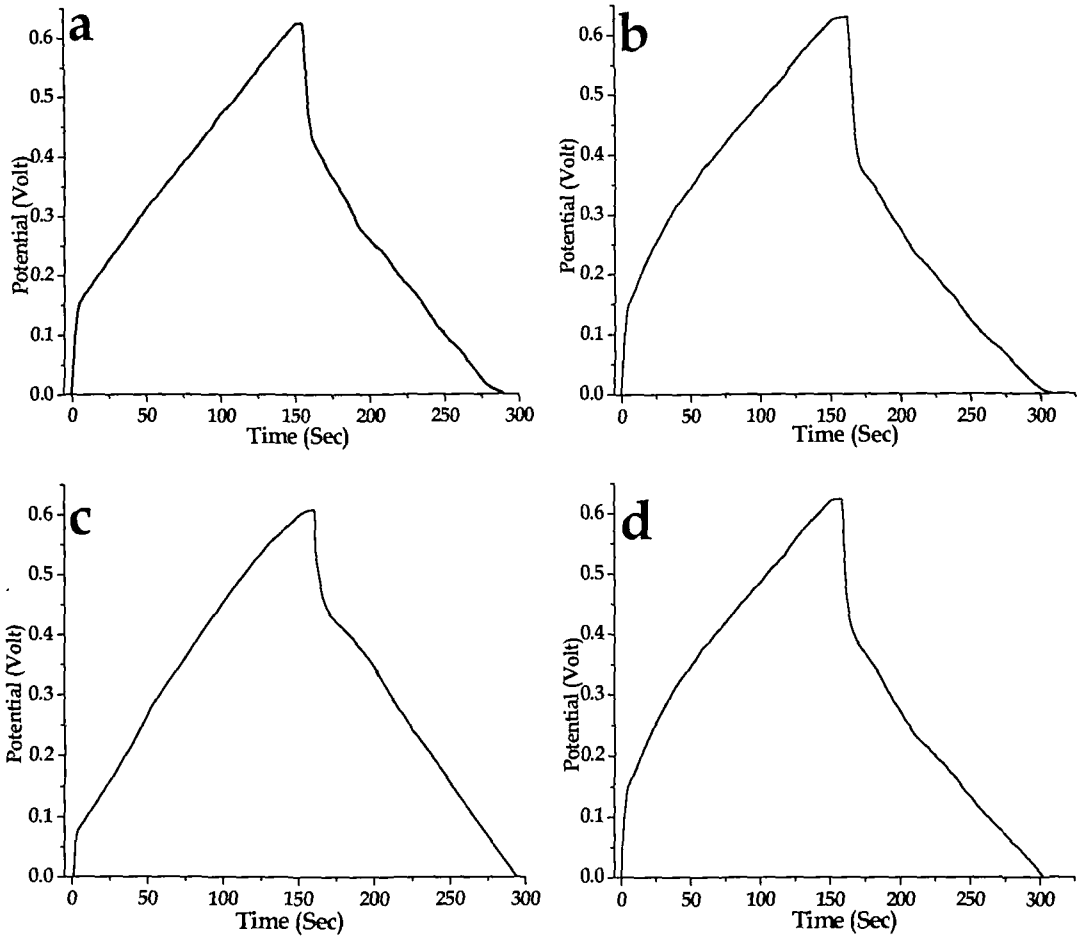


Figure 7.30: Charge-discharge plot of supercapacitors with poly(3-methylthiophene) electrodes doped with (a) $LiClO_4$, (b) $LiCF_3SO_3$, (c) $[CH_3(CH_2)_3]_4NBF_4$ and (d) $[CH_3(CH_2)_3]_4NPF_6$.

Table 7.10: Characteristic properties of supercapacitors with poly(3-methylthiophene) electrodes doped with different dopants.

| Dopant | Capacitance (F/gm) | | Discharge Capacitance | | Internal Resistance $R_i$ ($k\Omega cm^2$) | Coulombic efficiency $\eta$(%) | Energy Density (Wh/kg) |
|---|---|---|---|---|---|---|---|
| | Initial | Final | (mF/cm) | (F/gm) | | | |
| $LiClO_4$ | 221.3 | 171.69 | 43.70 | 218.50 | 1.46 | 85.90 | 10.95 |
| $LiCF_3SO_3$ | 223.0 | 174.29 | 44.09 | 220.45 | 1.51 | 89.51 | 11.02 |
| $[CH_3(CH_2)_3]_4NBF_4$ | 261.2 | 207.49 | 50.12 | 250.60 | 0.75 | 83.75 | 12.53 |
| $[CH_3(CH_2)_3]_4NPF_6$ | 282.7 | 238.52 | 54.98 | 274.90 | 1.44 | 90.51 | 13.75 |

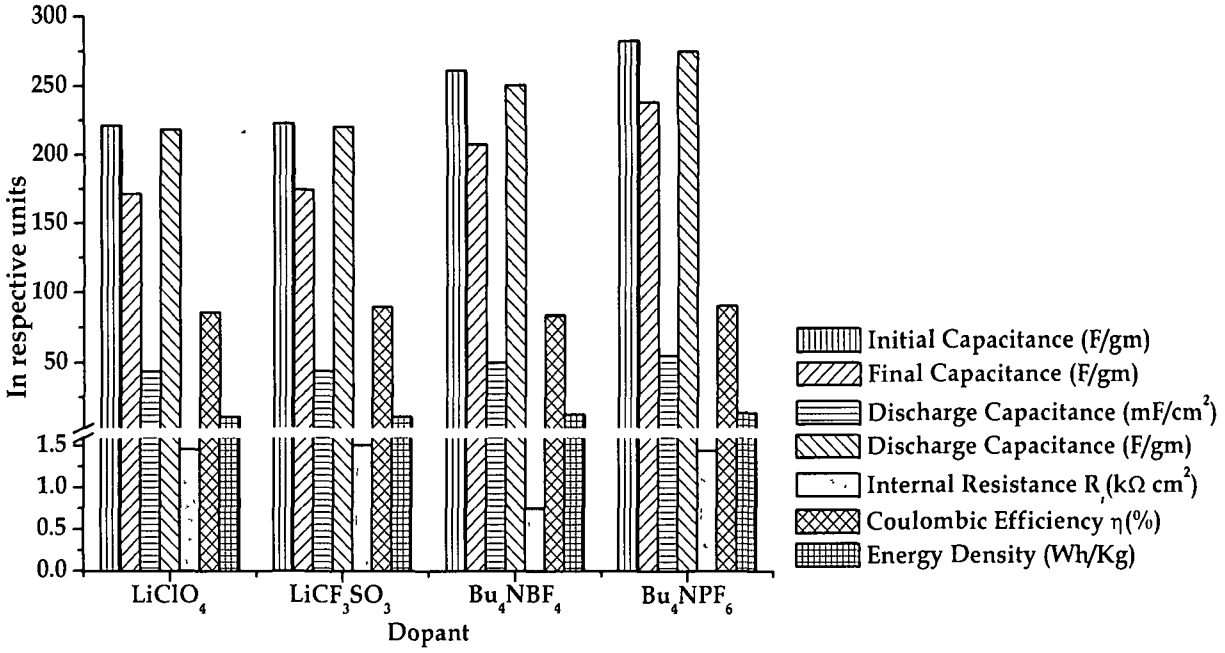


Figure 7.31: Characteristic properties of supercapacitors with poly(3-methylthiophene) electrodes doped with different dopants.

### *7.5.1 Type I supercapacitors with poly(3-methylthiophene) $LiClO_4$ doped irradiated electrodes:*

The lithium perchlorate ($LiClO_4$) p-doped poly(3-methylthiophene) conducting polymer electrodes irradiated with 120 MeV $Si^{9+}$ ion at three different fluences of $5x10^{10}$, $5x10^{11}$ and $3x10^{12}$ ions/cm$^2$ are used as electrodes to fabricate type I supercapacitors. The cyclic voltammograms of the supercapacitors with $LiClO_4$ doped irradiated poly(3-methylthiophene) conducting polymer electrodes recorded at different scan rates are presented in Fig. 7.32. The cyclic voltammograms show good capacitive behaviour upto scan rates of 100 mV/sec. The small increase in current towards higher potential observed in the cyclic voltammograms of the supercapacitor is due to the redox property of the conducting polymer electrodes. The capacitance values calculated from the cyclic voltammograms are presented in Table 7.11. The electrochemical stability of the supercapacitors with $LiClO_4$ doped irradiated poly(3-methylthiophene) electrode has been tested for 10,000 cycles of charging and discharging and the stability plots are shown in Fig. 7.33a. The initial decrease in the capacitance

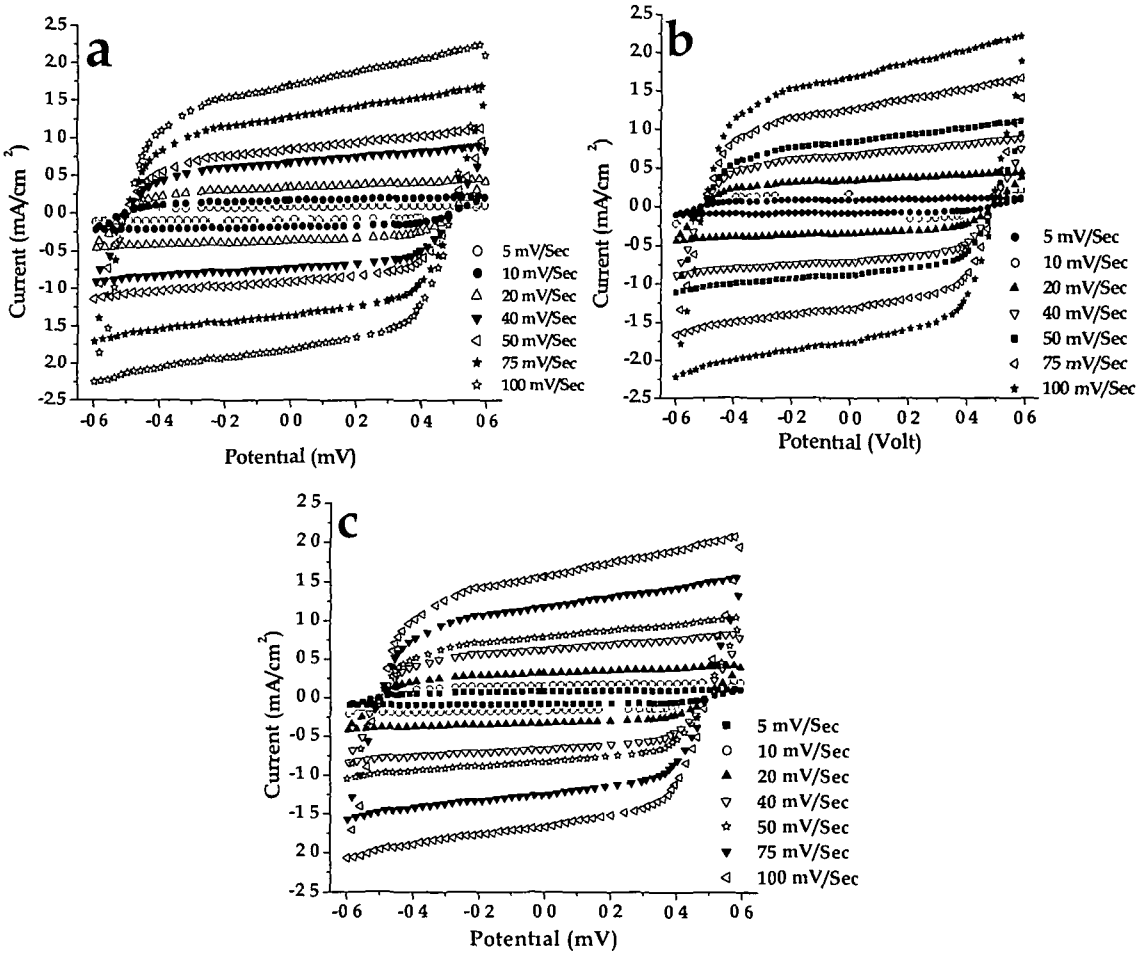


Figure 7 32 Cyclic voltammograms of supercapacitors with $LiClO_4$ doped poly(3-methylthiophene) irradiated electrode with fluence (a) $5X10^{10}$, (b) $5X10^{11}$ and (c) $3X10^{12}$ ions/$cm^2$

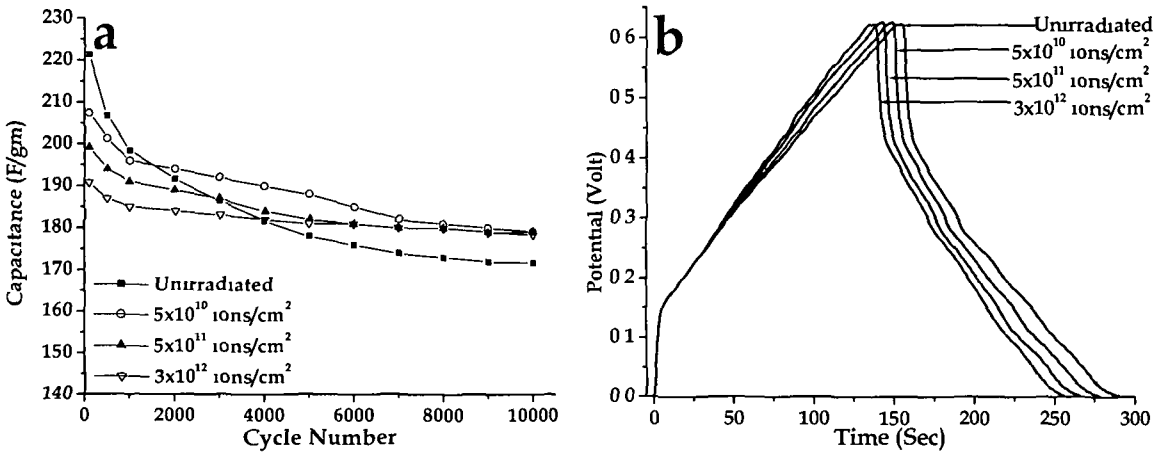


Figure 7 33 (a) Stability and (b) charge-discharge plots of supercapacitors with $LiClO_4$ doped poly(3-methylthiophene) electrodes before and after irradiation with different fluences

Table 7.11: Characteristic properties of supercapacitors with $LiClO_4$ doped Poly(3-methylthiophene) electrodes SHI irradiated with different fluences.

| Fluence (ions/cm²) | Capacitance (F/gm) | | Discharge Capacitance | | Internal resistance | Coulombic efficiency | Energy Density |
|---|---|---|---|---|---|---|---|
| | Initial | Final | mF/cm² | F/gm | (kΩcm²) | η(%) | (Wh/kg) |
| 0 | 221.3 | 171.69 | 43.70 | 218.50 | 1.46 | 85.90 | 10.95 |
| $5x10^{10}$ | 207.4 | 179.22 | 40.72 | 203. 60 | 1.46 | 85.33 | 10.18 |
| $5x10^{11}$ | 199.15 | 179.12 | 38.59 | 192.95 | 1.46 | 86.01 | 9.65 |
| $3x10^{12}$ | 190.8 | 171.41 | 37.37 | 186.85 | 1.45 | 84.17 | 9.34 |

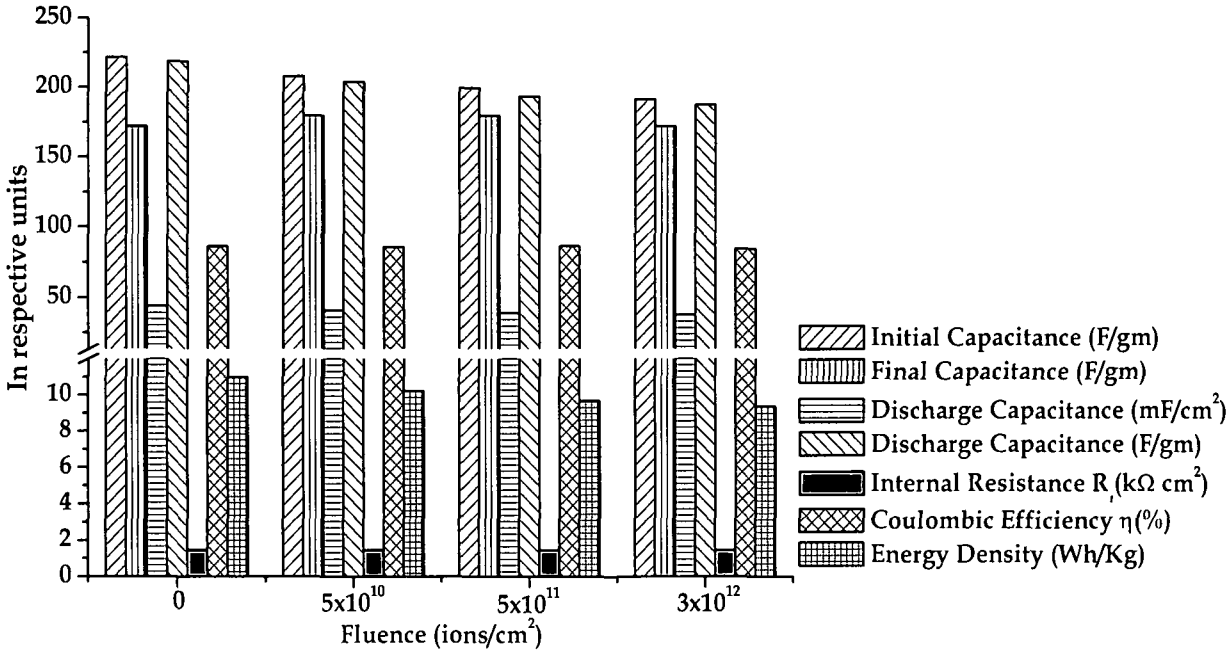


Figure 7.34: Characteristics of supercapacitors with $LiClO_4$ doped poly(3-methylthiophene) electrodes irradiated with different fluences.

value observed in the stability plots may be attributed to the irreversible faradic reaction occurring at the electrode surface due to the presence of volatile surface groups e.g., $OH^-$, $CN^-$, $CH_3^+$ etc., which cause loss of charge at the electrode. After SHI irradiation, the decrease in initial capacitance is observed to be less as compared to the capacitance of the supercapacitors with unirradiated polymer electrodes. This may be attributed to either stabilization or removal of the volatile and reactive surface groups from the electrode surface upon SHI irradiation. Thus the electrochemical stability of the

supercapacitors with irradiated electrode is enhanced at the cost of slight decrease in initial capacitance value. The decrease of capacitance value after SHI irradiation may be attributed to possible surface modification due to cross-linking induced by huge electronic energy loss mechanism and decrease in the concentration of the surface groups on the electrode surface, which decreases with the increase of fluence. The charge-discharge plots of the supercapacitors recorded galvanostatically at 100 μA are shown in Fig. 7.33b. The discharge capacitance values of the supercapacitors calculated from the charge-discharge plot using relation eqn. 7.2 are presented in Table 7.11. The characteristic values of various properties of the supercapacitors with unirradiated and irradiated $LiClO_4$ doped poly(3-methylthiophene) conducting polymer electrodes are presented graphically in Fig. 7.34. The value of discharge capacitance of the supercapacitors are found to be slightly less as compared to those calculated from the cyclic voltammograms, which may be due to the fact that the current obtained in cyclic voltammograms constitute in part due to the electronic current through the electrolyte because of continuous change of polarity of potential. The internal resistance of the supercapacitors with $LiClO_4$ doped poly(3-methylthiophene) electrode is small, of the order of 1.5 kΩ $cm^2$.

### *7.5.2 Type I supercapacitors with poly(3-methylthiophene) $LiCF_3SO_3$ doped irradiated electrodes:*

The cyclic voltammograms of the supercapacitors with 120 MeV $Si^{9+}$ ion irradiated $LiCF_3SO_3$ doped poly(3-methylthiophene) electrodes are shown in Fig. 7.35. The cyclic voltammograms of the supercapacitors with 120 MeV $Si^{9+}$ ion irradiated poly(3-methylthiophene) conducting polymer electrodes show good capacitive behavior up to a scan rate of 75 mV/Sec. At higher scan rate the cyclic voltammograms deviate from the rectangular shape. The increase in current towards higher potential at higher scan rates observed in the cyclic voltammograms may be due to the redox nature of the poly(3-methylthiophene) electrodes, which remains unchanged as observed in the cyclic voltammetry of the poly(3-methylthiophene) films after irradiation (Chapter 6, section 6.5.1).

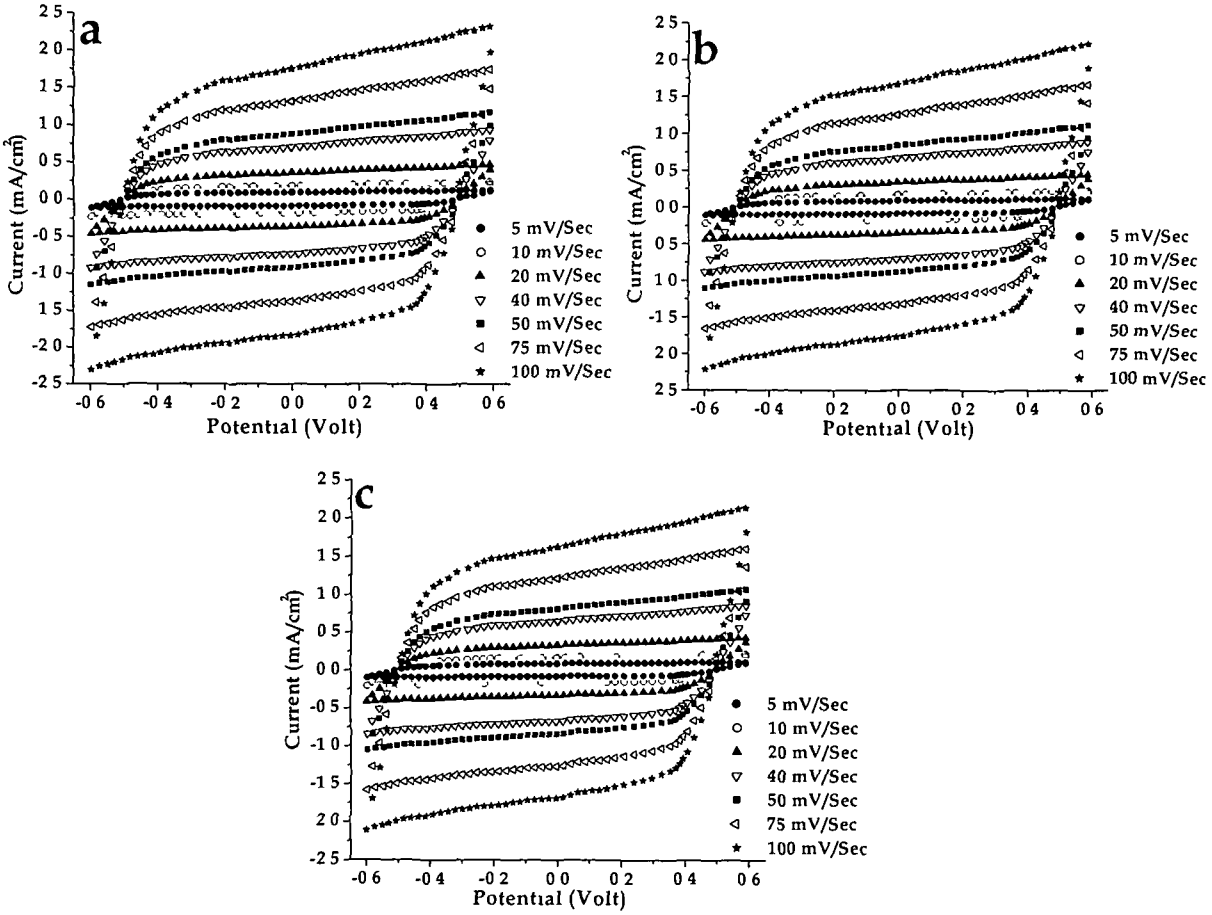


Figure 7 35 Cyclic voltammograms of supercapacitors with $LiCF_3SO_3$ doped poly(3-methylthiophene) irradiated electrodes with fluence (a) $5X10^{10}$, (b) $5X10^{11}$ and (c) $3X10^{12}$ ions/cm²

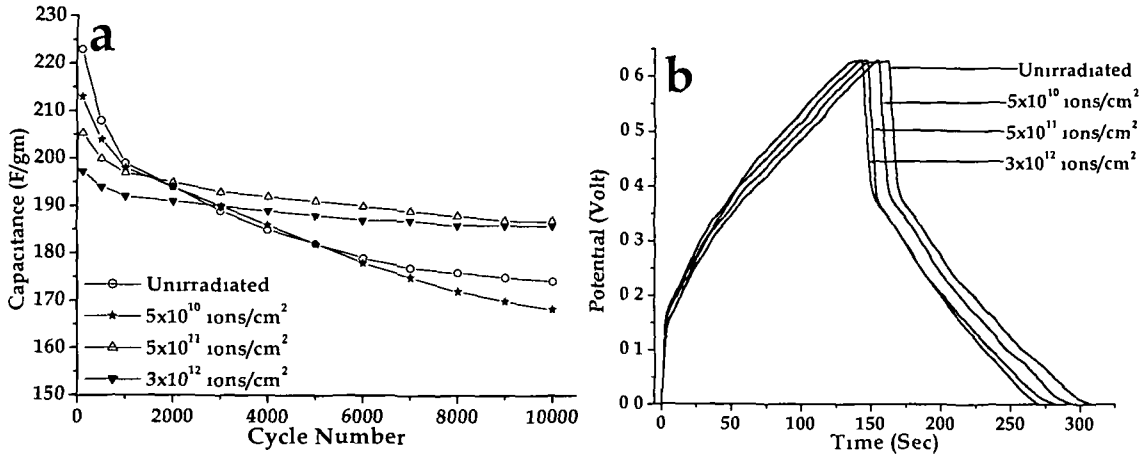


Figure 7 36 (a) Stability and (b) charge-discharge plots of supercapacitors with $LiCF_3SO_3$ doped poly(3-methylthiophene) electrodes before and after irradiation with different fluences

Table 7.12: Characteristic properties of supercapacitors with $LiCF_3SO_3$ doped poly(3-methylthiophene) electrodes irradiated with different fluences.

| Fluence (ions/cm²) | Capacitance (F/gm) | | Discharge Capacitance | | Internal resistance (kΩcm²) | Coulombic efficiency η(%) | Energy Density (Wh/kg) |
|---|---|---|---|---|---|---|---|
| | Initial | Final | mF/cm² | F/gm | | | |
| 0 | 223.0 | 174.29 | 44.09 | 220.45 | 1.51 | 89.51 | 11.02 |
| $5x10^{10}$ | 213.08 | 168.31 | 41.61 | 208.05 | 1.51 | 89.67 | 10.40 |
| $5x10^{11}$ | 205.4 | 186.87 | 40.27 | 201.35 | 1.49 | 89.86 | 10.07 |
| $3x10^{12}$ | 197.34 | 185.93 | 38.52 | 192.60 | 1.48 | 88.19 | 9.63 |

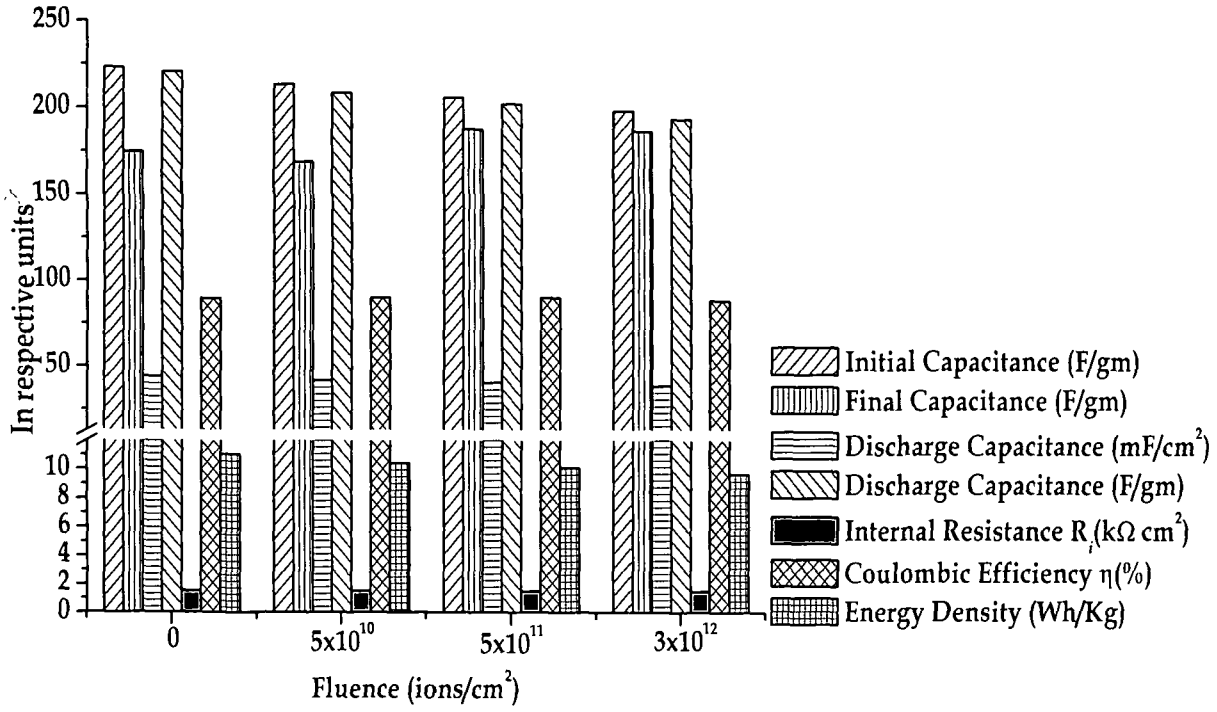


Figure 7.37: Characteristic properties of supercapacitors with $LiCF_3SO_3$ doped poly(3-methylthiophene) electrodes irradiated with different fluences.

The electrochemical stability plots of the SHI irradiated poly(3-methylthiophene) electrodes are shown in Fig. 7.36b. The stability plot of the supercapacitors with unirradiated as well as irradiated poly(3-methylthiophene) electrodes show initial sharp decrease in capacitance values, which may be attributed to the irreversible Faradic reaction of the highly

reactive surface groups like $OH^-$ $CN^-$, $CH_3^+$ etc., which gets attached to the electrode surface from the solvent and atmosphere. This initial decrease of capacitance of the supercapacitors with irradiated poly(3-methylthiophene) electrodes are less as compared to that of the supercapacitors with unirradiated electrodes. This may be due to the fact that the loosely bound volatile surface groups are stabilized or removed from the polymer electrodes upon SHI irradiation and hence the decrease of capacitance in initial charge-discharge becomes lesser with the increase in fluence. The charge-discharge plots of the supercapacitors with irradiated electrodes are shown in Fig. 7.36b. Decrease in the total charge-discharge time of the supercapacitors with irradiated electrodes is observed in the charge-discharge plots with small increase in coulombic efficiency. The decrease of charge-discharge time may be attributed to the increase in conductivity of the polymer electrodes after irradiation, which supports faster charge transport in the electrodes. The characteristic values of properties of the supercapacitors with irradiated $LiCF_3SO_3$ doped poly(3-methylthiophene) electrodes are presented in Table 7.12. The graphical representation of the characteristic values of properties of the supercapacitors with 120 MeV $Si^{9+}$ ion irradiated $LiCF_3SO_3$ doped poly(3-methylthiophene) electrodes are shown in Fig. 7.37.

### *7.5.3 Type I supercapacitors with poly(3-methylthiophene) $[CH_3(CH_2)_3]_4NBF_4$ doped irradiated electrodes:*

The cyclic voltammograms of supercapacitors with $[CH_3(CH_2)_3]_4NBF_4$ doped poly(3-methylthiophene), irradiated with 120 MeV $Si^{9+}$ ions with three different fluences of $5x10^{10}$, $5x10^{11}$ and $3x10^{12}$ ions/cm$^2$ recorded at different scan rates are shown in Fig. 7.38. The cyclic voltammograms show ideal capacitive behaviour of the supercapacitors at lower scan rates but deviated from the rectangular shape at higher scan rates (> 75 mV/sec) and an increase in current towards higher potential at the higher scan rates is observed. This may be due to the redox property of the conducting polymer electrodes, which

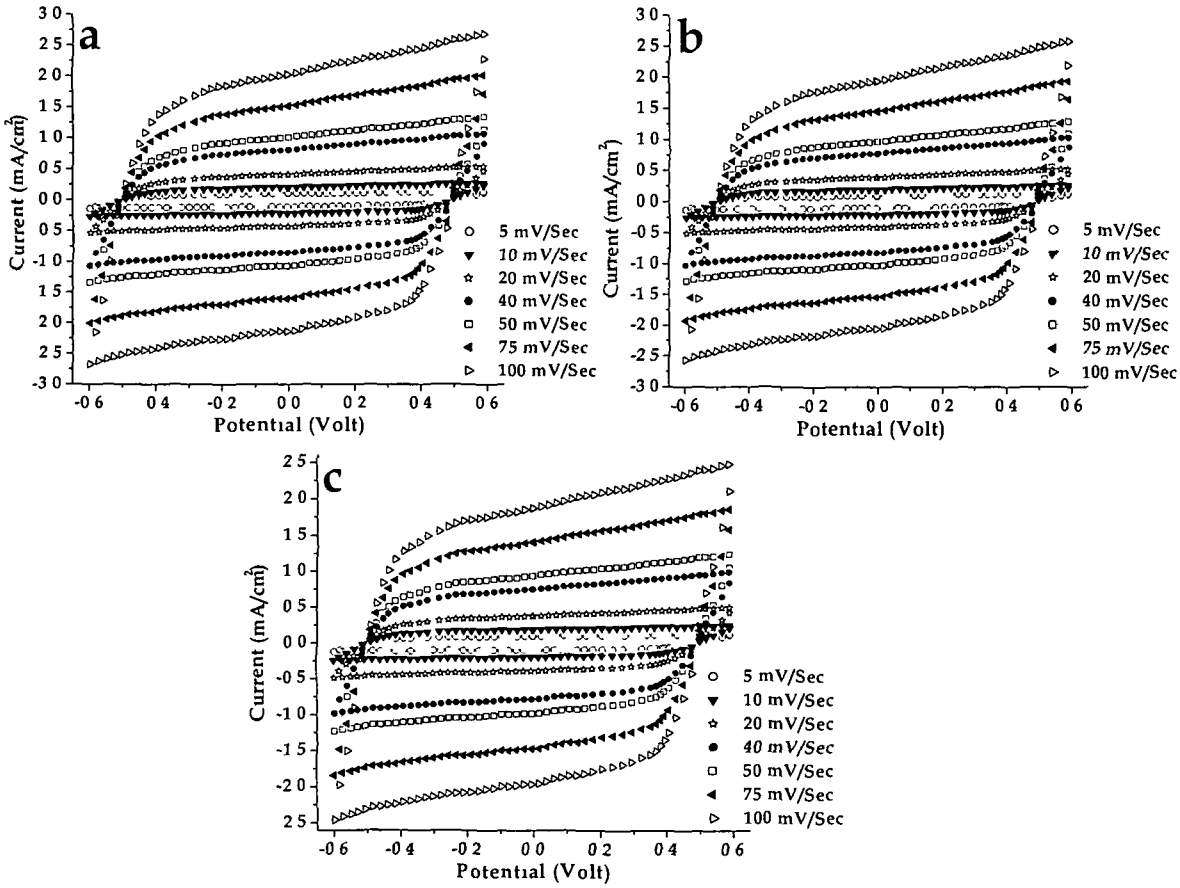


Figure 7 38 Cyclic voltammograms of supercapacitors with $[CH_3(CH_2)_3]_4NBF_4$ doped poly(3-methylthiophene) irradiated electrodes with different fluences (a) $5X10^{10}$, (b) $5X10^{11}$ and (c) $3X10^{12}$ ions/cm².

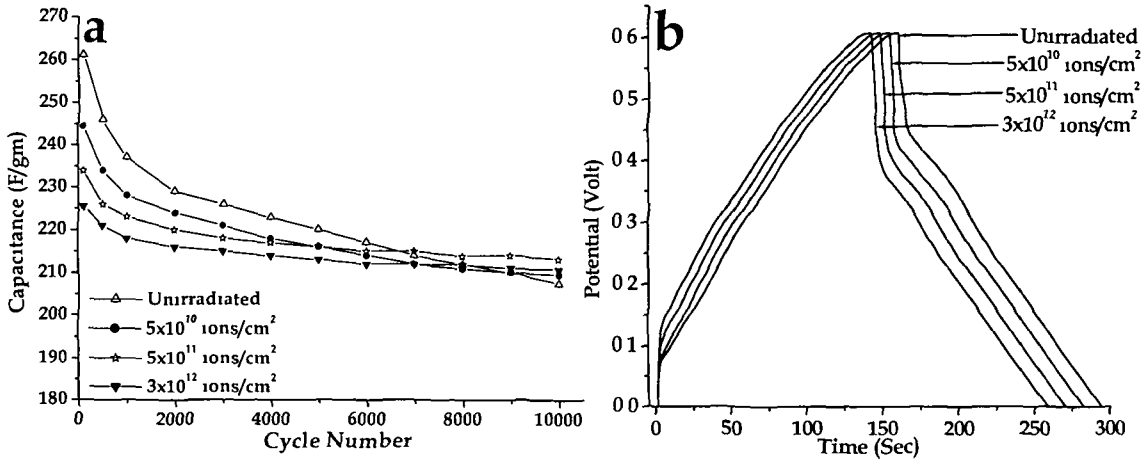


Figure 7 39 (a) Stability and (b) charge-discharge plots of supercapacitors with $[CH_3(CH_2)_3]_4NBF_4$ doped poly(3-methylthiophene) electrodes before and after irradiation

Table 7.13: Characteristics of supercapacitors with $[CH_3(CH_2)_3]_4NBF_4$ doped poly(3-methylthiophene) electrodes irradiated with different fluences.

| Fluence (ions/cm²) | Capacitance (F/gm) | | Discharge Capacitance | | Internal resistance (kΩcm²) | Coulombic efficiency η(%) | Energy Density (Wh/kg) |
|---|---|---|---|---|---|---|---|
| | Initial | Final | mF/cm² | F/gm | | | |
| 0 | 261.2 | 207.49 | 50.12 | 250.60 | 0.75 | 83.75 | 12.53 |
| $5x10^{10}$ | 244.4 | 209.56 | 48.05 | 240.25 | 0.76 | 83.12 | 12.01 |
| $5x10^{11}$ | 233.9 | 213.24 | 45.32 | 226.60 | 0.76 | 82.43 | 11.33 |
| $3x10^{12}$ | 225.5 | 210.87 | 43.89 | 219.45 | 0.77 | 82.98 | 10.97 |

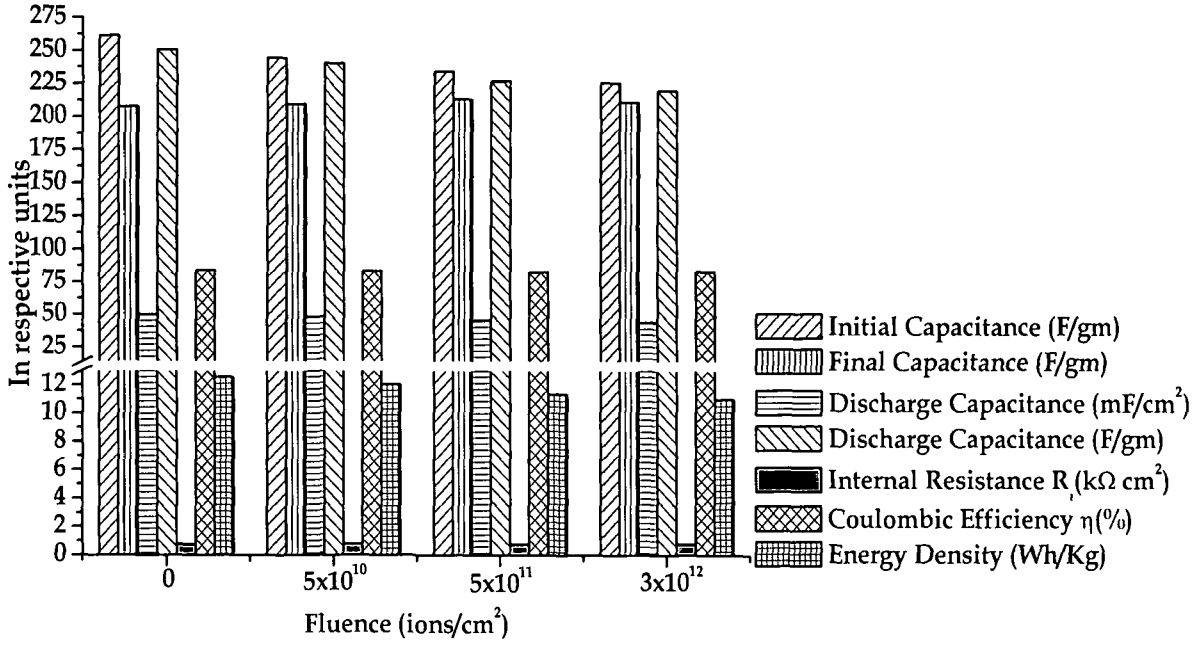


Figure 7.40: Characteristics of supercapacitors with $[CH_3(CH_2)_3]_4NBF_4$ doped poly(3-methylthiophene) electrodes irradiated with different fluences.

remains unchanged upon SHI irradiation. The capacitance values of the supercapacitors calculated from the cyclic voltammograms using relation eqn. 7.1 are presented in Table 7.13. The electrochemical stability of the supercapacitors has been tested for 10,000 cycles and the stability plots are presented in Fig. 7.39a. The initial sharp decrease of capacitance values for the supercapacitors occurs possibly due to the faradic reactions taking place on the electrode surface due to the presence of volatile and reactive surface groups e.g., $OH^-, CN^-, CH_3^+$ etc., causing loss of charge at the electrode. The SHI

irradiation causes stabilization or removal of the highly reactive surface groups that results in less initial decrease of capacitance and the decrease in capacitance becomes lesser with the increase of SHI irradiation fluence. The charge-discharge plots of the supercapacitors with unirradiated as well as irradiated electrodes recorded galvanostatically at 100 μA are presented in Fig. 7.39b. The characteristic values of properties of the supercapacitors with $[CH_3(CH_2)_3]_4NBF_4$ doped and irradiated poly(3-methylthiophene) conducting polymer electrodes are presented in Table 7.13 and are graphically shown in Fig. 7.40. The internal resistance of the supercapacitors with $[CH_3(CH_2)_3]_4NBF_4$ doped and irradiated poly(3-methylthiophene) electrodes is found to be very small (~ 0.7 kΩ $cm^2$), which is very promising for applications in high power devices.

### *7.5.4 Type I supercapacitors with poly(3-methylthiophene) $[CH_3(CH_2)_3]_4NPF_6$ doped irradiated electrodes:*

The tetrabutylammonium hexafluorophosphate ($[CH_3(CH_2)_3]_4NPF_6$) p-doped poly(3-methylthiophene) conducting polymer electrodes irradiated with 120 MeV $Si^{9+}$ ion at three different fluences of $5x10^{10}$, $5x10^{11}$ and $3x10^{12}$ ions/$cm^2$ are used as electrodes to fabricate type I supercapacitors. The cyclic voltammograms of the supercapacitors with $[CH_3(CH_2)_3]_4NPF_6$ doped and irradiated poly(3-methylthiophene) conducting polymer electrodes recorded at different scan rates are presented in Fig. 7.41. The cyclic voltammograms show good capacitive behaviour upto scan rates of 100 mV/Sec. The small increase observed in current towards higher potential is due to the redox property of the conducting polymer electrodes. The capacitance values calculated from the cyclic voltammograms are presented in Table 7.14. The electrochemical stability of the supercapacitors with $[CH_3(CH_2)_3]_4NPF_6$ doped and irradiated poly(3-methylthiophene) electrodes has been tested for 10,000 cycle of charging and discharging and the stability plots are presented in Fig. 7.42a. The initial decrease in the capacitance values observed in the stability plots may be

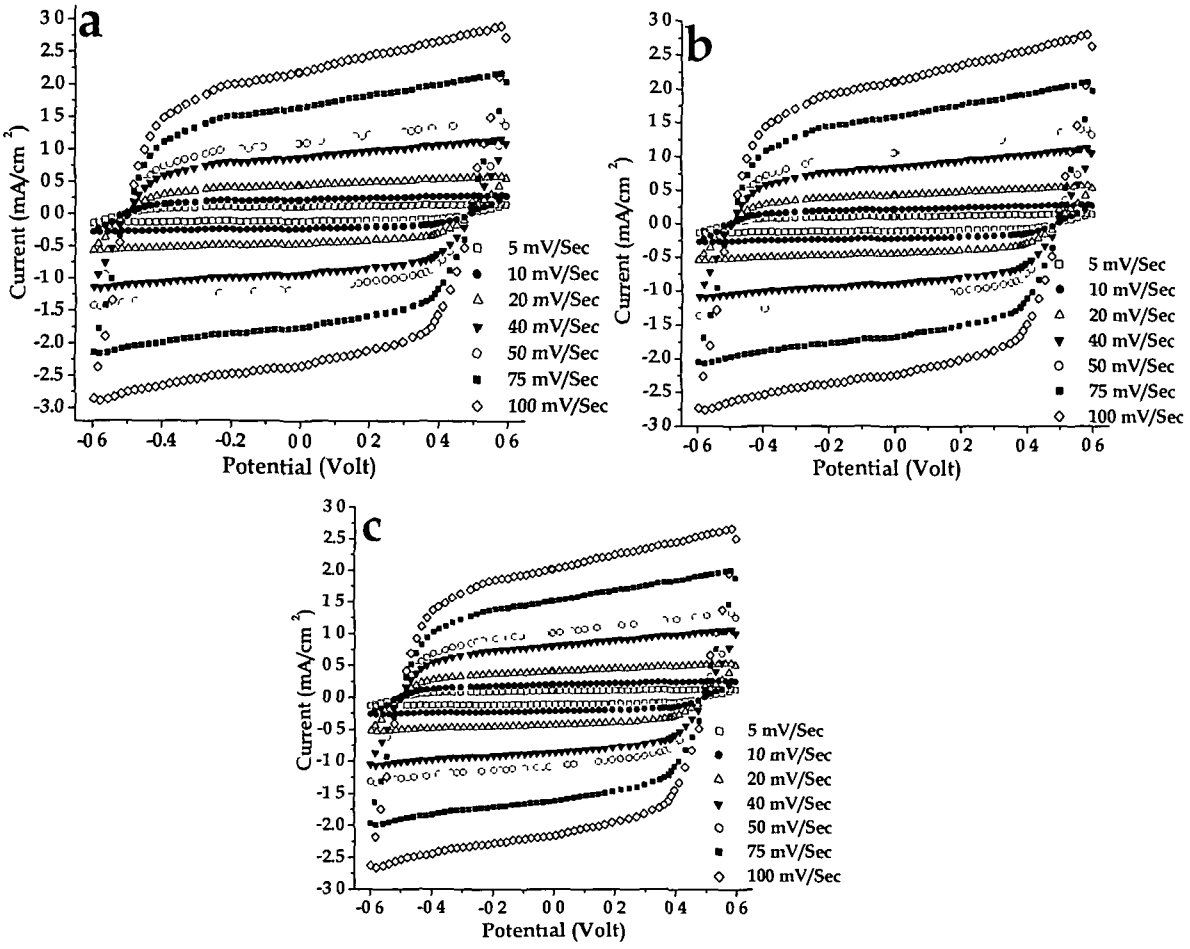


Figure 7.41: Cyclic voltammograms of supercapacitors with $[CH_3(CH_2)_3]_4NPF_6$ doped poly(3-methylthiophene) irradiated electrodes with different fluences (a) $5X10^{10}$, (b) $5X10^{11}$ and (c) $3X10^{12}$ ions/cm$^2$.

attributed to the irreversible faradic reaction occurring at the electrode surface due to the presence of volatile surface groups e g., $OH^-, CN^-, CH_3^+$ etc., which cause loss of charge at the electrode. After SHI irradiation, the decrease in initial capacitance is observed to be less as compared to the capacitance of the supercapacitors with unirradiated polymer electrodes. This may be due to stabilization or removal of the volatile and reactive surface groups from the electrode surface. Thus the electrochemical stability of the supercapacitors with irradiated electrodes is enhanced though the initial capacitance value is slightly decreased. The decrease of capacitance value after SHI irradiation may be attributed to possible surface modification due to cross linking induced by huge

electronic energy loss mechanism and decrease in the concentration of the surface groups on the electrode surface, which decreases with the increase of fluence, resulting in less decrease in initial capacitance values with the increase of fluence of SHI irradiation. The charge-discharge plots of the supercapacitors recorded galvanostatically at 100 μA are shown in Fig. 7.42b. The discharge capacitance of the individual supercapacitors, capacitance of the single electrode, internal resistance, Coulombic efficiency and energy density of the supercapacitors calculated from the charge-discharge plot using relations eqns. 7.2-7.4 are presented in Table 7.14. The characteristic values of the supercapacitors with unirradiated and irradiated $[CH_3(CH_2)_3]_4NPF_6$ doped poly(3-methylthiophene) conducting polymer electrodes are presented graphically in Fig. 7.43. The values of discharge capacitance of the supercapacitors are found to be slightly less as compared to those calculated from the cyclic voltammograms, which may be due to the fact that the current obtained in cyclic voltammograms constitutes in part to the electronic current through the electrolyte due to continuous change in polarity of potential. The internal resistance of the supercapacitors with $[CH_3(CH_2)_3]_4NPF_6$ doped poly(3-methylthiophene) electrode has been measured to be small of the order of 1.4 kΩ $cm^2$.

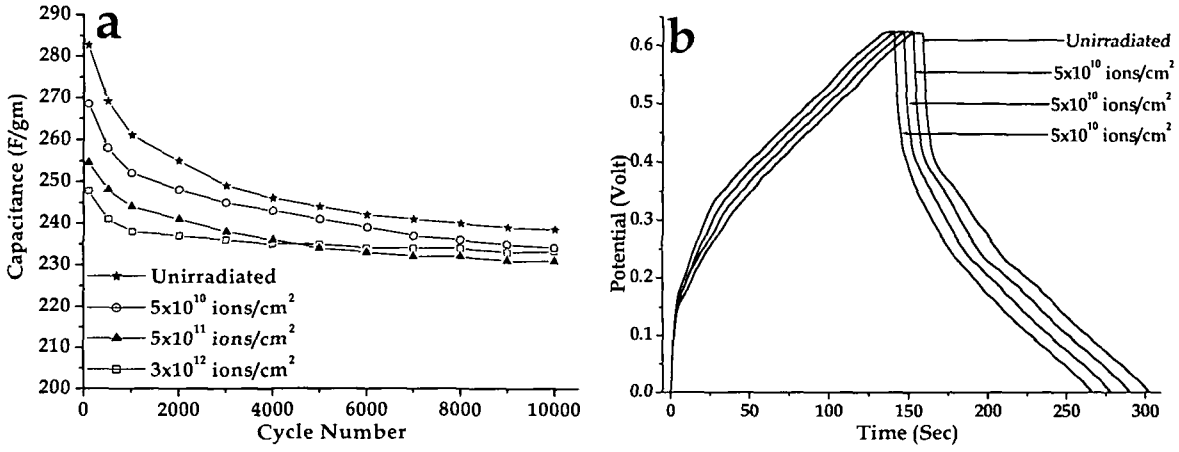


Figure 7.42: (a) Stability and (b) charge-discharge plots of supercapacitors with $[CH_3(CH_2)_3]_4NPF_6$ doped poly(3-methylthiophene) electrodes before and after irradiation with different fluences.

Table 7.14: Characteristic properties of supercapacitors with $[CH_3(CH_2)_3]_4NPF_6$ doped poly(3-methylthiophene) electrodes irradiated with different fluences.

| Fluence (ions/cm²) | Capacitance (F/gm) | | Discharge Capacitance | | Internal resistance | Coulombic efficiency | Energy Density |
|---|---|---|---|---|---|---|---|
| | Initial | Final | mF/cm² | F/gm | (kΩcm²) | η(%) | (Wh/kg) |
| 0 | 282.7 | 238.52 | 54.98 | 274.90 | 1.44 | 90.51 | 13.75 |
| $5x10^{10}$ | 268.5 | 234.11 | 52.19 | 260.95 | 1.43 | 90.79 | 13.05 |
| $5x10^{11}$ | 254.68 | 230.89 | 50.09 | 250.45 | 1.43 | 89.73 | 12.52 |
| $3x10^{12}$ | 247.75 | 233.34 | 48.41 | 242.05 | 1.41 | 89.23 | 12.10 |

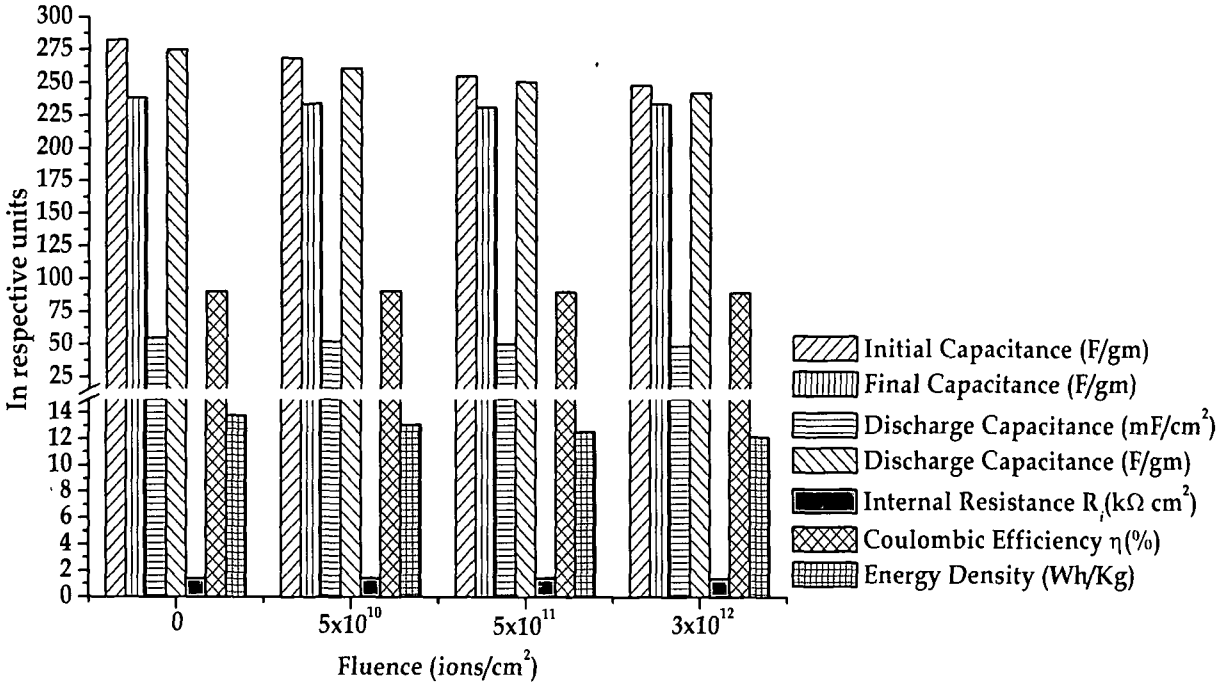


Figure 7.43: Characteristic properties of supercapacitors with $[CH_3(CH_2)_3]_4NPF_6$ doped poly(3-methylthiophene) electrodes irradiated with different fluences.

### *7.6 Type III supercapacitors with $LiClO_4$ p and n-doped poly(3-methylthiophene) unirradiated and irradiated electrodes:*

Type III supercapacitors have been fabricated with lithium perchlorate ($LiClO_4$) p and n-doped poly(3-methylthiophene) conducting polymer unirradiated and irradiated electrodes. The cyclic voltammograms of the supercapacitors with $LiClO_4$ p and n-doped irradiated poly(3-methylthiophene) conducting polymer electrodes recorded at different scan rates are presented in

Fig. 7.44. The cyclic voltammograms show good capacitive characteristics up to scan rates of 100 mV/sec. The small increase in the current towards higher potential observed in the cyclic voltammograms of the supercapacitors is due to the redox property of the conducting polymer electrodes. The capacitance values calculated from the cyclic voltammograms are presented in Table 7.15. The electrochemical stability of the supercapacitors with $LiClO_4$ p and n-doped irradiated poly(3-methylthiophene) electrode has been tested for 10,000 cycles of charging and discharging. The capacitance values have been calculated after every 1000 cycles and the stability plots of the supercapacitors are presented in shown in Fig. 7.45a. The initial decrease in the capacitance values observed in

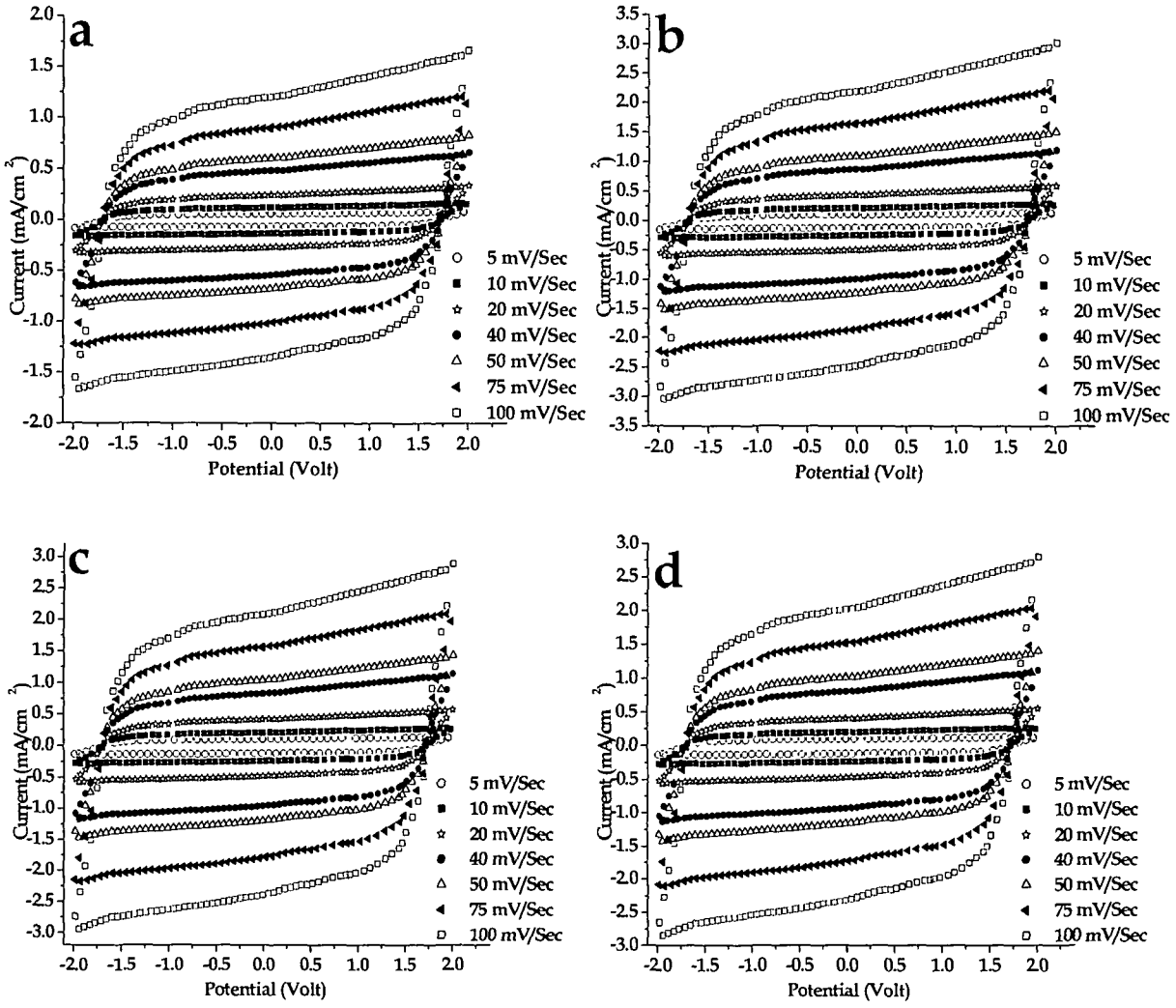


Figure 7.44: Cyclic voltammograms of type III supercapacitor with poly(3-methylthiophene) p and n-doped with $LiClO_4$ (a) unirradiated and irradiated electrodes with different fluences (b) $5X10^{10}$, (c) $5X10^{11}$ and (d) $3X10^{12}$ ions/cm$^2$.

the stability plots may be attributed to the irreversible Faradic reaction occurring at the electrode surface due to the presence of volatile surface groups e.g., $OH^-, CN^-, CH_3^+$ etc., which cause loss of charge at the electrode. After SHI irradiation, the decrease in initial capacitance is observed to be less as compared to the capacitance of the supercapacitors with unirradiated polymer electrodes. This may be due to stabilization or removal of the volatile and reactive surface groups from the electrode surface upon SHI irradiation. The electrochemical stability of the supercapacitors with irradiated electrode is enhanced, though the initial capacitance value is slightly decreased. The decrease of capacitance value after SHI irradiation may be attributed to possible surface modification due to cross linking induced by huge electronic energy loss mechanism and decrease in the concentration of the surface groups on the electrode surface, which decreases with the increase of fluence of SHI irradiation. The charge-discharge plots of the supercapacitors recorded galvanostatically at 100 μA are shown in Fig. 7.45b. The discharge capacitance of the individual supercapacitors, capacitance of the electrode material, internal resistance, Coulombic efficiency and energy density of the electrode have been calculated from the charge-discharge plot using

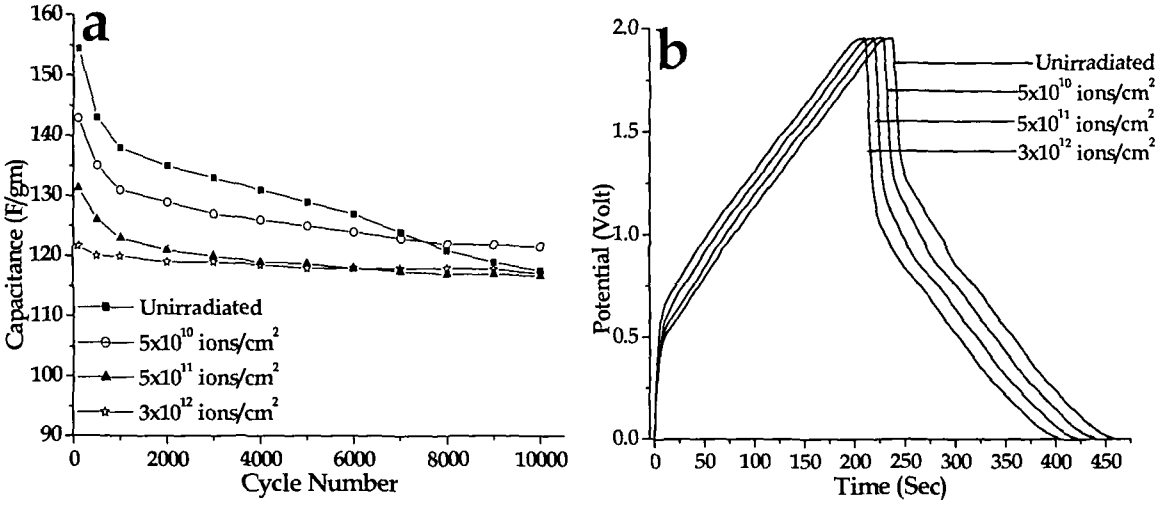


Figure 2.45: Stability (a) and charge-discharge (b) plot of type III supercapacitor with poly(3-methylthiophene) electrodes p and n-doped with $LiClO_4$ before and after irradiation.

Table 7.15: Characteristic properties of type III supercapacitor with poly(3-methylthiophene) electrodes p and n-doped with $LiClO_4$ irradiated with different fluences.

| Fluence (ions/cm²) | Capacitance (F/gm) | | Discharge Capacitance | | Internal resistance | Coulombic efficiency | Energy Density |
|---|---|---|---|---|---|---|---|
| | Initial | Final | mF/cm² | F/gm | (kΩcm²) | η(%) | (Wh/kg) |
| 0 | 154.5 | 117. 7 | 27.4 | 137.0 | 0.48 | 92.41 | 76.11 |
| $5x10^{10}$ | 142.9 | 121.6 | 26.51 | 132.6 | 0.47 | 85.33 | 73.67 |
| $5x10^{11}$ | 131.3 | 116.7 | 25.84 | 129.2 | 0.45 | 86.01 | 71.78 |
| $3x10^{12}$ | 121.7 | 117.2 | 23.82 | 119.1 | 0.41 | 84.17 | 66.17 |

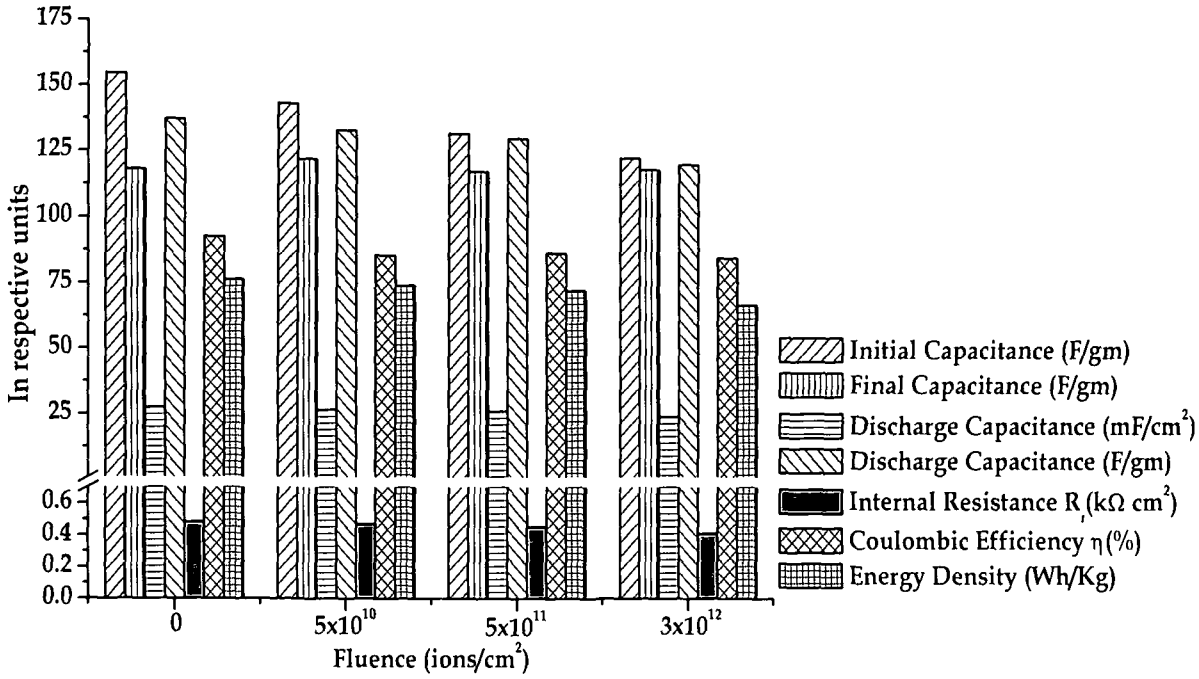


Figure 7.46: Characteristics of type III supercapacitor with poly(3-methylthiophene)
electrodes p and n-doped with $LiClO_4$ SHI irradiated with different fluences.

relations eqns. 7.2-7.4 and are presented in Table 7.15. The values of discharge capacitance of the supercapacitors are found to be slightly less as compared to that calculated from the cyclic voltammograms, which may be due to the fact that the current obtained in cyclic voltammograms is in part due to the electronic current through the electrolyte due to continuous swinging of polarity of potential. The characteristic values of the supercapacitors with

unirradiated and irradiated $LiClO_4$ p and n-doped poly(3-methylthiophene) conducting polymer electrodes are presented graphically in Fig. 7.46. The internal resistance of the type III supercapacitors with $LiClO_4$ p and n-doped poly(3-methylthiophene) electrode is quite small on the order of 0.4 $k\Omega\ cm^2$. The energy density of type III supercapacitors is found to be much higher than the type I and type II supercapacitors because of the higher working potential of about 2.5 Volt of the type III supercapacitors.

**7.7 Summary:**

All-polymer supercapacitors fabricated with polyaniline, polypyrrole and poly(3-methylthiophene) conducting polymer electrodes and PVDF-HFP(2)-PMMA(1)-$LiCF_3SO_3$(1)-PC+DEC(5.7)-$SiO_2$(0.3) gel polymer electrolyte show reasonably good capacitive behaviour with moderately high capacitance values consistent with those reported in the literature [342-345]. The capacitance values obtained for type III solid state supercapacitors are comparable with those using liquid electrolytes. The cyclic voltammetry studies carried out on all the supercapacitors show cyclic voltammograms of nearly rectangular shape at lower scan rates. At higher scan rates ($\geq$ 100 mV/Sec) the shape of the cyclic voltammograms deviated from the rectangular shape and an increase in current towards higher potential is observed. The rise in current towards higher potential could be attributed to the redox property of the conducting polymer electrodes, which get oxidized and consequently a rise in current occurs resulting in the deviation of the cyclic voltammograms from the ideal capacitive behaviour. The galvanostatic charge-discharge of the supercapacitors show good capacitive charging-discharging with small internal resistance. The discharge capacitance values of the supercapacitors calculated from the charge-discharge plots show slight lower values than those calculated form the cyclic voltammograms. In the cyclic voltammetry, the polarity of the potential keeps on changing and the potential of each electrode becomes positive and negative in every cycle. Thus the small electronic current passing through the electrolyte contributes to the total current obtained in the cyclic voltammograms giving

rise to slightly higher values of capacitance. The internal resistance of the solid state all-polymer redox supercapacitors calculated from the charge-discharge plots shows smaller values. A small decrease in internal resistance of the supercapacitors is found after SHI irradiation, which could be attributed to the increase in conductivity of the polymer electrodes after SHI irradiation. However, the decrease is not as much as expected from the increase in conductivity, which leads to the conclusion that the internal resistance arises mainly due to the interfacial resistance of the electrode/electrolyte interface, which depends on factors like surface morphologies of electrode and electrolyte. Coulombic efficiency of about 90% is obtained for all the fabricated supercapacitors. A decrease in total charge-discharge time is observed for supercapacitors with SHI irradiated electrodes. This may be attributed to the increase of conductivity of the electrodes after irradiation, which gives rise to faster charging and discharging of the supercapacitors. The energy density is directly dependent on the square of the working potential, hence highest energy density is obtained for the type III supercapacitors with p and n-doped poly(3-methylthiophene) electrodes, though the highest capacitance is obtained for type I supercapacitors with $[CH_3(CH_2)_3]_4NBF_4$ doped poly(3-methylthiophene) electrodes. The initial sharp decrease of capacitance with the unirradiated electrodes could possibly be attributed to the charge consumption or loss due to irreversible reactions with loosely bound volatile and reactive surface groups e.g., $OH^-$, $CN^-$, $CH_3^+$, etc. on the electrode surface, which initially contribute to charge storage at the electrode/electrolyte interface. The loosely bound volatile surface groups are stabilized or removed upon SHI irradiation leading to markedly less decrease of capacitance during initial charge-discharge cycles. Upon SHI irradiation, possible surface modifications due to cross-linking induced by huge electronic energy loss mechanism and decrease in the concentration of the surface groups on the electrode surface, which decreases with the increase of fluence, result in the decreased value of capacitance with the increase of fluence of SHI irradiation.

# CHAPTER VIII

## CONCLUSIONS AND FUTURE SCOPE

The present thesis is devoted to the electropolymerization of polyaniline, polypyrrole and poly(3-methylthiophene) conducting polymers and effects of swift heavy ion irradiation on them from the viewpoint of their application as electrodes in all-polymer solid state redox supercapacitors. The following are the main conclusions drawn from the studies carried out in the present work:

**1.** The electrochemical polymerization of conducting polymers produces better quality i.e., denser and smoother films in the potentiodynamic mode as compared to potentiostatic or other modes of electrodeposition. This could be attributed to the fact that electropolymerization in the potentiostatic method takes place at a constant potential. The oxidation potential of monomers is higher than that of dimers, trimers etc., resulting in the rapid and haphazard growth of dimers, trimers etc. growing at higher potential in the potentiostatic mode. On the other hand since in the potentiodynamic mode the potential keeps on varying and in the process becomes equal to the oxidation potential of the monomers, dimers, trimers etc., more orderly growth of the polymer films occurs making the films dense, smooth, uniform and less porous.

**2.** Cyclic voltammetry of the conducting polymer films shows remarkable electroactivity. The cyclic voltammograms constitute well constructed oxidation-reduction peaks during the potential sweep. The polyaniline conducting polymer films exhibit redox peaks accompanied by de-protonation and protonation peaks. The oxidation and de-protonation peaks have been observed in the range of 1.0 V- 1.1 V and 0.75 V – 0.85 V respectively. Similarly in the reverse sweep of potential, the reduction and protonation peaks have been observed in the range of 0.6 V - 0.4 V and 0.9 V -0.7 V respectively. The oxidation and reduction peaks for polypyrrole conducting polymer films have been observed in the range of 0.8 V-0.85 V and -0.15 V - 0.25 V in the forward and reverse sweep of potential respectively. Sharp and well constructed redox

peaks with dopant ion size dependent peaks shift have been observed in the cyclic voltammetry of polypyrrole. The oxidation and reduction peaks of p-doped poly(3-methylthiophene) conducting polymer films occur at ~1.1 V and ~0.45 V respectively and peak shift are observed, which could be attributed to the size of the dopant ions. The larger sized dopant ions have lower mobility in the electrolyte resulting in shift of oxidation/reduction peaks towards higher/lower potential. The redox response i.e., position of oxidation/reduction peaks of the conducting polymer films remains unchanged upon SHI irradiation. However there is increase in peak current values, which could be attributed to the increased conductivity of the polymer films upon SHI irradiation.

**3.** The conducting polymer films show change of colour with the applied electric field i.e., electrochromism, which is beautifully observed in the cyclic voltammetry. The bottle-green colour of reduced polyaniline films changes into dark green on oxidation in the forward sweep of potential and turns back to bottle-green in the reverse sweep on reduction. In the case of polypyrrole conducting polymer films, deep brown coloured reduced films turn blackish on oxidation and regain the deep brown colour on reduction in the forward and reverse sweep of potential respectively. The deep violet coloured poly(3-methylthiophene) reduced films on oxidation become black on oxidation, which again become deep violet on reduction in the reverse sweep of potential. The electrochromism of the conducting polymer films could be attributed to the change of the band gap of the conducting polymer films on oxidation/reduction.

**4.** The dc conductivity of the conducting polymer films has been observed to be dependent on the type of dopant ions, which could be explained in terms of electron affinities of the dopant ions. The highest conductivity of polyaniline conducting polymer film obtained for perchloric acid ($HClO_4$) dopant is ~78 S/cm, which increases to ~124S/cm upon SHI irradiation (120 MeV $Si^{9+}$ion, $3x10^{12}$ ions/$cm^2$). The $[CH_3(CH_2)_3]_4NBF_4$ doped polypyrrole exhibits conductivity of ~112 S/cm, which upon SHI irradiation (160 MeV $Ni^{12+}$ion,

$3x10^{12}$ ions/cm$^2$) increases to ~177 S/cm. The $LiClO_4$ doped poly(3-methylthiophene) shows highest conductivity of ~120 S/cm, which increases to ~198 S/cm upon SHI irradiation (120 MeV $Si^{9+}$ ion, $3x10^{12}$ ions/cm$^2$). The enhancement of dc conductivity upon SHI irradiation could be attributed to electronic stopping of the irradiated beam in the polymer, which creates large number of active chemical species, cations, anions, radicals and electrons along the ion track. Cross-linking of polymer chains upon SHI irradiation also decreases the resistance of the polymer films as the charge carriers can move from one chain to another through the cross-links, which otherwise takes place by inter-chain hopping resulting in high resistance. The redox peak height i.e., the magnitude of oxidation and reduction currents in cyclic voltammograms is increased in the SHI irradiated conducting polymer films, which could be attributed to the increase in the conductivity of polymer films after SHI irradiation as other experimental conditions of cyclic voltammetry are kept exactly the same as for the unirradiated polymer films.

**5.** The scanning electron microscopy of the conducting polymer films shows that the potentiodynamic polymerization method produced polymer films with better surface morphology as compared to those by the potentiostatic method. This could be attributed to the fact that monomer has higher oxidation potential than that of dimer and dimer has higher oxidation potential than that of the trimer and so on. In the potentiostatic mode the polymerization process nucleates at the monomer sites at the applied potential and dimers, trimers etc. don't grow further due to the unfavourable potential resulting in the haphazard growth due to preferential oxidation at monomer sites giving rise to rough, flaky and porous morphology. In the potentiodynamic method since the potential keeps changing and in the process becomes equal to the oxidation potentials of monomer, dimer, trimer etc., the polymerization and growth processes occur at all, monomer, dimer, trimer etc., sites steadily making the polymer film uniform, dense, smooth and less porous. Grain growth and densification of the polymer film surface have been observed upon SHI irradiation. The improvement observed in the morphology of the polymer films upon SHI

irradiation could be ascribed to the huge energy transfer due to electronic stopping mechanism and displacement of the polymer chains from hilly to valley regions under the impact of the huge energy transfer by incident swift heavy ions making the polymer films more uniform, denser and less porous.

**6.** The conductivity of the polymer films depend on the band gap i.e., $\pi-\pi^*$ transition as observed in the UV-Vis spectra. The polymer absorbing at higher wavelength in the UV-Vis spectra (i.e., lower band gap) shows better conductivity. It can be inferred that a conducting polymer film, which shows absorption in the higher wavelength region in the UV-Vis spectroscopy will have higher dc conductivity. The UV-Vis spectra of SHI irradiated conducting polymer films exhibited increase in carrier absorption intensities with slight shift of absorption peaks towards higher wavelength indicating lowering of band gap and increase in electrical conductivity. The decrease of band gap in conducting polymer occurs due to broadening of polaron/bipolaron band, which is attributed to the increase in carrier concentration in the polymer films as large number of cations, anions, radicals and charged particles are created upon SHI irradiation.

**7.** The dopant ion interaction absorption peaks, viz. C-Cl in HCl doped polyaniline, S=O in $H_2SO_4$ doped polyaniline and $LiCF_3SO_3$ doped polypyrrole and poly(3-methylthiophene), in the FTIR spectra of the conducting polymer films confirmed the presence of the dopants in the polymer films deposited by electrochemical polymerization. The presence of dopant ions after irradiation has also been confirmed from the FTIR spectra of the conducting polymer films after irradiation. The decrease of intensity of C-H twisting vibration absorption in polyaniline, decrease of N-H bending vibration absorption in polypyrrole and decrease of C-H stretching absorption of methyl groups in poly(3-methylthiophene) conducting polymer films have been observed, which could be attributed to the loss of hydrogen atoms upon SHI irradiation where the possible cross-linking of the conducting polymer chains occurs.

**8.** The XRD patterns of the unirradiated conducting polymer films show semi-crystalline nature of the conducting polymer films. The degree of

crystallinity has been observed to increase with the increase in fluence upon SHI irradiation. Besides degree of crystallinity, SHI irradiation causes enhancement in properties such as electrical conductivity and stability of conducting polymer films. This could be attributed to the cross-linking induced by deposition of huge amount of energy in the polymer by electronic stopping process. The degree of crystallinity of the conducting polymer films also largely affects the electronic conductivity, which is observed in the X-Ray diffraction and conductivity studies. The polymer with higher degree of crystallinity shows higher conductivity. More crystalline polymer morphology, i.e., increased cross-linking of the polymer chain after SHI irradiation facilitates the conduction of electrons between polymer chains resulting in the increased conductivity. The XRD patterns of the poly(3-methylthiophene) show semi-crystalline nature with less degree of crystallinity as compared to polyaniline and polypyrrole. Up on SHI irradiation up to 75% increase in crystallinity has been observed and also the loss of the methyl group is predicted from the FTIR spectroscopy, which leads to the conjecture that possibly steric hindrance due to the presence of the methyl group attached to the thiophene ring forbids systematic linear arrangement of the poly(3-methylthiophene) polymer chains making the unirradiated poly(3-methylthiophene) conducting polymer films more amorphous.

**9.** Type I (same p-doped), type II (different p-doped) and type III (same p and n-doped conducting polymer electrodes on either side) solid state all-polymer redox supercapacitors have been fabricated successfully using electrochemically deposited unirradiated and irradiated polyaniline, polypyrrole and poly(3-methylthiophene) films as electrodes and PVDF-HFP(20w/o)-PMMA(10w/o)-$LiCF_3SO_3$(10w/o)-PC+DEC(57w/o)-$SiO_2$(3w/o) gel polymer electrolyte. All the devices show capacitive behaviour with large value of capacitance on the order of 150-250 F/gm and Coulombic efficiency of about 90%. The cyclic voltammetry studies carried out on all the supercapacitors show cyclic voltammograms of nearly ideal rectangular shape at lower scan rates. However, at higher scan rates (~100 mV/Sec), the shapes of the cyclic

voltammogram deviate from the rectangular shape and an increase in current towards higher potential is observed. This is attributed to the redox property of the conducting polymer electrodes that get oxidized and consequently a rise in current in the cyclic voltammogram occurs resulting in the deviation of the voltammograms from the ideal capacitive structure.

**10.** Stability tests up to 10,000 charge-discharge cycles have been carried out on all the supercapacitors. Supercapacitors fabricated by using SHI irradiated conducting polymer films show similar (slightly less) capacitance and Coulombic efficiency but show markedly improved electrochemical stability. The internal resistance of the all solid polymer redox supercapacitors calculated from the charge-discharge plots shows smaller values. A very small decrease in internal resistance of the supercapacitors is found after SHI irradiation, which could be attributed to the increase of conductivity of the polymer electrodes after irradiation but the decrease is not as much as the increase obtained in conductivity. From this it can be inferred that the internal resistance mostly arises due to the interfacial resistance of the electrode and electrolyte contact, which depends on the surface morphologies of electrodes and electrolyte. The initial sharp decrease of capacitance with the unirradiated electrodes could be attributed to the charge consumption or loss due to irreversible faradic reactions with loosely bound volatile surface groups e.g., $OH^-$ $CN^-$, $CH_3^+$ etc. on the electrode surface, which initially contribute to charge storage at the electrode/electrolyte interface. The loosely bound volatile surface groups are stabilized or removed upon SHI irradiation leading to markedly less decrease of capacitance during initial charge-discharge cycles. Upon SHI irradiation, possible surface modifications due to cross-linking induced by huge electronic energy loss mechanism and decrease in the concentration of loosely bound surface groups on the electrode surface, which decreases with the increase of fluence, result in the decreased value of capacitance with the increase of fluence of SHI irradiation.

**11.** A decrease in total charge-discharge time has been observed for supercapacitors with SHI irradiated electrodes. This may be attributed to the

increase in conductivity of the polymer electrodes after SHI irradiation, which gives rise to faster charging and discharging of the supercapacitors. Highest energy density ~ 76 Wh/kg has been obtained for the type III supercapacitors with p and n-doped poly(3-methylthiophene) electrodes, which exhibit a working potential of ~3 V. The highest capacitance (~250 F/gm) has been obtained for type I supercapacitor with $CH_3(CH_2)_3]_4NBF_4$ doped poly(3-methylthiophene) electrodes even though its working potential is quite low ~ 0.6 V.

**Future scope of the work:**

Conducting polymers as novel electronic materials have tremendous scope of both fundamental and applied research. The conduction mechanism and effects of different dopants on the conduction process in conducting polymers are far from being fully understood. Solid state energy storage devices with higher power and energy densities possess tremendous potential for applications in transport and industrial sectors. Research in the field of conducting polymer based solid state supercapacitors holds tremendous future prospects for further improvement in the capacitance values and working potential range for higher energy density and to reduce the internal resistance of the devices for higher power density. Irradiation with swift heavy ion beams has become an integral part of numerous surface processing schemes and in the modification of surface layers of solids. Recently there has been a spurt of interest in high energy ion irradiation of polymers and other insulating materials. Swift heavy ion irradiation of conducting polymer films with different ion beams having different energies and fluences needs further studies for investigation of the effects of SHI irradiation on polymeric materials.

# REFERENCES


1. Y. Long, Z. Chen N. Wang, Y. Ma, Z. Zhang, L. Zhang and M. Wan, *Appl. Phys. Lett.*, **83** (2003) 1863.
2. K. Gurunathan, A.V. Murugan, R. Marimuthu, U.P. Mulik and D.P. Amalnerkar, *Mater. Chem. Phys.* **61** (1999) 173.
3. M. Winter and R.J. Brodd, *Chem. Rev.* **104** (2004) 4245.
4. D. Belanger, X. Ren, J. Davey, F. Uribe and S. Gottesfeld, *J. Electrochem. Soc.*, **147** (2000) 2923.
5. C. Sanchez and F. Ribot, *New J. Chem.* **18** (1994) 1007.
6. B. Ballarina, C. Zanardib, L. Schenettib, R. Seeberb and J.L. H. H. de Cisneros, *Synth. Metals* **139** (2003) 29.
7. P. Somani, A.B. Mandale and S. Radhakrishnan, *Acta Mater.* **48** (2000) 2859.
8. R. Jiang and D. Chu, *J. Electroanal. Chem.*, **527** (2002) 137.
9. P. Quan, Le T. Duan, C.X. Quang and P.H. Viet, *Analytical Sciences* **17** (2001) i749.
10. C.M.A. Brett and C. Thiemann, J. Electroanal. Chem. **538-539** (2002) 215.
11. J. Choi, J. Homes and P.K. Kahol, *Appl. Phys. Lett.*, **83** (2003) 2288.
12. H.H.S. Javadi, K.R. Cromack, A.G. MacDiarmid and A.J. Epstein, *Phys. Rev. B*, **39** (1989) 3579.
13. H. Letheby, *J. Chem. Soc.*, **15** (1862) 161.
14. D.M. Mohilner, R.N. Adams and W.J. Argersinger, Jr. *J. Am. Chem. Soc.*, **84** (1962) 3618.
15. A.F. Diaz and J.A. Logan, *J. Electroanal. Chem.*, **111** (1980) 111.
16. A. Dall'Olio, G. Dascola, V. Varacca and V. Bocchi *Compt. Rend. C*, **267** (1968) 433.
17. L. Gilchrist, *J. Phys. Chem.*, **8** (1904) 539.
18. A.G. Green and A.E. Woodhead, *Trans. Roy. Soc.*, **97** (1910) 2388.

19. T. Ohsaka, Y. Ohnuki, N. Oyama, G. Katagiri and K. Kamisako, *J. Electroanal. Chem.*, **161** (1984) 399.
20. R. Noufi, A.J. Nozik, J. White and L.F. Warren, *J. Electrochem. Soc.*, **129** (1982) 2261.
21. T. Kobayashi, H. Yonetama and H. Tamura, *J. Electroanal. Chem.*, **161** (1984) 419.
22. R. de Surville, M. Jozefowicz, L.T. Yu, J. Perichon and R. Buvet, *Electrochim. Acta*, **13** (1968) 1451.
23. A. Kitani, M. Kaya and K. Sasaki, *J Electrochem. Soc.*, **133** (1986)1069.
24. A.G. MacDiarmid, S.L. Mu, N.L.D. Somasiri and W.Q. Wu, *Mol. Cryst. Liq. Cryst.*, **121** (1985) 187.
25. T. Kobayashi, H. Yonetama and H. Tamura, *J Electroanal. Chem.*, **177** (1984) 281.
26. E.M. Genies, A.A. Syed and C. Tsintavis, *Mol. Cryst. Liq. Cryst.*, **121** (1985) 181.
27. A.F. Diaz, K.K. Kanazawa and G.P. Gardini, *J. Chem. Soc., Chem. Commun.* (1979) 635.
28. A.F. Diaz, A. Martinez, K.K. Kanazawa and M. Salmon, *J. Electroanal. Chem.*, **130** (1981) 181.
29. J. L. Bredas, R. R. Chance and R. Silbey, *Phys. Rev. B.*, **26** (1982) 5843.
30. J. L. Bredas and G. B. Street, *Acc. Chem. Res.*, **18** (1985) 309.
31. A.I. Nazzal, G.B. Street and K.J. Wynne, *Mol. Cryst. Liq. Cryst.*, **125** (1985) 303.
32. A.F. Diaz and B. Hall, *IBM J. Res. Dev.*, **27** (1983) 342.
33. H. Shigi, M. Kishimoto, H. Yakabe, B. Deore and T. Nagaoka, *Analytical Sciences*, **18** (2002) 41.
34. K.K. Kanazawa, A.F. Diaz, W.D. Gill, P.M. Grant, G.B. Street, G.P. Gardini and J.F. Kwak, *Synth. Metals*, **1** (1979/80) 329.
35. A.F. Diaz, J. Castillo, K.K. Kanazawa, J.A. Logan, M. Salmon and O. Fajardo, *J. Electroanal. Chem.*, **133** (1982) 233.
36. V. Meyer, *Chem. Ber.*, **16** (1883) 1465.

37. K. Fredenhagen, *J. Phys. Chem.*, **164** (1933) 176.
38. J. Bruce, F. Challenger, H.B. Gibson and W.E. Allenby, *J. Inst. Petrol.*, **34** (1948) 226.
39. M. Armour, A.G. Davies, J. Upadhyay and A. Wassermann, *J. Polym. Sci. Polym. Chem.*, **5** (1967) 1527.
40. S.L. Meisel, G.C. Johnson and H.D. Hartough, *J. Am. Chem. Soc.*, **72** (1950) 1910.
41. P. Kovacic and K.N. McFarland, *J. Polym. Sci. Polym. Chem.*, **17** (1979) 1963.
42. T. Yamamoto, K. Sanechika and Y. Yamamoto, *J. Polym. Sci. Polym. Lett.*, **18** (1980) 9.
43. O. Inganas, B. Liedberg, W. Chang-ru and H. Wynberg, *Synth. Metals*, **11** (1985) 239.
44. G. Zotti and G. Schiavon, *J. Electroanal. Chem.*, **163** (1984) 385.
45. S. Hotta, T. Hosakam and W. Shimotsuma, *Synth. Metals*, **80** (1984) 954.
46. K.-Y. Jen, G.G. Miller and R.L. Elsenbaumer, *J. Chem. Soc. Chem. Commun.*, 1986, 1346.
47. G. Tourillon and F. Garnier, *J. Electrochem. Soc.*, **130** (1983) 2042.
48. G. Touillon, D. Gourier, P. Garnier and D. Vivien, *J. Phys. Chem.*, **88** (1984) 1049.
49. G. P. Evans, *Advances in Electrochemical Science and Engineering*, Vol. 1, Cambridge Life Science, Cambridge, 1990.
50. R. Qian and J. Qiu, *Polym. J.*, **19** (1987) 157.
51. J. Roncali, F. Garnier, M. Lemaire and R. Garreau, *Synth. Met.*, **15** (1986) 323.
52. A. J. Bard and L. R. Faulkenr, *Electrochemical Metods*, John Wiley, New York, 1980.
53. P.G. deGennes, *Macromolecules*, **14** (1981) 1637.
54. H. Dahms, *J. Phys. Chem.*, **72** (1968) 362.
55. I. Ruff and V. J. Friedrich, *J. Phys. Chem.*, **75** (1971) 3297.
56. I. Ruff, V. J. Friedrich, K. Demeter and K. Csillag, *J. Phys. Chem.*, **75** (1971) 3303.

57. I. Ruff and V. J. Friedrich, *J. Phys. Chem.* **76** (1972) 162.

58. I. Ruff and V. J. Friedrich, *J. Phys. Chem.* **76** (1972)2957.

59. A.G. MacDiarmid and A.J. Heeger, *Synth. Metals,* **1** (1979/80) 101.

60. C.K. Chiang, C.R. Fincher Jr., Y.W.Park, A.J. Heeger, H. Shirakawa, E.J. Louis, A.G. MacDiarmid, *Phys. Rev. Lett.,* **39** (1977) 1098.

61. C.K. Chiang, M.A. Dury, S.C. Gau, A.J. Heeger, E.J. Louis, A.G. MacDiarmid, *J. Am. Chem. Soc.,* **100** (1978)1013.

62. P.J. Nigrey, A.G. MacDiarmid, A.J. Heeger, *J. Chem. Soc., Chem. Commun.,* (1979) 594.

63. D.MacInnes Jr., M.A. Druy, P.J. Nigrey, D.P. Nairns, A.G. MacDiarmid, A.J. Heeger, *J. Chem. Soc., Chem. Commun.,* (1981) 317.

64. A.J. Heeger, S. Kivelson, J.R. Schrieffer and W.-P. Su, *Rev. Mod. Phys.,* **60** (1988) 781.

65. K.E. Ziemelis, A.T. Hussain, D.D.C. Bradley, R.H. Friend, J. Rilhe and G. Wegner, *Phys. Rev. Lett.,* **66** (1991) 2231.

66. J.H. Burroughes, C.A. Jones and R.H. Friend, *Nature,* **335** (1988) 137.

67. J.H. Burroughes, D.D.C. Bradley, A.R. Brown, R.N. Marks and R.H. Friend, *Nature,* **347** (1990) 539.

68. A.G. MacDiarmid, *Synth. Metals,* **125** (2002) 11.

69. J.C. Chiang, A.G. MacDiarmid, *Synth. Metals,* **13** (1986) 193.

70. A.G. MacDiarmid, J.C. Chiang, A.F. Richter, A.J. Epstein, *Synth. Metals,* **18** (1987) 285.

71. Z.S. Tong, M.Z. Wu, T.S. Pu, F. Zhou and H.Z. Liu, *Synth. Metals,* **68** (1995) 125.

72. C.S. Wang, C.Y.-C. Lee and F.E. Arnold, "Mechanical and Electrical Properties of Heat-Treated Ladder Polymer Fiber", p-747 in L.Y. Chiang, A.F. Garito, D.J. Sandman (eds.), *Mat. Res. Soc. Symp. Proc.,* **247***: Electrical, Optical and Magnetic Properties of Organic Solid State Materials,* Materials Research Society, Pittsburgh, Pennsylvania, USA (1992).

73. E.H. Lee, Y. Lee, W.C. Oliver and L.K. Mansur, *J. Mater. Res.* **8** (1993) 377.

74. J.C. Pivin, *Thin Solid Films,* **263** (1995) 185.

75. M.V. Swain, A.J. Perry, J.R. Treglio and E.D. Demaree, *J. Mater. Res.* **12** (1997) 1917.

76. J. Dfavenas, X.L. Xu, M. Maitrot, C. Mathis and B. Franconis *Nucl. Instr. and Meth. B,* 32 (1988) 166.

77. J.-L. Zhu, Z.-M. Liu, Z.-W. Yu, Y.-P. Guo, Z.-T. Ma and R.-Z. Beng, *Nucl. Instr. and Meth. B,* **91** (1994) 469.

78. Y.Q. Wang, R.E. Giedd, M.G. Moss and J. Kauffmann, *Nucl. Instr. and Meth. B,* **127/128** (1997) 710.

79. A. Charlesby, *J. Polym. Sci.,* **10** (1953) 201; **11** (1953) 513; **11** (1953) 521.

80. A. Chapiro, *J. Chem. Phys.,* **51** (1954) 165; **52** (1955) 246; **53** (1956) 295; *Proc. Royal. Soc.* **215A** (1952) 187.

81. T. Venkatesan, L. Calcagno, B.S. Elman and G. Foti, *Beam Mod. Of Materials,* **Vol-2** (Elsevier Amsterdam, 1987) 301.

82. T.A. Scotheim (ed.) *Handbook of Cond. Polym.* Vol-1 and 2 (Dekker, NY, 1986).

83. H. Naarmann and N. Theophilou, *Synth. Met.,* **22** (1987) 1.

84. T. Venkatesan, *Nucl. Instr. and Meth.B* 7 (1985) 461.

85. M.S. Dresselhaus, B. Wasserman and G.E. Wnek, *Mater. Res. Soc. Symp. Proc.* **27** (1984) 413.

86. W.L. Brown, *Nucl. Instr. and Meth. B* **37/38** (1990) 270.

87. G. Maletta, *Nucl. Instr. and Meth. B* **46** (1990) 295.

88. J. Davenas, G. Boiteux, X.L. Xu and E. Adem, *Nucl. Instr. and Meth. B* **32** (1988) 136.

89. D.C. Weber, P. Brandt and C.A. Carosella, *Proc. Mat. Res. Soc.Symp. On Metastable Materials Formation by Ion Implantation.* **Vol-7** (North Holland, NY, 1982) 167.

90. J. Davenas, C. Dupuy, X.L. Xu, M. Maitrot, J.J. Andre and B. Franconis, *Radiation Effect* **74** (1983) 209.

91. J. Dfavenas, X.L. Xu, M. Maitrot, C. Mathis and B. Franconis *Nucl. Instr. and Meth. B* **32** (1988) 166.

92. S.H. Lin, K.L. Sheng, T.W. Rong, J.R. Rao, W.M. Wang, H.H. Wan, Z.Y. Zhou,X.F. Zhu and F.J. Yang, *Nucl. Instr. and Meth. B* **59/60** (1991) 1257.
93. H.K. Hu, J.A. Schultz and J.W. Rabalais, *J. Phys. Chem.* **86** (1982) 3364.
94. S. Lin, K. Sneg, J. Bao, T. Rong, Z. Zhou, L. Zhang, D. Zhu, Z. Shen and M. Yang, *Nucl. Instr. and Meth._B* **39** (1989) 778.
95. T. Wada, A. Takeno, M. Iwaki, H. Sasabe and Y. Kobayashi, *J. Chem. Soc. Commun.*_(1985) 1194.
96. N. Koshida and Y. Suzuki, *J. Appl. Phys.*, **61** (1987) 5488.
97. N. Koshida, Y. Suzuki and T. Aoyama, *Nucl. Instr. and Meth.B* **37/38** (1989) 708.
98. A. Das, S. Dhara and A. Patnaik, *Proceedings of the Solid State Physics Symp.* **42** (1999) 621.
99. S. Schiestel, W. Ensinger and G.K. Wolf, *Nucl. Instr. and Meth. B* **91** (1994) 473.
100. A.L. Evelyn, D. Ila, R.L. Zimmerman, K. Bhat, D.B. Poker and D.K. Hensley, *Nucl. Instr. and Meth._B* **127/128** (1997) 694.
101. B.E. Conway, V. Briss, and J. Wojtowicz, *J. Power Sources* **66** (1997) 1.
102. H.E. Becker (General Electric) *US Patent No. 2 800 616* (1957).
103. I.D. Raistick and R.A.Huggins, *Mater. Res. Bull.* **18** (1983) 337.
104. R. Kotz, and M. Carlen, *Electrochim. Acta,* **45** (1999) 2483.
105. D.C. Grahame, *Chem. Rev.*, **47** (1947) 441.
106. G. Gouy, *Ann. Phys.* **7** (1917) 183.
107. J.C. Currie in *Chem. And Phys. Of Composite Media,* Vol-85-5 eds.: M. Tomkiewicz and P.N. Sen, The Electrochemical Society, Pennington, NJ, USA. 1985 p.174.
108. A.F. Burke, Testing of ultracapacitors for electric vehicle applications, *Proc. 3rd Int. Seminar Double Layer Capacitors,* eds. S.P. Wolsky and N. Marincic, FL, USA, 1993, paper No.2.
109. J.W. Schultze and E. Koppitz, *Electrochim. Acta,* **21** (1976) 327.
110. J.W. Schultze and E. Koppitz, *Electrochim. Acta,* **21** (1976) 337.
111. P. Delahay, *J. Electroanal. Chem.*, **16** (1968) 131.

112. P. Delahay, *J. Phys. Chem.*, **70** (1966) 2373.

113. P. Delahay, *J. Phys. Chem.*, **71** (1967) 3360.

114. A. Rudge, I. Raistrick, S. Gottesfeld and J.P. Ferrarist, *Electrochim. Acta,* **39** (1994) 273.

115. A. Rudge, J.Davey, I. Raistrick, S. Gottesfeld and J.P. Ferrarist, *J. Power Sources,* **47** (1994) 89.

116. A.F. Diaz, J.F. Rubinson and H.B. Mark, *Adv. Polym. Sci.*, **84** (1988) 113.

117. G.P. Evans, *Advances in Electrochemical Science and Engineering (H. Gerischer and C.W. Tobias, eds.), Molecular Design of Electrode Surfaces*, J.Wley, New York, 1992.

118. I. Rubinstein, J. Risphon and S. Gottesfeld, *J. Electrochem. Soc.,* **134**(1987) 3087.

119. J. Tanguy, N. Mermilliod and M. Hoclet, *J. Electrochem. Soc.*, **134** (1987) 795.

120. P. Fiordiponti and G. Pistoia, *Electrochim. Acta,* **34** (1989) 215.

121. M. Kalaji and L.M. Peter, *J. Chem. Soc. Faraday Trans.* **87** (1991) 853.

122. S.W. Feldberg *J. Am. Chem. Soc.*, **106** (1984) 4671.

123. E.M. Genies, J.F. Penneau and E. Vieil, *J. Eletroanal. Chem.*, **283** (1993) 205.

124. T. Kobayashi, H. Yoneyama and H. Tamura, *J. Eletroanal. Chem.*, **177** (1984) 281.

125. C.M. Carlin, L.J. Kepley and A.J. Bard, *J. Electrochem. Soc.* **132** (1986) 353.

126. R.C.M. Jacobs, L.J.J. Janssen and E. Barendrecht, *Recl. Trav. Chim. Pays-Bas,* **103**(1984) 275.

127. N. Mermilliod, J. Tanguy, M. Hoclet and A.A. Syed, *Synth. Met.* **18** (1987) 359.

128. G. Inzlet and G. Horányi, *J. Electroanal. Chem.*, **230** (1987) 757.

129. G. Horányi and G. Inzlet, *Electrochim. Acta,* **33** (1988) 947.

130. G. Horányi and G. Inzlet, *J. Electroanal. Chem.*, **257** (1988) 311.

131. G. Inzlet and G. Horányi, *J. Electrochem. Soc.*, **136** (1989) 1747.

132. G. Horányi and G. Inzlet, *J. Electroanal. Chem.*, **264** (1989) 259.

133. V.E. Kazarinov, V.N. Andreev, M. A.Spytsin and A.V. Shlepakov, *Electrocim. Acta,* **35** (1990) 899.

134. C. Deslouis, M.M. Musiani and B. Tribollet, *J. Electroanal. Chem.*, **264** (1989)37, 57.

135. M. Kalaji, L.M. Peter, L.M. Abrantes and J.C. Mesquita, *J. Electroanal. Chem.*, **274**(1989) 289.

136. M. Kalaji, L. Nyholm and L.M. Peter, *J. Electroanal. Chem.*, **313** (1991) 271.

137. C.P. Andrieux, P. Audebert, P. Hapiot, M. Nechtschein and C. Odin, *J. Electroanal. Chem.*, **305** (1991) 153.

138. J.C. Lacroix, K.K. Kanazawa and A. Diaz, *J. Electrochem. Soc.*, **136** (1989) 1308.

139. G. Inzelt, *J. Electroanal. Chem.*, **279** (1990) 169.

140. S.H. Glarum and J.H. Marshall, *J. Electrochem. Soc.*, **134** (1987)142.

141. A.M. Waller and R.G. Compton, *J. Chem. Soc. Faraday Trans.*, **85** (1989) 977.

142. J.H. Kaufman, K.K. Kanazawa and J.B. Street, *Phys. Rev. Lett.*, **53** (1984) 2461.

143. S.H. Glarum and J.H. Marshall, *J. Electrochem. Soc.*, **134** (1987)2160.

144. M. Kaya, A. Kitani and K. Sasaki, *Chem. Lett. Chem. Soc. Japan*, **147** (1986).

145. J.C. Scott, P. Pfluger, M.T. Krounbi and G.B. Street, *Phys. Rev.* **B28** (1983) 2140.

146. M.E. Jozefowicz, R. Laversanne, H.H.S. Javadi, A.J. Epstein, J.P. Pouget, X. Tang and A.G. MacDiarmid, *Phys. Rev.* **B39** (1989) 12958.

147. J.M. Ginden, A.J. Epstein and A.G. MacDiarmid, *Solid State Commun.* **72** (1989) 987.

148. A.G. MacDiarmid and A.J. Epstein, *Faraday Discuss. Chem. Soc.*, **88** (1989) 317.

149. W.J. Albery, Z. Chen, B.R. Horrocks, A.R. Mount, P.J. Wilson, D. Bloor, A.T. Monkman and C.M. Elliot, *Faraday Discuss. Chem. Soc.* **88** (1989) 247.

150. M. Fujihira, *Topics in Organic Electrochemistry* (A.J. Fry and W.E. Britton, eds), Plenum Press, New York, 1986, p.255.

151. T.A. Skotheim (ed.), *Handbook of Conducting polymers*, Vols. 1 and 2, Marcel Dekker, New York, 1986.

152. J.-L. Bredas and G.B. Street, *Acc. Chem. Res.*, **18** (1985) 309.

153. E.M. Geniés and M. Lapkowski, *J. Electroanal. Chem.*, **236** (1987)199.

154. E.M. Geniés and M. Lapkowski, *Synth. Met.*, **24** (1988) 61.

155. W.-S. Huang, B.D. Humphrey and A.G. MacDiarmid, *J. Chem. Soc. Faraday Trans.*, **82** (1986) 2385.

156. B. Villeret and M. Nechstein, *Phys. Rev. Lett.* **63** (1989) 1285.

157. M. Lapkowski and E. M.Geniés, *J. Electroanal. Chem.*, **279** (1990) 157.

158. F. Genoud, M. Guglielmi, M. Nechstein, E.M. Geniés and M. Salmon, *Phys. Rev. Lett.*, **55** (1985)118.

159. M. Nechstein, F. Devreux, F. Genoud, E. Vieli, J.M. Pernaut and E.M. Geniés, *Synth. Met.*, **15** (1986) 59.

160. W.J. Albery, C.M. Elliot and A.R. Mount, *J. Electroanal. Chem.*, **288** (1990)15;

161. W.J. Albery, and A.R. Mount, *J. Electroanal. Chem.*, **305** (1991) 3.

162. F. Li and W.J. Albery, *J. Chem. Soc. Faraday Trans.*, **87** (1991) 2949.

163. M.E.G. Lyons, *Faraday Discuss. Chem. Soc.*, **88** (1989) 291.

164. M. Kalaji, L.M. Peter, L.M. Abrantes and J.C. Mesquita, *J. Electroanal. Chem.*, **274**(1989) 289.

165. S. Gottesfeld, A. Redondo, I. Rubinstein and S.W. Feldberg, *J. Electroanal. Chem.*, **265** (1989) 15.

166. K. Aoki, *J. Electroanal. Chem.*, **310** (1991) 1.

167. G. Inzelt and G. Horányi, *J. Electroanal. Chem.*, **230** (1987) 257.

168. C. P. Andrieux and J. M. Savéant, *J. Electroanal. Chem.* **111** (1980)377.

169. E. Laviron *J. Electroanal. Chem.* **112** (1980) 1.

170. P. J. Peerce and A. J. Bard, *J. Electroanal. Chem.* **114** (1980) 89.

171. F. B. Kaufman and E. M. Engler *J. Am. Chem. Soc.* **101,** (1979) 547.

172. L. Botár and I.. Ruff, *Chem. Phys. Lett.*, **126** (1986), 348.

173. I.. Ruff and L. Botár, *J. Chem. Phys.*, **83** (1985), 1292.

174. R.P. Buck, *J. Electroanal. Chem.*, **243** (1988), 279.

175. R.P. Buck, *J. Phys. Chem.*, **92** (1988) 4196.

176. P. He and X. Chen, *J. Electroanal. Chem.*, **256** (1988) 353.

177. I. Fritsch-Faules and L.R. Faulkner, *J. Electroanal. Chem.*, **263** (1988), 237.

178. S.W. Feldberg, *J. Electroanal. Chem.*, **198** (1986), 1.

179. J.R. Miller and J. Beitz, *J. Chem. Phys.*, **78** (1981) 6746.

180. J.R. Miller, K.W. Hartman and S. Abrash, *J. Am. Chem. Soc.*, **104** (1982) 4296.

181. R.K. Huddleston and J.R. Miller, *J. Chem. Phys.*, **79** (1982) 5337.

182. E. Leiva, P. Meyer and W. Schmickler, *J. Electrochem. Soc.* **135** (1988) 1993.

183. C.P. Andrieux and J.M. Savéant, *J. Phys. Chem.*, **92** (1988) 6761.

184. J.M. Savéant, *J. Electroanal. Chem.*, **242** (1988) 1.

185. F.C. Anson, D.N. Blauch, J.M Savéant and C.-F. Shu, *J. Am.Chem. Soc.* **113** (1991) 1922.

186. L. Srinivasa Mohan and M.V. Sangaranarayanan, *J. Electroanal. Chem.*, **323** (1992) 375.

187. D.N. Blauch and J.M. Savéant, *J. Am. Chem. Soc.*, **114** (1992) 3323.

188. D. M. Rück, *Nucl. Instr. and Meth. B* **166/167** (2000) 602.

189. T. Venkatesan, *Nucl. Instr. and Meth. B* **7/8** (1985) 461.

190. E. Balanzat, S. Bouffard, A. Le Moël and N. Betz, *Nucl. Instr. and Meth. B* **91** (1994) 140.

191. V. N. Popok, V. B. Odzhaev, I. P. Kozlov, I. I. Azarko, I. A. Karpovich and D. V. Sviridov, *Nucl. Instr. and Meth. B 129* (1997) 60.

192. J. Davenas, I. Stevenson, N. Celette, S. Cambon, J. L. Gardette, A. Rivaton and L. Vignoud, *Nucl. Instr. and Meth. B* **191** (2002) 653.

193. A. Laskarakis, C. Gravalidis and S. Logothetidis, *Nucl. Instr. and Meth. B* **216** (2004) 131.

194. M. Guenther, G. Gerlach, G. Suchaneck, K. Sahre, K. -J. Eichhorn, V. Baturin and S. Duvanov., *Nucl. Instr. and Meth. B* **216** (2004) 143.

195. V. Chailley, E. Balanzat and E. Dooryhee, *Nucl. Instr. and Meth. B* **105** (1995) 110.

196. E. H. Lee, *Nucl. Instr. and Meth. B* **151** (1999) 29.

197. M. Toulemonde, C. Trautmann, E. Balanzat, K. Hjort and A. Weidinger, *Nucl. Instr. and Meth. B* **216** (2004) 1.

198. A. Chatterjee and H.J. Schafer, *Radiat. Environ. Biophys.*, **13** (1973) 479.

199. J.L. Magee and A. Chatterjee, *Radiation Chemistry: Principles and application,* eds: Farhataziz and M.A.J. Rogers, Chapter 1,5 and 6, VCH Publishers, New York, 1987.
200. J.J. Butts and R. Katz, *Radiation Research,* **30** (1967) 855.
201. M.P.R. Waligorski, R.N. Hamm and R. Katz, *Nucl. Tracks Radiat. Meas.,* **11** (1986) 309.
202. G.D. Zeiss, W.J. Meath, J.C.F. MacDonald and D.J. Dawson, *Radiat. Res.,* **63** (1975) 64.
203. J.D. Hunn and C.P. Chriustensen, *Solid State Technol.,* **37** (1994) 57.
204. E.H. Lee, G.R. Rao, M.B. Lewis and L.K. Mansur, *J. Mater. Res.,* **9** (1994) 1043.
205. M.B. Lewis, E.H. Lee and G.R. Rao, *J. Nucl. Mater.,* **211** (1994) 46.
206. Nishino, A., *Journal of power sources,* vol. 60, pp. 137-147, 1996.
207. Endo, M., Takeda, T., Kim, Y.J., Koshiba, K. and Ishii, K., *Carbon science,* **1** (2001) 117.
208. C.J. Currie (Sohio), *US Patent No. 4 730 239* (1988).
209. B.E. Conway, *Progress in Surface Science,* **16** (1984)1.
210. D. Saikia and A. Kumar, *Euro. Polym. Jour.,* **41** (2005) 563.
211. S. Stever, in C.F. Coombs, edt. *Electronic Instrument Handbook.* McGraw-Hill, New York, (1995) pp13.11-13.14.
212. J.F. Rubinsion and H.B. Mark in *Interfacial Electrochemistry- Theory, Experiments and Applications,* edited by A. Wieckowski, Marcel Dekker Inc. New York (1999).
213. B. E. Conway, and W. G. Pell, *Journal of Power Sources,* **105,** (2002) 196.
214. R.J. Mortimer, *Chem. Soc. Rev.,* **26** (1997) 147.
215. H. Xue, Z. Shen and Y. Li, *Synth. Metals,* **124** (2001) 354.
216. J. Joo and A.J. Epstein, *Appl. Phys. Lett.,* **65** (1994) 2278.
217. A. Mirmohseni and A. Oladegaragoze, *Synth. Metals,* **114** (2000) 105.
218. Y.H. Rho and K. Kanamura, *J. Electroanal. Chem.,* 559 (2003) 69.
219. A.D. Pasquier, A. Laforgue and P. Simon, *Journal of Power Sources,* **125** (2004) 95.

220. H. Karami, M. F. Mousavi and M. Shamsipur, *Journal of Power Sources,* **117** (2003) 255.

221. H. Karami , M. F. Mousavi and M. Shamsipur , *Journal of Power Sources,* **124** (2003) 303.

222. H.H. Rehan, *Journal of Power Sources,* **113** (2003) 57.

223. M. Morita, S. Miyazaki, M. Ishikawa, Y. Matsuda, H. Tajima, K. Adachi, and F. Anan, *Journal of Power Sources,* **54** (1995) 214.

224. M. Mastragostino, C. Arbizzani and F. Soavi, *Solid State Ionics,* **148** (2002) 493.

225. J.D.S. -Smith, C.K. Webber, N. Anderson, A. P. Chafin, K. Zong and J.R. Reynolds, *J. Electrochem. Soc.,* **149** (2002) A973.

226. Y.U. Jeong and A. Manthiram, *J. Electrochem. Soc.,* **149** (2002) A1419.

227. D.W. Hatchett, M. Josowicz and J. Janata, *J. Electrochem. Soc.,* **146** (1999) 4535.

228. P. Novak, K. Muller, K.S.V. Santhanam and O. Hass, *Chem. Rev.,* **97** (1997) 207.

229. J.P. Ferraris, M.M. Eissa, I.D. Brotherson and D.C. Loveday, *Chem. Matter.,* **10** (1998) 3528.

230. Y. Wei, X. Tang, Y. Sun and W.W. Focke, *J. Polym. Sci., Polym. Chem.,* **27** (1989) 2385.

231. K.R. Prasad and N. Munichandraiah, *Synth. Metals,* **126** (2002) 61.

232. K.R. Prasad and N. Munichandraiah, *Synth. Metals,* **130** (2002) 17.

233. W-C. Chen, T-C Wen and A. Gopalan, *Synth. Metals,* **128** (2002) 179.

234. S. das Neves, C.N.P. da Foseca and M.-A. De Paoli, *Synth. Metals,* **89** (1997) 167.

235. N. Ahmed and A.G. MacDiarmid, *Synth. Metas,* **78** (1996) 103.

236. M. Grzeszczuk and P. Poks, *J. Electrochem. Soc.,* **146** (1999) 642.

237. F. Fusalba, P. Gouéree, D. Villers and D. Bélanger, *J. Electrochem. Soc.,* **148** (2001) A1.

238. A.A. Pud, *Synth. Metals,* **66** (1994) 1.

239. M.C. Miras, C. Barbero, R. Kötz and O. Haas, *J. Electrochem. Soc.*, **138** (1991) 335.

240. T. Osaka, T. Nakajima, N. Kaoi and B.B. Owens, *J. Electrochem. Soc.*, **137** (1990) 2139.

241. S. Yonezawa, K. Kanamura and Z.-I. Takehara, *J. Electrochem. Soc.*, **142** (1995) 3309.

242. E. Naudin, P. Gouérec and D. Bélanger, *J. Electrochem. Soc.*, **145** (1998) 1.

243. S. Tawde, D. Mukesh and J.V. Yakhmi, *Synth. Metals*, **125** (2002) 401.

244. L. Lizarraga, E.M. Andrade and F.V. Molina, *J. Electroanal. Chem.*, **561** (2004) 127.

245. L. Wen and N.M. Kocherginsky, *Synth. Metals*, **106** (1999) 19.

246. S. Kaul, S.K. Dhawan and R. Chandra, *Synth. Metals*, **124** (2001) 295.

247. A.B. Samui, A.S. Patankar, R.S. Satpute, and P.C. Deb, *Synth. Metals* **125** (2002) 423.

248. E.S. Matveeva, C.F. Gimenez and M.J.G. Tejera, *Synth. Metals*, **123** (2001) 117.

249. G.B. Blanchet, C.R. Fincher and F. Gao, *Appl. Phys. Lett.*, **82** (2003) 1290.

250. M. Camposy and B. Bello Jr. *J. Phys. D: Appl. Phys.* **30** (1997) 1531

251. M. Karakisàla, M. Sacàak, E. Erdem and U. Akbulut, *J. Appl. Electrochemistry*, **27** (1997) 309.

252. K.H. An, K.K. Jeon, J.K. Heo, S.C. Lim, D.J. Bae and Y.H. Lee, *J. Electrochem. Soc.*, **149** (2002) A1058.

253. C.K. Jeong, J.H. Jung, B.H. Kim, S.Y. Lee, D.E. Lee, S.H. Jang, K.S. Ryu and J. Joo, *Synth. Metal*, **117** (2001) 99.

254. J.E. Albuquerque, L.H.C. Mattoso, D.T. Balogh, R.M. Faria, J.G. Masters and A.G. MacDiarmid, *Synth. Metals*, 113 (2000) 19.

255. F. Yan and G. Xue, *J. Mater. Chem.*, **9** (1999) 3035.

256. R.H. Baughman, *Proc. of Ann. Int. Conf. IEEE Eng. in Medicine and Biology Soc.*, **13** (1991) 1785.

257. M.V. Kulkarni and A.K. Viswanath, *J. Macromol. Sci., Part A – Pure and Applied Chemistry*, **A41**, (2004) 1173.

258. A.M. P. Hussain and A. Kumar, *Bull. Mater. Sci.* **26** (2003) 329.

259. M.G. Han, Y.J. Lee, S.W. Byun and S.S. Im, *Synth. Metals,* **124** (2001) 337.

260. A.L. Schemid, L.M. Lira and S.I.C. Torresi *Electrochim. Acta* **47** (2002) 2005.

261. J.L. Koenig 1999 *Spectroscopy of polymers* (Amsterdam: Elsevier) 2nd ed., D.L. Pavia, G.M. Lampman and G.S. Kriz *Introduction to spectroscopy* (Fort Worth: Harcourt College Publishers) 3rd ed.( 2001).

262. *Handbook of Chemistry and Physics*, R. C. Weast and J. Astle, Ed. CRC Press, Boca Raton, 1978, p 255.

263. K. G. Neoh, M. Y. Pun, E. T. Kang and, K. L. Tan *Synth. Metals*, **73** (1995) 209.

264. E. C. Venancioa, L.H.C. Mattoso and A. J. Motheoa *J. Braz. Chem. Soc.*, **12** (2001) 526.

265. A.A. Athawale, B. Deore, M. Vedpathak, S.K. Kulkarni, *J. Appl. Polym. Sci.* **74** (1999) 1286.

266. M. Shaolin, C. Chuanxiang and S. Yujun, *Chem. J. Internet*, **3** (2001) 036026pe (http://china.chemistrymag.org/cji/2001/036026pe.htm).

267. A. Balamurugan, S. Kannan, V. Selvaraj and S. Rajeswari, *Trends Biomater. Artif. Organs*, **18** (2004) 41.

268. *Applications of Electroactive Polymers* ed. by Bruno Scrosati, Chapman and Hall, London (1993).

269. L.Calcagno and G.Foti, *Nucl. Instr. and Meth.* B19/20 (1987) 895.

270. S. Koul, S.K. Dhawan and R. Chandra, *Synth. Metal,* **124** (2001) 295.

271. J. Liu and M. Wan, *Synth. Metals,* **124** (2001) 317.

272. C.K. Chiang, Y.W. Park, A.J. Heeger, H. Shirakawa, E.J. Louis and A.G. MacDiarmid, *J. Chem. Phys.*, **69** (1978) 5098.

273. Y. Harima, Y. Kunugi, K. Yamashita and M. Shiotani, *Chem. Phys. Lett.*, **317** (2000) 310.

274. M. Zhou, M. Pagels, B. Geschke and J. Heinze, *J. Phys. Chem. B,* **106** (2002) 10065.

275. A. Wanekaya and O.A. Sadik, *J. Electroanal. Chem.*, **537** (2002) 135.

276. C. Petrillo, S. Borra, R. Cagnolati and G. Ruggeri, *J. Chem. Phys.*, **101** (1994) 11004.

277. K. Yakushi, L.J. Lauchlan, T.C. Clarke and G.B. Street, *J. Chem. Phys.*, **79** (1983) 4774.

278. J.L. Toto, T.T. Toto, C.P. de Melo and K.A. Robins, *J. Chem. Phys.*, **102** (1995) 8048.

279. G. Zotti, S. Zecchin, G. Schiavon, B. Vercelli, A. Berlin, E. Dalacanale and L.B. Groenendaal, *Chem. Mater*, **15** (2003) 4642.

280. J.W. Gardner and P.N. Bartlett, *Sensors and Actuators A*, **51** (1995) 57.

281. R.H. Baughman, *Synth. Metals*, **78** (1996) 339.

282. G. Horowitz, *Adv. Mater.*, **10** (1998) 365.

283. M. Su, L. Fu, N. Wu, M. Aslam, and V.P. Dravid, *Appl. Phys. Lett.*, **84** (2004) 828.

284. G.M. Spinks, T.E. Campbell and G.G. Wallace, *Smart Mater. Struct.*, **14** (2005) 406.

285. E.A. Moschou, S.F. Peteu, L.G. Bachas, M.J. Madou and S. Daunert, *Chem. Mater.*, **16** (2004) 2499.

286. Y. Yang and M. Wan, *J. Mater. Chem.*, **11** (2001) 2022.

287. V. Saxena and B.D. Malhotra *Curr. Appl. Phys.*, **3** (2003) 293.

288. F. Zhang, A. Petr, and L. Dunsch, *Appl. Phys. Lett.*, **82 (2003)** 4587.

289. C.D. Dimitrakopoulos, S. Purushothaman, J. Kymissis, A. Callegari and J.M. Shaw, *Science*, **283** (1999) 822.

290. M. Gross, D.C. Müller, H. Nothofer, U.H scherf, D. Neher, C. Bräuchle and K. Meerholz, *Nature* **405** (2000) 661.

291. M.D. Ingrama, H. Staeschea and K.S. Ryder, *Solid State Ionics*, **169** (2004) 51.

292. A.M. White and R.C.T. Slade, *J. Mater. Chem.*, **13** (2003) 1345.

293. A. Malinauskas, J. Malinauskienÿe and A. Ramanavičius, *Nanotechnology* **16** (2005) R51.

294. X. Zhang and R. Bai, *Langmuir*, **19** (2003) 10703.

295. C.O. Yoon, H.K. Sung, J.H. Kim, E. Barsoukov, J.H. Kim and H. Lee, *Synth. Metals,* **99** (1999) 201.

296. C.C. Hu, X.X. Lin, J. Electrochem. Soc. 149 (2002) A1049.

297. L. Qu, G. SHI, J. Yuan, G. Han and F. Chen, *J. Electroanal. Chem.,* **561** (2004) 149.

298. M. Tang, T.-Y. Wen, T.-B. Du, Y.-P. Chen, *Euro. Polym. Jour.,* **39** (2003) 143.

299. M. Bazzaoui, L. Martins, E.A. Bazzaoui, J.I. Martins *J. Electroanal. Chem.,* **537** (2002) 47.

300. A.M.P. Hussain, A. Kumar, D. Saikia, F. Singh and D.K. Avasthi, *Nucl. Instr. and Meth. B* **240(4)** (2005) 871.

301. D.-H. Han, H.J. Lee and S.M. Park, *Electrochim. Acta,* **50** (2005) 3085.

302. M.J. van der Sluijs, A.E. Underhill and B.N. Zaba, *J. Phys. D: Appl. Phys.,* **20** (1987) 1411.

303. J. Chen, C. O. Too, G.G. Wallace and G.F. Swiegers, *Electrochimica Acta,* **49** (2004) 691.

304. M. Karakışla, L. Aksu and M. Saçak, *Polym. Int.,* **51** (2002) 1371.

305. H. Neugebauer, *J. Electroanal. Chem.,* **563** (2004) 253.

306. M.C. Bernard, A.H.L. Goff and W. Zeng, *Electrochimica Acta* **44** (1998)781.

307. M.C. Bernard, S.C. Torresi and A.H.L. Goff, *Electrochimica Acta* **44** (1999)1989.

308. T.M. Hall, A. Wagner and L.F. Thompson, *J. Appl. Phys.,* **53** (1982) 3397.

309. P. Chandrasekhar, *Conducting polymers, Fundamentals and Applications- A practical approach,* Kluwer Academic Publishers, Boston (1999).

310. H.E.A. Huitema, G.H. Gelinck, J.B.P.H. Van der Putten, K.E. Kuijk, C.M. Hart, E. Cantatore, P.T. Herwig, A.J.J.M. van Breemen, D.M. de Leeuw, *Nature,* **414** (2001) 599.

311. Z.L. Li, S.C. Yang, H.F. Meng, Y. S. Chen, Y.Z. Yang, C.H. Liu, S.F. Horng, C.S. Hsu, L.C. Chen, J.P. Hu and R.H. Lee, *Appl. Phys. Lett.,* **84** (2004) 3558.

312. W.U. Huynh, J.J. Dittmer, A.P. Alivisatos, *Science,* **295** (2002) 2425.

313. B. Sun, E. Marx, N.C. Greenham, *Nano Lett.,* **3** (2003) 961.

314. G. Yu, J. Gao, J.C. Hummelen, F. Wudl, A.J. Heeger, *Science* **270** (1995) 1789.

315. A.A. Argun, A. Cirpan, J.R. Reynolds, *Adv. Mater.*, **15** (2003) 1338.

316. D. DeLongchamp, P.T. Hammond, *Adv. Mater.*, **13** (2001) 1455.

317. B. Crone, A. Dodabalapur, Y.-Y. Lin, R.W. Filas, Z. Bao, A. LaDuca, R. Sarpeshkar, H.E. Katz, W. Li, *Nature*, **403** (2000) 521.

318. C.J. Drury, C.M.J. Mutsaers, C.M. Hart, M. Matters, D.M. de Leeuw, *Appl. Phys. Lett.*, **73** (1998) 108.

319. A. Cravino, N.C. Sariciftci, *Nat. Mater.*, **2** (2003) 360.

320. J.R. Bredas, S. Marder, *Adv. Funct. Mater.*, **12** (2002) 555.

321. C. Hagleitner, A. Hierlemann, D. Lange, A. Kummer, N. Kerness, O. Brand, H. Baltes, *Nature*, **414** (2001) 293.

322. G. Chen, Z. Guan, C.T. Chen, L. Fu, V. Sundaresan, F.H. Arnold, *Nat. Biotechnol.*, **15** (1997) 354.

323. T. Nagatomo, O. Omoto, *J. Electrochem. Soc.*, **135** (1988) 2124.

324. A. Laforgue, P. Simon, C. Sarrazin, J.-F. Fauvarque, *J. Power Sources* **80** (1999) 142.

325. F. Tran-Van, M. Carrier and C. Chevrot, *Synth. Metals*, **142** (2004) 251.

326. M. Catellani, S. Luzzati, N.-O. Lupsac, R. Mendichi, R. Consonni, F. Giacalone, J.L. Segura and N. Martin, *Thin Solid Films*, **451/452** (2003) 2.

327. J. Dai, J.L. Sellers and R.E. Noftle, *Synth. Metals*, **139** (2003] 81.

328. N.M. Alpatova, E.V. Ovsyannikova, M.Y. Grosheva, V.V. Topolev, S. Kirchmeyer, F. Joans, V.M. Bazhenov and V.A. Nikanorov, *Synth. Metals*, **138** (2003) 507.

329. C. Roth, S. Hintschich, A.P. Monkman, M. Svensson and R. Anderson, *J. Chem. Phys.*, **116** (2002) 10503.

330. K.E. Aasmundtveit, E.J. Samuelsen, K. Hoffmann, E. Bakken and P.H.J. Carlsen, *Synth. Metals*, **113** (2000) 7.

331. G. Zebi, B. Chierichetti and O. Ingänas, *J. Chem. Phys.*, **94** (1991) 4637.

332. L. S. Roman, A. C. Arias, M. Theander, M. R. Andersson and O. Ingan¨as *Braz. J. Phys.*, **33** (2003) 376.

333. T. Kowalewski, R.D. McCullough and K. Matyjaszewski, *Eur. Phys. J. E,* **10** (2003) 5.

334. S. Kuwabata, S. Ito and H. Yoneyama, *J. Electrochem. Soc.,* **135** (1988) 1691.

335. S. Kiralp, Z. Kücükyavuz_ A.F. Qasrawi, *Turk. J. Chem.,* **27** (2003) 417.

336. G. Zotti and A. Berlin, *Synth. Metals,* **105** (1999) 135.

337. R.A. Huggins, *Solid State Ionics,* **134** (2000) 179.

338. B.E. Conway, *J. Electrochem. Soc.,* **138** (1991) 1539.

339. A. Clemente, S. Panero, E. Spila and B. Scrosati, *Solid State Ionics,* **85** (1996) 273.

340. C. Arbizzani, M. Mastragostino and F. Soavi, *J. Power Sources,* **100** (2001) 164.

341. S.A. Hashmi, R.J. Latham, R.G. Linford and W.S. Schlindwein, *Ionics,* **3** (1997) 177.

342. K. S. Ryu, X. Wu, Y-G. Lee and S. H. Chang, *J. Appl. Polym. Sci.,* **89** (2003) 1300.

343. K. Rajendra Prasad and N. Munichandraiah, *Electrochem. and Solid-State Lett.,* **5** (2002) A271.

344. A. K. Shukla, S. Sampath and K. Vijayamohanan, *Current Science,* **79** (2000) 1656.

345. J.Y. Lee, K. Liang, K. H. Ana and Y. H. Lee, *Synth. Metals,* **150** (2005) 153.

# LIST OF PUBLICATIONS

**A. Papers published in journals:**

1. A.M.P. Hussain, A. Kumar, F. Singh and D.K. Avasthi, *J. Phys. D, Appl. Phys.*, (In press).
2. D. Saikia, A.M.P. Hussain, F. Singh, D.K. Avasthi and A. Kumar, *Nucl. Instr. and Meth. B* (In press).
3. A.M.P. Hussain, A. Kumar, D. Saikia, F. Singh and D.K. Avasthi, *Nucl. Instr. and Meth. B* **240(4)** (2005) 871.
4. A.M.P. Hussain, D. Saikia, F. Singh, D.K. Avasthi and A. Kumar *Nucl. Instr. and Meth. B* **240(4)** (2005) 834.
5. A.M.P. Hussain, D. Saikia, A. Kumar, F. Singh and D.K. Avasthi, *Ind. J. of Phys.* **79(7),** (2005) 783.
6. D. Saikia, A.M.P. Hussain, A. Kumar, F. Singh and D.K. Avasthi, *Ind. J. of Phys.* **79(7),** (2005) 803.
7. A.M.P. Hussain and A. Kumar, *Ind. J. of Phys.*, **79(9),** (2005) 1033.
8. A. Kumar, D. Saikia and A.M.P. Hussain, *Elec. Micro. Soc. Ind. Bull.*, **5(1)** (2004) 2.
9. A.M. P. Hussain and A. Kumar, *Bull. Mater. Sci.*, **26 (3)** (2003) 329.

**B. Presented in conferences:**

1. A.M.P. Hussain, D. Saikia, F. Singh, D.K. Avasthi and A. Kumar, *Indo-German workshop Synthesis and modification of nano-structured Materials by energetic ion beam'*, NSC, New Delhi, Feb. 20-24, 2005.
2. A.M.P. Hussain, D. Saikia, A. Kumar, F. Singh and D.K. Avasthi, *International Conference on Electroactive Polymers: Materials and Devices (ICEP 2004)*, Dalhousie (India), 1-5 Nov. 2004.
3. A.M.P. Hussain, D. Saikia, A. Kumar, F. Singh and D.K. Avasthi, *6th National Conference on Solid State Ionics (NCSSI)*, Jadavpur University, Kolkata, 5-7 Oct. 2004.

4. A.M.P. Hussain and A. Kumar, *Condensed Matter Days-04*, NEHU, Shillong, 25-27August, 2004.
5. A. Kumar, D. Saikia and A.M.P. Hussain, *XXVII Annual Meeting of Electron Microscopy Society of India (EMSI) and Conference on Electron Microscopy and Allied Fields*, NPL, New Delhi, April 1-3, 2004.
6. D. Saikia, A. Kumar, A. M. P. Hussain, F. Singh and D. K. Avasthi, *National Conference of Materials and Application*, Kurukshetra University, Kurukshetra 11-13 February, 2004, pp-335.
7. A.M.P. Hussain and A. Kumar, *14th Annual General Meeting-Materials Research Society of India*, BARC Mumbai, 11-13 Feb, 2003.
8. A.M.P. Hussain and A. Kumar, Proc. of *3rd Regional conf. on Physics Research in the north East*, Dibrugarh University, Dibrugarh, 9 Nov. 2002, pp. 57.

**C. In annual reports:**

1. A.M.P. Hussain, D. Saikia, A. Kumar, F. Singh and D.K. Avasthi, *NSC Annual Report*, (2004-2005) pp-217.
2. D. Saikia, A.M.P. Hussain, A. Kumar, F. Singh, N. C. Mishra and D. K. Avasthi, *NSC Annual Report*, (2004-2005) pp-213.
3. D. Saikia, A.M.P. Hussain, A. Kumar, F. Singh, and D. K. Avasthi, *NSC Annual Report*, (2003-2004) pp-157.
4. D. Saikia, A.M.P. Hussain, A. Kumar, F. Singh, D. K. Avasthi and N. C. Mishra, *NSC Annual Report*, (2002-2003) pp-214.